NISTIR 5825

NIST Construction Automation Program Report No. 1 Non-Line-of-Sight (NLS) Construction Metrology

William C. Stone

February 1996
Building and Fire Research Laboratory
National Institute of Standards and Technology
Gaithersburg, Maryland 20899

U.S. Department of Commerce
Ronald H. Brown, Secretary
Technology Administration
Mary L. Good, Under Secretary for Technology
National Institute of Standards and Technology
Arati Prabhakar, Director

ABSTRACT

This paper addresses the subject of automated metrology (surveying) for use on construction sites. Specifically, the research is directed to the development of a novel Non-Line-of-Sight (NLS) system with which the real-time position and orientation (attitude) of any object on a construction jobsite may be determined, irrespective of the presence of intervening obstacles that would otherwise render optical and/or electro-optical techniques useless. Tests were conducted using a specially configured broad-band, low-frequency spread-spectrum radar. The transmission and receiving antennae, which in normal radar are typically one and the same, were physically separated so as to create a system with a fixed broadcast unit and a "roving" receiver, whose range was to be determined relative to the transmission antenna by means of time-of-arrival measurements. Time domain response was synthesized by means of fourier theory from a broad spectrum of data sampled in the frequency domain. Numerous field experiments were performed in which typical construction site obstacles were placed between the transmitter and receiver with separation distances of up to 80 meters. The obstacles included a half-meter thick, heavily reinforced concrete wall, varying combinations of masonry block and brick up to more than a meter in thickness, and metal pre-fabricated wall panels. In all but the latter case, repeatable distances were obtained . Range detection was lost in the presence of extensive metal panels that contained no windows. However, the presence of even small openings permitted range acquisition. Sources of error, limits of resolution and accuracy, and factors affecting time of flight measurement are discussed.

KEYWORDS: Construction automation, dielectric constant, diffraction, metrology, multipath, NLS, non-line-of-sight, penetration capacity, positioning system, propagation delay, spread spectrum radar, surveying.

Table of Contents

Chapter One : Introduction:

Surveying has traditionally been defined as the science and art of determining relative positions of points on, above, or beneath the surface of the earth, or establishing such points. It is one of the oldest and most important arts, stemming from the need to mark boundaries and divide land.

In modern structural and civil engineering, surveying is an essential element required to plan, construct, and maintain highways, railroads, rapid-transit systems, buildings, bridges, tunnels, canals, dams, drainage works, and land subdivisions, to name but a few. Such surveys will generally fall under categories of establishing local topography and land boundaries prior to commencement of construction; in-progress assessments conducted during actual construction to provide control elevations, horizontal positions, dimensions, and configurations; and as-built data to provide exact final location and layout of engineering works, their positional verification, and records that include design changes and retrofits.

The surveying process, as practiced at a typical construction site generally involves the following steps:

- **Research and analysis**: selecting the survey method and equipment.
- **Field work or data acquisition**: making measurements and recording data in the field.
- **Computing or data processing**: performing calculations based on the recorded data to determine locations, areas, volumes, and so on.
- **Mapping or data representation**: plotting measurements or computed values to produce a map, or chart, or portraying the data in a numerical or computer format.
- **Stakeout:** setting monuments and stakes to delineate boundaries or guide construction operations.

The past 15 years have seen significant improvements in surveying technology, the most important being the development of electronic distancing equipment and the integration of these devices into "total stations", which contain onboard microcontrollers which automatically reduce inclination, azimuth, and distance to provide cartesian coordinates of a survey target relative to the survey instrument. New technologies that are just now beginning to see limited use on construction sites include Differential GPS (satellite based positioning relative to an orbiting constellation of time-encoded transmitters) and "fanning" laser systems operating in the ultraviolet range of the electromagnetic spectrum. These latter technologies possess the important attribute of being capable of providing nearly instantaneous, or "real time", position information.

The advantages and disadvantages of each of these systems will be described below. However, all share the common limitation of requiring a direct line of sight between the instrument and the point for which the position is desired. At a typical construction site, where optically opaque walls, beams, girders, slabs, and ceilings are constructed as a matter of course, component obstructions will constitute a severe impediment to real-time surveying.

In the context of present day construction, line of sight surveying instruments meet the existing needs. However, the traditionally conservative construction industry has long been identified as one which is overdue to reap the benefits of "information age" technology. Global competition is now forcing a reconsideration of this status quo. Unlike the manufacturing and shipping industries, construction has been unsuccessful at delivering improved value over time. The potential benefits from improvement in performance of the construction process are enormous, given the scale of the industry and its impact on national and global economies. The construction process itself must be re-designed as a system if technology innovation is to be effectively exploited by the U.S. construction industry. Construction automation has been proposed as a central enabler to the better use of limited global resources (capital, human and material) and therefore has a key role in achieving development which is environmentally sustainable. Innovation through construction automation is also central to competitiveness of the industry.

Construction automation addresses the following problems: decreasing worker productivity; poor working conditions; injuries to workers; decreasing desirability of building and construction jobs; declining quality of the constructed project; over-run schedules; high project costs; decreasing skill level of workers; hazardous materials or site conditions (both known and unexpected); manual handling of heavy and awkward assemblies; and time consuming inspection, repair and maintenance. Construction automation embodies a systems engineering approach to hardware, software and interface technologies, as well as to condition assessment and real-time site metrology.

Accurate and flexible simulation tools for the construction process, in all its dimensions, are central to solving the problem of performance of the constructed facility over its entire life cycle. In the design stage , simulations of constructability and maintainability, as well as performance under natural and manmade environments during the facility's use, must be undertaken. Simulation includes performance of construction equipment; environmental factors and impacts; and behavior of human participants. Thus, simulations of construction and maintenance or renovation activities are essential to design as they are to selection of optimal alternative construction processes.

Within the above construction automation context the problem distills to one of knowing where everything is at all times. This requirement for global position knowledge when components, machines, and people move about outside and within the constructed facility poses metrology problems which exceed present day capabilities. What is needed is a metrology system -- a "Non-Line-of-Sight" (NLS) survey system -- in which position at a construction site may be determined irrespective of the presence of intervening obstacles.

It is the objective of the research described below to enable the development of such a metrology system.

The Automated Construction Site

In 1994, NIST began a research initiative in construction automation. The broad-based objectives of this program are to develop standards to permit the construction industry to achieve the benefits of large scale automation and systems integration that have heretofore been possible only in controlled factory environments. Several architectures have been proposed for automated integration of construction site tasks (see Figs. 1.1.1, 1.1.2, and 1.1.3).

Common features depicted in the above architectures which are necessary to permit one-of-a-kind, large-scale manufacturing at highly varied construction sites include:

- **Sensors for Real-Time Construction Site Metrology**
- **Wide Band Telemetry and Data Acquisition**
- **Virtual Site Simulation and Object Representation Standards**
- **Person-in-Loop Systems Feedback**
- **Construction Robotics**

As suggested in Fig. 1.1.4 (BFRL pyramid slide), these technologies may be viewed of as a pyramid, with each successively more sophisticated capability being dependent on those beneath it. Described below are these five topical areas, identified by NIST as necessary to achieve a global closure of the construction automation process from real-time data acquisition at the job site through the return of that information, in a processed format, in numerous useful ways on-demand.

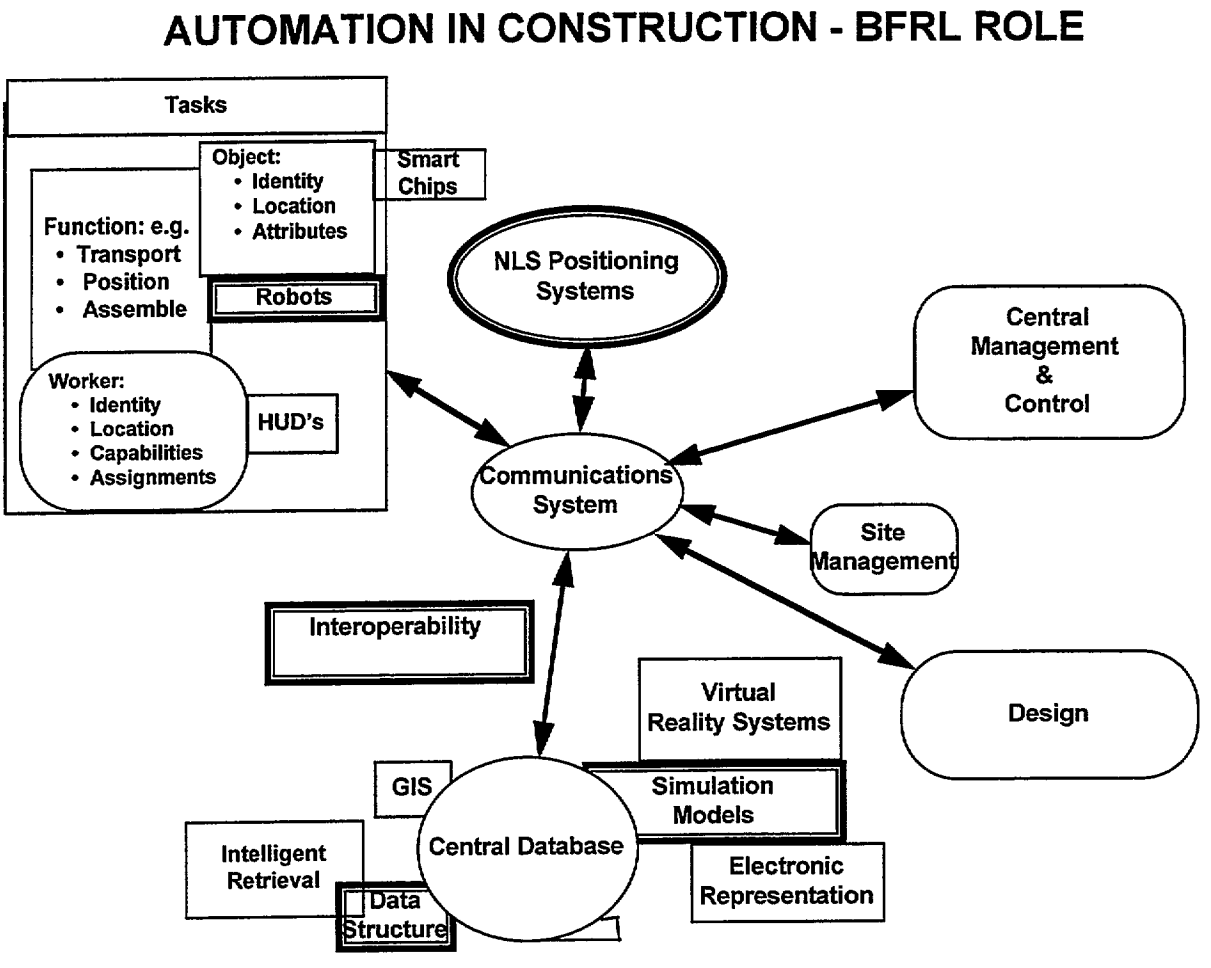

Figure 1.1.1: Early BFRL vision of open architecture for construction automation. Key facets include metrology; wireless communications; global interactive databases; worker feedback, training, and teleoperation systems; and semi-automated and fully automated machinery.

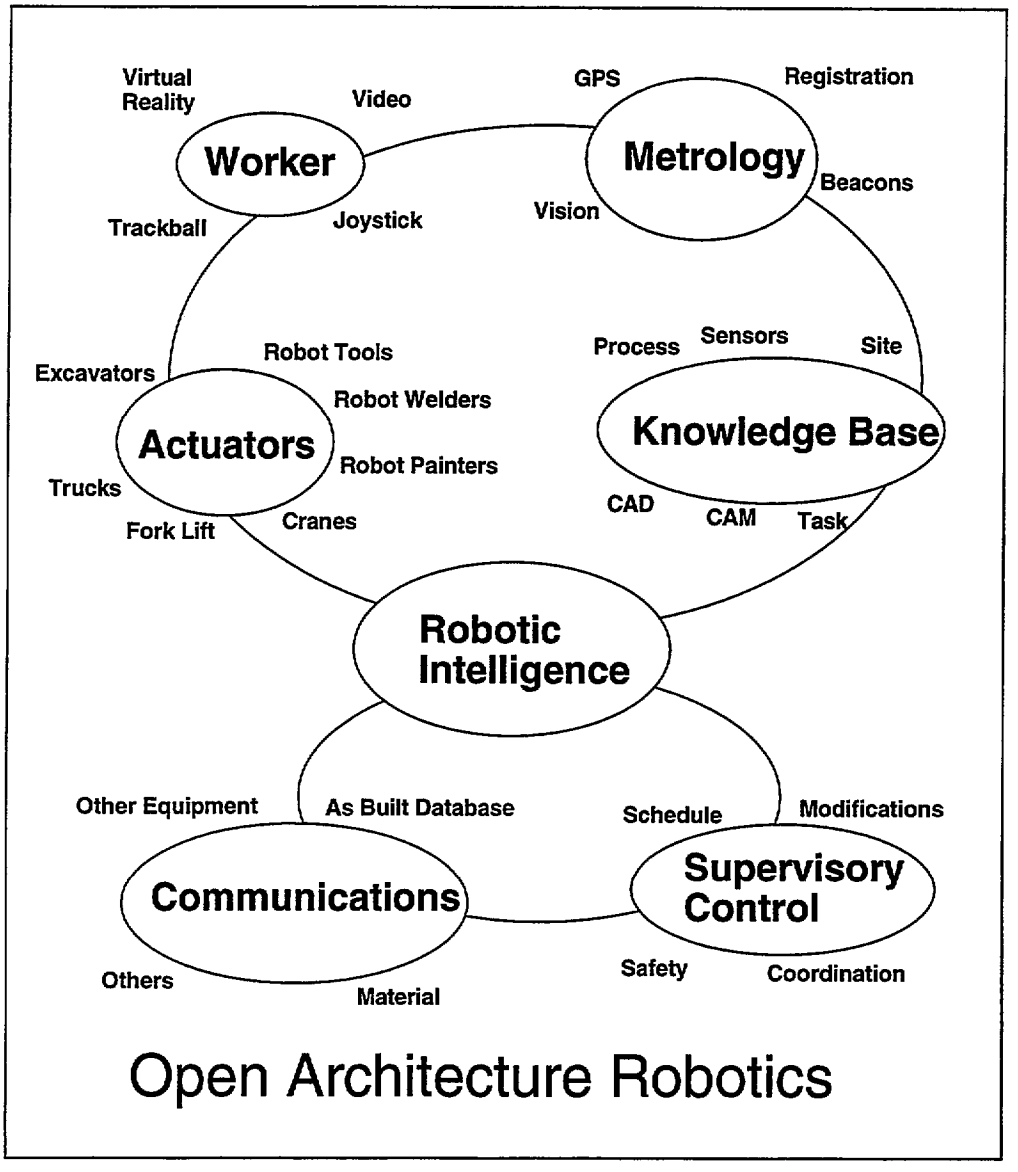

Figure 1.1.2: Construction automation open architecture proposed by Cybo Robotics.

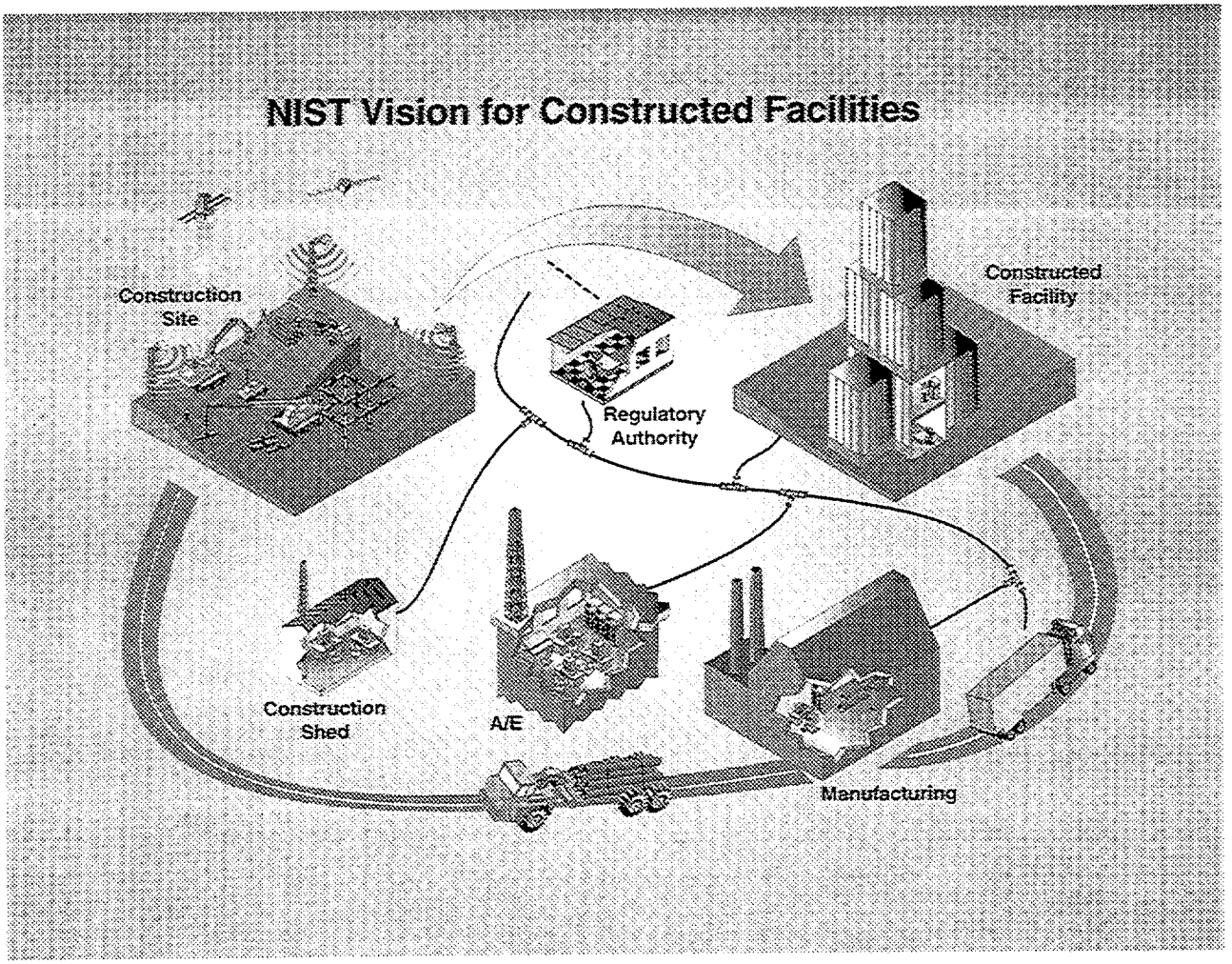

Figure 1.1.3: NIST Vision for construction automation. Jobsite wireless communications links workers and machines to the local construction shed which is in turn linked to the information superhighway via a miniimum T1 data link (1.5 Mbits/sec). Automated routers permit design office engineers and project planners, manufacturing job shops and fabricators, and regulatory authorities to subscribe to various portions of this data flow. Workers and foremen at the construction site will be able to ascertain in real-time the status and location of raw materials and fabricated components.

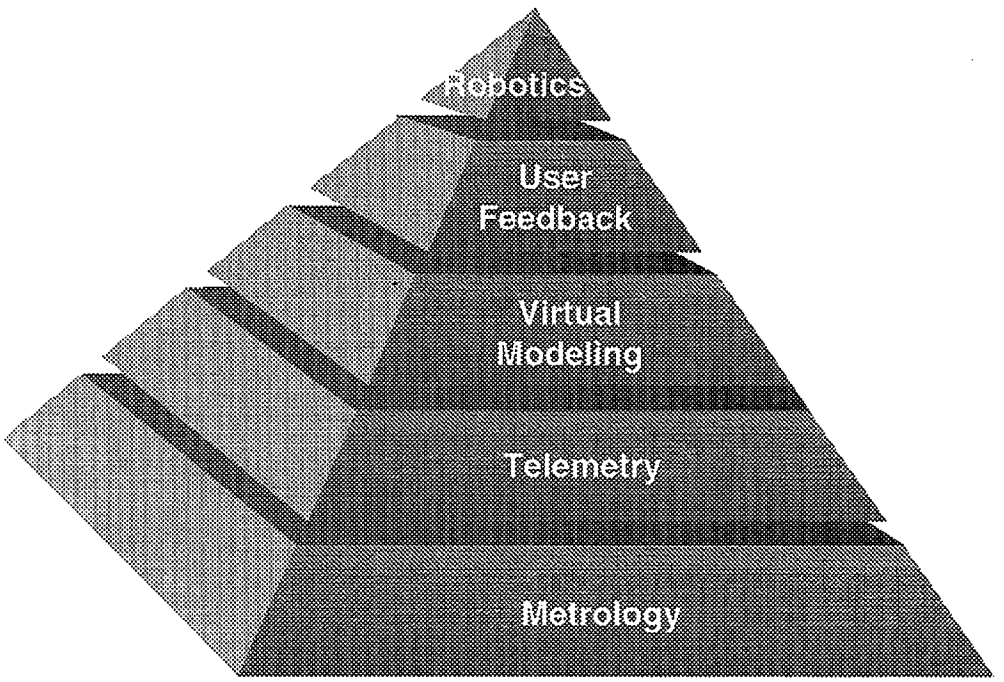

Construction Automation Hierarchy

Figure 1.1.4: Technological underpinnings of construction automation. Real-time measurement (metrology) forms the foundation of all automation. Wireless jobsite communications involving potentially hundreds to thousands of data channels is required to uplink information in a fashion which is unintrusive to on site operations. Virtual modeling and the development of a real-time global database is needed to store all project data, including that uplinked from the jobsite as well as that from design offices and fabricators, and to make this available to all authorized subscribers in a format which provides realistic assessment at a glance. User feedback systems and training systems include helmet-mounted displays (HMDs) and head-up displays (HUDs) both for data interrogation, machinery operation, and machinery simulation. Semi-automated and eventually fully automated (robotic) machinery will begin to see effective use at job sites only after the first four foundation levels have been effectively implemented.

1.1.1 Real Time Metrology and Sensing Needs

The fundamental problem with any construction site is that it is continually in a state of semi-controlled chaos. One reason for this is the lack of instantaneous knowledge about what needs to be done next, where it needs to be done, and where the people and/or machines, materials and tools are that are needed to do it. Thus the underpinning, as suggested by Fig. 1.1.4, is real-time metrology.

Before addressing how one might conduct such surveying, it will be useful to establish how much accuracy is needed. The required accuracy depends primarily on the purpose of the survey. For horizontal and vertical control surveys standards have been established by the Federal Geodetic Control Committee [Berry, 1976], as shown in Table 1.1.1. Accuracy is expressed as a relative fraction, for example, 1 part in 100,000 for a First Order survey. At a typical construction site, where survey distances realistically are less than 100 m, First Order accuracy amounts to a +/- 1 mm error band ; Third Order, Class I accuracy would be +/-10 mm over the same distance.

Table 1.1.1: Horizontal Control Survey Accuracy Standards

Order and Class	*Relative Accuracy Between Adjacent Points*	*Accuracy on 100 m Survey Line*
First Order	1 part in 100,000	1 mm
Second Order:		
Class I	1 part in 50,000	2 mm
Class II	1 part in 20,000	5 mm
Third Order		
Class I	1 part in 10,000	10 mm
Class II	1 part in 5,000	20 mm

Typically, Third Order, Class II accuracy is specified for local construction site work and is sufficient for grade line control for earth moving, where +/- 20 m m over 100 m (1 part in 5,000) is commonly specified for plane control of, for example, paved parking lots [Allegheny Excavating, 1995]. Building stakeouts typically involve accuracies of 1 part in 10,000 [Dewberry & Davis, 1995]. First order surveys are typically commissioned only for the setting of control points where position and/or alignment are critical. For example, the Washington DC Metro requires First Order accuracy for all rail lines.

For the placement of steel framework the American Institute of Steel Construction [AISC, 1980] provides the position and alignment tolerances shown in Table 1.1.2.

Table 1.1.2: Steel Construction Position and Alignment Tolerances

Task	Relative Accuracy Between Adjacent Points	Accuracy on 100 m Survey Line
Horizontal Alignment of Exterior Columns	1 part in 2400	42 mm
Vertical Alignment of Exterior Columns (inter-story slope)	1 part in 2000	50 mm
Vertical Alignment of Exterior Columns (total deviation from column line)	1 part in 864	116 mm

More stringent accuracies are required by AISC for the installation of anchor bolts and embedded items. Table 1.1.3 lists typical requirements for these types of connections.

Table 1.1.3: Installation of Anchor Bolts and Embedded Items

Category	Absolute Error Tolerance
Center-to-Center of any two bolts within a group	3.2 mm
Center -to-Center of adjacent bolt groups	6.4 mm
Elevation of tops of bolts	+/- 12.7 mm
Deviation of bolt group Centerline from Column Line	6.4 mm

The absolute error limits established in Table 1.1.3 represent a class of common construction related assembly operations, and similar values could be prescribed, for example, in the error tolerance that might be acceptable for an automated robot designed to place structural steel in a high rise structure. From the above discussion it is apparent that a graded accuracy scale might be developed for general automation at a construction site. Many items that will require position monitoring, such as the location of supplies, equipment, and personnel, do not require as great a level of accuracy. Table 1.1.4 presents what the author feels to

be a representative first cut at establishing standard metrology needs for the automated construction workplace:

Table 1.1.4: NIST Proposed Working Model for Automated Construction Site Metrology Accuracy

Category	Absolute Error Tolerance (over 100 m radius)
Vehicle position (remote reporting)	+/- 500 mm
Personnel (remote reporting)	+/- 500 mm
Material stockpiles and discrete components within those stockpiles (remote reporting)	+/- 500 mm
General earthmoving (coarse machine control)	+/- 100 mm
Structural alignment (remote reporting)	+/-50 mm
Final Grade earthmoving (machine control)	+/- 20 mm
Final component position (remote reporting)	+/- 10 mm
Component Placement Full Registration Coarse Alignment	+/- 5 mm
Component Placement Full Registration Fine Alignment	+/- 2mm

There are several emerging technologies which are poised to address portions of the accuracy spectrum described in the above table. All of these technologies, described in greater detail in Section 1.2, have the common requirement of an unobstructed line-of-sight between the survey instrument and the target, whose position is desired.

In addition to position acquisition (three degrees of translational freedom), there will also be a requirement in the automated construction workplace for several

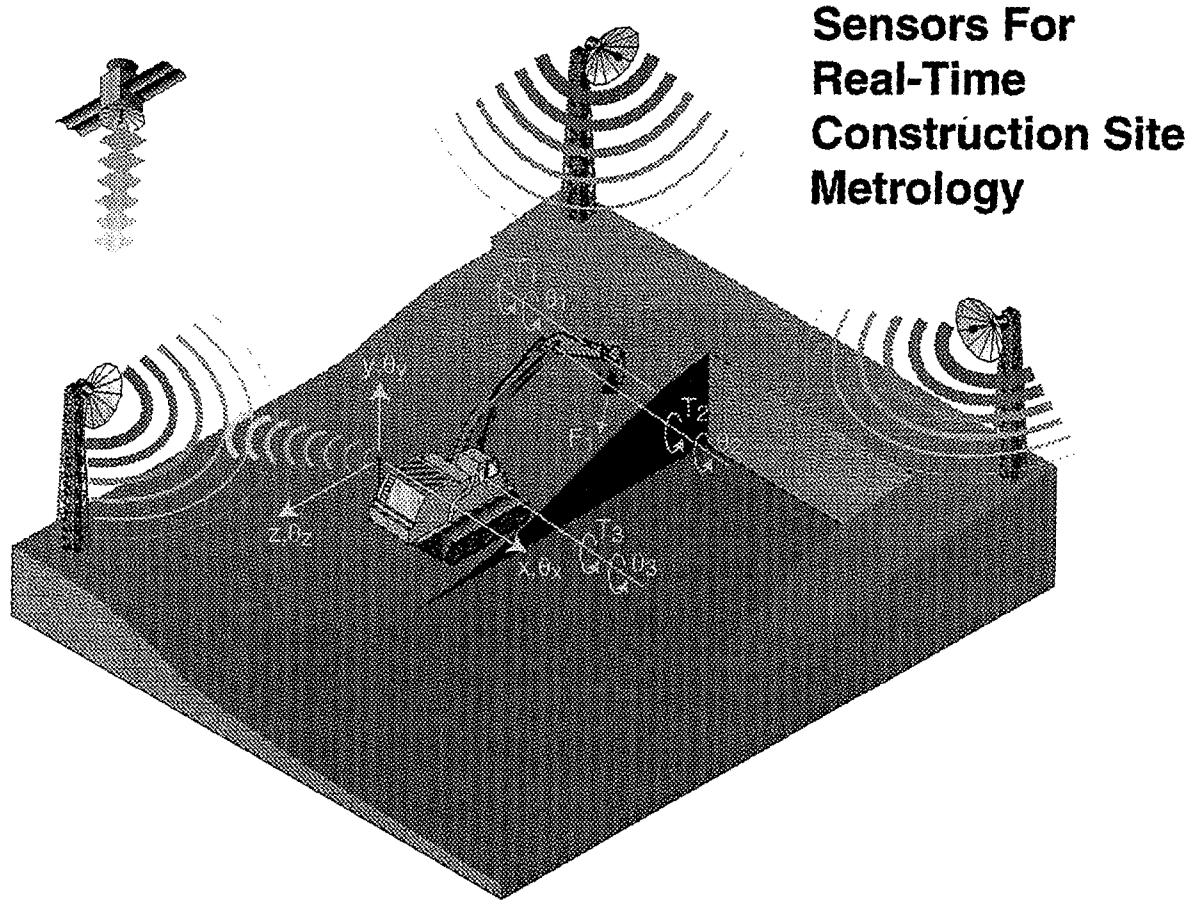

Figure 1.1.5: Sensors for Real-Time Construction Site Metrology. In order to track and eventually place machinery under semi-autonomous and eventually fully autonomous control the position and attitude of the vehicle must be known at all times. Additionally, for collision avoidance, the status of all other kinematic degrees of freedom must also be known, such as the angles associated with articulated arms. The first six degrees of freedom (vehicle position and attitude) can be determined by several approaches including differential phase GPS (which requires no additional jobsite metrology equipment) or by an array of onsite pseudolites, fanning laser, or NLS (non-line-of-sight) surveying systems now under developement. These external reference metrology systems may be aided by auxiliary onboard IMUs (inertial measurement units). The development of generic, low cost "strap-down" units for vehicle tracking will be essential to fully realize the potential of construction automation.

other sensed characteristics, including attitude (three degrees of rotational freedom); joint rotations, actuator and/or cable extensions, and various strains, loads, pressures, and temperatures which are needed to completely describe the state of machinery, vechicles, and robotic hardware (Figure 1.1.5).

Furthermore, a means for uniquely identifying each item that can move about, including machines, people, components and raw materials must be developed. Acquisition of this identification code, which might take the form of a bar code or "smart chip," will be part of the sensing technology that will one-day be integral with the positioning system. From the view point of "real-time" operations, such position, state, and identification actions will need to take place at sufficient update frequencies to permit remote operation (teleoperation) of vehicles and realistic virtual representations of the site to be created at remote offices.

A simple example of the identification task is: suppose one has a pile of rebar on the construction site. A construction *foreman,* or worker, needs to know

- what that rebar is... is it a #4 bar, a # 6 bar etc.
- where is it located right now and
- where is it supposed to go.

The *engineer and planner,* on the other hand, would like to know

- is it Grade 60?
- what mill did it come from?
- what is its stress-strain data
- when was it manufactured
- is it supposed to be epoxy coated or bare? etc.

It is assumed that there will be some type of bar code or smart chip identifier for every significant item entering a construction site (Figure 1.1.6). It would not be unreasonable for a deformed bar manufacturer to automatically stamp a bar code in each bar as it comes off the mill. What that code would mean, and what its format should be remains to be defined. The same approach could be adapted to wide flange sections and other standard construction materials and components. Although initially an inspector will be responsible for keeping track of scanning codes, counting components and acquiring positions, this task will eventually be done by erection crews as they do their job. NIST has chosen to concentrate initially on development of standards for identification systems for construction site components, including familiar items like rebar and rolled sections and eventually proceeding onward to complete kinematic descriptions of vehicles that would allow manufacturers to easily enter their machinery into a standard

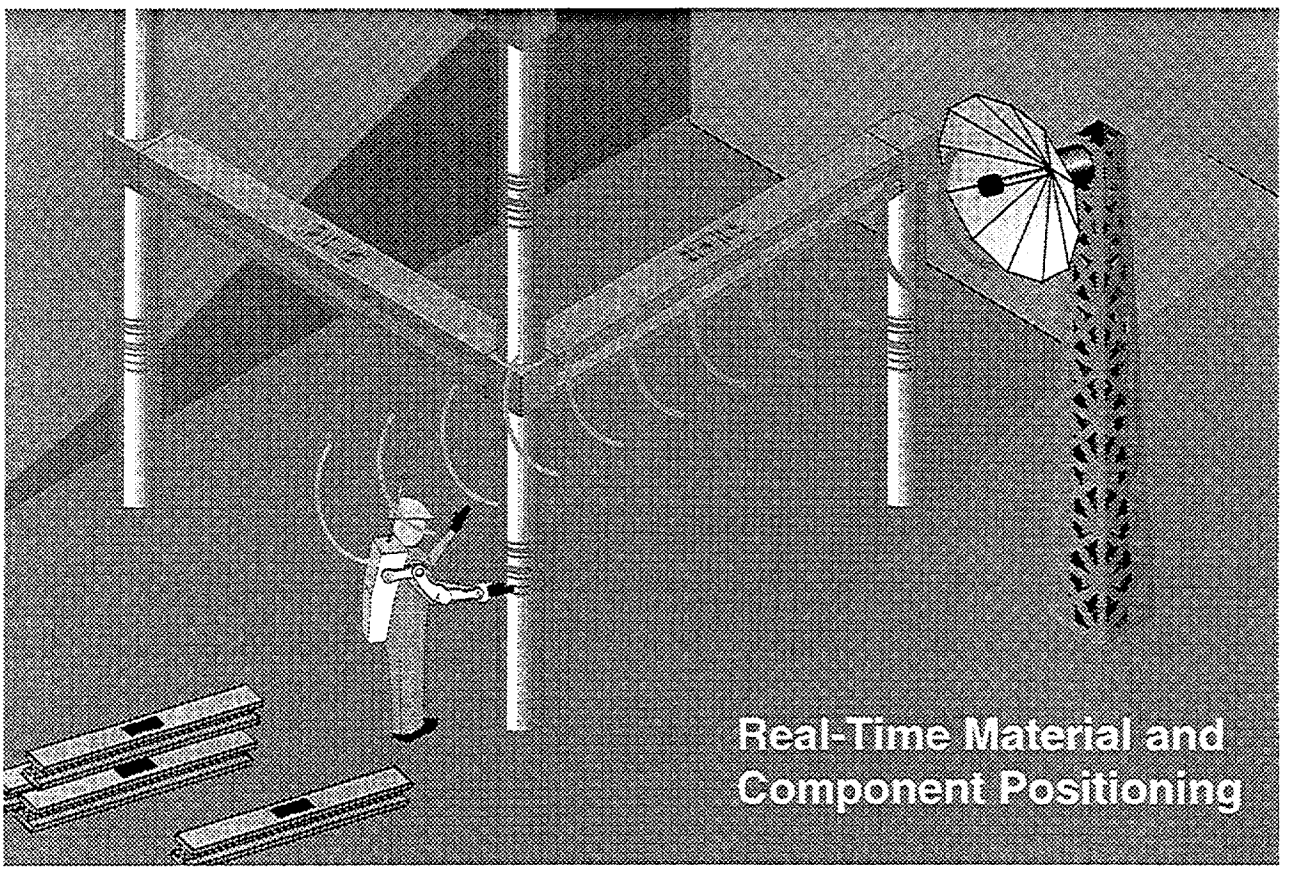

Figure 1.1.6: Real-Time Material and Component Positioning: In addition to vehicle tracking, the position of all construction materials and constructed components must be known. This permits near instantaneous knowledge of the as-built status of the structure as well as provides information to construction foremen and workers of the location of hardware and materials. Unilke vehicle tracking, Q/A workers will be tasked with tracking onsite movements of these items. Bar codes and smart chips will permit component recognition, but the location must be spatially derived by touching key points (pre-marked) on components which will be referenced in the global database, so that the location and orientation of each component (once installed) is known. As shown above, one possibility for acquiring key point positions is though the use of an articulated scanning arm connected to a roving backpack receiver. The backpack will use the same positioning systems described earlier for vehicle tracking and the articulated arm will account for the offset relative to a sensing element directed by the worker to the component keypoints.

identification system that would permit menu-select entry of that item into a virtual world model of a construction site.

1.1.2 Data Telemetry

It is one thing to acquire bar codes and positions. One can presume that for a large construction site that will eventually see controlled vehicles and tracked positions of every moving object, that there will be hundreds if not thousands of such position and identification transactions occurring each second. In order for any sense to be made of this data it must reach a global database to which remote and local queries can be made. The transfer of data must be accomplished via telemetry (wireless communications), although for a few specific cases fiber optic lines can be considered. This massive transfer of data from independent sources will require novel approaches to prevent radio frequency chaos and the intervention of the FCC (Federal Communications Commission) that might prevent or hamper implementation. Key issues to be resolved include:

- Interfacing hundreds of on site positioning systems with a global jobsite database
- Maximizing real time data reliability (inter-city construction will involve transmission from within a congested location and competetion with similar transmitters at nearby jobsites).
- Federal communications laws.
- Data security
- Cost

It is anticipated that many techniques developed during the past ten years for battlefield command and control will be brought to bear on this issue.

1.1.3 Virtual Site / Simulator Standards

The third step in closing the automation loop is the development of simulations and simulation tools to model the performance of individual pieces of construction equipment, e.g., earth moving equipment or cranes, and other objects which move about the construction site either under their own means of locomotion (e.g. human workers) or materials and components which may, from time to time, be moved by either of the afforementioned agents. These simulations and software tools will permit users to determine key characteristics of construction equipment and processes, e.g. the productive output of the equipment and the response, or failure, of the equipment to its environmental factors such as weather and soil conditions. Manufacturers and commercial software companies will develop the "commercial" simulation capabilities, but

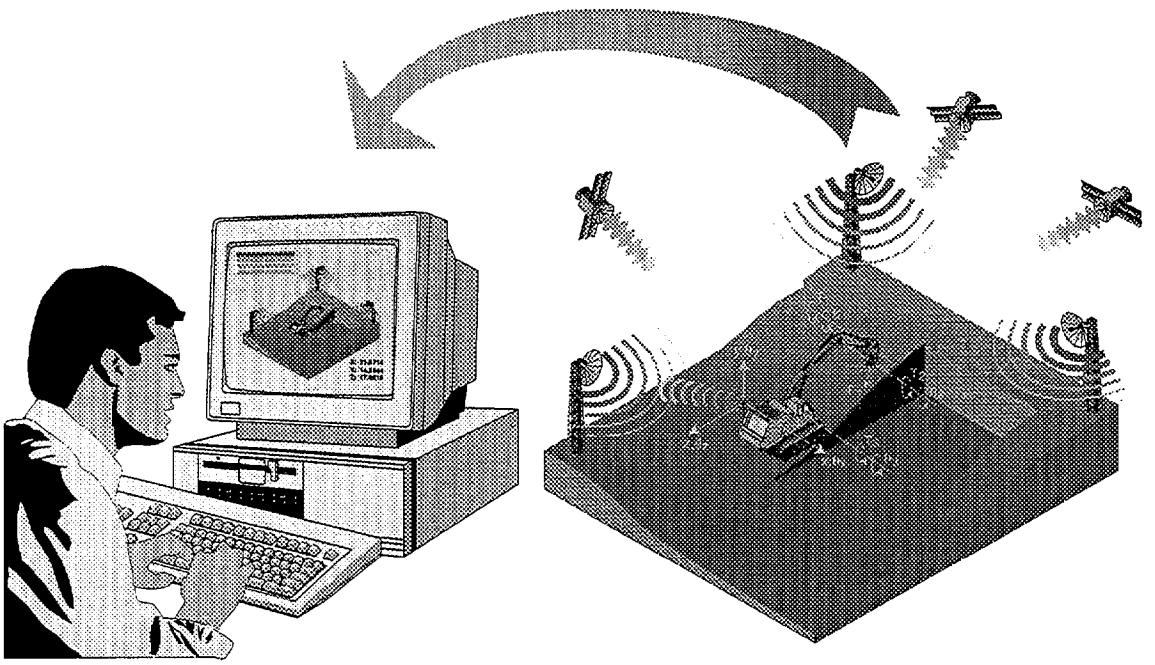

Virtual Site Simulation
and Object Representation Standards

Figure 1.1.7: Virtual Site Simulation: Data telemetered from the construction site will be used to update full three-dimensional kinematically realistic representations of the items and machines which exist at the at the construction site, in addition to the present site geometry (which may be modified by the actions of machines and workers). Any node connected to the information superhighway and possessing the proper authorization (see Figure 1.1.3) can subscribe to the global database and view either numerical or three dimensional renderings of the status of the site from any perspective. Standard formats for storing and displaying component and machine representations remains to be developed.

will make use of common standards for data exchange, thus facilitating inter-operability and flexibility. Federal R&D will focus on fundamental and enabling research needed, e.g., dynamic properties of soil, nonlinear response of mechanical systems, vision/user interface technologies, control algorithms, automated site metrology/telemetry, data exchange standards (e.g. for kinematic virtual models), and planning/reasoning techniques.

Simulations will be developed of the construction process at various levels of detail. Critical path scheduling is simulated at a high level of abstraction, whereas simulation of mechanical tasks (for example, back hoe loading of a truck) is at a very detailed level. Eventually, there should be capability to move through a hierarchy of planning detail for the construction process. Commercial organizations are expected to provide the "commercial" versions of these simulations, but construction contractors, equipment manufacturers and academic and federal researchers will be principals in the development and verification of algorithms, database standards, and proof-of-concept demonstrations through virtual construction test-beds.

Construction process simulation (Figure 1.1.7) includes simulations of interactions with the environment and people; static and dynamic, linear and non-linear response of materials and systems to forces, displacements and temperatures; behavior of equipment considering its position and attitude, its flexibilities and degrees of freedom, component inertias, environment, control systems and operator interventions; and gaming-type models for effects of operations with time. Simulations of maintenance, renovation, and demolition are within this scope provided that removals as well as placement of materials and components are simulated.

Federal R&D can facilitate development of effective, neutral standards in the form of guide specifications to manufacturers of the physical systems and equipment that will utilize automation, advanced metrology and sensing capabilities and the software/data interface standards that will link all these disparate sub-systems. These standards and guides will act as a framework, evolving under industry consensus and technological innovation, that equipment manufacturers can use to ensure acceptance of new and innovative equipment and systems. Standards will support robust and reliable equipment which will yield attractive production rates and high quality construction.

Three dimensional graphics (including virtual reality technologies) will be a key aspect of the simulation tools, so that construction workers, managers and engineers can understand the reasons for problems in the construction process and easily identify improvements. Non-graphic analytical and reasoning techniques also will be needed to identify opportunities and needs for improvements and recommend changes in construction processes. Commercial software companies will be involved in developing and marketing construction

simulations, with research activities involving research organizations and contractors.

1.1.4 User-in-the-Loop Feedback

Once one has position and identification, what can be done with the information? One promising use would be to enter it into a 3D immersive simulator that would permit a management level project planner to assess what is happening at the site and where things are. Establishing such a virtual environment is a big job and will, by nature, involve many iterations in which concepts shown to work on testbed simulators are put before industry for common concensus of practicality. However, once agreed upon, the impact of this system will carry all the way to the indivdual hardhat worker on the jobsite who will, on demand, have interactive access to this information..

Human factors and display research will be essential to close the loop and bring the database information back to the construction site worker and foreman where it can be put to practical use in the form of selected access to registered 3D as well as alphanumeric data, updated in realtime, on the jobsite. The development of lightweight, robust, inexpensive helmet mounted displays (HMDs) and head-up displays (HUDs) are crucial to this process [Chinnock, 1995], as are human factors design to determine methods of displaying data, while avoiding information overload, eye strain, and disorientation typical of such systems today. Voice activation and recognition technologies, high capacity, compact, local storage media, and inter-worker communications will also be crucial technologies to this effort. It is presumed that Federal R&D will develop the initial proof-of-concept technologies, with the private sector subsequently manufacturing commercial versions of these systems.

One variant of this technology envisioned at NIST is that of a Head-up Construction Database Interrogator: a flip down, see-through visor that mounts to a standard construction helmet (Figures 1.1.8 and 1.1.9). A hands-off voice activated menu system would come up which would permit the worker to identify the section of the jobsite he is working at and call up a blueprint if there is a question concerning what goes there. If the question really is: "where are the 135-degree bent #8 bars that are supposed to go here?" the database can be accessed and the answer displayed on the visor. It may be appreciated that this system could extend far beyond this level; supervisors could request shipment status, locate and call meetings with key workers, interactively flag problems to management etc. Many of the required base technologies to achieve this already exist; assembling them in a fashion that meets the "effective, cheap, and robust" criterion will prove the measure of the problem.

Retractable HUD (Heads Up Display) for Database Interrogator

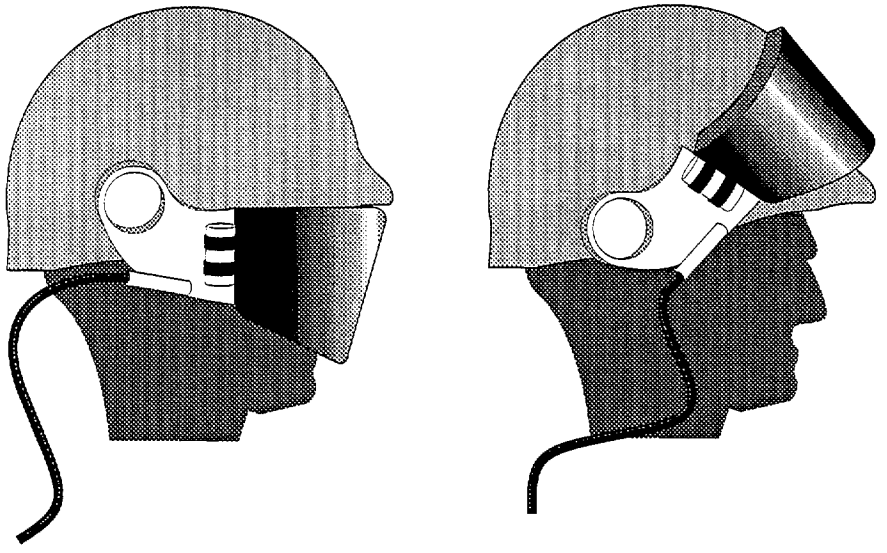

Figure 1.1.8: One possible manifestation of an individual helmet-mounted database interrogator. An on-site worker is able to querry, for example, regarding the location of a particular component. More advanced versions will permit full *registration* of the virtual world database three dimensional site representation model with that of the real world in real-time. This will permit placement of components without the need for on site surveying or measuring.

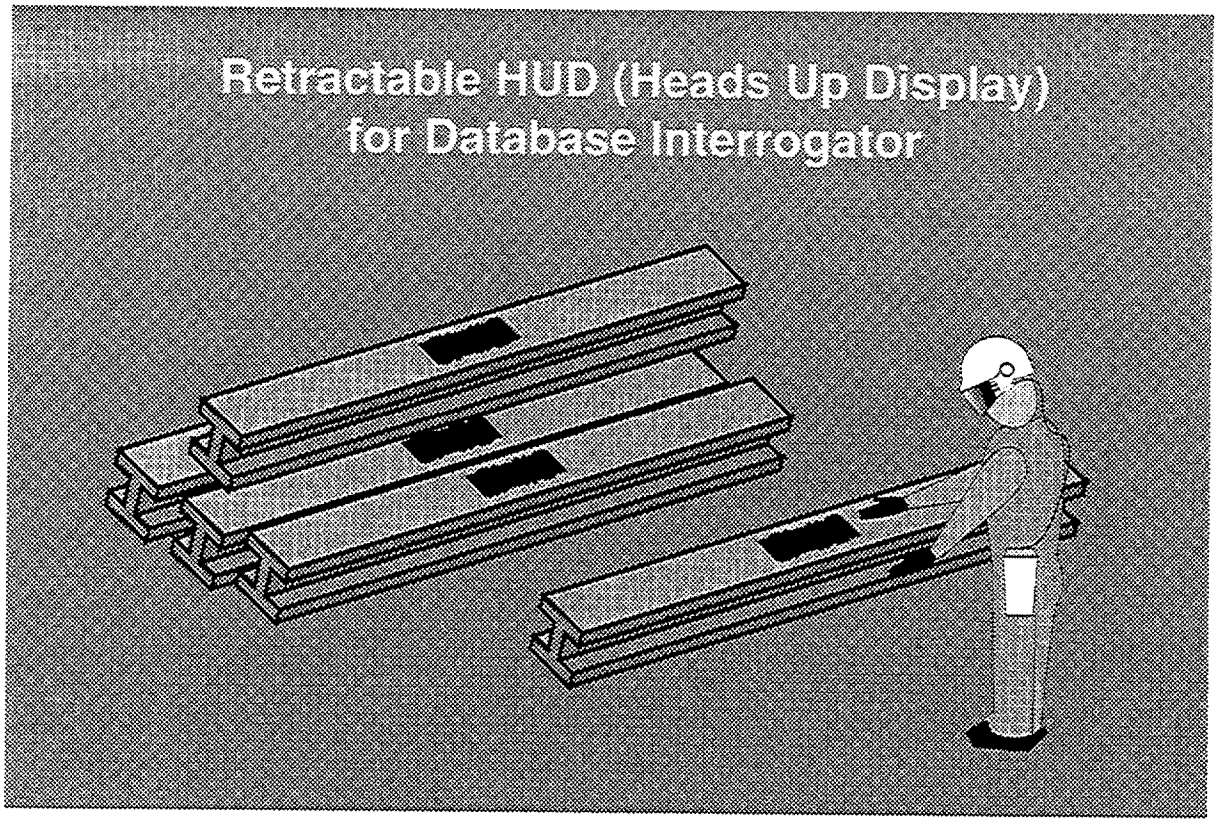

Figure 1.1.9: Using the portable Database Interrogator to identify the intended final destination for an on site component. Each component will have a bar stripe or smart chip identifier installed at the fabricators. Erection sequencing programs assigned at the design office will indicate when and where a particular component is called for, thus preventing mistaken installation.

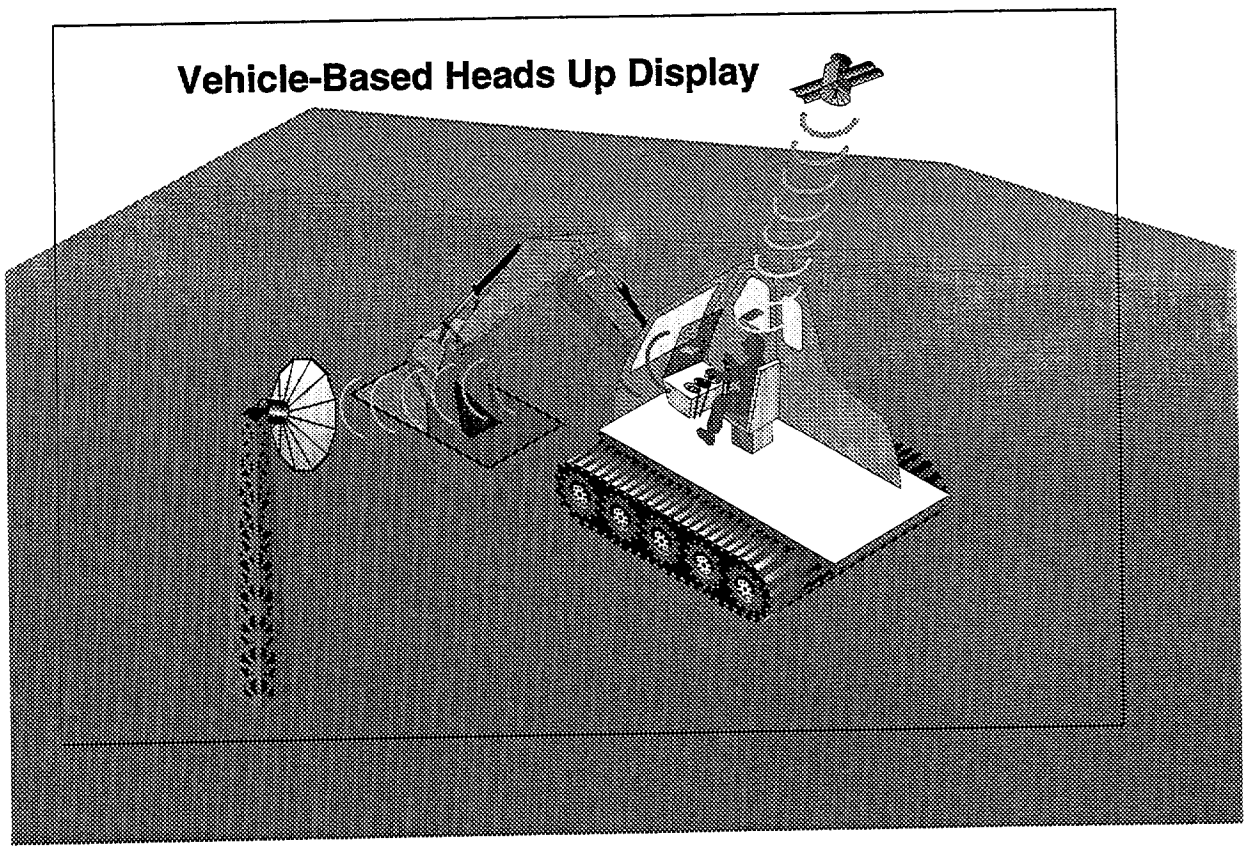

Figure 1.1.10: Vehicle-Based Heads Up Display (HUD). Real-time information concerning the *desired* site geometry may be downlinked to a see-through projection HUD to a machine operator who can then guide the earthmoving operation to match the registered geometry of the final desired landscaped surface. These actions can be semi-automated to the extent that the operator should be able to request "auto-pilot" control through a particular maneuver, after which the machine will carry out the necessary actions. Operators will be able to over-ride the automated system at any time. Since complete kinematic models are kept in real time for each vehicle, each piece of machinery in effect becomes a real-time surveying instrument, relaying the present state of the site geometry local to the vehicle to the global database.

The feedback from the global database may come on a hierarchy of levels, beginning with the above mentioned construction worker interface. The next level would be dedicated head-up displays mounted in construction vehicles. But the concept can be taken much further, effectively turning the real vehicle cab into a virtual receiving port (Figure 1.1.10) that would make it indistinguishable from a virtual training simulator for the same piece of machinery. The person operating the actual vehicle can call up the virtual image of the site indicating what needs to be done and providing recommended maneuvers. This is easy to envision with earth moving, but can be extended to all forms of construction machinery. By building realistic virtual simulators to match the actual cabs and by equipping the cabs with virtual feedback systems one immediately obtains the spinoff product of tele-operation, if desired, since an operator working in a high fidelity virtual cab should be able to operate the actual machinery without actually being in it. The fidelity will be limited by the time-of-flight of the transmission signals and will be a factor on some very long distance control operations.

1.1.5 Construction Robotics

The final level of feedback is autonomous and/or semi-autonomous control, in essence "robotics." The slow pace of development in the robotics world during the last decade, as opposed to the early, and wildly optimistic, expectations of the degree to which robots would penetrate everyday life, has given way to a cautious re-assessment of what is achievable and what is "futuristic" with respect to construction robots. It is now generally accepted among researchers that turning loose a 1000 horsepower bulldozer or a 50 ton crane on a construction site without human supervision is not likely in the foreseeable future. More likely it will come to pass that a full time operator does the setup, fixturing, initialization, and choice of process to be performed and then the machine performs the task.

In effect, the strategy is to let the human operator do what is easy and natural for a human, and let the computer do what is easy and natural for the computer. The resulting machine-operator team may be 5-10 times more productive than present, conventional methods.

Initial, tentative steps in this direction will take place during the next five years. NIST is presently studying various aspects of construction operations in order to logically downselect the most desirable task candidates for automation. Initial demonstration projects in semi-automated robot operations are anticipated to involve on-site setup by construction personnel, followed by autonomous task execution by the robot. The operator must, at all times, have the ability to over-ride and stop the robotic process. One example expected to see early implementation is semi-automated three dimensional terrain profiling within a

controlled area (Figure 1.1.11) and semi-automated grade level controls on earth moving and paving machinery (PWRI, 1995).

References:

Berry, R.M, (1976), "History of Geodetic Leveling in the United States," Surveying and Mapping 36 (no. 2):137

Allegheny Excavating, (1995) personal communication, Gary Sippel, President, Allegheny Excavating, Inc., Butler, PA

Dewberry & Davis, (1995) personal communication Barry Kendel, surveying division, Dewberry & Davis, Gaithersburg, MD.

AISC, (1980), Manual of Steel Construction, Eighth Edition, American Institute of Steel Construction, Inc., Chicago, ILL.

Chinnock, (1995), "Flat Panels Launch Helmet-Mounted Display Market," Military & Aerospace Electronics, Feb. 1995, pp. 11-13.

PWRI (1995), "Start of Experiments on ETC and ARTS/AHS at PWRI Test Course," PWRI Newsletter, No. 62, Oct. 1995, Public Works Research Institute, Ministry of Construction, Tsukuba, Japan, pp. 1-4.

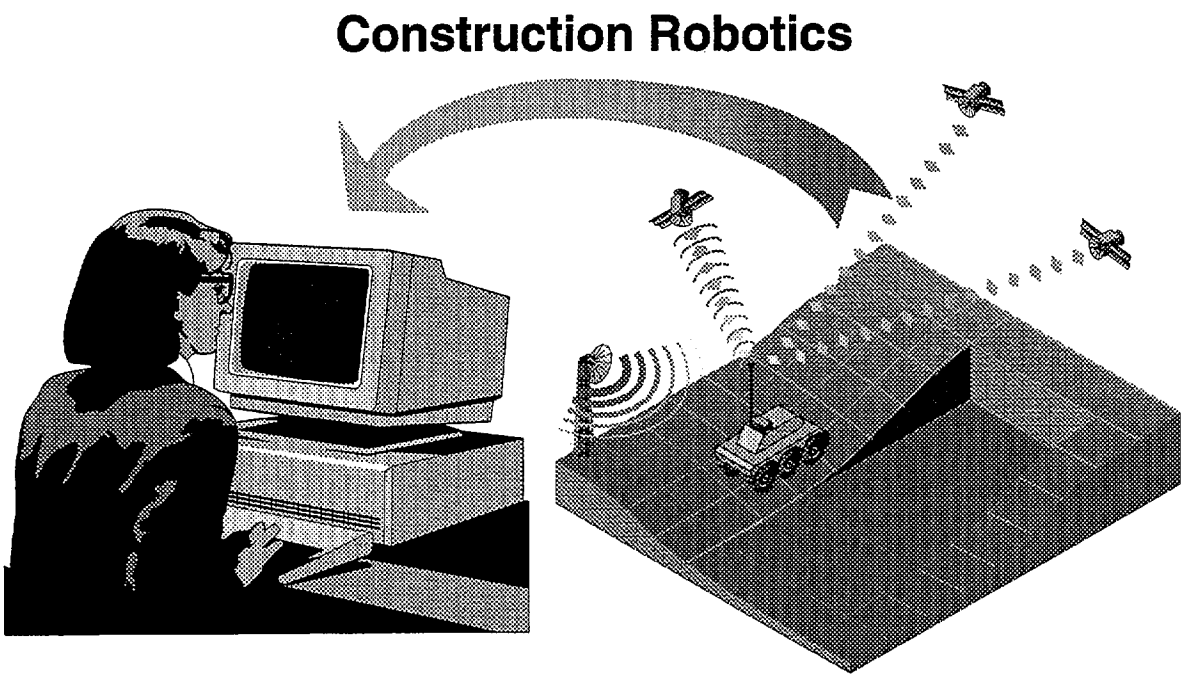

Figure 1.1.11: Ultimately, fully autonomous machinery will see use on construction sites. Much earlier, however, will come semi-autonomous vehicles in which an operator will have the ability to make on site judgements and override the operation of the machine if an unstructured event occurs for which the machine is not programmed. Also, remote operation (tele-operation) of un-manned vehicles (with remote operator override capability) will begin to see wide use in hazardous environments such as toxic waste and nuclear cleanup.

Chapter 2: A Review of Present Electronic Positioning Technologies

2.1 Electronic Distance Measurement (EDM)

During the past 15 years, electronic distance measuring (EDM) instruments have seen wide acceptance among surveyors and have almost completely surplanted the use of stadia and tapes for this purpose. These devices determine lengths based on phase changes that occur as electromagnetic energy of known wavelength travels from one end of a line to the other and returns.

Early forms of these instruments tranmitted visible light and were capable of measuring distances up to 40 km at night; they were degraded during daylight hours. These were followed with microwave-based systems capable of 80 km range in daylight. Figure 2.1.1 [Brinker & Wolf, 1984] shows frequency and wavelength values for the electromagnetic spectrum along with identification of bands commonly used for the above distancing technology as well as some other common electronic instruments.

The chief advantages of electronic surveying are the speed and accuracy with which distances can be measured. If a line of sight is available, long or short lengths can be measured over bodies of water or terrain that is inaccessible or rugged (e.g. a virgin construction site). Present EDM systems can be classified by the wavelength of the transmitted electromagnetic energy and fall into two general categories:

a) Electro-optical systems which transmit either modulated laser light between 400-900 nm (visible spectrum through far ultraviolet: 4.5-7.5 $(10)^{14}$ Hz).

b) Microwave systems which transmit microwaves. Although microwaves occupy a large portion of the electromagnetic spectrum (from $3(10)^5$ - $1(10)^9$ nm), most measurement geodetic survey instruments fall in the 8.6 to 100 $(10)^6$ nm range (3 to 35 GHz).

In general, EDM equipment measures distances by comparing a line of unknown length to the known wavelength of modulated electromagnetic energy. Electromagnetic energy propagates through the atmosphere as:

$$V=f^*\lambda \qquad \text{eq(1.1)}$$

Where V = velocity of electromagnetic radiation, in meters per second; f = the frequency of modulation, in hertz (cycles/second); and λ = the wavelength, in

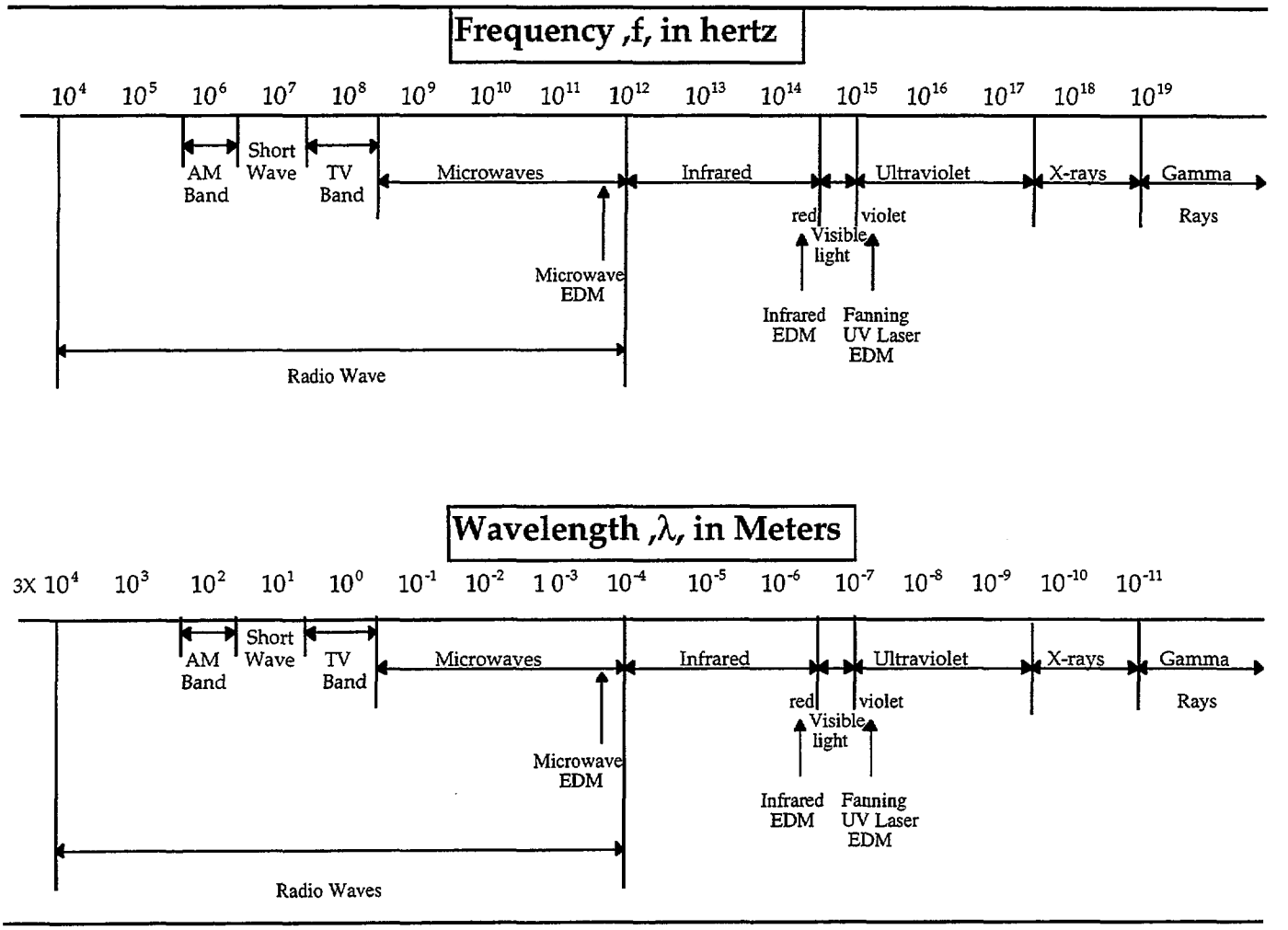

Figure 2.1.1: Frequency spectrum and Wavelengths for electromagnetic radiation

meters. In a vacuum, V is equal to the relativistic constant c = 299,792,500 m/second. In the earth's atmosphere this velocity is reduced in accordance with the local index of refraction (n) as:

$$V = c/n \qquad \text{eq (1.2)}$$

Where n is dependent on the pressure, temperature, and humidity of the air column and has a sea level value of approximately 1.0003. Because of this, and the interdependence of equations 1.1 and 1.2, accurate electronic distance measurement using phase information requires that the atmosphere be sampled local to the measurements and corrections made either to the instrument or to the results. **In general, the higher the frequency of operation, the finer the range accuracy. But with higher frequency, atmospheric effects also become greater.** Most instruments are now specified with both an instrumental accuracy (a function of the physics of the device) and an atmospheric error, usually expressed in parts-per-million (ppm) of the surveyed distance.

The general EDM distancing procedure is shown in Figure 2.1.2 (from Brinker & Wolf, 1984). An EDM device, centered by means of a plumb bob or optical plummet over the reference transmitting station, transmits a carrier signal or electromagnetic energy upon which a reference frequency has been superimposed, or modulated. The signal is returned from the receiving station to the receiver, located on the EDM instrument, so that the travel path is double the slope distance. In Figure 2.1.2 the modulated electromagnetic energy is represented by a series of sine waves having wavelength lambda. Any position along a given wave can be specified by its phase angle, which is 0-degrees at its beginning, 180-degrees at the midpoint, and 360-degrees at its end.

EDM devices used in surveying operate by measuring phase shift. In this procedure, the returned energy undergoes a complete 360-degree phase change for each even multiple of exactly one-half the wavelength separating the line's endpoints. When a line is not exactly an even multiple of the half wavelength (which would usually be the case), the fractional part is measured by the instrument as a nonzero phase angle. If the precise length of a wave is known (via eq(1.1) with atmospheric compensation) then the fractional part can be converted to distance.

There is a problem, however, in that EDMs using this technique can directly resolve only a fractional part of a wavelength, but not the number of full wavelengths over the full transit path to and from the reflector system. In commercial systems this ambiguity is resolved by transmitting additional signals of lower frequency and longer wavelength, so that the true distance, within the design range of the device, can be uniquely determined.

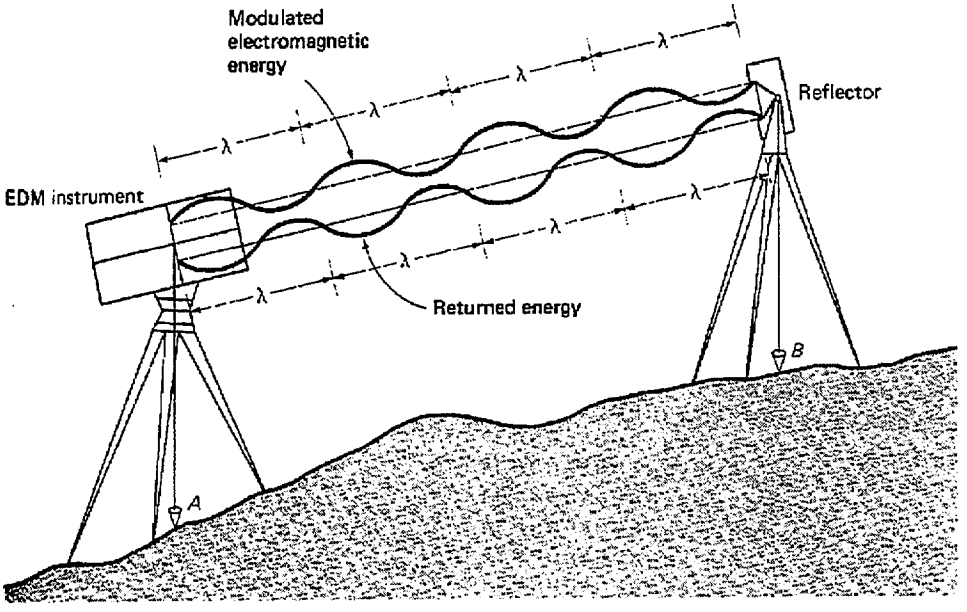

Figure 2.1.2: Standard EDM surveying system in which a carrier frequency is transmitted from the survey instrument to a retroreflector target. The phase of the returned signal is compared with that of the transmitted signal. The phase difference is used to determine the total transit distance to and from the retroreflector. The true line-of-sight survey distance is half the round trip distance.

As an example, if a system used four separate frequencies of 50 MHz, 5 MHz, 500 kHz, and 50 kHz (with associated wavelengths of 6, 60, 600, and 6000 m, respectively) then the total range of the instrument over which the distance could be ascertained unambiguously is 6,666 m. The accuracy of the instrument is determined by the shortest wavelength (highest frequency) and the resolution of the digital phase detectors used to measure the fractional wavelength. For example, if the phase detector was only accurate to 1-degree , then the accuracy would be given by 6 m / 360-degrees = 0.0167 m = 16.7 mm, not accounting for atmospheric effects. Most practical instruments involve the use of retro-reflectors (corner cube mirrors) which return the transmitted signal to the EDM instrument, and so the actual unambiguous range would be half the above amount or 3,333 m, which is beyond that typically required of most site-surveying total stations. Some present-day instruments use only two frequencies (e.g. 75 kHz and 15 MHz), with a commensurate shortening of the unambiguous range. Typical accuracies and ranges for various EDM units are given in Table 1.3.1. Figures 2.1.3 and 2.1.4 show on site use of a typical two-frequency "total station" and its associated target retroreflector.

Table 1.2.1: Typical EDM Instrument Accuracies

Instrument	Range	Accuracy
Wild TC500	400-1300 m	+/-5 mm + 5ppm
Wild TC010	400-1300 m	+/-3 mm + 2 ppm
Wild TC 1610	400- 1300 m	+/-2 mm + 2 ppm
MicroFix 100C	60,000 m	+/-15 mm + 3 ppm

References:

Brinker, R.C., and Wolf, P.R. (1984), "Elementary Surveying," Seventh Edition, Harper & Row, Publishers, New York.

2.2 GPS-Based Metrology

Background

The GPS (Global Positioning) system presently consists of a constellation of 24 satellites, four in each of six circular 20,321 km orbits with inclinations of 55 degrees.

The fundamental navigation technique for GPS is to use one way ranging from the GPS satellites which are also broadcasting their estimated positions. Ranges are measured to four (or more) satellites simultaneously in view by matching (correlating) the incoming signal with a user generated replica signal and measuring the received phase against the user's (relatively crude) crystal clock.

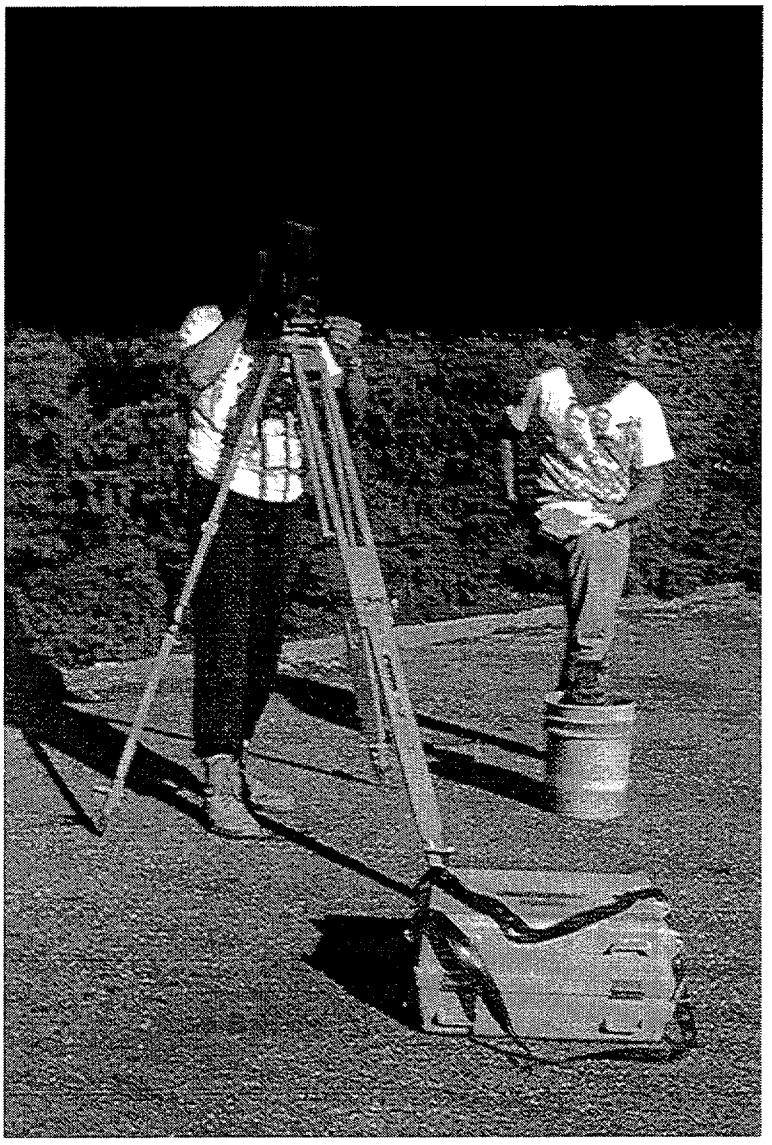

Figure 2.1.3a: Survey crew setting up a typical Total Station survey shot. Azimuth and vertical angles are are alighed using the optical sight and digitally displayed on an integral LCD panel. EDM distance is obtained using the same sighting arrangement. The received signal from a retroreflector located at the target station is processed onboard and displayed as well on the LCD.

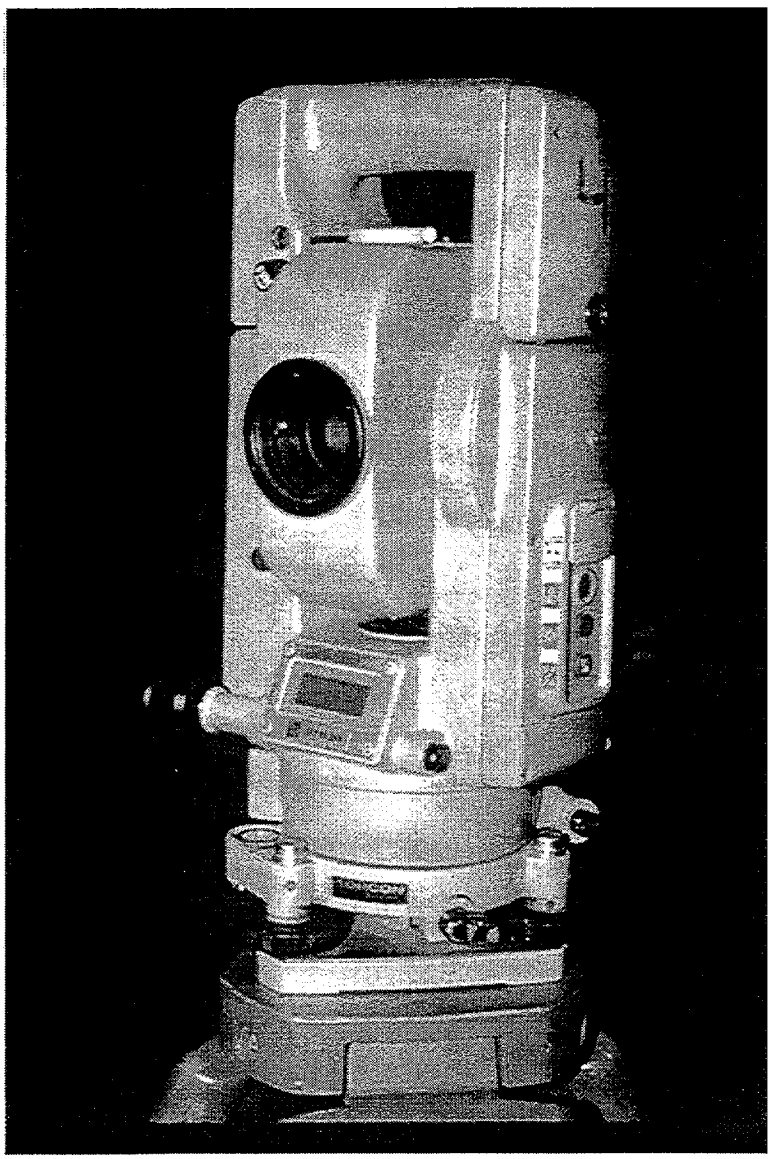

Figure 2.1.3b: Closeup photo of a typical Total Station transmitter/ receiver unit. Optical alignment with a retroreflector target is achieved via the central lens; digital values for azimuth, inclination, and computed distance are accessed sequentially in the LCD display located just below the lens body.

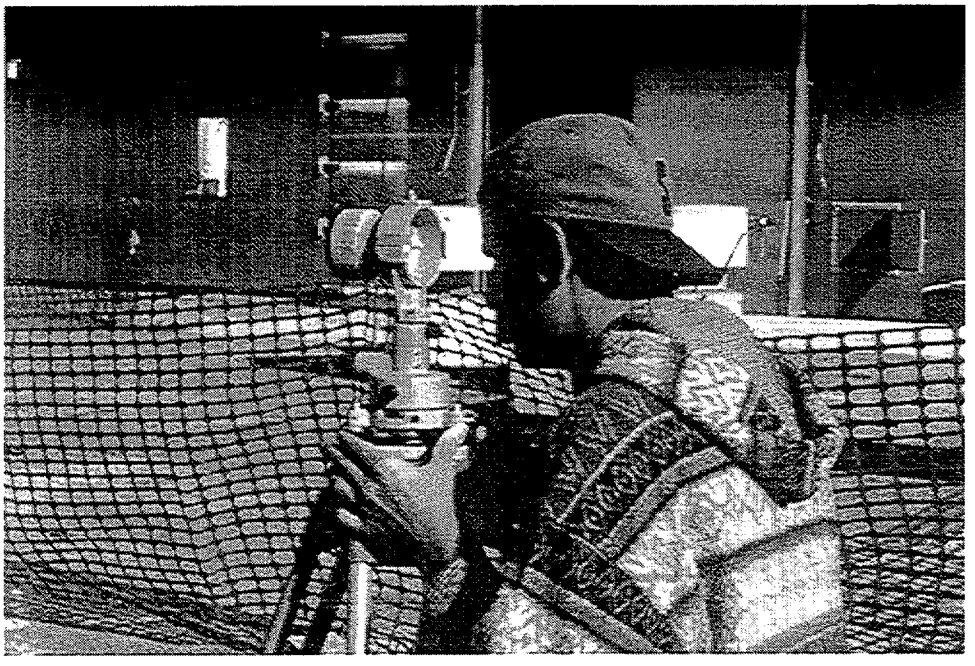

Figure 2.1.4a: Survey crew member setting up a typical retroreflector to be used in a Total Station survey shot. The optical center of the retroreflector is aligned, using an optical plumb, over the target station.

Figure 2.1.4b: Closeup photo of typical retroreflector unit set up on station for an EDM shot from a Total Station. Accuracies using this technology can achieve +/- 2 mm survey error and 2 ppm error due to propagation delays resulting from variance in atmospheric conditions (humidity, temperature, barometric pressure.)

With four satellites and appropriate geometry, four unknowns can be determined; typically, they are: latitude, longitude, altitude, and a correction to the user's clock. If altitude or time are already known, a lesser number of satellites can be used. Each satellite's future position is estimated from ranging measurements taken at world wide monitoring stations. These stations calculate, and upload, future satellite locations and future satellite clock corrections. Excellent summaries of various aspects of general GPS technology are presented in [Parkinson et.al., 1995; Lichtenegger & Collins, 1992; Stein et.al., 1994; Trimble, 1994; Hurn, 1989; ION, 1980; ION, 1984; ION, 1986; and ION, 1993].

A key feature of the GPS design is that the satellites need not be continuously monitored and controlled. To achieve this autonomy, the satellites must be preditable in four dimensions: three of position and one of time. Predictability, in the orbital position, is aided because the high altitude orbits are virtually unaffected by atmospheric drag. In order to insure that all satellite clocks remained synchronized, provisions were developed to fly accurate timing standards. The only type of clock sufficiently accurate to achieve the error tolerance specifications for GPS (5 feet accumulated error per day) is an atomic standard. GPS has traditionally used two types of atomic clocks: Rubidium and Cesium.

The GPS ranging signal is broadcast at two frequencies: a primary signal at 1575 MHz (called L1) and a secondary broadcast at 1227 MHz (called L2). These signals are generated synchronously, so that a user who receives both signals can directly calibrate the ionospheric group delay and apply appropriate corrections. Civilian users are limited to the L1 band.

Both the L1 and L2 frequencies can carry two independent modulations through the use of phase quadrature. The present GPS system permits two modulations for the L1 signal and one, known as protected mode, on L2. These modulations are defined in the following sections.

2.2.1 GPS Ranging Modes

Code Solution

The primary intent of the GPS system was to provide 5 to 10 meter accuracy absolute point positions for the U.S. Department of Defense using coded information on two carrier frequencies, the L1 frequency at 1575.42 MHz and the L2 frequency at 1227.60 MHz. The high-accuracy service is call the Precise Positioning Service (PPS) and uses what is called P-code (Precise-code). The use of PPS is restricted and is not available for civilian use when Selective Availability (S/A) is turned on. A lower level of precision is available at all times and is called the Standard Positioning Service (SPS) which uses the Coarse

Acquisition or C/A-code. In this a short pseudo-random noise code is broadcast at a rate of 1.023 megabits/second and contains satellite position and time. The P-code is broadcast at ten times the rate of C/A, 10.23 megabits/second. Because of its higher modulation bandwidth, the P-code ranging signal is more precise. This code , when encrypted, becomes the Y code. The military uses this encryption capability in such a way as to prevent the more precise positioning service from being used by an unauthorized user. During S/A the satellite frequency is dithered, limiting the point position to an accuracy of 100 m in the horizontal and 150 m in the vertical components. An example of the variation in position using SPS with S/A on is shown for 2.5 hours of data collected at UNAVCO using a Trimble SSe receiver (Figures 2.2.1.1 and 2.2.1.2). During this period the position varied up to 50 meters horizontally and 100 meters vertically.

Code Differential Solution

Considerable improvement is obtained by combining observations from two receivers; the second unit comprises the "reference" receiver (Figure 2.2.1.3). Both receivers, because of their proximity, see essentially the same range error to each satellite and therefore the same corresponding error in position. With one receiver at a known position, the range errors can be determined and transmitted to the roving receiver. The roving receiver applies these corrections to the observed ranges in real-time [Hurn, 1993]. The standard format for code differential corrections is RTCM. Almost all GPS receivers with a serial interface are capable of accepting RTCM corrections. For small inexpensive receivers (~$300) the accuracy is limited by the noise level of the code measurement, which is typically 2 to 10 meters. A newer class of enhanced C/A code tracking receivers such as the Trimble 4000 SSe and Ashtech Z12 have noise levels at the 0.5 meter level and advertise 1 meter level differential position accuracy. A pair of Trimble 4000 SSe's were connected using a radio link with one set as a reference station and the other to accept RTCM corrections. The majority of the horizontal positions differ by less than +- 50 cm with the exception of a nearly 2 meter horizontal excursion near the start of the time series (Figure 2.2.1.4). The vertical solution variation is up to +- 5 meters but more typically less than +- 1 meter.

The precision of the differential solution using only C/A code will degrade with increasing distance due to ionospheric effects, tropospheric effects and errors in the broadcast orbit ephemeris. Current development is directed toward increasing the range of code differential GPS (DGPS) beyond about 100 km. From a software point of view, the techniques are relatively straightforward and the reliability is high.

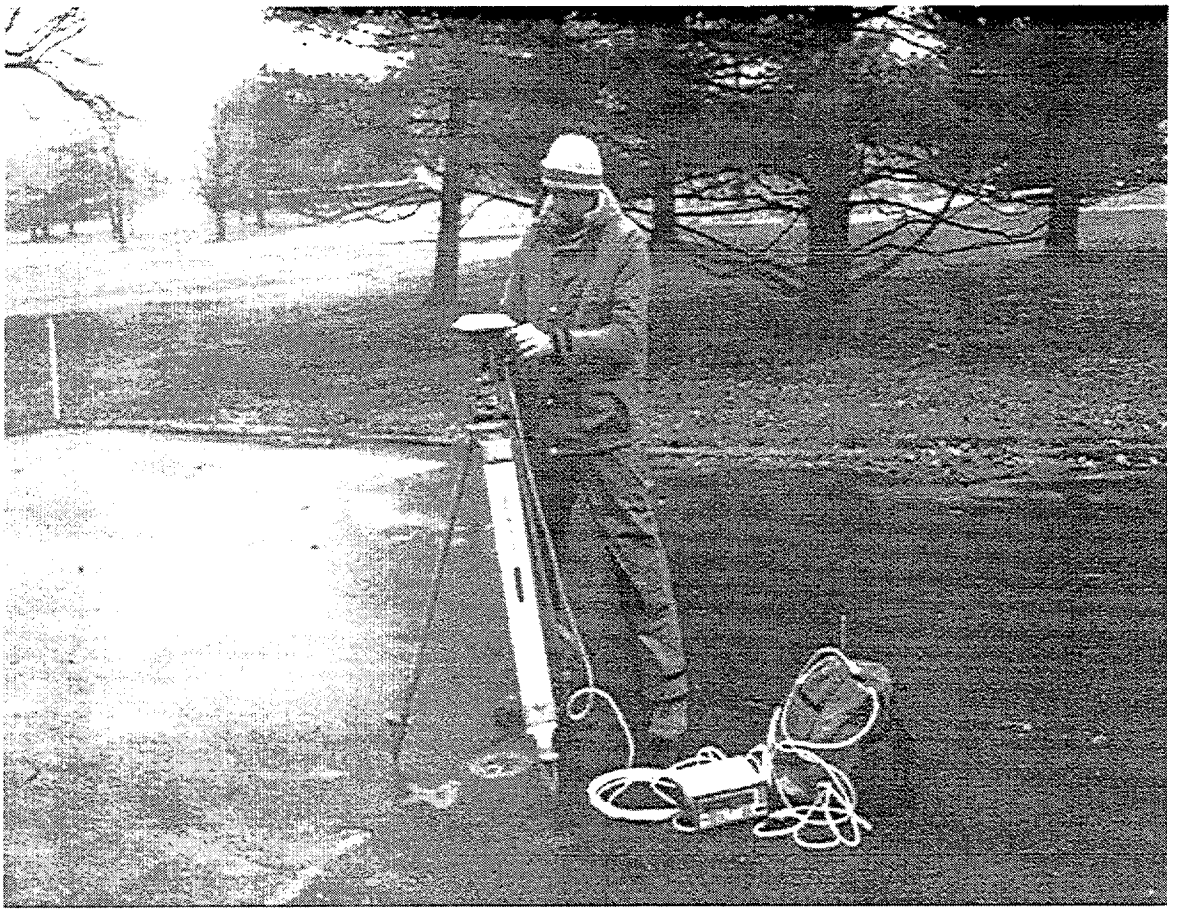

Figure 2.2.1.1: Setting up a single GPS receiver over a benchmark station for C/A code solution test. Typical accuracy attained was +/- 50 m horizontally and +/- 100 m vertically.

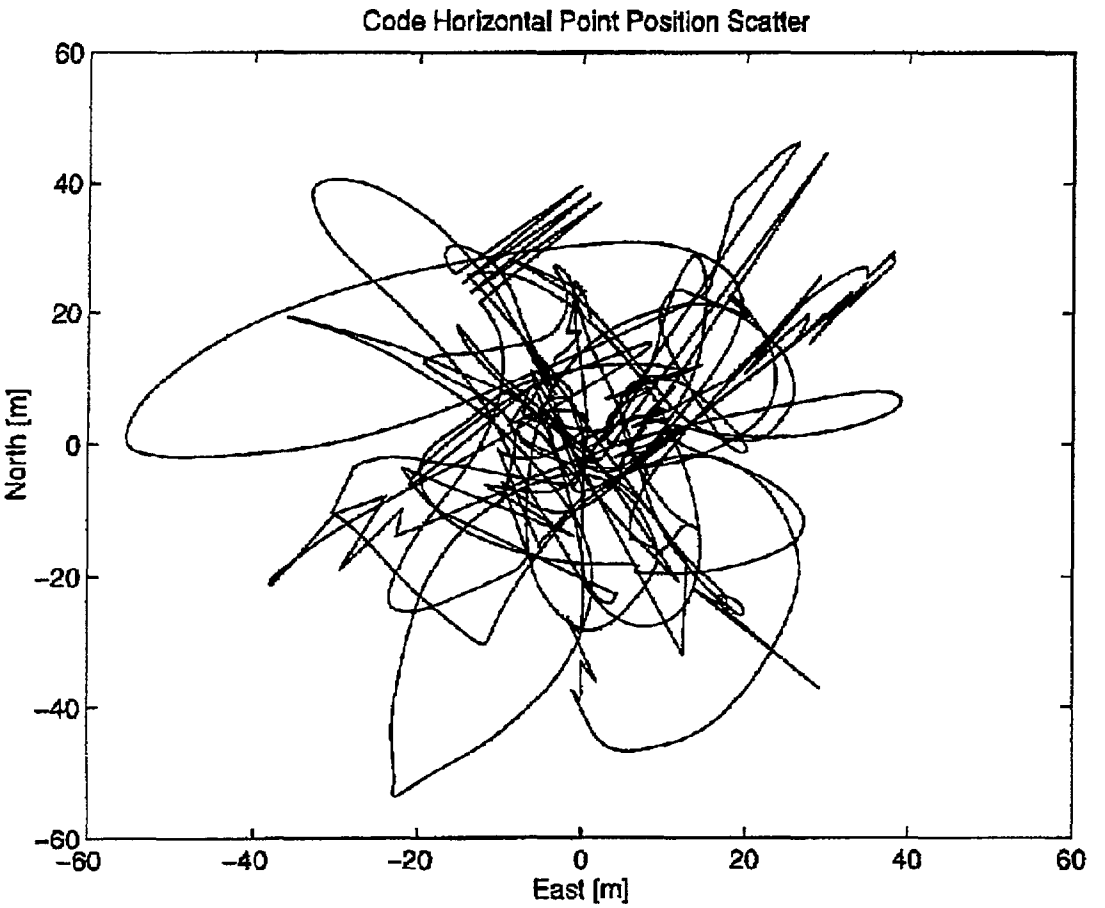

Figure 2.2.1.2: Typical time-varying results from a single C/A code solution GPS receiver sampling continuously over a benchmark station. Typical accuracy attained was +/- 50 m horizontally and +/- 100 m vertically.

Figure 2.2.1.3: GPS Phase Differential reference receiver and RF transmitter set up atop the NIST MON-102 benchmark on the NOAA/NIST GPS evaluation range. Position corrections are transmitted via the RF link to the roving GPS receiver for RTK (real-time kinematic) surveying.

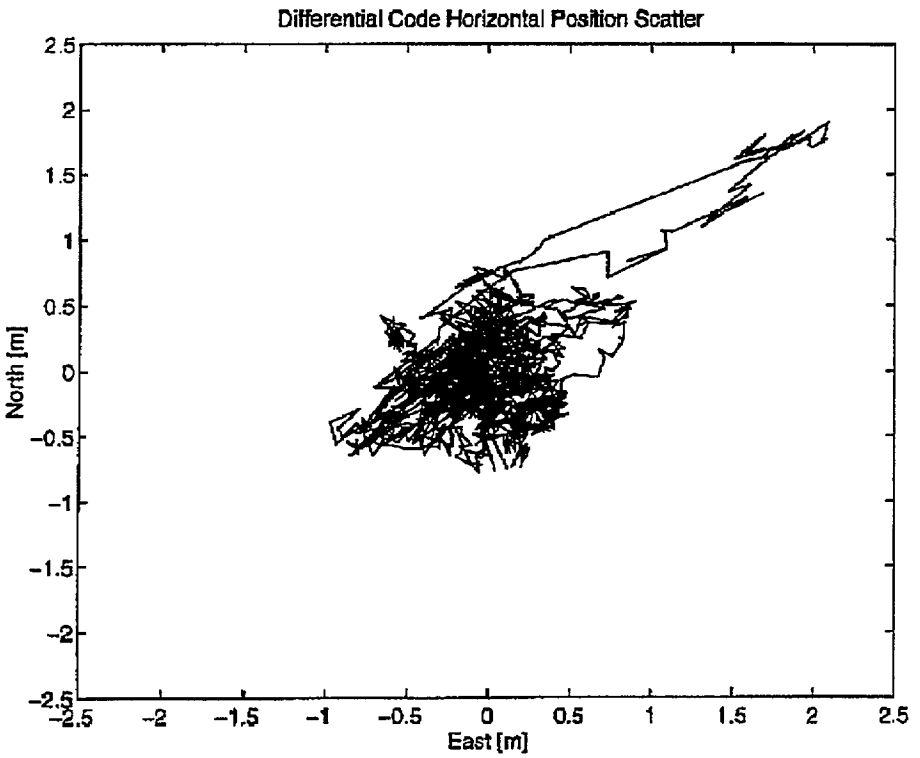

Figure 2.2.1.4: Typical time varying horizontal error results for a GPS receiver set up to measure position using a differential code (not phase) solution. Errors of +/- 2 m are observed. Differential solutions will result for an RTK survey system when phase lock information information is lost but RF communications link, with correction updates, is still available from the reference receiver station. Such accuracies are acceptable for material location at a large jobsite, but not for vehicle control and final component position verification.

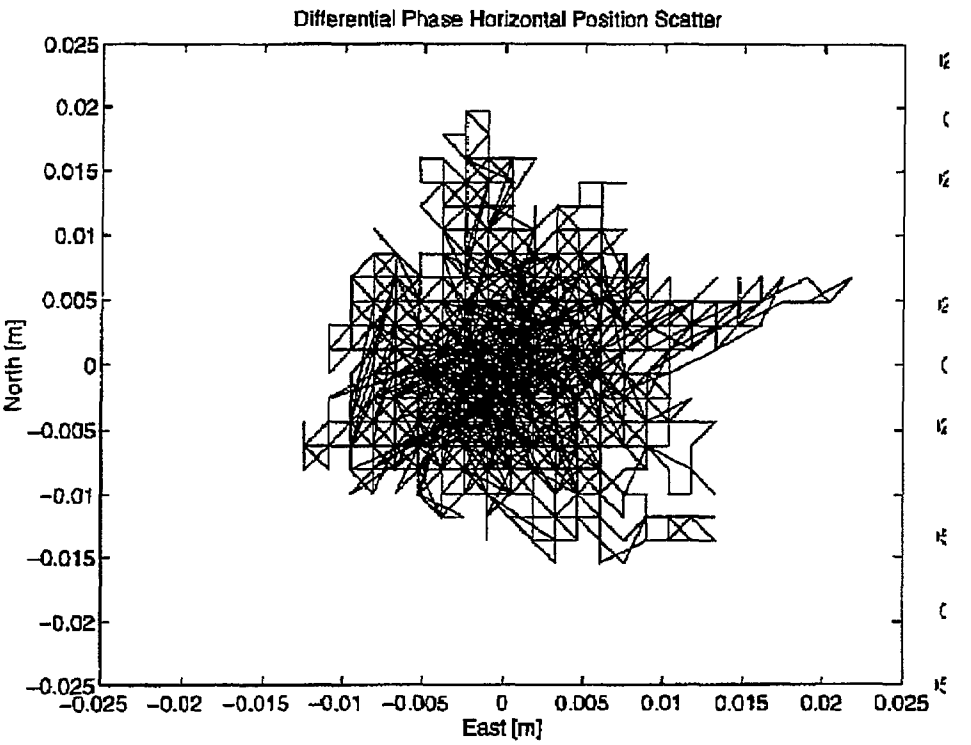

Figure 2.2.1.5: Time varying results for a typical real-time kinematic (RTK) differential phase GPS receiver stationed atop a fixed benchmark. Accuracy over time is +/- 20 mm. Drift over a short period of time can be significantly less (see Figure 2..2.3.5).

Phase Differential Solution

The highest degree of position precision is obtained using carrier phase data. The receiver noise level of the carrier phase measurement is approximately 1 mm as opposed to about 50 cm for the better C/A code receivers (Figure 2.2.1.5). With an antenna the carrier phase noise level typically increases to about 1 cm or larger due to multipath. High quality geodetic-quality GPS receivers recording L1 and L2 carrier phase measurements and static surveys (many hours of data at a fixed point) can achieve mm- to cm-level precisions on base- lines up to 1000s of km in length. The difficulty with using carrier phase measurements is that, while the fractional phase can be determined to high precision, there is an inherent initial integer cycle ambiguity (i.e. the number of whole wavelengths between the satellite and receiver is unknown). The integer number of cycles of the carrier phase must be determined where a cycle is 19 cm in the L1 and 24 cm in the L2 frequencies. With static surveys, the initial ambiguity is estimated along with the coordinate solution using as much continuous data as is available. For short breaks, called "cycle slips", the fractional phase is recovered when tracking resumes, but the integer cycles is lost. Cycle slips can usually be corrected in post-processing for over short gaps or when the loss does not occur to all satellites at once. Over longer gaps, cycle slips cannot be uniquely determined and a new ambiguities must be estimated.

GPS Static Accuracy

In addition to the afforementioned operating modes, a number of other factors, including geometric errors (Position Dilution of Precision or PDOP) related to the satellite constellation configuration, and ranging errors associated with satellite ephemeris, satellite clocks, ionospheric group delay, tropospheric group delay, multipath and receiver errors, all affect the final precision of the system. Table 1.2.2 summarizes the expected accuracy for code tracking receivers:

Table 1.2.2: Typical Single Receiver GPS Accuracy

	Precise Positioning Positioning Service (PPS) [not available to civilian users]		Standard Positioning Service (SPS) [available to all users] [specification]	
	Specification	Measured	No S/A	With S/A
Ranging Accuracy	6 m	2.3 m	6 m	20 m
CEP (Horizontal)		4.6 m	12 m	40 m
SEP (3D)		8.3 m	22 m	72 m

CEP = Circular Error Probable
SEP = Spherical Error Probable

2.2.2 Kinematic GPS

Once the ambiguity is determined (initialized), it is possible to determine precise positions using carrier phase as long as there is no loss of lock to the satellites. The use of GPS carrier phase data for determining continuous cm-level relative positions for stationary or moving platforms is called "kinematic" (in some cases, real-time kinematic, or "RTK") positioning or surveying. This concept has generally been attributed to Dr. Ben Remondi at the National Geodetic Survey and has been in limited use for surveying applications since the late 1980's. The principle advantage of kinematic techniques for surveying is the ability to occupy sites for only a few minutes before going to the next mark--as long as there was not a break in tracking. In the early stages of development, only L1 carrier phase measurements were used. Due to the need to maintain uninterrupted lock on the GPS satellites, and the computing power needed to perform real-time calculations, survey data were typically collected and then post-processed afterwards. After the fact, data could also be processed backwards in time to the point of loss of lock, a technique clearly not possible for real-time applications. Ambiguity initialization was accomplished by antenna swapping between two marks or by using an initialization plate of known baseline length and orientation or by occupation of a point with known coordinates. For further information on RTK aspects of GPS, see [Abidin, 1994; Cohen et.al., 1994; Frodge et.al., 1994; Griffen et.al., 1993; Trimble, 1992; and Meertens & Johnson, 1995].

Gap Analysis

Two possible failure modes can cause a loss of data. The first is a loss of lock on the satellites, the second is a loss of communication between the reference and rover receivers. The longest gap occurs when there is a loss of lock, also known as "cycle slip", resulting in tracking to fewer than 4 satellites. This type of break can occur when passing by tall building, trees or under a bridge. RTK phase tracking can recovers by automatic reinitialization, either in a stationary mode or "On-the-fly" ("OTF") while moving. The initialization can occur only after the receiver again tracks at least 5 satellites. Once there is initialization, the number of satellites simultaneously tracked can drop to 4. The specifications for the Trimble 4000 SSe Total Station indicate typical automatic initialization in less than one minute. This would be the time after 5 satellites are again tracked. As we shall show, shorter breaks occur when there is a loss of receiver-to-receiver radio link.

2.2.3 Brief Summary of GPS Field Tests Conducted at NIST

A series of field measurements were conducted at NIST in late 1994 [Meertens & Johnson, 1995] in order to ascertain the capabilities of real-time GPS positioning of vehicles for automated construction applications. A pair of Trimble 4000SSe

receivers with real-time kinematic (RTK) and on-the-fly ambiguity resolution (OTF) were used. Three levels of accuracy can be obtained with this system. The first is non-differential point positioning with an accuracy limited by Selective Availability to ±100 meters in the horizontal and ±150 meters in the vertical. Second is real-time differential code positioning using RTCM corrections transmitted from reference to mobile receiver. The code-differential precision using the Trimble 4000SSe system is typically better than 1 meter in all components relative to the reference station position, though there were extremes of 2 meters horizontal and 5 meters vertical in one test. The carrier phase-differential precision of the RTK results are also consistent with advertised specifications showing a maximum horizontal excursion of up to 20 mm, but typical scatter of less than 10 mm, and a vertical scatter is up to ± 40 mm, but more typically ±20 mm.

Static Surveys.

Three sets of static survey data were collected. The first static survey, an RTK survey of the NGS Kinematic test network at the NIST site, was made with the reference station located at monument NIS MON-102 for which we had published coordinates. We then measured RTK GPS-determined positions for the test network (for which we did not have coordinates) and converted all results to local (X,Y horizontal and Z vertical) coordinates with respect to an origin station (KINC, the reference for the NIST ground survey). For the four separate occupations of station KINC, the maximum scatter did not exceed ±7 mm in all components.

A second set of benchmarks was surveyed with RTK in the parking lot of the NIST Large Scale Structures Test Facility located about 500 meters west of the reference monument. Whereas the Kinematic test network is located in open fields, the parking lot marks were located adjacent to a tall building and the purpose of the test was to see the effect of the building on solution accuracy. In most cases we were able to obtain RTK phase solutions with repeatabilities of 3 to 10 mm horizontal and 10 to 60 mm vertical. For the stations nearest the building, only a code differential solution was possible. Tracking ability depended entirely on how many satellites were obscured by the 5 story building to the east. at the time of observation. Note that although the differential code solution scatter is relatively small (± 3 cm), there is a 35 cm difference from the phase solution. This indicates that for short periods of time the code solutions are correlated giving a small scatter which is not representative of the systematic (decimeter level) error.

RTK phase measurements could not be made during the third survey of the points located the woods near the Test Facility. Tracking proved to be even worse than near the building. At best only code differential solutions could be

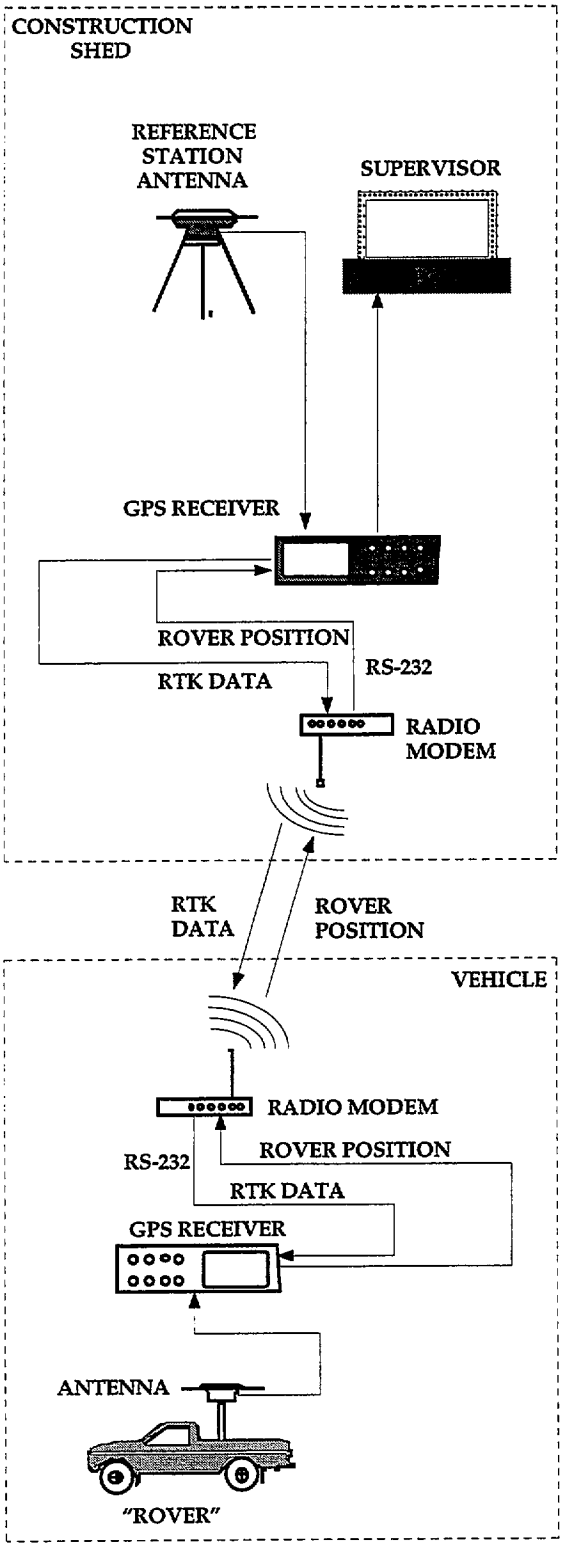

Figure 2.2.3.1: Schematic of GPS configuration used for RTK vehicle position acquisition tests at NIST (from Meertens and Johnson, 1995).

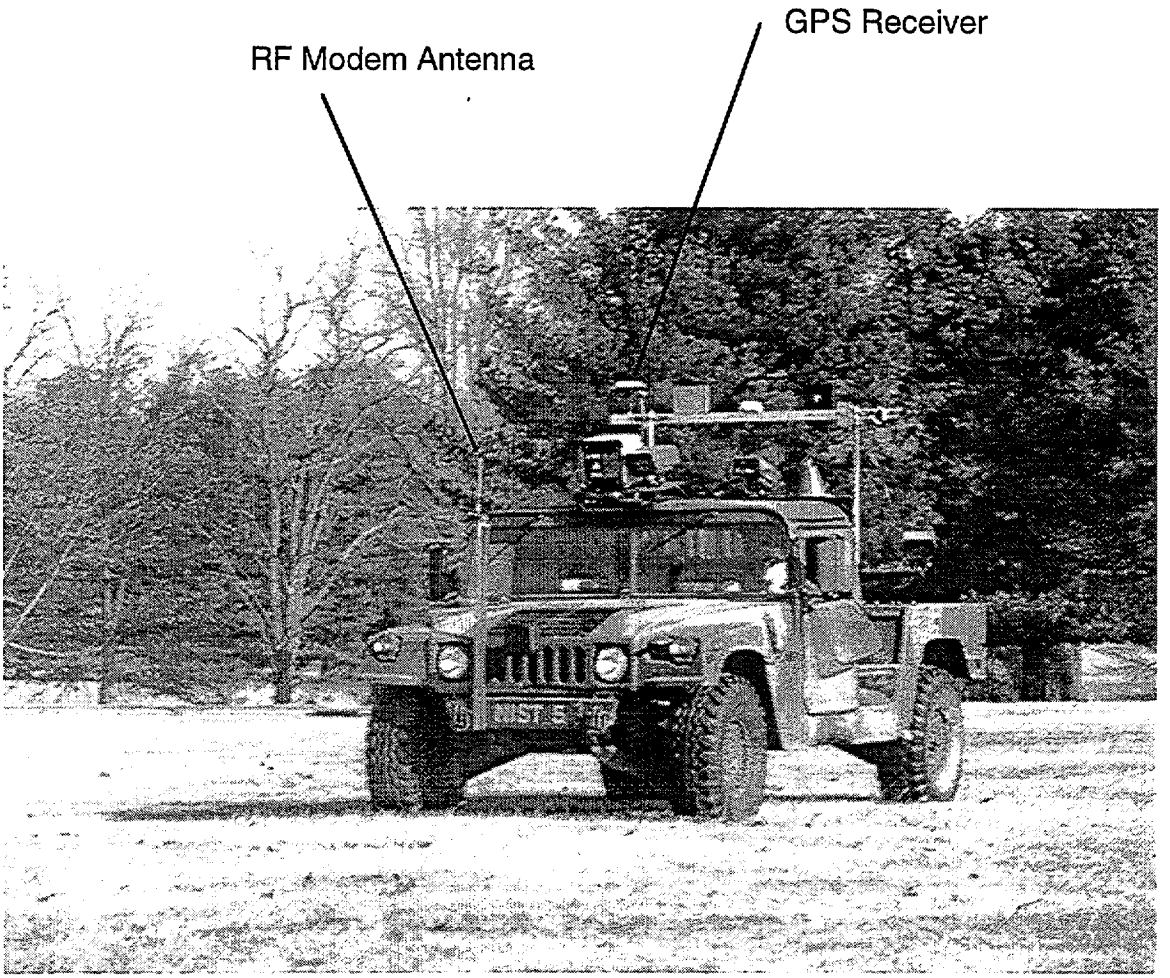

Figure 2.2.3.2: RTK "construction vehicle" on the NIST GPS test range. This arrangement was used for three dimensional terrain profiling. Plan and 3D isometric views of the surveyed area are shown in Figures 2.2.3.3 and 2.2.3.4. Vertical and horizontal position errors due to the tilt of the vehicle on steep terrain were not accounted for in this study. For registered user feedback full 3D models of the construction vehicle and the position of the strap down position/attitude acquisition system relative to that model will be necessary.

obtained and for one case only a 2d point position (100 m accuracy) was possible. The trees had already lost their leaves so the results could be expected to even be worse when there is full foliage.

Moving RTK Surveys.

There were three sets of RTK moving vehicle tests conducted at NIST. The test setup is shown in Figures 2.2.3.1 and 2.2.3.2. The first experiment was conducted along the roads; the second involved a topographic mapping survey of a field north of South Drive; and the third test was set in the field south of South Drive. The road tests show good agreement between the 15 and 25 mph speed tests and no loss of data. The 35 mph tests failed near the start and did not reinitialize before the drive was over.

An analysis of the data gaps showed two types of breaks. The first, a complete loss of lock on the satellites, required reinitialization either statically or on-the-fly. These breaks lasted on average about 120 seconds. A shorter type of break was caused by a break in the ground receiver-to-receiver radio link either on the outgoing or incoming side. The average break in this case was only 14 seconds. These results highlight the need for more rapid reinitialization or the need for alternate navigation methods such as inertial or magnetic systems.

The topographic mapping results using RTK were used to generate contoured maps with an interval of 50 cm over a total range of only 7 meters. A detailed analysis of the intersecting points showed the vertical difference of crossing tracks was no worse than ± 10 cm and had a standard deviation of only ± 3.7 cm. The intersections were only approximate and did not include a correction for the attitude of the vehicle, but still clearly demonstrate the vertical precision of the RTK system. Again, the loss of lock was quite evident when the vehicle was moving, and there clearly is need for rapid OTF reinitialization or backup navigation systems.

A note on real-time tracking using RTK.

Using the two-way radio modem link it was easy to log the data from the moving receiver onto a laptop PC at the fixed site. Although we had the software to plot the position observations on the screen in real-time, this proved to be too cumbersome with our off-the-shelf software and slow laptop PC. The data could, for example, have been plotted onto the Autocad site drawing, but due to the size of the file, this was not practical taking up to 10's of minutes to be updated. Furthermore, it would have been necessary to pre-reference the GPS data to the drawing. Again, not a technical problem, just a time consuming one requiring reliable and consistent survey coordinates in the drawing file.

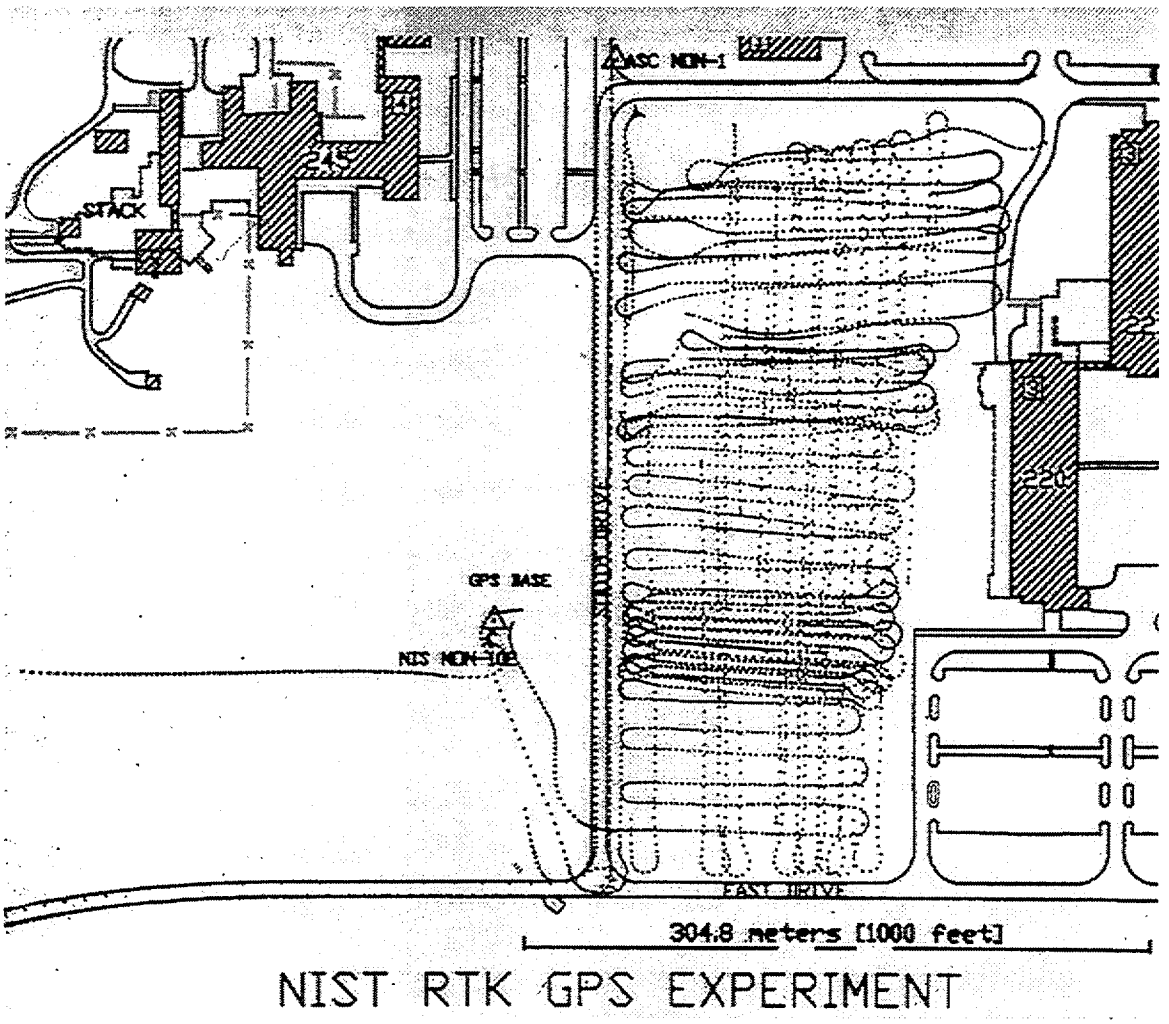

Figure 2.2.3.3: Plan view of the vehicle track (see Figure 2.2.3.2) over the south portion of the NIST, Gaithersburg campus. The RTK reference receiver was located at NIST Mon-102 (small triangle at left center). Note the spaced dots along the roads (East and South Drive) indicating the vehicle path relative to a CAD model of the NIST campus. In general, phase differential solution was maintained, but there were notable exceptions when the vehicle was close to the buildings shown at right, when near trees, and in some cases when making rapid turns. The road traces were conducted at velocities of up to 55 km/hour.

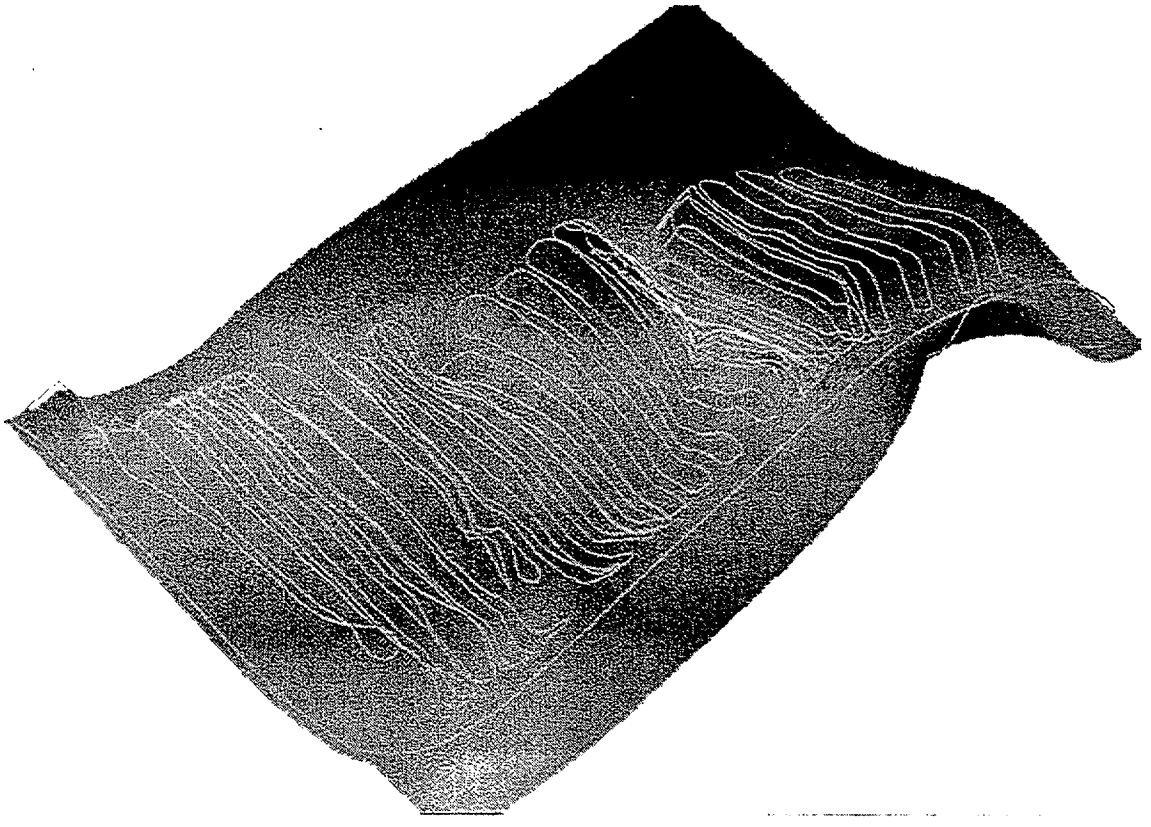

Figure 2.2.3.4: Three dimensional surface contour of the NIST field surveyed using the RTK phase differential GPS receiver mounted on a generic construction vehicle. Once such a digital site model exists the geometry can be modified in real-time by earthmoving equipment. Provided sufficiently robust kinematic CAD models exist for the earthmoving equipment, and that they are equipped with strap down position/attitude acquisition units and other necessary sensors and transmitters, it will be possible to account for removed earth in the site model in real-time.

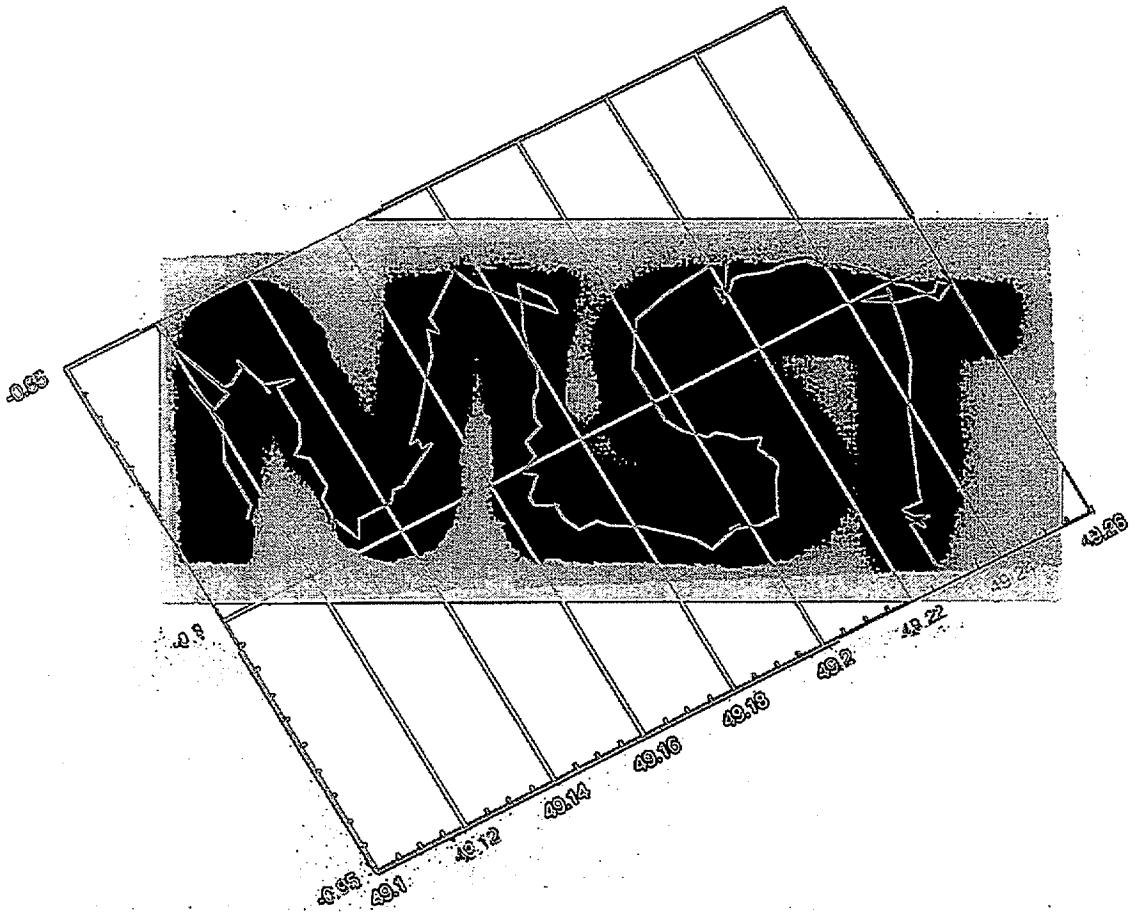

Figure 2.2.3.5: Final test of RTK phase differential GPS. Hand-held GPS receiver antenna was used to trace the NIST logo (actual size = 60 mm high by 160 mm long). The individual letter thickness is approximately 20 mm. This indicates an instantaneous accuracy of approximately +/- 5-10 mm.

Enhancing the tracking system to handle multiple vehicles at a single job site would require additional development work. Supplying the RTK corrections is not a problem with more receivers. A single reference receiver can broadcast on the same frequency and on a one-way link to an unlimited number of roving receivers. Each receiver could then perform it's own RTK calculations. The challenge is to simultaneously return the positions of all the vehicles to the tracking/ monitoring site or, via telemetry, to the job site database.

Final RTK TEST: Writing with GPS

As a final demonstration of RTK precision the rover antenna was placed on the top of a pencil and the operator traced out the letters "NIST" by hand (Figure 2.2.3.5). At 1 second sampling, the writing took 1.5 minutes to complete. The letters are easily distinguished. Slight imperfections reflect in part the measurement noise and in part the limits to how steady the operator can hold the pencil/antenna while trying not to block the satellite signals.

References:

Parkinson, B.W., Spilker, J.J. Jr., Sr. Editors; Axelrad, P., and Enge, P. Editors, (1995), SP 940100/32/01/95 Stanford University Custom Course Material SU 951 0-18-189437-8, Spring 1995, Course AA 272C Vols. 1 and 2.

H.Z. Abidin, (1994), On the Construction of the Ambiguity Searching Space for On-the-fly Ambiguity Resolution, Navigation 40, p. 321-338.

C.E. Cohen, B.S. Pervan, D.G. Lawrence, H.S. Cobb, J.D. Powell and B.W. Parkinson, (1994), Real-Time Flight Testing Using Integrity Beacons for GPS Category III Precision Landing., Navigation, 41, p. 145-158.

Frodge, S.L., S.R. Deloach, B. Remondi, D. Lapucha, and R. A. Barker, (1994), Real-time on-thefly kinematic GPS system results, Navigation, 41, p. 175-186.

Griffioen, P., T. Allison, and S. Dreier, (1993), "Real-time Kinematic: The Next Surveying Tool", Proceedings of the 1993 ION Technical Meeting, San Francisco, January, 1993.

Lichtenegger, H. and Collins, J., (1992), GPS Theory and Practice, Hofmann-Wellenhof, 1992, 326 pages.

Stein, S. R., Lieutenant Fox, C., Bartholomew, T. R., and Gifford, G. A., (1994) "GPS Time Determination and Dissemination -A Tutorial," Timing Solutions, Inc., Boulder, CO.

Trimble, (1995), "GPS Surveyor's Field Guide : A Field Guidebook for Static Surveying," Trimble Navigation Limited, Sunnyvale, CA, 1991.

Hurn, J. (1993), "Differential GPS Explained," Trimble Navigation, Sunnyvale, CA, 1993.

Meertens, C., and Johnson, J. (1995), "High Precision Real Time GPS Site Positioning Development and Demonstration," University Navstar Consortium (UNAVCO), Boulder, CO, Report to the National Institute of Standards and Technology, Gaithersburg, MD, August 22, 1995, 41 pp.

Trimble, (1992), "GPS Survryor's Field Guide: A Field Guidebook for Dynamic Surveying," Trimble Navigation, Sunnyvale, CA, 1992.

Hurn. J. (1989), "GPS A guide to the Next Utility," Trimble Navigation, Sunnyvale, CA, 1989.

ION, (1980), "Global Positioning System," The Institute of Navigation, Vol. 1, Alexandria, VA, 1980.

ION, (1984), "Global Positioning System," The Institute of Navigation, Vol. 2, Alexandria, VA, 1984.

ION, (1986), "Global Positioning System," The Institute of Navigation, Vol. 3, Alexandria, VA, 1986.

ION, (1993), "Global Positioning System," The Insitiute of Navigation, Vol. 4, Alexandria, VA, 1993.

Meertens, C., and Johnson, J., (1995), "High Precision Real Time GPS Site Positioning Development and Demonstration," University Navstar Consortium GCR Contractor Report to NIST, August, 1995 (available from NIST).

2.3 Pseudolites

Prior to implementing the satellite system, a system of solar powered GPS transmitters was deployed on the desert floor at the Yuma Proving Ground in order to test the initial GPS concept. These transmitters all radiated one of the unique orthogonal GPS codes (at the approved frequencies) which were synchronized to each other and to the satellites as they were launched. These transmitters were called pseudolites (from psuedo-satellites). They provided a geometry that approximated that of the satellites, although the signals were coming from negative elevation angles. The psuedolite concept has since been expanded as a potential technique to improve accuracy and integrity of GPS for civil landing of aircraft.

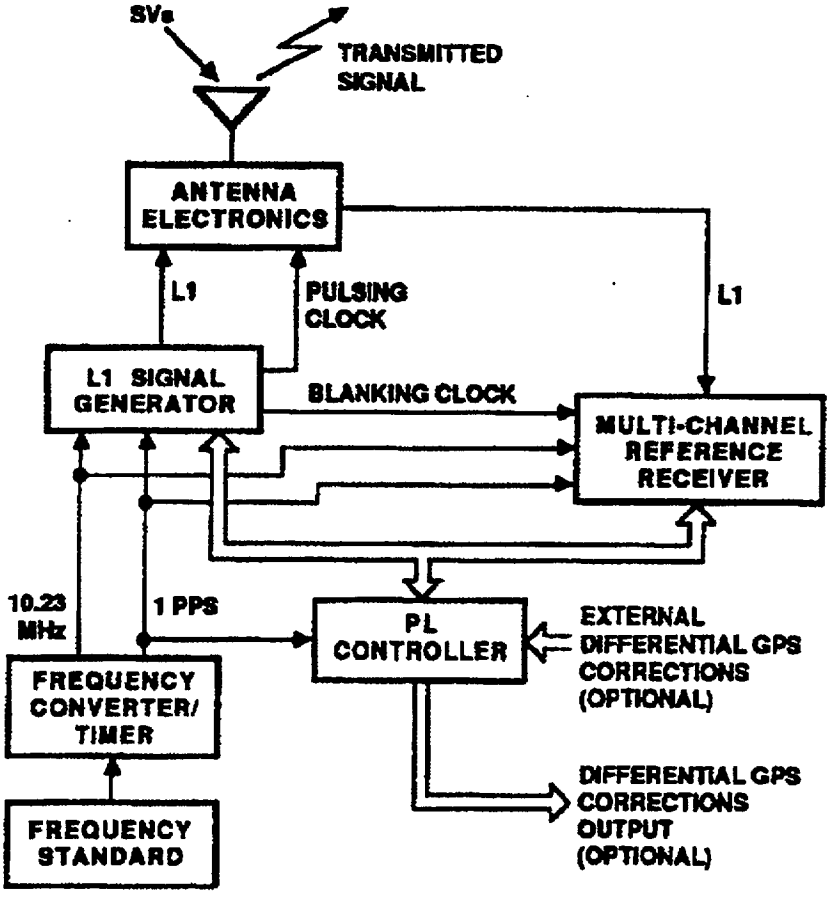

Figure 2.3.1: Collocated Pseudolite/ Reference Receiver Configuration (from Dierendonck, 1990)

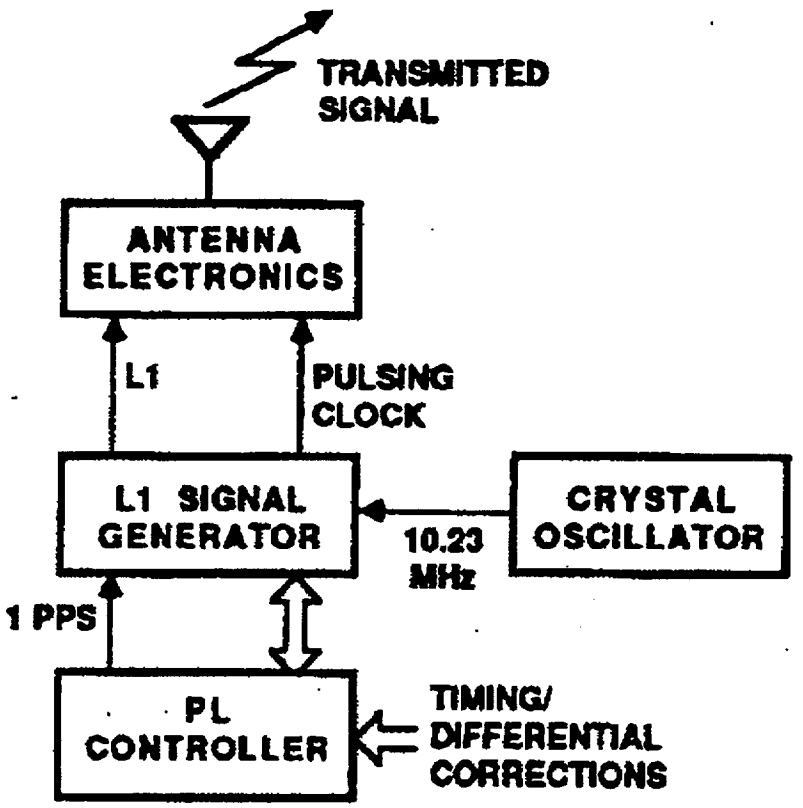

Figure 2.3.2: Remote Pseudolite Configuration (from Dierendonck, 1990)

Pseudolites have two functions: to provide signal augmentation to the GPS satellites with better GDOP in the local region and to transmit DGPS corrections to the participating GPS receiver units in the local area.

The method of synchronizing the pseudolites to the GPS satellites can be achieved in one of two ways -- one in which a pseudolite is collocated with a DGPS reference receiver, and one in which it is remote from the reference receiver that is tracking its transmitted signal. In the latter case, the reference receiver sends time corrections to the pseudolite plus the DGPS corrections to be modulated onto its transmitted signals. The two different pseudolite configurations are illustrated in Figures 2.3.1 and 2.3.2. For the case of the collocated configuration, the reference receiver shares the transmit/receive antenna with the pseudolite, which also allows self calibration.

The type of configuration used would depend upon whether or not there is more than one pseudolite at a given local region. If there is only one, the collocated approach is more desirable, especially if line-of-sight visibility to a reference receiver might be a problem. If there is more than one pseudolite, the remote approach is more desirable to provide a common sychronization source. However, if line-of-sight visibility problems exist, having a receiver collocated with the pseudolite is a necessity for synchronization, although a multi-channel version would not be required for each pseudolite. In this case, a Master pseudolite that contains the reference receiver is designated, and the rest of the pseudolites are Slave pseudolites, receiving DGPS corrections for the GPS satellites from the Master pseudolite [Van Dierendonck, 1990].

Collocated Pseudolite Configuration

Both the reference receiver and the pseudolite L1 signal generator derive their timing coherently from the same stable atomic frequency standard. The signal generator pulses the transmission of the pseudolite signal, in order to minimize interference to both participant and non-participant GPS users. This pulsing also allows the reference receiver to receive the GPS satellite signals via the same antenna by blanking its input signal during the pulse period. By providing a suitable calibration path the reference receiver can also track the output of the signal generator when the pulses are not present, because the signal can be generated continuously. Only the transmitter power amplifier is pulsed on and off. The collocated pseudolite can be self-calibrating, and the transmitted pseudolite signal will be synchronized to the same clock that is used to derive the DGPS corrections. This is true even in the multiple pseudolite scenario, where the slave pseudolites receive differential corrections from the master pseudolite. The time solutions for the slave pseudolite receivers will be referenced to the master pseudolite's clock, since the DGPS corrections are computed with respect to that clock.

Remote Pseudolites

Remote pseudolites to not need to have receivers if they can be tracked by the reference receiver. The reference receiver supplies corrections to the pseudolite for correcting its local clock and provides the DGPS corrections for modulation of the pseudolite signal. Since the reference receiver can update the pseudolite continuously, the remote pseudolite does not require an atomic frequency standard. Otherwise, its configuration is identical t the collocated configuration without the reference receiver, the self-calibration path, and low-noise amplifier in the antenna electronics.

Advantages of Pseudolite Technology for Construction Metrology

As suggested in both the immediate discussion above, as well as in the general discussion of GPS, there is marked degradation of accuracy when the receiver is not in full view of at least four satellites. This can happen as a result of interference from, for example, foliage or the intervening presence of a building or wall. In the case of foliage, there is a degradation of signal (not instantaneous loss as with an interfering building) proportional to the height of the trees. The model for predicting this loss is known as the Modified Exponential Decay (MED) model [Stein & Tsang, 1990]. It is generally valid for frequencies ranging from 230 MHz through 95 Ghz, and is applicable to cases in which the ray path is blocked by dense, dry, in-leaf trees found in temperate-latitude forests. The MED model is given by:

$$L = 1.33\, F^{0.284} d_f^{\,0.58} \quad \text{for } 14 \le d_f \le 400$$

$$L = 0.45\, F^{0.284} \quad \text{for } 0 \le d_f \le 14$$

where L is the loss due to the trees in dB, F is the frequency in Ghz, and d_f is the depth (vertical height) of the trees in meters. With an assumed tree depth of 20 m, attenuation losses are approximately 7.6 dB for L band (GPS) frequencies. This represents a 6 fold decrease in power from the signal reaching the treetops. Given the low power levels received from the actual GPS transmitters at the earth's surface under ideal conditions, the foliage related signal loss is normally sufficient to cause loss of differential lock (as illustrated in the general discussion of GPS above). Degradation can also occur even when four satellites are visible when one or more satellites are low on the horizon, and thus have to penetrate more atmosphere, leading to the so-called PDOP and GDOP errors.

Loss of differential phase solution, in the case where vehicles are being operated using DGPS data, means that precision control is no longer possible (indeed the position may instantaneously be unknown) and the vehicle, for safety reasons, must be halted until the signal can be re-acquired. If DGPS is to become a day-to-

day utility at construction sites there is a pressing need to develop a means to insure that differential phase lock is never lost.

The elegance behind the use of pseudolites, which are time synchronized to the orbiting satellite system and also transmit using similar code sequencing, is that COTS (commercial off-the-shelf) receivers can be used without further modification and the pseudolite simply appears as another satellite, but with the distinct advantage of having a fixed position at the local site, presumably within view of the operations for which position monitoring is desired, and with a **much stronger** signal. In doing so we are not evading the requirement for line-of-sight (LOS). However, by employing many such transmitters one could effectively guarantee that each floor of a building or obscure corner of a construction site would be covered and that a position could be acquired. If a pseudolite system is to work seamlessly with the real GPS system for local augmentation, then the transmission power of the pseudolite must be carefully considered so as not to swamp the orbiting signals.

The pseudolite approach is thus not a panacea: it will require setting and reclaiming of a multitude of small transmitters and receivers and will not be effective in non-line-of-sight and rapid entry, unstructured situations... e.g. firefighters entering a burning building; sending teleoperated vehicles into a hazardous site etc. Until such issues as multi-path signal resolution, required power and transmitter distribution density can be resolved for the typically cluttered environment of the average construction site (as opposed to, for example, their use in air traffic control [Pervan et.al., 1994]) pseudolites will remain laboratory curiosities. Their potentially low cost, small size, and ability to utilize COTS position receivers, on the other hand, should fuel research towards the resolution of the above problems. For further reading on pseudolites see [Zimmerman et.al., 1994; Klein & Parkinson, 1986; Schuchman et.al., 1986; Stansell, 1986; Stein & Tsang, 1988; and Weissberger, 1982].

References:

Zimmerman, K.R., and Cannon, R.H. Jr., (1994), "GPS-Based Control for Space Vehicle Rendezvous," Proceedings of the Institute of Navigation GPS-94 Conference, Salt Lake City UT, September 1994.

Pervan, B.S., Cohen, C.E. and Parkinson, B. W., (1994), Integrity Monitoring for Precision Approach Using Kinematic GPS and a Ground-Based Pseudolite, Navigation, 41, p. 159-174.

Van Dierendonck, A.J., (1990), "The Role of Pseudolites in the Implementation of Differential GPS," CH2811-8/90/0000/0370 1990 IEEE pp 370-377.

Klein, D., and Parkinson, B.W., (1986), "The Use of Pseudo-Satellites for Improving GPS Performance," Global Positioning System, Vol. III, Institute of Navigation, 1986.

Schuchman, L., Elrod, B.D., and VanDierendonck, A.J., (1986), "Applicability of an Augmented GPS Nagivation in the National Airspace System, " Proceedings of the IEEE Special Issue on Air Traffic Control, Nov. 1989.

Stansell, T., Jr., (1986), "RTCM SC-104 Recommended Pseudolite Signal Specification," Global Positioning System, Vol. III, Institute of Navigation, 1986.

Stein, B.A., and Tsang. W.L., (1990), "COTS GPS C/A-Code Receivers with Pseudolites for Range PLS Application," CH2811-8/90/0000/0191 1990 IEEE.

Stein, B., A., and Tsang, W.L., (1988), "Pseudolite-Aided GPS: A Comparison," CH2675-7/88/0000-0329 1988 IEEE.

Weissberger, M.A., (1982), "An Initial Critical Summary of Models for Predicting the Attenuation of Radio Waves by Trees," ESD-TR-81-101, Department of Defense, Electromagnetic Compatibility Analysis Center, Annapolis, MD July 1982.

2.4 Fanning Lasers

A novel method of position determination has been developed over the past four years which involves the use of rotating, inclined, fan-shaped laser beams. The system operates under the fundamental geometric principle that the intersection of three planes uniquely defines a point in space. Three inclined fan-shaped laser beams are rotated about an axis at high speed. When the rotation of a laser beam is such that it strikes a roving receiver, a photosensitive detector generates a signal. These signals are sent to a processing unit which uses pre-existing reference data to calculate the angle of the rotation at which the laser beam intersects the receiver. Each transmitter provides intersection data from which the 3D position of the receiver can be determined.

Several variations of this approach are detailed in U.S. patents 5,100,229; 5,110,202; 5,247,487; and 5,294,970 [Beliveau et.al., 1993; Dornbusch et.al., 1992; Dornbusch et.al., 1994; and Lundberg et.al., 1992, respectively]. The invention provides a spatial position system utilizing at least three fixed referent stations, although four may be used, to determine the position of one or more portable position sensors. Each fixed station includes a laser and a strobe transmitter. The laser produces a laser beam having a predetermined divergence or spread which is rotated at a constant angular velocity in a direction perpendicular to the spread. Each time the spread laser beam passes a specific point in its rotation, the

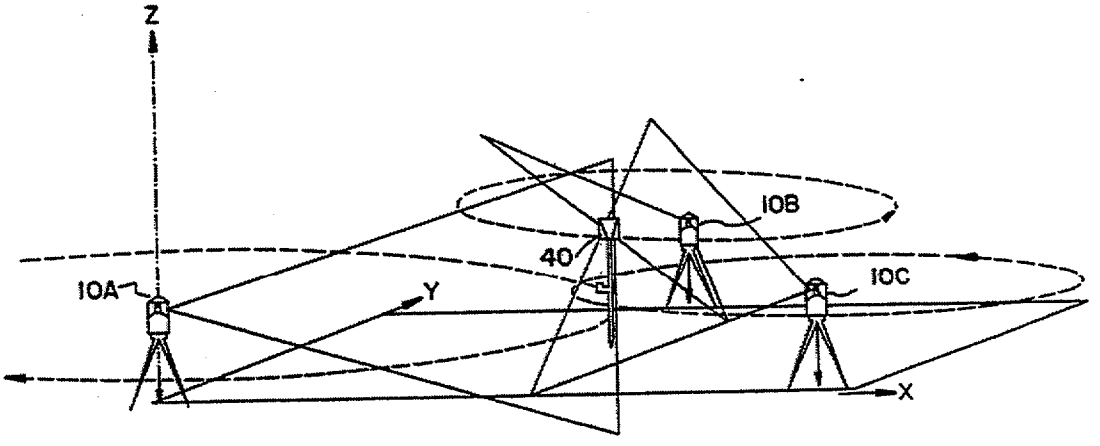

Figure 2.4.1: Early concept for the fanning laser positioning system. Three laser transmitter stations, based at known benchmarks, transmit inclined fans. A computer and light sensitive detector is contained in the roving receiver. For any point which is crossed by two intersecting laser beams, a horizontal angle can be determined from the time difference between the time of crossing of the primary and reflected laser beam. Once these horizontal angles are known for three fixed referent stations, the point of intersection of the three planes, and hence the position, is known. (from U.S. Patent 5,110,202)

strobe transmitter is triggered and a pulse is emitted. This point in the rotation is referred to as the rotation datum. The rotation datum is thus defined as an arbitrarily chosen actuation or trigger line selected internally for the corresponding fixed station independently of the other fixed stations. The strobe transmitter can be of the type emitting a light pulse (light strobe transmitter) or the type emitting a radio pulse (radio strobe transmitter).

There are two types of fixed stations, horizontal and vertical. In the horizontal fixed station, the laser beam is rotated in a horizontal plane. In the vertical fixed station, the laser beam is rotated in a vertical plane. Preferably, at least three horizontal fixed stations and one vertical fixed station are used to ensure consistent x,y, and z positioning across an entire site.

An alternate solution is to use only three fixed stations set on different axes (Figure 2.4.1). A unique position solution exists for all points covered by the rotating laser beams from the fixed stations. The axes selected would be such that the area to be measured was covered by each of the spread laser beams emitted from the fixed stations.

The portable position sensor includes a light sensitive detector, a computer and a display. The light sensitive detector is generally a disk of predetermined thickness oriented in a horizontal plane having a photosensitive area covering the circumference of the disk. When struck by either the laser beam or the strobe pulse, the detector generates an electric pulse which is sent to the computer. If a radio strobe pulse transmitter is used instead of a light strobe pulse transmitter, the portable position sensor also includes a radio receiver which generates an electric pulse upon receipt of a radio strobe pulse. Once the computer has accepted, time labeled, and recorded two strobe pulses and an intermediate laser pulse from each fixed station, it can determine the three dimensional position of the detector and present this information to the operator on the display for determination of a position on the site.

The horizontal position of the portable position sensor is determined through a trigonometric algorithm which uses horizontal angles determined from time information of the rotating lasers beams and the strobe signals of the horizontal fixed stations. The vertical position of the portable position sensor is generated using a trigonometric algorithm, which uses the horizontal distance to a vertical fixed station system, as calculated above, and an angle which is calculated from time information from the rotating laser beam and the strobe signal broadcast by the vertical fixed station system.

Since the rotation datum of each fixed station is self-contained, i.e. each rotation datum is determined internally of the particular station, and the signal corresponding to the rotation datum is generated at the same fixed detector, multiple fixed detectors can be quickly set up, without the need to align the laser

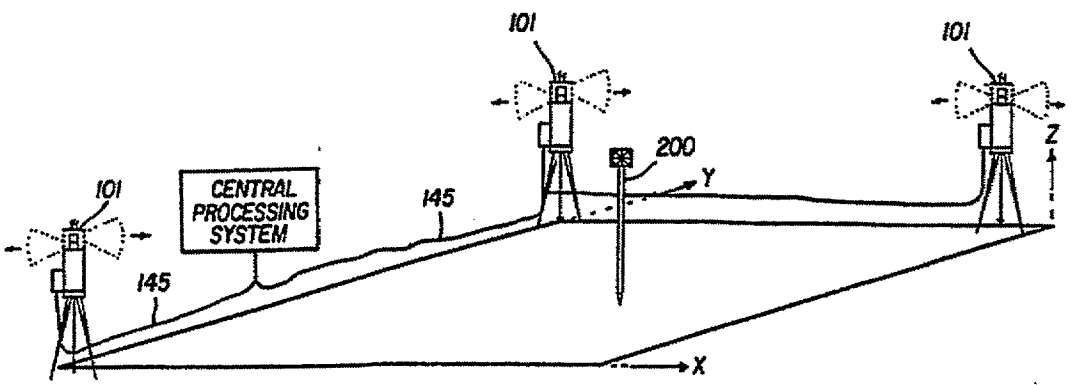

Figure 2.4.2: Alternate manifestation of the fanning laser positioning concept. The survey system consists of fixed referent stations which emit rotating, divergent laser beams and a portable reflector. Each fixed station also includes a detector and a processor. The portable reflector may include retroreflectors or transponders. When the rotation of the laser beam is such that it is in line with a portable reflector, the transmitted laser beam is reflected off the portable reflector and received at the fixed receiver. For any point which is crossed by the fanned laser beams of a fixed station, a horizontal angle can be determined. Once these horizontal angles are known for three fixed stations, the point of intersection of three planes, and thus the three-dimensional position of the point, is determined. (from U.S. Patent 5,294,970).

beams of opposite reference stations. Moreover, the fixed stations need not be located at the same elevation.

This approach provides a unique solution for x,y, and z position measurement through the use of spread laser beams from the horizontal fixed stations to accurately determine x, y position. To determine z, a vertical fixed station rotates a spread laser beam in a vertical plane. The spread beam strikes the portable position sensor, and through a self-contained rotation datum, the difference in time of the spread beam strike and the rotation datum provides a horizontal interior angle. Since the x-y position is known from measurements made with the horizontal fixed stations, the z-coordinate determination can be done with the same relative accuracy as the x-y coordinate determination.

The circular detector will produce an output pulse when crossed by a laser beam, which has a peak which consistently corresponds to the laser beam crossing the center of the portable position sensor. In this approach, the origin of the laser beams which strike the portable position sensor each have unique rotation rates. Thus the computer establishes a window of time when a laser beam or a strobe pulse from a particular fixed station is expected to arrive. The computer will continually update the windows of time to accomodate for movement of the portable position sensor and drift in the rotation rates of the motors. Alternatively, the laser beams may be identified through modulation of the wavelength of the lasers at differnet rates or by using lasers of differing wavelengths.

An alternate, and more recent approach (Figure 2.4.2) to the above uses a system wherein the reference stations are able to determine their location in reference to one another, establishing a local coordinate system. This information may then be transferred to a portable position sensor for use in determining its location.

In this approach, three fixed broadcast stations (items 101 in Figure 2.4.2) are used to determine the position of one or more portable positioning reflectors (as opposed to processing sensors). Each fixed station produces a set of rotating fan-shaped laser beams which rotate at constant angular velocity. Each fixed station also includes a receiving device, which is light sensitive. When the rotation of the laser beam is such that it is in line with a portable positioning reflector, the transmitted laser beam is reflected off the portable position reflector and received at the fixed receiver.

For any point which is crossed by the fanned laser beams of a fixed station, an angle perpendicular to the rotation of the laser beam angle can be determined. Once these angles are known for three fixed stations, the point of intersection of the three planes, and thus the three-dimensional position of the point, is determined.

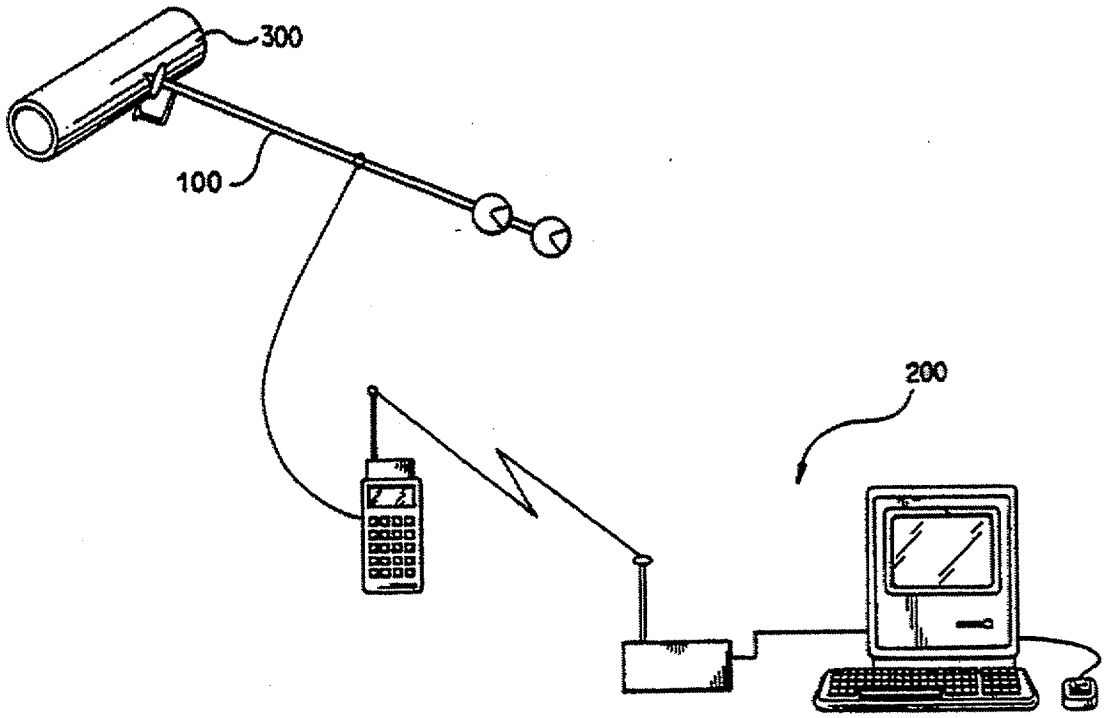

Figure 2.4.3: Component position verification using the fanning laser system and a local data logger. The system includes a data gathering apparatus and a model building apparatus. The data gathered may then be transformed into a CAD model of an as-built or as-is environment, or to otherwise map a building structure and its elements in three dimensions. (from U.S. Patent 5,247,487).

The portable positioning reflector (termed the "P-reflector," item 200 in Figure 2.4.2) includes a reflective surface or surfaces, which redirect the incoming laser light back toward the fixed station. A retroreflector, which is used with an electronic distance measurement device (EDM, as described above in section 2.1), is an example of a reflector which could be used as the reflective surface of the P-reflector. A number of retroreflectors preferably would be used to provide a 360-degree horizontal reflecting capability.

The fixed position sensor preferably includes a light sensitive detector and a computer. The detector includes a lens system which directs light to a photosensitive detector. The detector generates an electrical pulse when struck by a laser beam. This pulse is sent to a computer. The computer time labels each received pulse, which corresponds to the time the reflected laser beam from the P-reflector strikes the optical receiver. Once the computer has accepted, time-labeled and recorded a reflected primary pulse and reflected secondary pulse from the P-reflector, it can determine the directional angles or the P-reflector relative to the fixed station.

The directional angles are sent to a central processor system, via a communications link. The central processor system receives angle information from a number of fixed stations. If the central processor system receives angle information from at least three fixed stations, the position of the retroreflector can be determined.

In yet another variation in the above theme, a portable positioning transponder (Figure 2.4.3) may be substituted for the retroreflector. The transponder includes a light sensitive detector which is capable of sensing light about 360 degrees in the horizontal plane. An energy beam (light or radio) is emitted by the transponder when light from a fixed station is received by an optical detector on the transponder. The emitted wave is received back at the fixed station by a transponder receiver. The use of such a transponder increases the range of the positioning system by eliminating the reflected path of the laser beam.

Some specifications for a representative commercial fanning laser positioning systems are presented in Table 1.2.4.1. The absolute accuracy for this system, while having a finer specific range resolution (1 mm) than that for a typical EDM system (2-5 mm), is dominated by the second term which reflects the ambiguity resulting from propagation of the laser beam through the atmosphere. An error of 100 ppm over a typical survey distance of 100 m represents an error of 10 mm. This is a direct result of the significantly higher frequency of operation of this type of system (370 terahertz, versus 80 MHz for a typical RF-based EDM system).

Table 1.2.4.1: Nominal Specifications for a Fanning Laser Positioning System (SPSI "Odyssey")

Accuracy	
Horizontal	±(1mm+100ppm)
Vertical	±(1mm+100ppm)
Range	
Outdoor Receiver	150m
Indoor Receiver	75m
Measurement Rate	
Frequency	5Hz
Transmitter Optics	
Scan Rate	50Hz
Emission Wavelength	810nm±10nm
Field of View	120° x 30°

Like pseudolites, fanning laser systems can be deployed in such a fashion as to insure coverage of specific areas. Because of the narrower field of view, however, a greater density of fanning laser systems would be required to cover a specified work area.

References:

Beliveau, Y.J., Lundberg, E.J., Dornbusch, A., and Pratt, T., (1993), "Spatial Measurement Recovery System," U.S. Patent 5,247,487, Sept. 21, 1993.

Dornbusch, A., Beliveau, Y.J., Lundberg, E.J., , and Pratt, T., (1992), "Spatial Positioning and Measurement System," U.S. Patent 5,110,202, May 5, 1992.

Dornbusch, A., Lundberg, E.J., Beliveau, Y.J., and Pratt, T., (1994), "Spatial Positioning System," U.S. Patent 5,294,970 March 15, 1994.

Lundberg, E.J., Beliveau, Y.J., and Pratt, T., (1992), "Spatial Positioning System," U.S. Patent 5,100,229 March 31, 1992

2.4 Summary

As part of the NIST initiative in Construction Automation, research is being directed towards the assessment and development of real-time construction site metrology and to determining what can be done with such information in order to improve jobsite efficiency. The objectives are to develop new measurement technologies and to promote data exchange standards among all automated

measurement systems so as to permit the real time position and orientation updates of any object on the jobsite -- including materials, personnel, and machinery -- to be ascertained and made available to a remote management office by means of telepresence and virtual reality interfaces.

From the above discussion, it is apparent that there are certain limitations to line-of-sight (LOS) data acquisition. In the balance of the present report we discuss the nacent experiments conducted at NIST as part of an effort to investigate alternative technologies for resolving these issues and leading towards the development of what we refer to as NLS (Non-Line-of-Sight) construction metrology.

The problem of eliminating the line-of-sight requirement while achieving high precision is a difficult one. All of the systems previously described above rely on the use of high frequency radiation (UV laser light in one case, and mid to high band RF in the others) which has the unfortunate characteristic of substantial dissipation when encountered by objects typical at most construction sites. Research is planned at NIST involving the use of pseudolite networks for vehicle control. However, even pseudolite signals will not penetrate reinforced concrete.

In order to survey *through* engineering materials, a different approach must be used. The research reported herein involves the use of ultra wide band transmission techniques, which are sometimes referred to as "impulse radar", "spread-spectrum radar," and "base-band radar." All prior work with these technologies appears to have been directed to surveillance, where it was not possible to have a "cooperative" receiver on the inside of the target structure. Fundamental work remains to be done with cooperative receivers to determine which part of the EM spectrum is most effective in penetrating engineering materials.

Following extensive literature reviews, a series of experimental projects were initiated at NIST in cooperation with MIT Lincoln Laboratories. The objective of the preliminary laboratory investigation was to determine the effectiveness of spread spectrum radar transmissions, with a bandwidth of approximately 2 GHz (from 50 MHz through L-band (2 GHz)), to penetrate various engineering materials and structures and to experiment with a "cooperative" positioning receiver located beyond such obstacles. This was the first-ever experiment in NLS metrology for the purposes of surveying. Preliminary results (described below) show that it is possible to locate, via time-of-flight measurements, the position of a receiver beyond a meter-thick reinforced concrete wall, or beyond several brick and masonry block walls, and beyond typical interfering stacks of wide flange girders. The specific accuracies obtained under these varying circumstances, and the factors affecting the range resolution, are discussed in the remainder of this report.

Chapter 3: Impulse Radar Tutorial:

3.1 Basic Radar Principles

Radar is an electromagnetic system for the detection and location of objects. The name is an acronym for Radio Detection and Ranging. Traditional radar operates by transmitting a particular type of waveform, a pulse-modulated sine wave for example, and detects the echo signal. A portion of the transmitted signal is back-scattered by the object (known in military terms as "the target") and is reradiated in all directions. In fact, as will be discussed in further detail below, electromagnetic waves are completely reflected by conducting bodies; non-conductors will both absorb and re-radiate the incident signal. The distance to the target, known as *range*, is determined by measuring the time taken for the radar signal to travel to the target and back and is given by:

$$R = \frac{cT_R}{2} \qquad \text{eq.(3.1.1)}$$

where c = 3×10^8 m/s (the propagation velocity of electromagnetic radiation in a perfect vacuum) and T_R is the time taken for the signal to propagate to the target and return. The factor 2 appears in the denominator because of the two-way propagation of radar. Each nanosecond of round-trip travel time corresponds to a distance of approximately 150 mm. The propagation speed is dependent on the index of refraction of the medium through which the wave is propagating. For engineering materials this can result in significantly slower transit times than for a vacuum.

Many radar systems employ a single antenna which is used both for transmission and reception. In some designs these tasks are performed by physically separate antennas, in which case the two antennas are mounted next to each other. For the work conducted at NIST the antennas were separated and the receiver became the roving element whose position was to be determined while the transmitter became a fixed broadcast station, whose position was known to high accuracy. For this case the range equation simplifies to:

$$R = cT_R \qquad \text{eq.(3.1.2)}$$

and each nanosecond of propagation time between the transmitter and receiver corresponds to 300 mm of traverse distance. The use of three such transmitters whose positions are known and which are positioned in a roughly triangular pattern about a contruction provide for a unique position determination in Cartesian space of the roving receiver.

Conventional radars generally have been operated at frequencies extending from about 220 MHz to 35 GHz. These are not hard limits. Some over-the-horizon radars have been operated at 4 to 5 Mhz. Laser radars operate at significantly higher frequencies (in the terahertz range). The selection of the appropriate frequency or band of frequencies to be used for construction metrology, in which the objective is maximum material penetration, is discussed in greater detail below.

Range Performance and Signal Detection

The simple form of the radar equation is given by

$$R_{\max} = \left[\frac{P_t G A_e \sigma}{(4\pi)^2 S_{\min}} \right]^{1/4} \qquad \text{eq.(3.1.3)}$$

where P_t= transmitted power, watts
G= antenna gain
A_e= antenna effective aperture, m^2
σ= radar cross section, m^2
S_{min}= minimum detectable signal, watts

and relates the maximum detectable range, in meters, of a potential target. This presumes that a signal propagates through the atmosphere as a spherical wave and is reflected by the target and subsequently detected by the receiving antenna located at the origin of the radar pulse. If the "target" happens to be a reinforced concrete wall *through which* we desire to obtain range to a receiving antenna on the opposite side, then the radar cross section term becomes meaningless and additional terms relating to the complex propagation of the electromagnetic wave through the material must be added. The ratio of received to transmitted power for one-way transmission is given by the Friis Transmission equation as:

$$\frac{P^R}{P^T} = \frac{\lambda^2 G_T G_R L}{16\pi^2 R^2} \qquad \text{eq.(3.1.4)}$$

where P^T= transmitted power, watts
P^R= transmitted power, watts
G_T= transmission antenna gain
G_R= receiver antenna gain
L = Total loss due to transmission through media + all other losses
R = True range between the antennas, meters
λ = Wavelength of transmitted signal, meters

An important factor that must be considered in this equation is the statistical or random nature of several of the parameters. The minimum detectable signal is

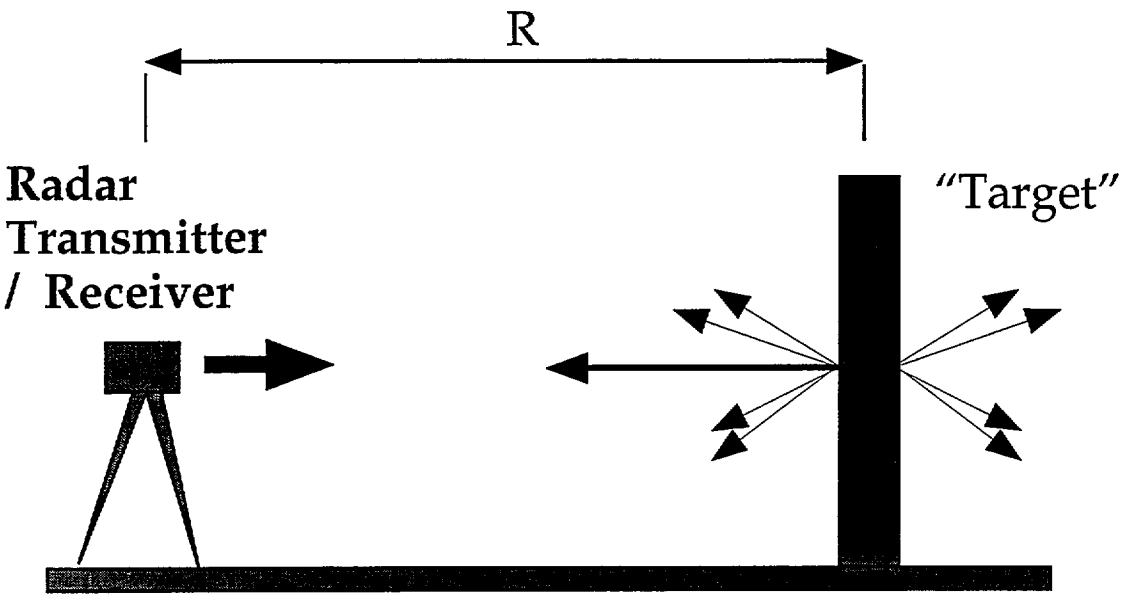

Figure 3.1.1: Traditional Radar. Transmitted pulse hits "target". Some energy is reflected from the target and is sensed by a radar receiver which is coincident with or immediately adjacent the transmitter. The range, R, is given by cTr /2, where c is the speed of light, and Tr is the time for the signal to propagate to the target and return.

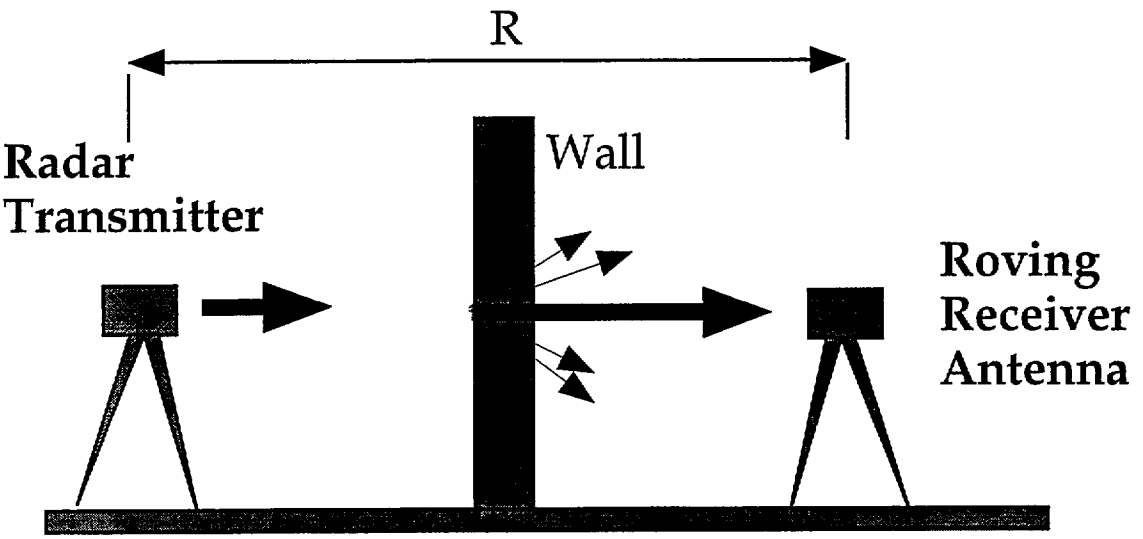

Figure 3.1.2: Roving receiver approach used for NLS tests at NIST. Transmitted signal propagates through engineering materials and reaches receiver located on the inside of the structure. Time of flight, Tr, is used to determine the one-way travel distance of the transmitted pulse: R=vTr, where v is less than c and is governed by the characteristics of the material through which the pulse travels.

statistical in nature. Other factors affecting radar transmission performance are the meteorological conditions along the propagation path and the nature and variability of the construction material properties that may be blocking that path. Thus the practical use of such apparatus for construction metrology will ultimately entail the development of statistical models for the various factors affecting range calibration.

From a practical systems design standpoint, it is useful to note the power relationship in eq.(3.1.4) indicates that a doubling of range requires a 4-fold increase in transmited power to achieve the same received power level. Unlike normal radar installations, construction workers would be continuously active beneath the transmission umbrella were such a metrology system to be deployed at a construction site. Design tradeoffs will necessarily have to balance accepted transmission power in the presence of humans; FCC interference rules; while maximizing the ability to penetrate substantial thicknesses of engineering materials and still obtain accurate position estimates.

The ability of a radar to detect a weak signal is limited by the noise energy that occupies the same portion of the frequency spectrum as does the signal energy. Detection is generally based on establishing a threshold level at the output of the receiver, as shown in Figure 3.1.3. A general rule of thumb is that the amplitude of a true target should be at least 12 dB above that for the noise peak amplitude. In the case of propagation of the radar pulse through, for example, a series of reinforced concrete and masonry walls, there will in general, not be a single well defined peak in the arrival pulse. More likely, there will be a rounding of the pulse peaks due to scatter and diffraction -- known as dispersion -- as well as additional peaks on the timeline which may or may not have higher amplitudes than the first peak. The latter effect is known as "clutter" or "multipath" and results from the fact that for a complex geometry there are many paths by which the transmitted radiation can reach the receiver. Each of these paths is subject to propagation delays, either through the atmosphere or through the respective material layers. For simple geometries it can generally be anticipated that the first signal to arrive will represent the shortest possible distance between the transmitter and receiver and hence the true traverse distance. Propagation through dispersive media is discussed in greater detail below.

3.2 Why single frequency systems cannot be used for Ranging

It will be useful at this point to briefly review the merits of various radar systems. One of the simplest approaches involves broadcasting on a single continuous frequency (CW) and measuring the doppler shift of the reflected signal. Historic experiments in the 1920s and 30s used this approach almost exclusively. It was the basis for the "proximity" fuse which saw wide use towards the end of World War II.

In the following discussion, we address the special variation of radar used for the

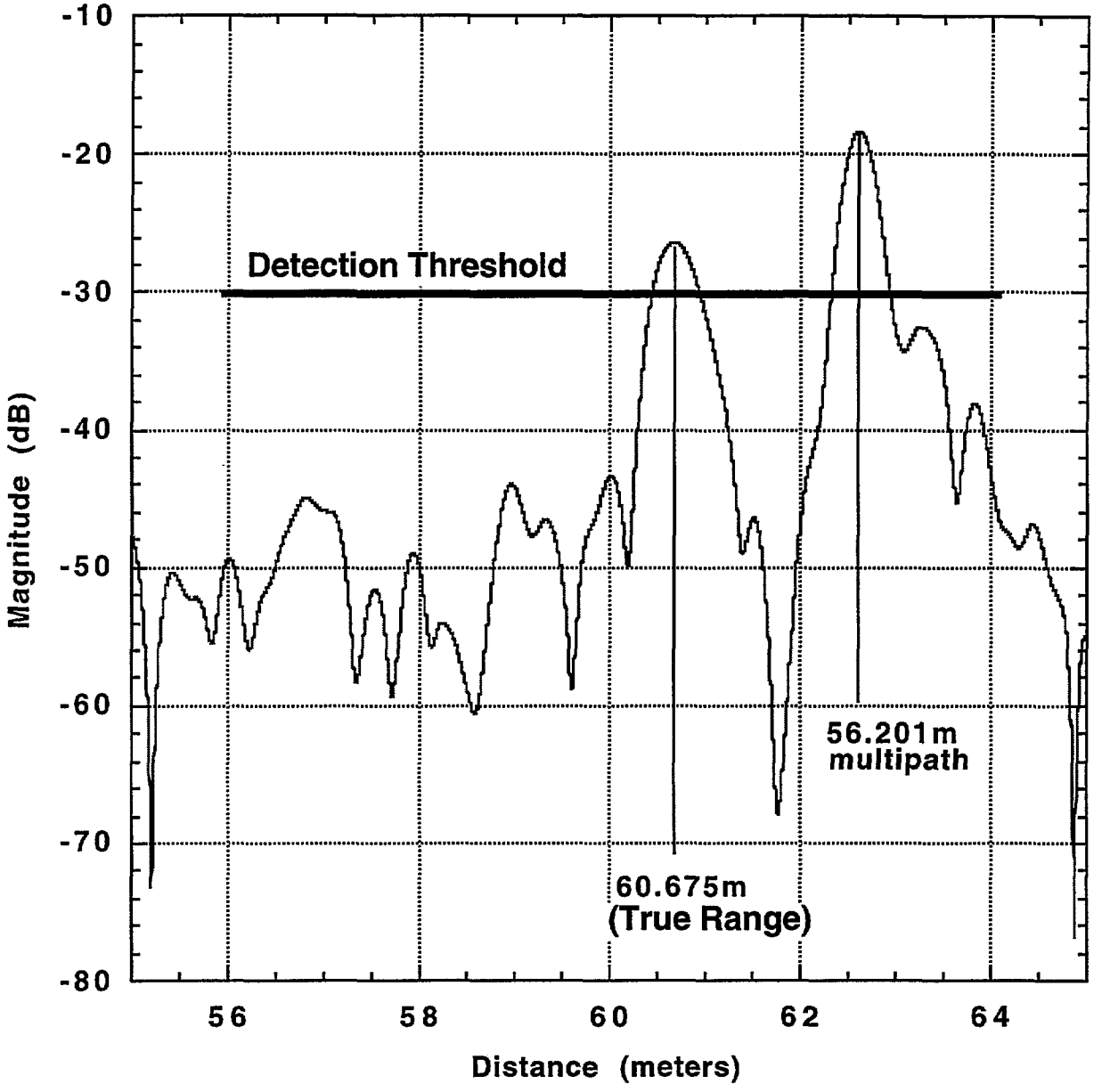

Figure 3.1.3: Typical envelope of the radar receiver output as a function of time. The peak at 60.675 m represents the true distance between transmitter and receiver; The peak at 56.201 m represents a false target created by multipath effects. Threshold for target detection is arbitrarily set to -30 dB. This plot was created from actual NIST test data in which the receiving antenna was placed behind a 500 mm thick reinforced concrete wall.

NIST experiments, in which the transmitter and reciever are not co-located and the intent is to measure the straight line distance between the transmitter and receiver. If a single-frequency CW radar is set up in the above configuration with a transmitter and receiver separated by a distance R in free space, as depicted in Figure 3.2.1, and a single frequency signal, $\cos(2\pi f_0 t)$, is applied to the transmitter.

The received signal will be given by:

$$\cos(2\pi f_0(t-T) \qquad \text{eq.(3.2.1)}$$

where:

T = time for signal to traverse the distance R in free space.
R = range in meters.
f_0 = operating frequency

The traverse time is given by:

$$T = R/c \qquad \text{eq. (3.2.2)}$$

where

c = the speed of light in a vacuum. The actual velocity will be affected by the presence of intervening atmosphere (with its variations in humidity, temperature, and pressure) and physical obstacles and is given by:

$$v = c/n \qquad \text{eq.(3.2.3)}$$

where n = index of refraction for the given media.

The phase difference between the transmitted and received signals is given by:

$$\begin{aligned} \Delta\varphi &= 2\pi f_o[t-(t-T)] \\ &= 2\pi f_o T \\ &= 2\pi f_o R/c \end{aligned} \qquad \text{eq.(3.2.4)}$$

This phase difference can be used to measure range as a function of the phase difference in much the same fashion as that described for use by EDM systems (see Section 2.1) as:

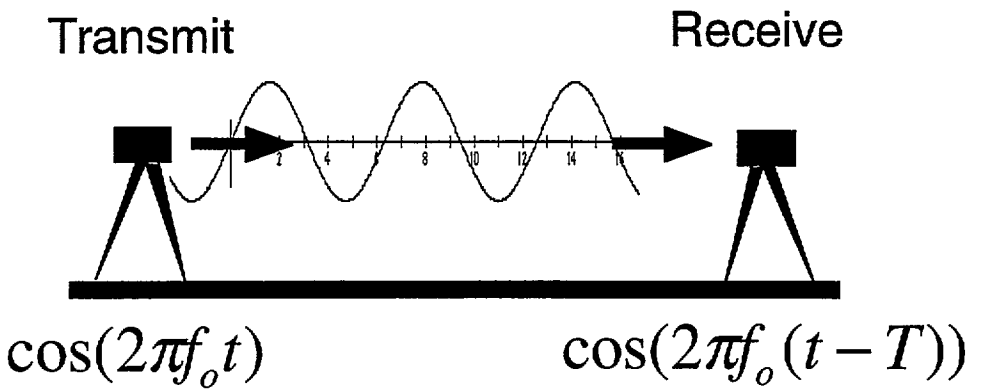

Figure 3.2.1: CW radar setup in opposition mode where the receiver becomes the "target" and the object is to obtain the straight line distance between the transmitter and receiver.

$$R = \frac{c\Delta\varphi}{2\pi f_o} \qquad \text{eq.(3.2.5)}$$

However, the measurement of $\Delta\phi$, the phase difference, is ambiguous, since $\Delta\phi$ (actual) = measured $\Delta\phi$ + n*2π, where n is an arbitrary integer. The region of *unambiguous range,* R_u is defined as the distance the signal travels for each 2π radians of phase change. If we substitute 2π into eq.(3.2.5) we obtain:

$$R_u = \frac{c2\pi}{2\pi f_o} = \frac{c}{f_o} = \lambda_o \quad \text{(wavelength)} \qquad \text{eq.(3.2.6)}$$

Recalling the discussion of EDM distancing above, one can only know for sure what the distance is if the transmitter and receiver are a) less than one wavelength distance apart, and b) one can precisely measure the phase. If the distance between the transmitter and receiver is greater than one wavelength there is no means of uniquely determining that distance: At radar frequencies, R_u is too small to be of practical use, making a single-frequency ranging system untenable for construction metrology.

3.3 Dual-Frequency Radars

The unambiguous range, R_u , can be expanded by using two separate CW signals that are at slightly different frequencies. For example:

Transmit: $\cos(2\pi f_1 t)$ and
$\cos(2\pi f_2 t)$ where $f_2 = f_1 + \Delta f$

Receive: $\cos(2\pi f_1 (t-T))$ and
$\cos(2\pi f_2 (t-T))$

At each frequency, the phase difference between the transmitted and received signal is:

$\Delta\varphi_1 = 2\pi f_1 T = 2\pi f_1 R/c$
$\Delta\varphi_2 = 2\pi f_2 T = 2\pi f_2 R/c$

from this:

$\Delta\varphi_2 - \Delta\varphi_1 = 2\pi(f_2 - f_1)R/c = 2\pi\Delta f R/c$

$R = c(\Delta\varphi_2 - \Delta\varphi_1)/\ 2\pi\Delta f \qquad \text{eq.(3.3.1)}$

and the *unambiguous* range is then given by:

$$R_u = 2\pi c/(2\pi\Delta f) = c/\Delta f \qquad \text{eq.(3.3.2)}$$

From eq.(3.3.2) , the alias-free range, R_u , can be made very large by making Δf very small.

Operational Aspects of Dual Frequency Radars

At the transmitter, the two signals (at f_1 and f_2) are in phase. As the signals progress away from the transmitter, the relative phase between the two increases because of their difference in frequency.

When the two signals slip in phase by one cycle, the measurement of phase, and hence range, becomes ambiguous. In a single-target (single propagation path), noise free environment, this two-frequency CW radar can be made to work.

If noise is present, the two-frequency radar will have a finite accuracy. It can be shown (Skolnik, 1980) that the error in time delay for a radar pulse travelling from a transmitter to a receiver is given by:

$$\delta T_R = \frac{1}{2\pi B\sqrt{\frac{2E}{N_0}}} \qquad \text{eq.(3.3.3)}$$

where: E = energy in the received signal
N_0 = Noise power per hertz of bandwidth
B = bandwidth, Hz

However, from the above discussion, the time delay for a direct transit from transmitter to receiver (no echo as for traditional radar) is given by:

$$T = c/R \qquad \text{eq.(3.3.4)}$$

hence: $\delta T_R = c/\delta R$

we may also, for the case of a two frequency radar, make the substitution

$$B = \Delta f \qquad \text{eq.(3.3.5)}$$

by substituting the above into eq.(3.3.3) we obtain the estimate for the range error for a two frequency radar as:

$$\delta R = \frac{c}{2\pi\Delta f\sqrt{\frac{2E}{N_0}}} \qquad \text{eq.(3.3.6)}$$

From this equation, it is apparent that a large value of Δf results in a small range error δR. Thus, Δf must be small enough to yield an acceptably large *unambiguous range*, R_u, but large enough to provide acceptable *range accuracy*. Intuitively, the use of many frequencies will improve accuracy and range ambiguity. The concept of one and two frequency systems helps illustrate the significance of phase and indeed is the underpinning of EDM type survey systems. However, for the situation of a target inside a complex construction site this approach will not work. As with an EDM system, which employs a retro-reflector to ensure an unambiguous target, there must be only one target and only one propagation path.

If the propagation from the transmitter follows more than one path, as shown in Figure 3.3.1, with path distances r_1 and r_2 in free space, then the received signal becomes complicated.

In this case, the received signal is given by:

$$S_R(t) = \cos(2\pi f_0(t - T_1) + \cos(2\pi f_0(t - T_2) \qquad \text{eq.(3.3.7)}$$

In this case, the meaning of the phase measurement is doubtful. An approach is needed that can separate the signal in time. This has been accomplished in the radar community by means of pulse compression.

3.4 Pulsed Radar

We consider the situation presented in Figure 3.4.1, which depicts an ideal time-of-arrival (TOA) measurement system in which a perfect rectangular impulse of pulse width, τ, is launched from a transmitter at time t=0 and is received by a receiving antenna at time t=T.

Just as for the CW radar described above, this pulsed radar will have a finite accuracy due to real world noise and the precision in the measurement of time. The ability of a radar to detect the presence of an echo signal is fundamentally limited by noise. Noise also limits the accuracy of the range obtained. The parameters usually of interest in radar applications are the range (time delay), the range rate (doppler velocity), and the angle of arrival. Only the first of these is critical to NLS construction metrology.

The measurement of range is equivalent to measurement of time delay $T_R = R/c$.

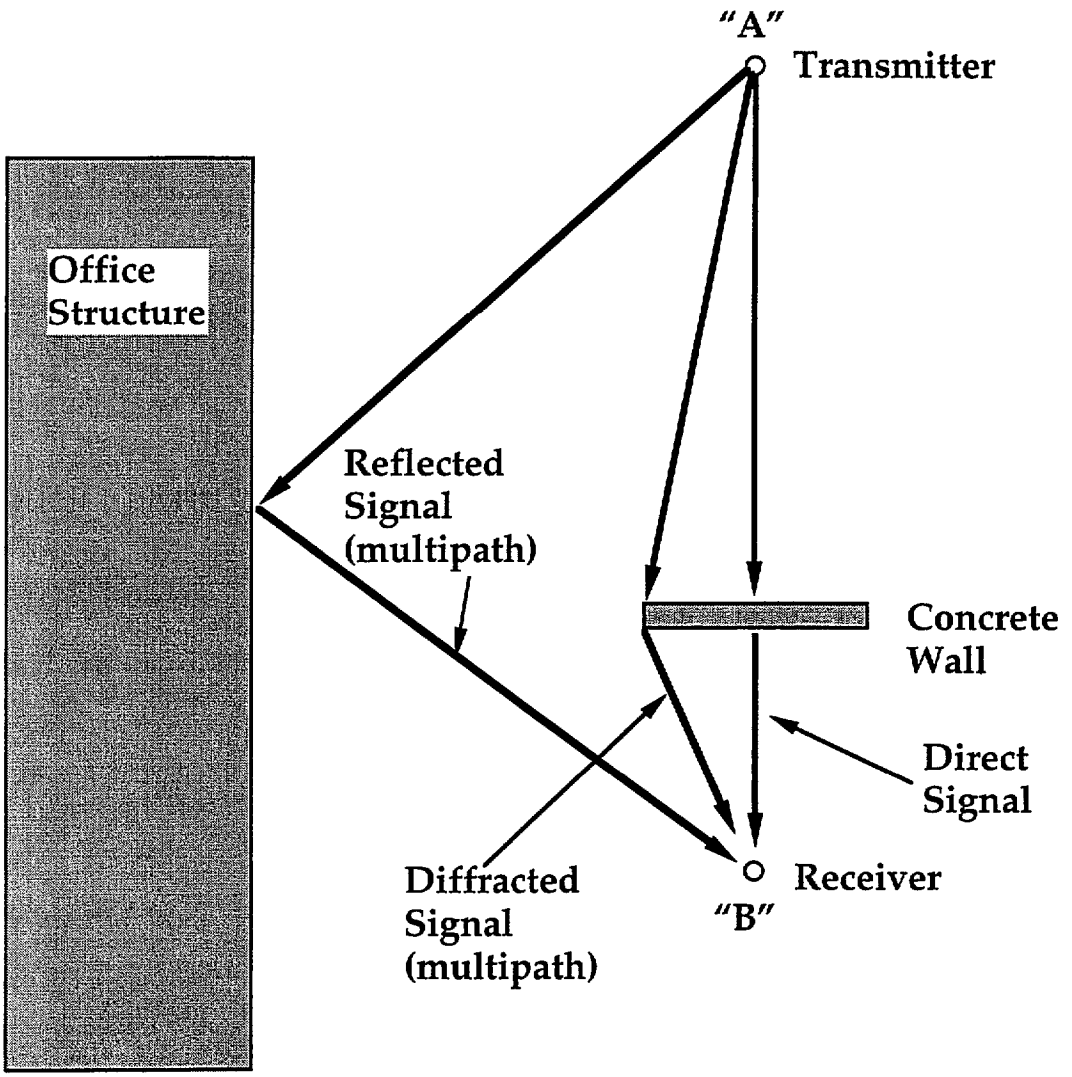

Figure 3.3.1: Multipath effects at a real construction site. Transmitted signal from point A can follow several alternate paths to reach the roving receiver, located at point B, including diffraction around the concrete wall and reflection from nearby structures. Intuition says that the first detected peak, representing the shortest distance between points A and B, and therefore the "true" distance, will be produced by the ray which travels in a straight line from point A to point B. However, in reality, the propagation speed through the concrete wall is significantly less than that through the surrouding air, leading to potential ambiguities over which signal in fact arrives first, especially for diffracted/reflected paths that are almost straight lines. Furthermore, the magnitude (power) of the direct signal is significantly dissipated during its transit through the concrete wall, leading to the possibility that either the amplitude associated with the true distance will not pass the detection threshold and will therefore be falsely rejected, or two peaks will smear together, biasing the result.

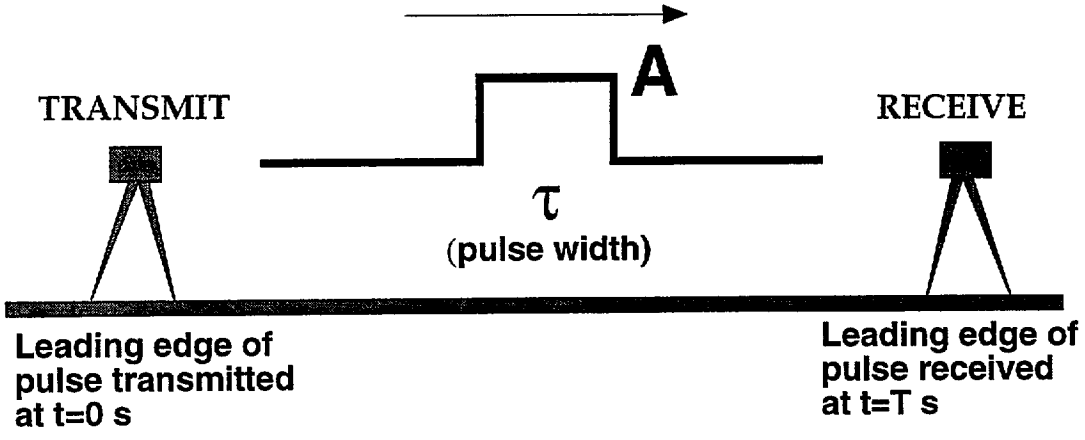

Figure 3.4.1: Ideal time-of-arrival metrology system in which a rectangular impulse is launched from a transmitter and received some time later by a receiving antenna. The time-of-flight determines the distance between the two antennas.

Note that this is true only for one-way NLS survey operations; the traditional radar time delay equation, $T_R = 2R/c$, accounts for the two-way travel time of the wave which is reflected off a distant target and received by an antenna co-located with the transmitting antenna. In both cases c is the velocity of light. One method of determining range with a pulsed waveform is to measure the time at which the leading edge of the pulse crosses some threshold, as shown in Figure 3.4.2. The ideal pulse is given by the solid curve. The shape of the pulse is not perfectly rectangular and the rise and decay times are non-zero. A perfectly square pulse would require an infinite bandwidth.

The effect of noise is to perturb the shape of the pulse and to shift the time of threshold crossing as shown by the dashed curve. The maximum slope is given by the pulse amplitude A divided by the rise time, t_r. For large signal-to-noise ratios the slope of the pulse corrupted by noise is effectively the same as the slope of the un-corrupted pulse. The slope of the pulse in noise may be written as $n(t)/\Delta T_R$, where n(t) is the noise voltage in the vicinity of the threshold crossing and ΔT_R is the error in the time delay measurement. These two slope relationships yield:

$$\Delta T_R = \frac{n(t)}{A/t_r} \qquad \text{eq.(3.4.1)}$$

or

$$\left[(\Delta T_K)^2\right]^{1/2} = \delta T_R = \frac{t_r}{(A^2/n^2)^{1/2}} = \frac{t_r}{(2S/N)^{1/2}} \qquad \text{eq.(3.4.2)}$$

where A^2/n^2 is the video signal to noise (power) ratio. The video signal to noise ratio is equal to twice the IF signal to noise power ratio (S/N), assuming a linear detector law and a large signal to noise ratio. If the rise time of the video pulse is limited by the bandwidth B of the IF amplifier, then $t_r \approx 1/B$. Letting $S=E/\tau$ and $N=N_0B$, where E is the signal energy, N_0 the noise power per unit bandwidth, and τ the pulse width, the error in the time delay can be written as:

$$\delta T_R = \left(\frac{\tau}{2BE/N_o}\right)^{1/2} \qquad \text{eq.(3.4.3)}$$

If a similar independent time delay measurement is made at the trailing edge of the pulse, the two combined measurements will be improved by

$$\delta T_R = \left(\frac{\tau}{4BE/N_o}\right)^{1/2} \qquad \text{eq.(3.4.4)}$$

For constant pulse amplitude, A, the rms time-delay error is proportional to the rist

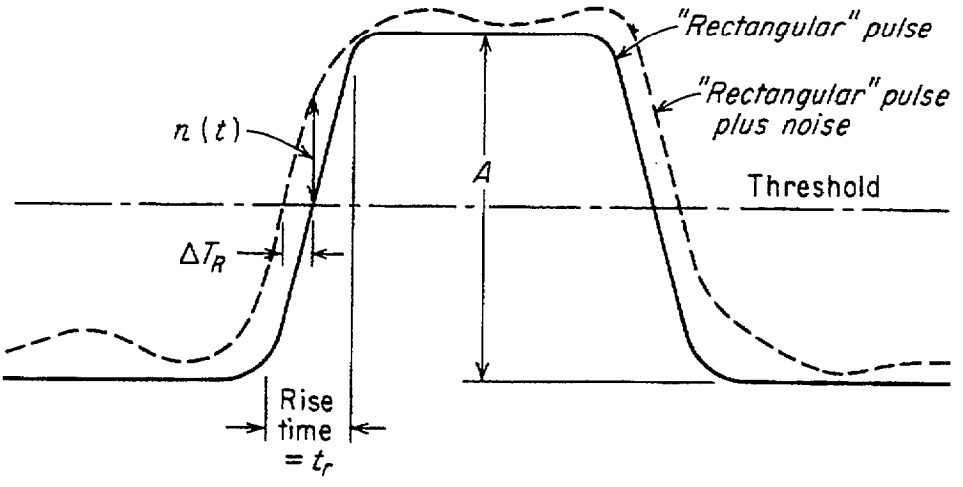

Figure 3.4.2: Determining range based on leading edge measurements of a "rectangular" pulse (Skolnik, 1990).

time and is independent of the pulse width. An improvement in accuracy is obtained, therefore, by decreasing the rise time (increasing the bandwidth) or by increasing the signal to noise ratio.

It follows from the above that the pulsed radar range accuracy is:

$$\delta R = c\delta T = c\sqrt{\frac{\tau N_0}{4BE}} \qquad \text{eq.(3.4.5)}$$

Eq. 3.4.5 shows that the range accuracy can be improved by transmitting a narrower pulse, τ , or transmitting a pulse with larger energy , E.

This τ/E relationship represents a design problem, because E and τ are related. For a transmitted pulse of amplitude A (see Figure 3.4.1) it can be shown that:

$$E \cong A^2\tau \qquad \text{eq.(3.4.6)}$$

Therefore, τ/E becomes

$$\frac{\tau}{A^2\tau} = \frac{1}{A^2} \qquad \text{eq.(3.4.7)}$$

This amplitude dependence is a problem, because there are practical limitations to the transmission of high amplitude pulses. This issue can be avoided by synthesizing a high-energy, narrow-width pulse with a technique known as pulse compression.

3.5 Pulse compression techniques

Pulse compression allows a radar to utilize a long pulse to achieve large radiated energy, but simultaneously to obtain the range resolution of a short pulse. It accomplishes this by employing frequency or phase modulation to widen the signal bandwidth. The received signal is processed in a matched filter that compresses the long pulse to a duration 1/B, where B is the modulated pulse spectral bandwidth. There are several advantages to this approach over all of the previously mentioned systems, including:

- improved range resolution
- improved range accuracy
- resolution of multipath signals
- reduction of clutter effects

A short pulse radar is not without its disadvantages. It requires large bandwidth with the possibility for interference to other users of the band. The shorter the pulse the more information there is available from the radar, and therefore the greater will be the demands on the information processing systems and the display systems. If the radar transmitter is peak power limited (which it will be for work at a construction site where workers are present) the shorter the pulse, the less total energy is transmitted. This results in limitations of range for short pulse radars.

Pulse compression is a method for achieving most of the benefits of a short pulse while keeping within the practical constraints of the peak-power limitation. It is usually a suitable substitute for the short-pulse waveform except when a long minimum range might be a problem. Pulse compression radars, in addition to overcoming the peak-power limitations, have an electromagnetic compatibility advantage in that they can be made more tolerant to mutual interference. This is achieved by allowing each pulse-compression radar that operates within a given band to have its own characteristic modulation and its own particular matched filter.

Linear FM Pulse Compression

Figure 3.5.1 shows a block diagram for a pulse compression radar. In this device, the transmitter is frequency modulated and the receiver contains a pulse compression filter (which is identical to a matched filter). The transmitted waveform consists of a rectangular pulse of constant amplitude A and of duration T, as shown in Figure 3.5.2a. The frequency increases linearly from f_1 to f_2 over the duration of the pulse (Figure 3.5.2b). The time waveform of the signal described by Figure 3.5.2a and b is shown schematically in Figure 3.5.2c. On reception, the frequency modulated signal is passed through the pulse compression filter, which is designed so that the velocity of propagation through the filter is proportional to frequency. When the pulse compression filter is thought of as a dispersive delay line, its action can be described as speeding up the higher frequencies at the trailing edge of the pulse relative to the lower frequencies at the leading edge so as to compress the pulse to a width 1/B, where $B=f_1-f_2$. When the pulse compression filter is considered as a matched filter, the output is the autocorrelation function of the modulated pulse, which is proportional to

$$\frac{(\sin \pi Bt)}{\pi Bt}$$

The peak power of the pulse is increased by the pulse compression ratio BT after passage through the filter.

The FM waveform in the block diagram of Figure 3.5.1 is generated by directly modulating the high power transmitter. Alternatively, the waveform may be generated at a low power level and amplified in a power amplifier, as is the more

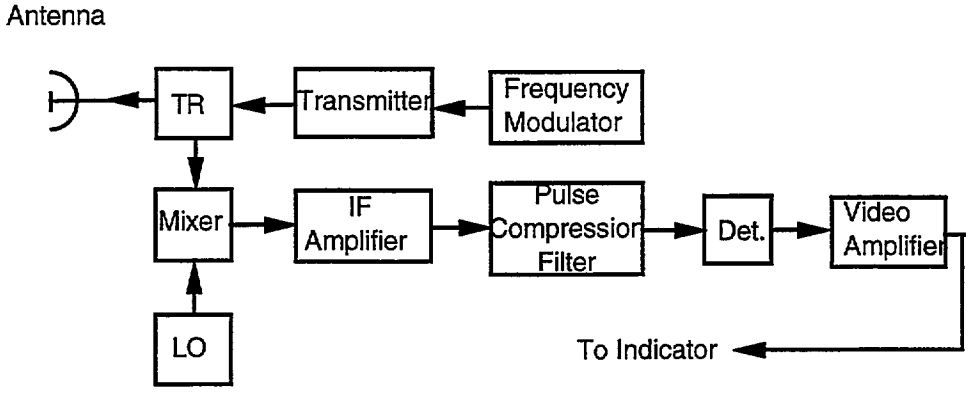

Figure 3.5.1: Block diagram for an FM pulse compression radar (Skolnik, 1990).

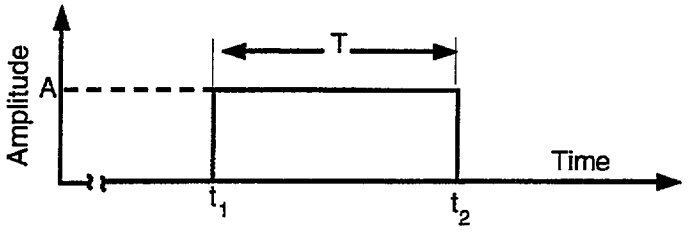

a) Transmitted waveform

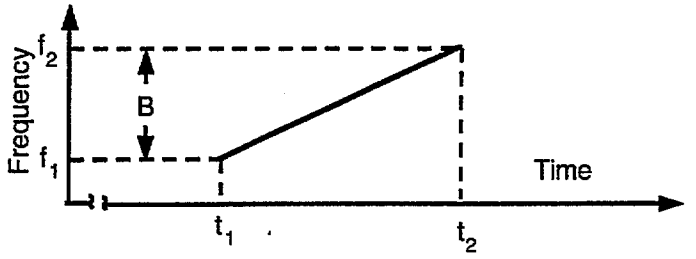

b) Frequency variation of the transmitted waveform

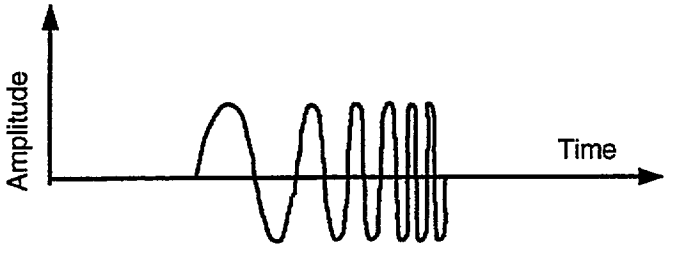

c) Time representation of the transmitted waveform

Figure 3.5.2: Linear FM pulse compression
(Skolnik, 1980)

usual procedure. The waveform may be generated by a voltage-controlled oscillator whose frequency is made to vary with an applied voltage, or by any of a half dozen active and passive methods described in detail by Skolnik (Skolnik, 1980).

Pulse compression is not without its disadvantages. It requires a transmitter that can be readily modulated and a receiver with a matched filter which is more sophisticated than that of a conventional pulse radar. Although it may be more complex than a conventional long-pulse radar, the equipment for a high-power pulse compression radar is more practical than would be required of a short-pulse radar with the same pulse energy. The time sidelobes accompanying the compressed pulse are objectionable, since they can mask desired targets or create false targets. When limiting is employed, there can be small-target suppression and possibly spurious false-targets as well. The long uncompressed pulse can restrict the minimum range and the ability to detect close-in targets. A conventional short pulse at a different frequency might have to be generated at the end of the long pulse to provide coverage of the close-in range that is blanked by the long pulse. since it only has to cover the range blanked by the long pulse, it need not be of large power. A separate receiver, or matched filter, might be needed for this short range pulse. A pulse-compression waveform does not have the immunity to interference inherent in the short-pulse radar.

3.6 Operating Principles from Fourier Theory

It is possible to achieve pulse compression (at high power) through the synthesis of of many separate independently transmitted signals, each at a different frequency. This is possible because a target's frequency response and time domain impulse response are Fourier transform pairs. In other words, the response to a series of uniformly stepped frequency scans can be converted to time domain response by using the inverse Fourier transform:

$$x(t) = \int_{-\infty}^{\infty} X(f) e^{j2\pi ft} df \qquad \text{eq.(3.6.1)}$$

Examination of eq.(3.6.1) shows that the Fourier transform integral apparently requires an infinite bandwidth of frequency data to generate a true time domain impulse response. In practice, frequency data of a significant magnitude may only exist over a finite band. Even so, it is not safe to assume that the measurements available will completely span this band (Scarborough, 1995). Therefore, the measured data will be used in the Fourier transform to generate a bandlimited estimate of the target's impulse response, making sure that this estimate is accurate enough so that the results are of use.

The bandwidth of the measurements can be represented by the rectangular function:

$$RECT\left(\frac{f}{2b}\right)=\begin{cases}1 & if|f|\le b\\ 0 & if|f|>b\end{cases} \qquad \text{eq.(3.6.2)}$$

The bandlimited estimate of the impulse response x(t) is denoted by:

$$\bar{x}(t)=\int_{-b}^{b}X(f)RECT\left(\frac{f}{2b}\right)e^{j2xft}df \qquad \text{eq.(3.6.3)}$$

Multiplication of two functions in the frequency domain corresponds to convolution in the time domain, and the Fourier transform of eq.(3.6.2) yields:

$$RECT\left(\frac{f}{2b}\right)=2b\sin c(bt) \qquad \text{eq.(3.6.4)}$$

where

$$\sin c(x)=\frac{\sin(2\pi x)}{2\pi x} \qquad \text{eq.(3.6.5)}$$

Therefore,

$$\bar{x}(t)=x(t)\otimes 2b\sin c(bt) \qquad \text{eq.(3.6.6)}$$

where the symbol $\otimes$ represents convolution.

Convolving a function with the sinc function results in a weighted averaging effect regulated by the width of the sinc function's main lobe. The width of this main lobe decreases with increasing bandwidth B. *The end result of limited bandwidth in the frequency domain is limited resolution in the time domain.* Therefore, choice of frequency range depends on two things: The bandwidth must be large enough to provide the desired amount of resolution, and the frequency range must include frequencies at which the scattering mechanism under study exists.

The inverse Fourier transform described in eq.(3.6.1) requires X(f) to be a continuous frequency function (analogous to a continuous timeline function). In modern applications of analog signal processing it is preferable to sample the signals to take advantage of the processing and storage capabilities of digital computers. The measured data is recorded and calibrated in this manner, and so the Fourier transform must be modified to make it suitable for computer-oriented Fourier transform computation.

Sampling of the continuous input signal can be described by multiplying the signal by a periodic impulse train:

$$S(f) = \sum_{n=-\infty}^{\infty} \delta(f - n\Delta f) \qquad \text{eq.(3.6.7)}$$

where Δf is the sampling interval, in Hertz. The sampled waveform, $X_s(f)$ is given by:

$$X_s(f) = X(f)S(f) \qquad \text{eq.(3.6.8)}$$

The inverse Fourier transform of $X_s(f)$ is:

$$x_s(t) = x(t) \otimes s(t) \qquad \text{eq.(3.6.9)}$$

where the inverse Fourier transform of S(f) is given by:

$$s(t) = \frac{1}{\Delta f} \sum_{n=-\infty}^{\infty} \delta(t - \frac{n}{\Delta f}) \qquad \text{eq.(3.6.10)}$$

As can be seen in Figure 3.6.1, $x_s(t)$ is a periodic function made up of shifted and scaled versions of x(t). Thus the effect of sampling in one domain results in periodicity in the other domain. Taking this one step further, we realize that the computer will represent the continuous time domain results of this transform with a sampled version as well. Therefore, sampling occurs in both domains and so both members of the Fourier transform pair may be considered periodic. This, in effect, equates the Fourier transform of sampled data to a Fourier series representation where, as can be seen in eq.(3.6.7) and eq.(3.6.10), the sampling rate in one domain determined the rate of periodicity in its dual, thus:

$$period, T = \frac{1}{\Delta f} \qquad \text{eq.(3.6.11)}$$

One important aspect of this is that if the sampling interval is too large, the period in the dual will be too small, and the shifted replicas of x(t) will overlap, a phenomenon known as aliasing. Aliasing distorts the final results so that they do not accurately represent x(t).

The effects of aliasing can be minimized by choosing the time domain period of T large enough to contain the entire signal. If the signal has settled to negligible values at the limits of the period, then no overlap can occur. The necessary period T can be determined by relating maximum target length to the travel time of the radar impulse.

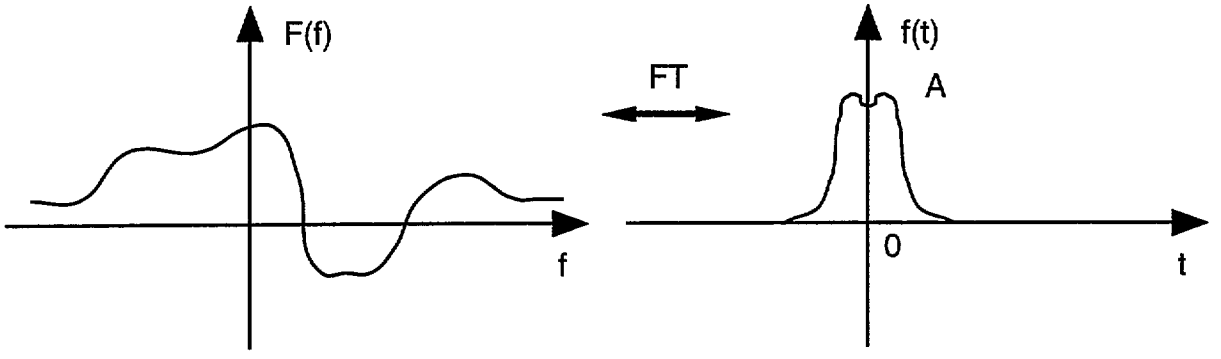

a) Frequency Domain Data

b) Time Domain Data

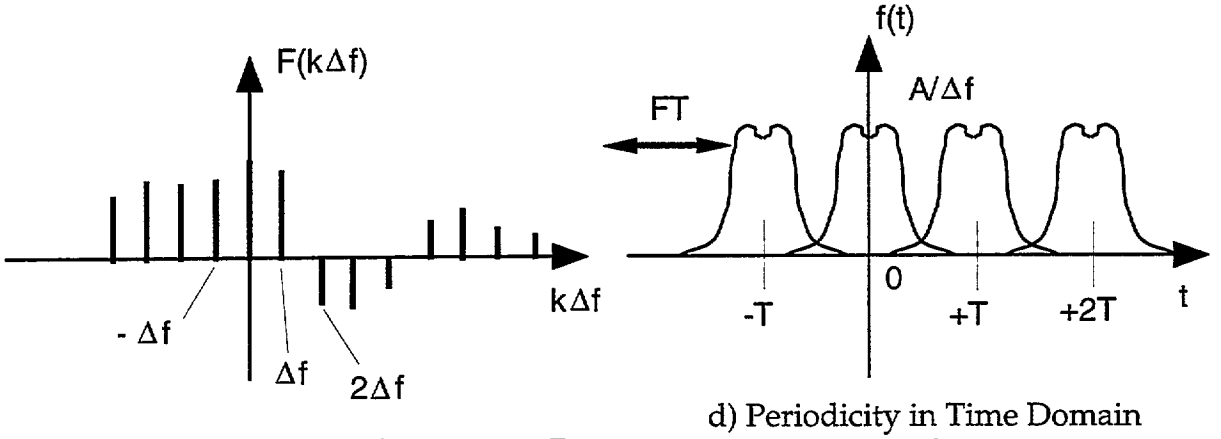

c) Discrete Sampling of Frequency Data

d) Periodicity in Time Domain Data Resulting from Discrete Sampling in Frequency Domain

Figure 3.6.1: Sampling Effects on the discrete Fourier Transform

$$T = \frac{D}{c} \qquad \text{eq.(3.6.12)}$$

where, in classical radar theory, D = the maximum target dimension and c = the speed of light. For construction metrology, D may be taken as the shortest one-way distance between the transmitter and roving receiver, whose position is desired.

Generally, a constant must be included to account for non-ideal filtering in the measurement, as well as delayed transmissions resulting from scattering mechanisms associated with the construction materials being penetrated. Therefore:

$$T \geq (1+k)\frac{D}{c} \qquad \text{eq.(3.6.13)}$$

Substitution of eq.(3.6.11) yields:

$$\Delta f \leq \frac{c}{(1+k)D} \qquad \text{eq.(3.6.14)}$$

which defines the maximum sampling interval needed to properly reconstruct x(t) f at a specified target distance. Now that the implications of sampling have been discussed, the integral shown in eq.(3.6.1) can be modified. Solving the integral over one period of X(f) using Riemann sum approximation results in:

$$x(t) = \Delta f \sum_{n=0}^{N-1} X(n\Delta f) e^{j2\pi n\Delta f t} \qquad \text{eq.(3.6.15)}$$

where N is the number of samples and Δf is the sampling interval. The function x(t) must be in a sampled form as well, so take N samples of x(t) over its period $1/\Delta$f. This defines the sample rate in the time domain as

$$\Delta t = \frac{1}{N\Delta f} \qquad \text{eq.(3.6.16)}$$

Substitution into eq.(3.6.16) yields:

$$x(k\Delta t) = \Delta f \sum_{n=0}^{N-1} X(n\Delta f) e^{j2\pi n\Delta f k\Delta t} \qquad \text{eq.(3.6.17)}$$

for k=0, ..., N-1 and

$$\Delta f \Delta t = \Delta f \frac{1}{N\Delta f} = \frac{1}{N} \qquad \text{eq.(3.6.18)}$$

Thus:

$$x(k\Delta t) = \Delta f \sum_{n=0}^{N-1} X(n\Delta f) e^{\frac{j2xnk}{N}} \qquad \text{eq.(3.6.19)}$$

This equation is known as the discrete Fourier transform. It can also be represented as an operation on N samples without reference to sample rates as:

$$x(k) = \sum_{n=0}^{N-1} X_s(n) e^{\frac{j2xnk}{N}} \qquad \text{for k=0, ..., N-1} \qquad \text{eq.(3.6.20)}$$

3.7 Developing a Practical NLS Survey System

As described above, it is possible to synthesize a narrow pulse result, with its inherently greater resolution, by summing the responses for a series of discrete frequency transmissions as indicated in eq.(3.6.20). In order to do this on a practical basis we make use of phasor notation, as shown in Figure 3.7.1

As suggested by Figure 3.7.1, any single sinusoidal transmission is fully characterized by three parameters, as:

$$A\cos(2\pi f_0 t + \varphi) \qquad \text{eq.(3.7.1)}$$

where

- A = amplitude
- φ = phase angle
- f_0 = oscillation frequency

The phase *shift* , in seconds, is given by:

$$\text{Phase shift} = \frac{-\phi}{2\pi f_o} \qquad \text{eq.(3.7.2)}$$

Phasor notation is commonly used to describe such waves in the frequency domain and is based on the equality:

$$e^{j\theta} = \cos\theta + j\sin\theta \qquad \text{eq.(3.7.3)}$$

where:

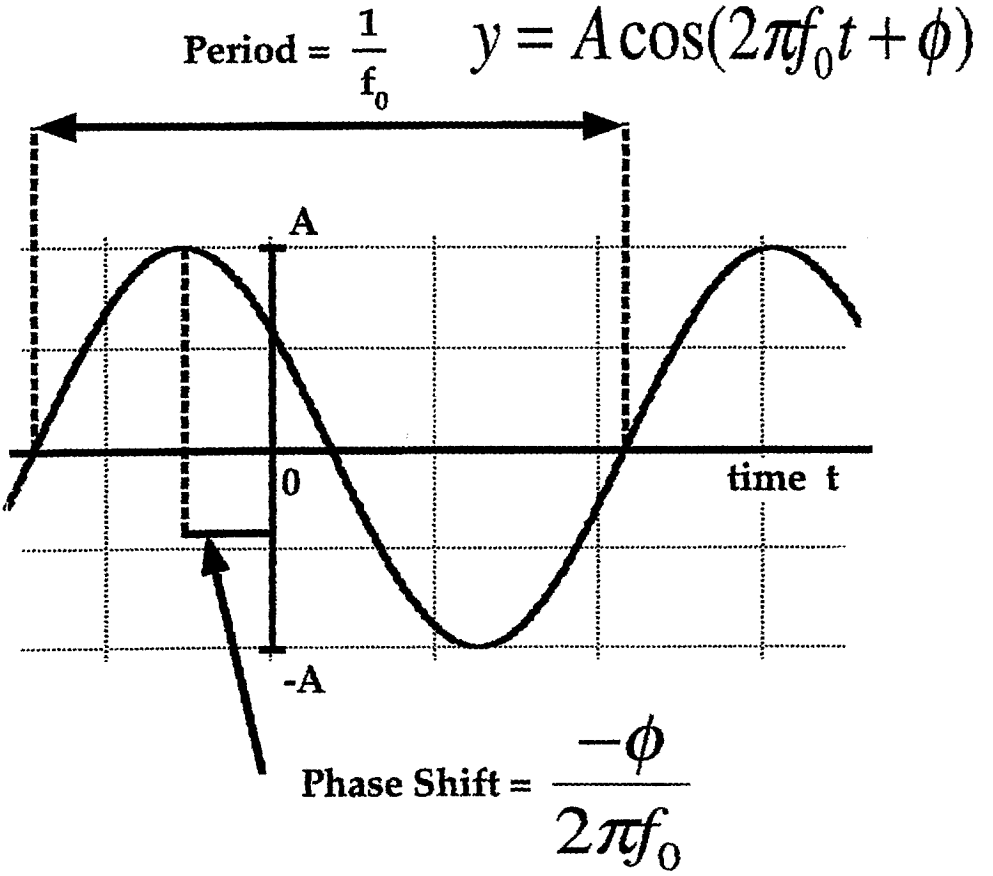

Figure 3.7.1: Phasor notation for a single frequency sinusoidal transmission.

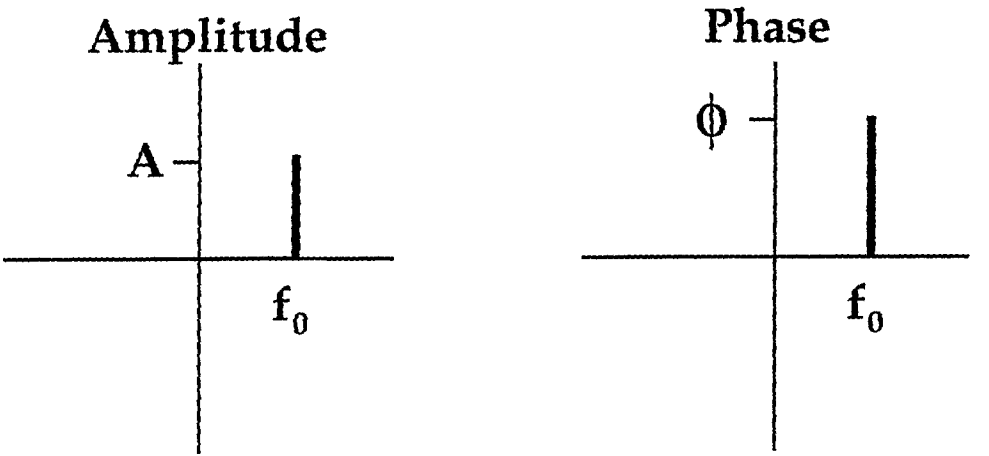

Figure 3.7.2: Amplitude versus frequency and Phase versus frequency plots for a single frequency sinusoidal transmission.

$$j = \sqrt{-1} \qquad \text{eq.(3.7.4)}$$

The real component, cos(θ) is defined as:

$$\cos\theta = \text{Real}\left\{e^{j\theta}\right\} \qquad \text{eq.(3.7.5)}$$

Substitution into eq.(3.5.1) yields:

$$\begin{aligned} A\cos(2\pi f_o t + \phi) &= A\ \text{Real}\left\{e^{j(2\pi f_o t+\phi)}\right\} \\ &= A\ \text{Real}\left\{e^{j2\pi f_o t}e^{j\phi}\right\} \\ &= \text{Real}\left\{Ae^{j\phi}e^{j2\pi f_o t}\right\} \end{aligned} \qquad \text{eq.(3.7.6)}$$

The term, $Ae^{j\varphi}$, is called the phasor representation of the sinusoid, $A\cos(2\pi f_0 t + \varphi)$. By plotting this phasor as a function of frequency, the sinusoid is completely characterized by the terms A, φ, and f_0, as shown in Figure 3.7.2

As suggested in section 3.4 above, complicated waveforms can be represented as a summation of multiple sinusoids, each sinusoid with a unique value of A, φ, and f_0. This can be expressed mathematically as:

$$x(t) \cong \sum_{n=0}^{N} A_n \cos(2\pi f_n + \phi_n) \qquad \text{eq.(3.7.7)}$$

alternatively, eq.(3.5.7) may be expressed in phasor notation as:

$$x(t) \cong \sum_{n=0}^{N} \text{Real}\left\{A_n e^{j\phi n} e^{j2\pi f_n t}\right\} \qquad \text{eq.(3.7.8)}$$

In this form, eq.(3.7.8) may be viewed as a method for converting sampled frequency domain data to the time domain. We now return to the concept of the time-of-arrival distancing system shown in Figure 3.4.1. The range error associated with this approach, as given in eq.(3.3.3) and eq.(3.3.6) is inversely proportional to the bandwidth, B. Thus, the wider the synthesized bandwidth, the finer the measurement. Practical hardware considerations will generally limit achievable bandwidths for NLS systems to approximately 20 Ghz. For tests conducted at NIST as part of this report, a bandwidth of 1.95Ghz was used.

The approach used for the NIST NLS experiments is shown in Figure 3.7.3. A sinusoidal pulse, $\tilde{A}$, with amplitude and phase at a single frequency, is launched from a transmitting antenna. This electromagnetic wave travels through free space

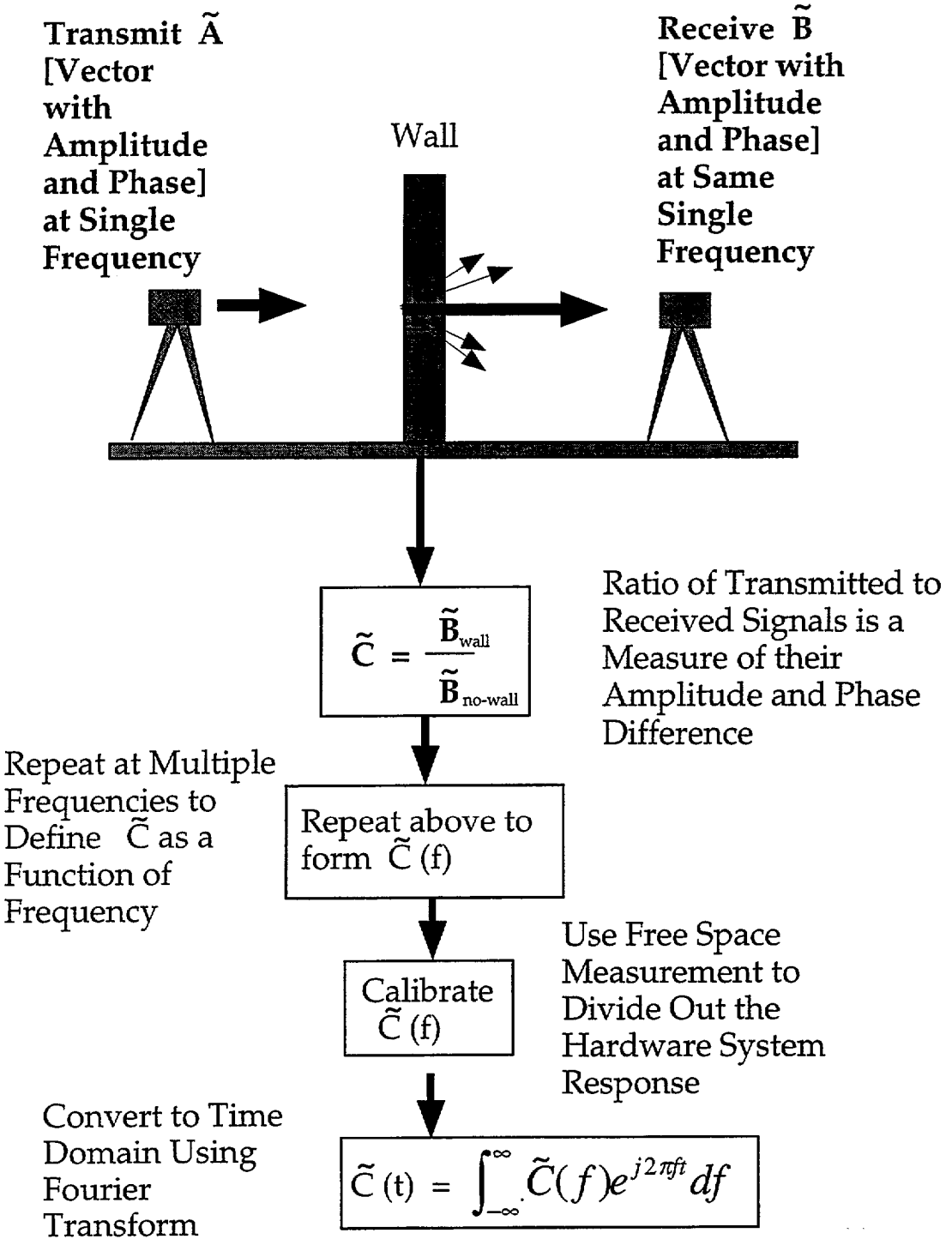

Figure 3.7.3: Impulse synthesis approach used for NIST tests. Composite signal with a bandwidth of 1.95 GHz was achieved by recording the response for discrete single frequency transmissions with a frequency step of 2 MHz. The composite time domain response was synthesized via fourier transform from the discrete frequency response data.

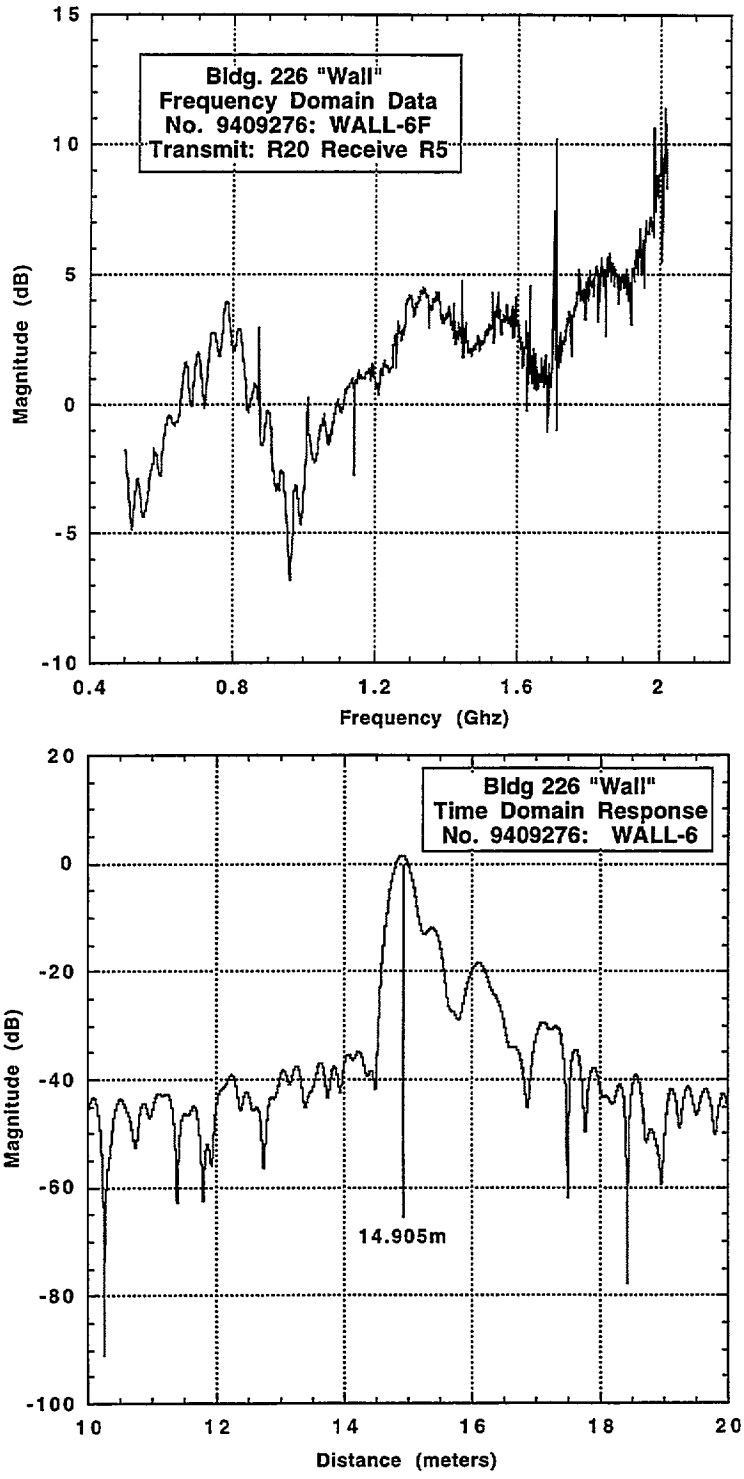

Figure 3.7.4: Frequency and Time domain response for a radar signal penetrating a 500 mm thick reinforced concrete wall at NIST. The time domain abscissa is expressed for convenience in meters, as opposed to seconds, where the distance is given by the transit time multiplied by the speed of light. This particular test was a "free space" calibration in which there were no obstacles between the transmitter and receiving antennas, other than atmospheric air. The exact (total station surveyed) distance between the electrical centers of the two antennas was 14.905 m.

and intervening obstacles , e.g. a reinforced concrete wall, and is eventually sensed at a receiving antenna. The received vector, $\tilde{B}$, will be different than the signal originally sent, owing to power (amplitude) losses and phase changes associated with propagation through lossy media. The ratio of the transmitted to received signals may be used as a measure of these amplitude and phase differences:

$$\tilde{C} = \frac{\tilde{B}}{\tilde{A}} \qquad \text{eq.(3.7.9)}$$

where:

$\tilde{A}$ = the measured signal when the target wall is <u>not</u> present.
$\tilde{B}$ = the measured signal when the target wall is present.

At this point the measurement is repeated for multiple frequencies to define the function $\tilde{C}$ as a function of frequency over the available bandwidth. Typical frequency steps used during the NIST study were 2 MHz, over a range from 50 MHz through 2 GHz, representing 975 discrete transmissions. Prior to a series of actual survey tests, free space measurements, in which the antenna pairs were placed on a grid with known distances separating the transmitter and receiver and with no intervening obstacles (save for atmospheric air), were conducted. The measured response for these free space measurements was used to compensate for the hardware system response. Finally, the time domain response is given by the Fourier transform as:

$$\tilde{C}(t) = \int_{-\infty}^{\infty} \tilde{C}(f) e^{j2\pi ft} df \qquad \text{eq.(3.7.10)}$$

This can be re-written for the discrete sampling case at NIST as:

$$\tilde{C}(t) = \sum_{n=0}^{N} \tilde{C}(f_n) e^{j2\pi f_n t} \qquad \text{eq.(3.7.11)}$$

where N = the total number of different frequencies used to synthesize the composite signal and f_n is the frequency corresponding to the currently sampled response. If uniform frequency steps, Δf, are employed (as was the case at NIST) then $f_n = n*\Delta f$. Typical results for a free space calibration of two radar antenna are shown in Figure 3.7.4.

References:

General Radar

Skolnik, M.I., (1980), "Introduction to Radar Systems," 2nd Ed., McGraw-Hill, New York, NY. ISBN 0-07-057909-1.

Pollard, Ernest C., (1982), "Radiation," 'One Story of the M.I.T. Radiation Laboratory,' The Woodburn Press: Science and People, Box 5653/ Duke Station, Durham, N.C., 1982.

Fink, Donald G., (1942), "Microwave Radar," Vol. 1: Theory and Practice of Pulsed Circuits, The Radiation Laboratory, Massachusetts Institute of Technology, Cambridge, MA, July, 1942.

M.I.T Radar School (1944), "Principles of Radar,", The Technology Press, Massachusetts Institute of Technology, Cambridge, MA 1944

Papoulis, A., (1977), "Signal Analysis," McGraw-Hill Inc., New York, NY, 1977. ISBN 0-07-048460-0.

Impulse Radar

Black, D. L., (1992), "An Overview of Impulse Radar Phenomenon," Proceedings IEEE 1992 National Aerospace and Electronics Conference, ASD/ENACR Wright-Patterson AFB, Ohio, 45433-6503; p. 320-6 Vol. 1.

Mccorkle, John W., (1992), "Overview of the HDL Impulse Synthetic Aperture Radar," IEEE Antennas and Propagation Society International Symposium, 1992 Digest; New York; p 1236 Vol. 3.

Strifors, H.C., Gaunaurd, G.C., Abrahamson, S., and Brusmark, B., (1993), "Scattering of Short EM-Pulses by Simple and Complex Targets in the Combined Time-Frequency Domain Using Impulse Radar," IEEE, 0-7803-0934-0, New York, 1993; pp. 70-75.

Stratis, G. K., Naik, V., Boerner, W., and Cole, J. B., (1992), "Wideband Polarimetric Radar Imaging," IEEE Antennas and Propagation Society International Symposium, 1992 Digest. p 1130 Vol. 2.

Daniels, D.J., (1993), "Developments in Impulse Radar Technology for Surface Penetrating Radar," IEE, Lodon, U.K., 1993, pp. 2/1-2/11.

Fowler, Charles A., (1992), "The UWB (Impulse) Radar Caper or "Punishment of the Innocent"," IEEE AES Systems Magazine, New York, 1992, pp. 3-5.

Chung, T., Carter, C.R., Masliwec, T., and Manning, D.G., (1992), "Impulse Radar Evaluation of Asphalt-Covered Bridge Decks," IEEE Transactions on Aerospace and Electronic Systems, Vol. 28, No. 1, New York, 1992, pp. 125-137.

Marcus, R. B., (1990), "Electromagnetic Compatibility Aspects of Impulse Radars," IEEE, CH2903-3/90/0000-0185, New York, 1990. pp. 185-188.

Fowler, C., Entzminger, J., and Corum, J., (1990), "Assessment of Ultra-Wideband (UMB) Technology," IEEE AES Magazine, Washington D.C., 1990, pp. 45-49.

Caldecott, R., Poirier, M., Scofea, D., Svoboda, D.E., and Terzuoli, A.J.,(1988), "Underground Mapping of Utility Lines Using Impulse Radar," IEE Proceedings, Vol. 135, Pt. F, No. 4, New York, 1988, pp. 343-353.

Blejer, D., Frost, C., and Scarborough, S., (1994), "VHF Ground Penetration Measurements of Buried and Partially Buried Trihedrals," Massachusetts Institute of Technology, Lexington, MA., 1994,

Blejer, D.J., Wittmann, R.C., and Yaghjian, A.D., (1992), "On-Axis Fields From a Circular Uniform Surface Current," Proceeding of International conference on Ultra-Wideband Short-Pulse electromagnetics, 1992, pp. 1-8.

Scarborough, S., (1995), "Tutorial on Spread Spectrum Radar," Massachusetts Institute of Technology, Lexington, MA., 1995, personal communication to Bill Stone, NIST, Gaithersburg, MD.

RF Propagation Through Engineering Materials

de Toledo, A. F., and Turkmani, A. M. D., (1992), "Propagation Into and Within Buildings at 900, 1800 and 2300 MHz," IEEE, 0-78030673, New York., 1992, pp. 633-636.

Zabela, R., and Bostian, C. W., (1992), "Measurements of Building Penetration by Low Orbit Satellite Signals at VHF," IEEE, 0-78030730, New York, 1992, pp. 604-607.

Matthews, P. A., and Abu Bakar, A. H., (1994), "Direction of Arrival of Radio Signals inside and outside Buildings," IEEE 44th Vehicular Technology Conference, The Univ. of Leeds, U.K.; p 1754-8, Vol. 3.

de Toledo, A. F., Lewis, D. G., and Turkmani, A. M. D., (1990), "Radio Propagation Into Buildings at 1.8 GHz, IEEE Colloquium on University Research in Mobile Radio, Digest No. 143, p. 3/1-5; Dept. of Electrical Engineering and Electronics, The University of Liverpool, Liverpool, U.K.

Iwasaki, T., Freundorfer, A. P., and Iizuka, K., (1994), "A Unidirectional Semi-Circle Spiral Antenna for Subsurface Radars," IEEE, Vol. 36, No. 36, 0018-9375, New York, 1994, pp. 1-6

Nicollin, F., Barbin, Y., Kofman, W., Mathieu, D., Hamran, S., Bauer, P., Achache, J., and Blamont, J., (1992), "An HF Bi-Phase Shift Keying Radar: Application to Ice Sounding in Western Alps and Spitsbergen Glaciers," IEEE, Vol. 30, No. 5, 0196-2892, New York, 1992, pp. 1025-1033.

Damosso, E., Paraboni, A., and Protto, F., (1993), "Indoor Propagation Measurements: Application to Mobile Channel Modeling," IEE, London, U.K., 1993, pp. 146-149.

Kashyap, S., Burton, M., and Louie, A., (1992), "EM Field Penetration Inside the Bridge of a Ship," Defense Research Establishment Ottawa, Ottawa, Ontario, Canada, 1992, pp. 10)

Yamaguchi, Y., Honda, T., Sengoku, M., Motooka, S., and Abe, T., (1992), "On the Reduction of Wave Propagation Loss in Tunnels," IEEE, Vol. 34, No. 2, 0018-9375, New York, 1992, pp. 78-85.

Turkmani, A.M.D., de Toledo, A.F., (1991), "Radio transmission at 1800MHz Into, and Within Multistory Buildings," IEEE Proceedings-1, Vol. 138, No. 6, 1991, New York, pp. 577-584.

Aguirre, S., Loew, L.H., and Yeh, L. (1994), "Radio Propagation into Buildings at 912, 1920, and 5990 Mhz using Microcells," 1994 3rd Annual International Conference on Universal Personal Communications, IEE, New York, Sept. 27-Oct. 1, 1994. p 129-34.

<u>**Potential Modeling & Compensation for Propagation Delay**</u>

Blejer, Dennis J., (1981), "Some Mathematical Aspects of EMP Propagation Through A Conducting Medium," GTE Memorandum 0070-I-2764.

Kiang, Jean-Fu, (1992), "Geometrical Ray Tracing Approach for Indoor Wave Propagation in a Corridor," IEEE, 0-7803-0591, 1992, pp. 04.06.1-04.05.6.

Miyazaki, Y., and Tanoue, K., (1989), "Tapered and Graded Index Type Electromagnetic Absorbers Using Inhomogenous Lossy Dielectric Layers," IEEE, New York, U.S.A., 1989, pp. 803-807.

Miyazaki, Y., and Tanoue, K., (1990), "Electromagnetic Absorption and Shield Properties of Lossy Composite Multilayers," IEEE, CH2903, New York, 1990, pp. 370-374

Linner, L.J., (1989), "Exact Formulas for Wave Impedance and Propagation Constants of Homogenous, Lossy Dielectric and/or Magnetic Materials," IEEE Transactions on Antennas and Propagation, 0018-926x, Vol. 37, No. 3, New York, 1989. pp. 410-411.

Chapter 4: Surveying Through a 500 mm Reinforced Concrete Wall

4.1 Test Description

As part of the initial study to determine the feasibility of NLS metrology an experiment was conducted on the grounds of the NIST campus in Gaithersburg, Maryland. In this experiment a 500 mm thick, reinforced concrete wall was placed between the transmitter and receiver to simulate a significant radar obstacle that would typically be found at a construction site.

4.1.1 Radar Hardware

The radar system was based on a Hewlett-Packard HP8530 network analyzer/microwave receiver combined with an HP 83623A frequency synthesizer, HP 8511A frequency converter, and an HP 85330A multiple channel controller. A 486 PC-based computer network performs radar control functions, while data calibration and data management are handled with a Pentium PC. The wideband pulse modulators used for hardware gating and the computer software for system control and data processing were custom developed by Flam and Russell, Inc. of Horsham, PA. MIT Lincoln Lab developed the overall system (detailed in Figure 4.1.1.1) and cooperated with NIST researchers on all aspects of the field research and subsequent data reduction. The radar was field-portable with the electronics and computational hardware based in a mid-size van. Table 4.1.1 lists characteristics of this system.

Table 4.1.1: Wideband Radar Specifications

Frequencies	0.5-2 GHz, 2-18 GHz
Bandwidth	Antenna limited
Waveform	Gated CW
Pulse Width	10 ns to 500 ns
PRF	50 kHz to 5 MHz
Polarization	Fully polarimetric
Output Power	20 dBm
Dynamic Range	80 dB
Noise Floor	-100 dBm

The radar is fully polarimetric and operates over two frequency bands (0.5-2 GHz and 2-18 GHz; only the former was used for the tests reported herein). A dual-polarized Quad-Ridged Horn antenna, model WJ-48450 from Watkins-Johnson (Figure 4.1.1.2), was used for the NIST experiments. This unit has a frequency

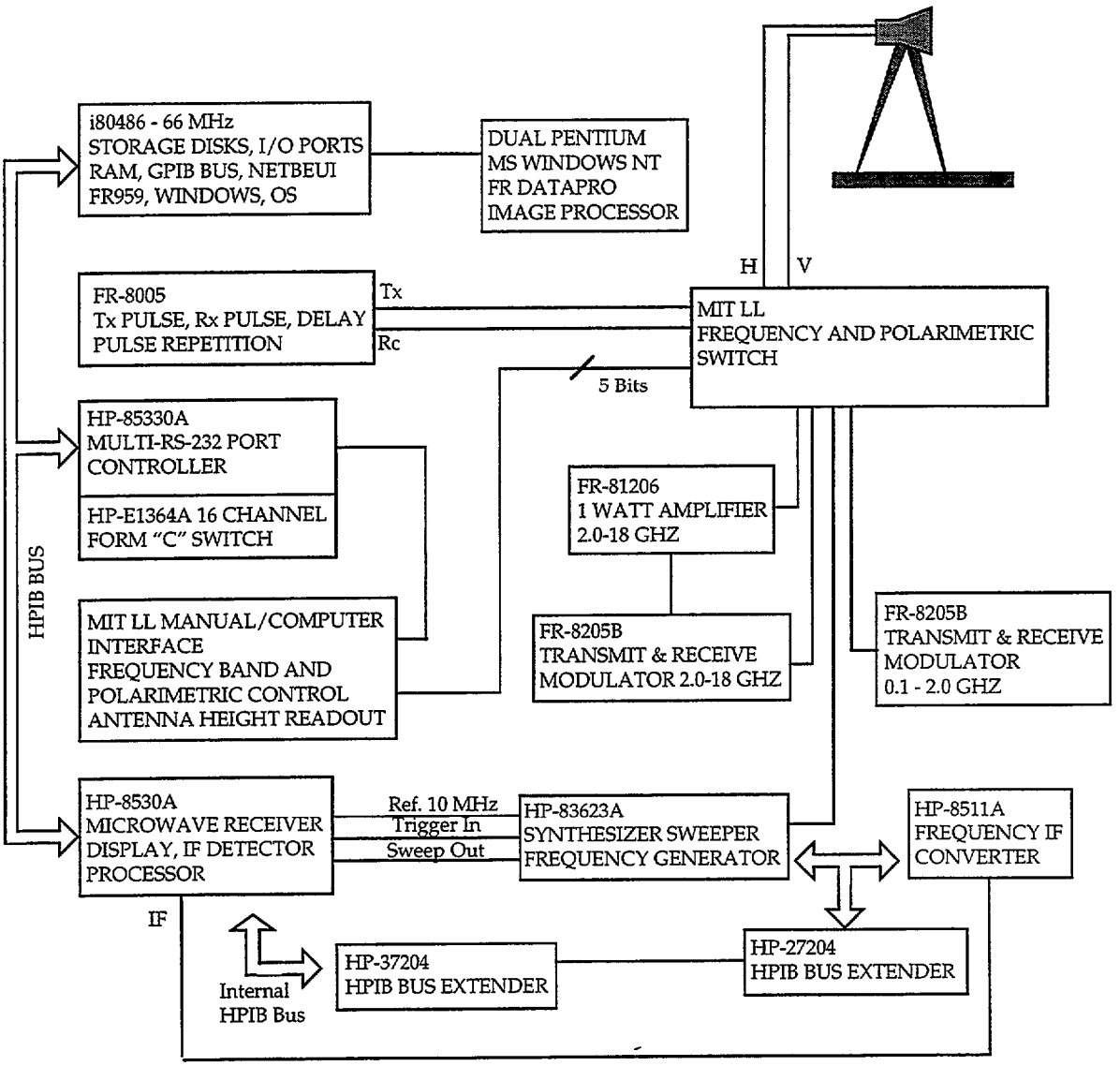

Figure 4.1.1.1: Schematic of the spread spectrum radar developed by MIT/Lincoln Labs which was used for the initial NLS experiments at NIST.

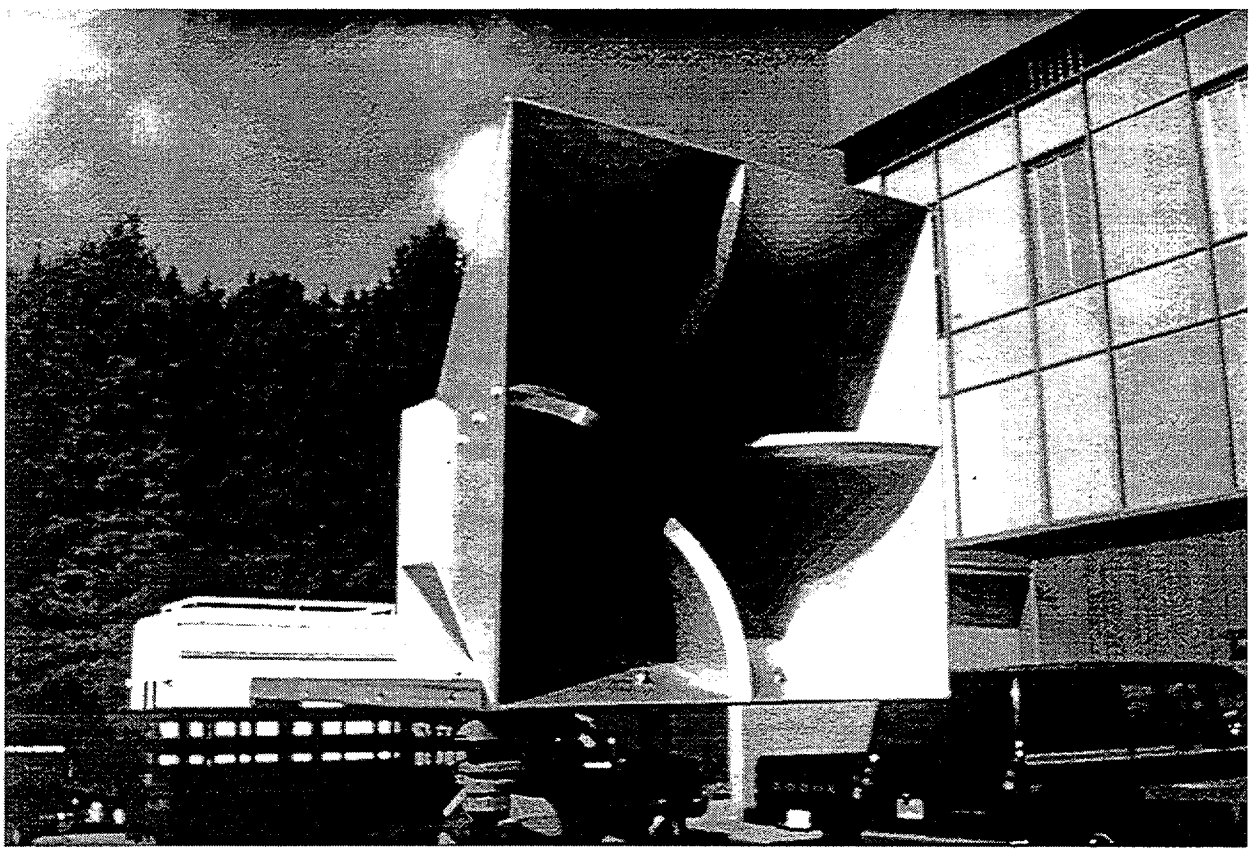

Figure 4.1.1.2: Watkins-Johnson WJ-4850 Quad-Ridged Horn antenna used for the NLS tests at NIST. Frequency coverage is 0.5-2.0 GHz. The unit is capable of simultaneous (or independent) horizontal and vertical polarization.

coverage of 0.5-2 Ghz and is capable of simultaneous horizontal and vertical polarization. Complete specifications are given in Table 4.1.2. These are high gain, directional antennas which were used both for transmission and reception of the radar signals and served well for the purposes of straight line distance measurements. In an actual construction site operation, where several independent transmitters would need to be deployed to insure a unique 3D position location, the receiving unit must be omnidirectional.

Table 4.1.2: Performance Specifications for NLS Antenna

Model No.	WJ-48450
Frequency Range	0.5-2GHz
VSWR (Max.)	3.0:1
Gain (Nominal)	7-12 dBi
Polarization	Dual Linear
F-to-B Ratio	20 dB
3 dB Bandwidth; E-Plane	70°- 50°
3 dB Bandwidth; H-Plane	70°- 25°
Cross Polarization	20 dB Min.
Squint (Max.)	5°
CW Power (Average)	70 w
CW Power (Peak)	3 kw

4.1.2 Test Wall

At the inception of this project it was presumed possible, but not certain, that the concepts described in Chapter 3 could be used to obtain repeatable distances between a spread spectrum radar transmitter and a receiver located on the opposite side of a reinforced concrete wall -- a typical serious EM transmission obstacle that would be encountered in everyday practice at a construction site. It was felt that if the concept could be shown to work for a 500 mm thick reinforced concrete wall that it would prove a viable system at a large number of locations both for original construction as well as retrofit and repair. With this in mind, a reinforced concrete wall of known properties and geometry was erected on the grounds of the NIST Gaithersburg campus in the loading bay outside of Building 226.

The "wall" consisted of two existing 500 mm thick reinforced concrete slab specimens which had been cast some years earlier for research in non-destructive testing. The bottom slab measured 4.5 x 2 m and formed the base of the stack. A smaller 2 m wide x 2.5 m tall slab was stacked on top of the former and was grouted in place to insure stability. This target wall (see Figure 4.1.2.1) was then placed at the zero datum of a linear test grid (Figure 4.1.2.2) which had previously been laid out. A precision survey (total station & EDM) was conducted to establish the three

a) (below): Side view of reinforced concrete target wall.

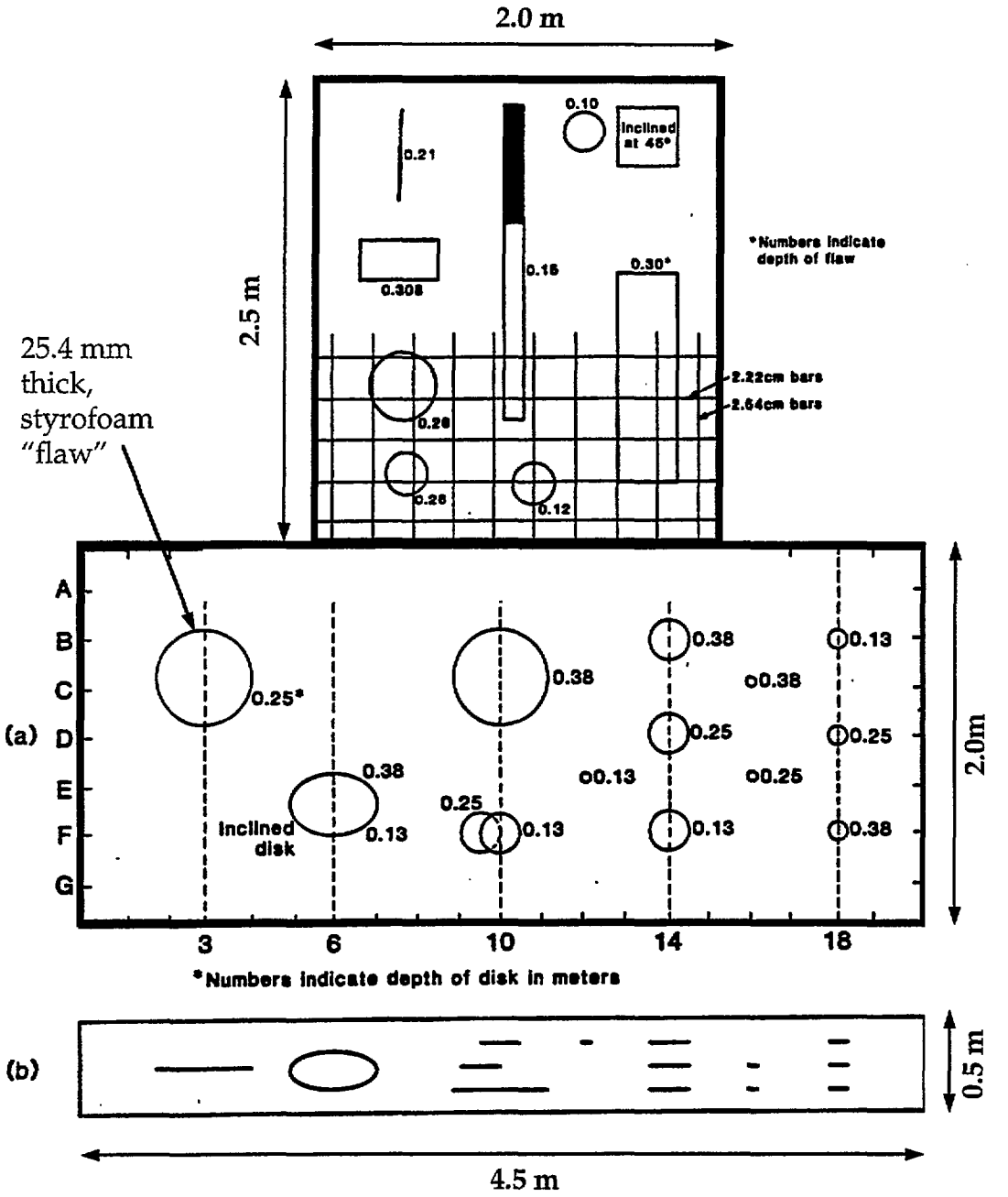

b) (above) Top view of target wall.

Figure 4.1.2.1: Details of the reinforced concrete target wall used for the Building 226 test series conducted at NIST.

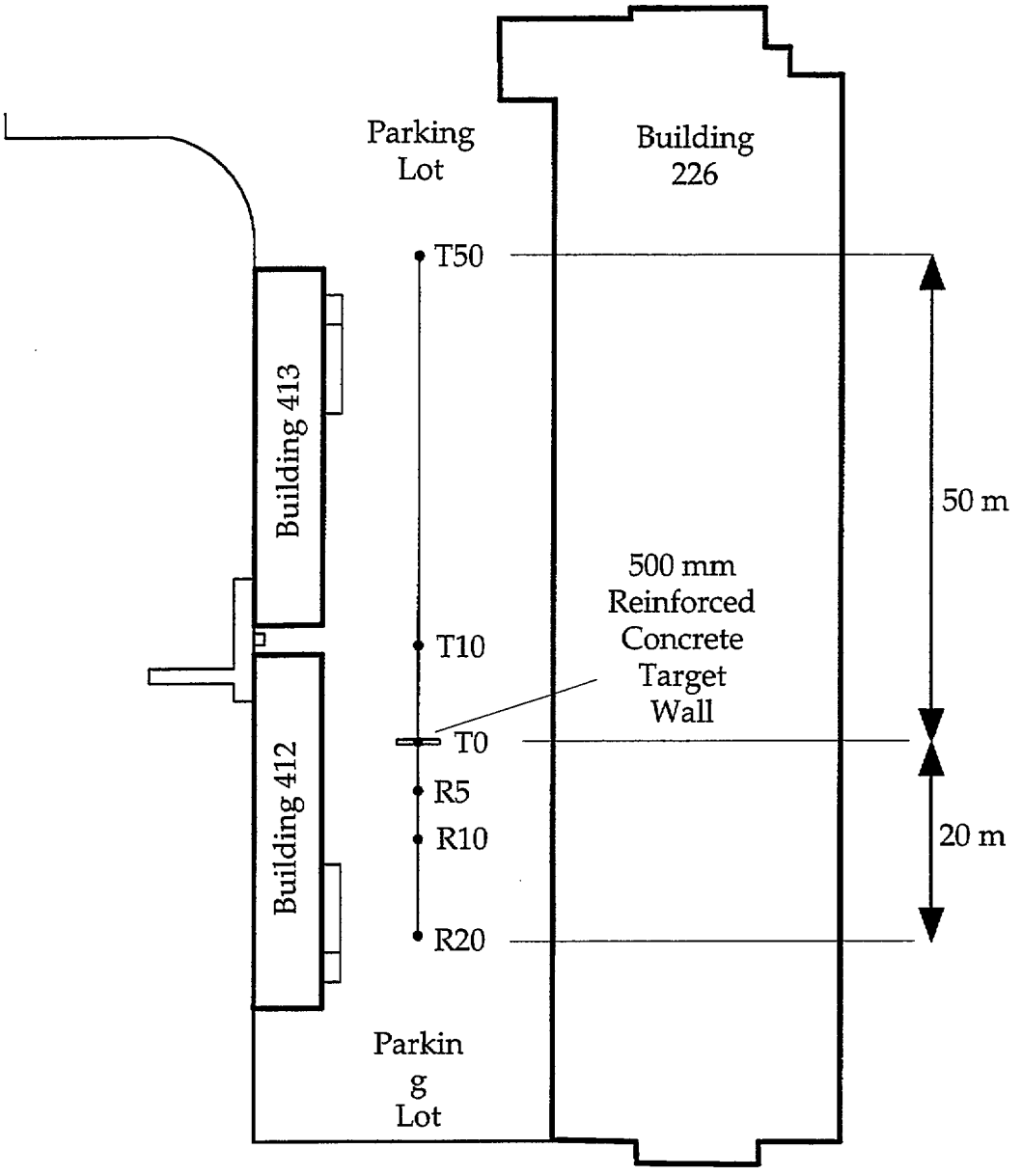

Figure 4.1.2.2: Building 226 NLS Test Setup Geometry. Reinforced concrete wall (500 mm thick) obstacle is centered on station T0. "T" station prefix indicates nominal Transmitter antenna benchmark; "R" station prefix indicates nominal Receiver antenna benchmark. Station numbers indicate nominal distance of benchmark from the wall centerline in meters. The test setup was established in a paved parking lot located between NIST buildings 226 and 413/412.

dimensional coordinates of the various points along this grid. The station was a Topcon GTS3B 1-second EDM with an accuracy of 2 mm over a 100 m baseline. Thes grid location data are presented in Table 4.1.3.

Table 4.1.3: Building 226 Linear NLS Test Range

All units are mm relative to the NIST master site coordinate system

NORTH	EAST	UP	NAME
4408843.	4247367.	3048.	"T-50"
4409563.	4286962.	3064.	"T-10"
4409760.	4297867.	3058.	"T-0"
4409849.	4302962.	3047.	"R-5"
4409934.	4307869.	3044.	"R-10"

4.2 Test Procedure

Special mounting fixtures were developed in order to adapt the Watkins-Johnson Quad-ridged antennas to standard surveyors field tripods. The antenna mount was designed to attach to a standard tripod tribrack (a removable puck-like adapter to the top of the tripod which usually contains its own optical plummet). The assembly was optically aligned with the benchmark station (one of the five listed inTable 4.1.3) and the height of the center of the antenna recorded in a logbook for each particular setup geometry (see Figure 4.2.1). The same was done for both transmitting and receiving antennas. These elevations were factored into the distance calculation when comparing to the previously surveyed benchmarks (see Table 4.3.1). A typical test setup, transmitting at T50 and receiving at R5, is shown in Figure 4.2.2.

Prior to any day's testing, a "free space" measurement was made to establish system frequency response characteristics. In this test, the transmission and receiving antennas were set up on benchmarks with no intervening obstacles between the two. This response was later used, as described in Section 3.5, to divide out system response from the desired response signal.

For each possible combination of receiver and transmitter position, as defined in Table 4.1.3, there were also two transmission plane wave polarizations and two receiver polarizations were possible. Two such combinations were used for the NIST tests: horizontal (HH for horizontal transmit, horizontal receive) and vertical (VV for vertical transmit, vertical receive). The efficacy of these combinations for building material penetration was unknown at the time of testing, but it was believed that HH polarization would lead to unwanted ground plane reflection as the beam bounced off the parking lot pavement, leading to multipath effects. For each test configuration, 20 sets of data scans were taken in order to arrive at an averaged response signal in the frequency domain. This averaged frequency

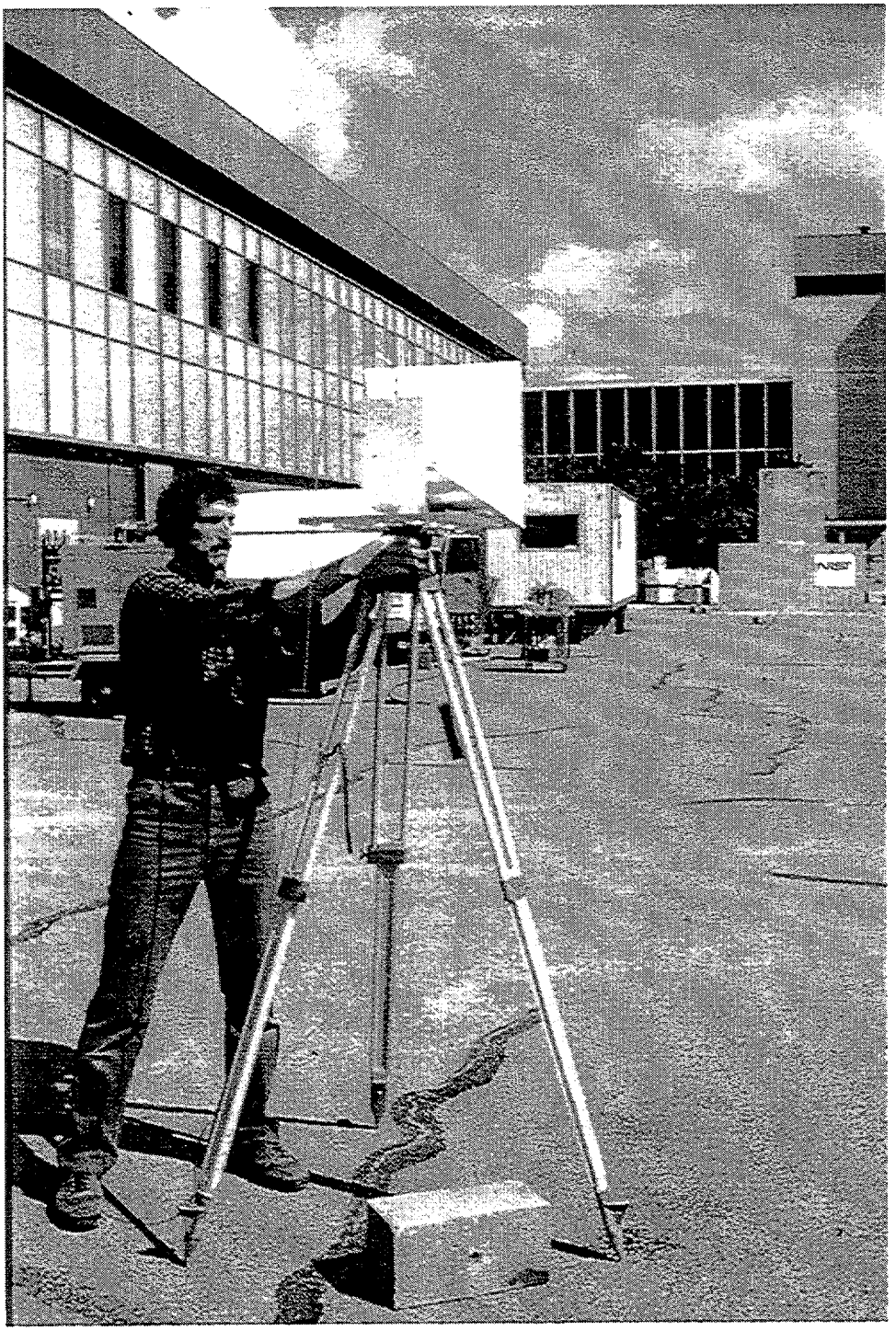

Figure 4.2.1: Setup and leveling of the transmission antenna over pre-surveyed benchmark. Antenna was affixed to a special adapter plate such that its electrical center coincided with the axis of a standard surveyor's tribrach optical leveling adapter. Height of the antenna center to the benchmark was recorded.

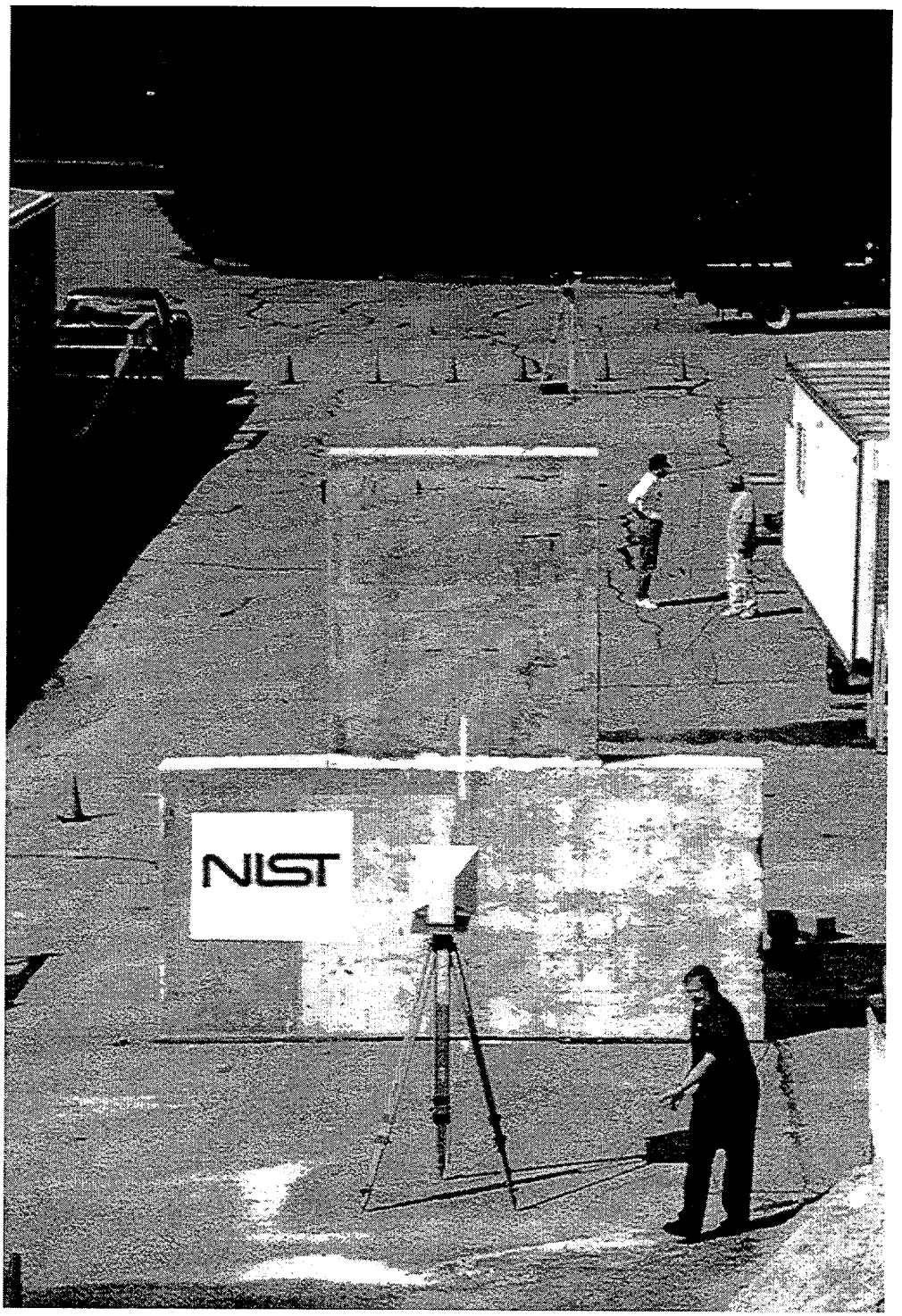

Figure 4.2.2: Field test at Building 226. Transmitter antenna (top) is positioned atop benchmark T50; receiving antenna is positioned over benchmark R5. Office trailers at left and right produced spurious reflected signals while other multipath routes originated via diffraction around the test specimen.

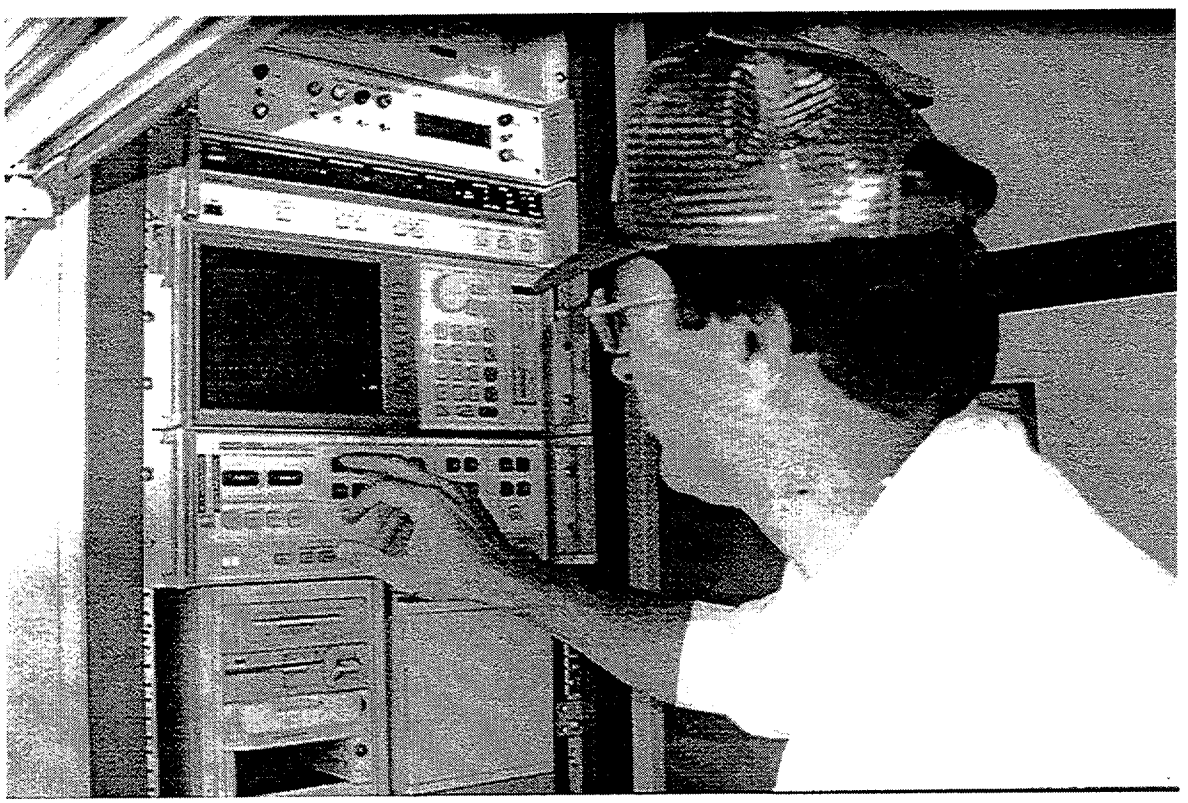

Figure 4.2.3: Field processing of the frequency domain response was carried out in the Lincoln Lab mobile van.

response was then fed into the real time "chirp-z" transform in order to obtain a time domain response. Both data acquisition and real time processing took place in the mobile Lincoln van (see Figure 4.2.3). Due to new digital signal processing (DSP) circuitry, such data processing can be economically conducted in real time at a field construction site -- a requirement if this type of technology is to make its way into the construction industry.

4.3 Results

The results of the first series of NLS tests on the Building 226 test range are presented in Table 4.3.1 (complete frequency and time domain plots are provided in Appendix A). There are several points regarding this data that require elaboration. As described earlier, data was acquired in the frequency domain as a series of discrete amplitude (voltage) responses at each frequency in the sweep range. The first response was at 0.5 GHz with subsequent responses obtained at 2Mhz intervals through 2 Ghz. A typical sample of this data is shown in Figure 3.7.4a. Unless noted as a "free space" measurement, the intended transmission path was through the 500 mm thick reinforced concrete wall described in Section 4.1. The magnitude (y-axis) in Figure 3.7.4a is representative of the response for each frequency, expressed in dB, and it can be inferred that greater amounts of radar energy were transmitted through the wall at those frequencies having a greater magnitude value in the plot shown in Figure 3.7.4a. If a particular band of frequencies were shown to have markedly better transmission properties through reinforced concrete, then this would be of significance in the design of NLS systems targeted for the construction community. When the data shown in Figure 3.7.4a is processed using the chirp-z transform it produces the time domain plot shown in Figure 3.7.4b. Keeping in mind that light in air travels at approximatelly 0.33 m per nanosecond, we may convert the time domain response to magnitude as a function of distance, rather than nanoseconds. The x-axis scale in Figure 3.7.4b, and all subsequent time domain plots, are thus given in meters, since this directly bears on the information of interest, which is the determination of the distance between the transmitter and receiver. Figure 3.7.4b is typical of radar response data in which a region of noise surrounds the response of a true target, represented as a peak on the time domain plot. In general, any signal peak which lies in excess of 10 dB above the noise level represents a valid target distance. For reasons described below, however, there may be more than one valid peak associated with one true transmitter to receiver distance.

Shortly after the preliminary data became available, it was apparent that the results were being affected by both "clutter" (unwanted reflections from obstacles other than the target wall) and diffraction scattering around the finite sized barrier wall. The transmitting radar acts like a flashlight, illuminating the area ahead of it in a broad cone. Adjacent to the test wall was a line of temporary office buildings with aluminum side walls. Just as with a flashlight, a portion of the radar beam reached

those walls and was reflected towards the receiving antenna which subsequently registered its arrival. Likewise, a portion of the beam followed a path leading to the inside corner formed at the mid-height of the stacked wall and was diffracted (bent) around this in such a fashion that a portion of this signal also reached the receiving antenna. The third possible transmission path was the intended one, i.e. directly through the wall. The first two situations produce what is known in the electronic communications and radar communities as "multipath effects." Their effect is to produce false targets which appear as peaks in the time domain plot. For reasons which will be explained in further detail in Chapter 6, the second arrival peak was generally (but not always) the one associated with the direct through-the-wall transmission for this particular set of tests. In all but one case conducted at the enclosed test range at Building 202 (Chapter 5) the first arrival peak was the one associated with the direct transmission signal.

The Δ Error column in Table 4.3.1 gives the difference, in meters, between the precision surveyed distance between a pair of benchmarks, identified as T-Pos and R-Pos, and the NLS time-of-flight derived distance between the same set of benchmarks. Nearly all of this error results from delayed propagation of the transmitted wave as it passes through the reinforced concrete wall. At the particular frequency range employed for these tests it is apparent, and will be derived later in Chapter 6, that the reinforced concrete acts as a medium which slows the wave. Just as a glass lens will alter, and scatter, incoming light rays, so to will a non-conducting construction material. Further, light traveling through such a lens (both for the visible spectrum being transmitted through a transparent lens and an invisible radar beam being transmitted through an opaque concrete wall) will travel at some speed less than c, its velocity in a vacuum. Depending on the material, it may travel up to ten times slower than it does in a vacuum.

The critical conclusion that can be drawn from Table 4.3.1 (and as detailed in Section 6.3 later in this report) is that it <u>is</u> possible to "survey through solid concrete." Many secondary questions -- such as what are the range limitations?; what are the accuracy limitations?; and can the errors be compensated or calibrated? -- may be addressed through analytical simulations and further experiments and empirical modeling.

It is important to note that the power levels employed for these tests were extremely low -- on the order of a milliwatt. That is around two orders of magnitude less than that permitted for un-licensed walkie-talkies sold at children's toy stores. The radiation is non-ionizing at these levels and in fact could be safely increased 1000-fold and still fall within the purview of mobile communications power levels permited by the FCC. Because these are broad-band signals, special permits may be required for operation at higher power levels in urban environments.

Table 4.3.1: Building 226 Test Range NLS and EDM Survey Data

T-Pos = Survey position of transmitter; R-Pos = Survey position of receiver
T-Hgt = Height of transmitter; R-Hgt = Height of receiver
Survey = Separation distance as surveyed by NIST using mm precision EDM equipment.
Radar = Separation distance as seen by Lincoln radar
Δ Error = Difference between survey and radar results
ND = valid radar detection not available.
Note: Total Penetration = 500 mm Reinforced Concrete Wall

File	Polarity	T-Pos	R-Pos	T-Hgt	R-Hgt	Survey	Radar	Δ Error
94092703	Vertical	T-10	R-5	1.98	2.027	16.0026	16.766	0.763
94092704	Horizontal	T-10	R-5	1.98	2.027	16.0026	16.765	0.762
94092705	Horizontal	T-10	R-5	1.98	2.027	16.0026	ND	ND
94092706	Vertical	R-20	R-5	2.00	2.027	14.9052	Free Space	Free Space
94092707	Horizontal	R-20	R-5	2.00	2.027	14.9052	Free Space	Free Space
94092708	Horizontal	R-20	R-5	2.00	2.027	14.9052	Free Space	Free Space
94092709	Horizontal	T-50	R-5	2.01	2.027	55.6041	ND	ND
94092710	Vertical	T-50	R-5	2.01	2.027	55.6041	56.580	0.976
94092711	Vertical	R-10	T-50	1.978	N/A	60.5118	ND	ND
94092712	Horizontal	R-10	T-50	1.978	N/A	60.5118	61.274	0.762
94092713	Horizontal	R-20	T-50	N/A	N/A	70.5093	71.420	0.911
94092714	Vertical	R-20	T-50	N/A	N/A	70.5093	71.400	0.891
94092715	Vertical	R-20	T-10	N/A	1.978	30.9078	31.720	0.812
94092716	Horizontal	R-20	T-10	N/A	1.978	30.9078	31.840	0.932
94092717	Horizontal	R-10	T-10	2.03	1.978	20.9103	21.780	0.870
94092718	Vertical	R-10	T-10	2.03	1.978	20.9103	ND	ND
94092719	Vertical	R-5	T-10	2.07	1.978	16.0027	16.790	0.787
94092720	Horizontal	R-5	T-10	2.07	1.978	16.0027	16.940	0.937
94092721	Vertical	R-5	T-50	2.07	1.986	55.6042	56.580	0.976
94092722	Horizontal	R-5	T-50	2.07	1.986	55.6042	ND	ND
94092723	Horizontal	T-50	R-10	1.985	1.986	60.5118	ND	ND
94092724	Vertical	T-50	R-10	1.985	1.986	60.5118	61.330	0.818
94092725	Vertical	T-50	R-20	1.985	1.970	70.5093	71.280	0.771
94092726	Horizontal	T-50	R-20	1.985	1.970	70.5093	71.330	0.821
94092727	Horizontal	T-10	R-20	1.955	1.970	30.9078	31.840	0.932
94092728	Vertical	T-10	R-20	1.955	1.970	30.9078	31.800	0.892
94092729	Vertical	T-10	R-10	1.955	1.990	20.9103	21.750	0.840
94092730	Horizontal	T-10	R-10	1.955	1.990	20.9103	21.765	0.855

Chapter 5: Surveying Through Building Walls

5.1 Test Description (Building 202)

The second phase of the NLS proof-of-concept tests were conducted at Building 202 on the grounds of the NIST, Gaithersburg campus. As with the previous tests of the reinforced concrete wall, a grid of precision surveyed benchmarks were established at the test. In this particular case approximately half of the points were located in a 90° arc around the outside parking lot on the northwest corner of the building (see Figure 5.1.1 and 5.1.2). The remainder were permanently drilled and set into the concrete slab comprising the floor of the Large Scale Structures Test Facility. These two grids provided a wealth of real-world NLS surveying situations, including obstacles such as brick and masonry block walls (in some cases multiple sets of such walls), stacks of wide flange steel girders; rollup metal doors; metal wall paneling; and a 2 m thick, heavily reinforced concrete structural reaction wall. As will be discussed below, varying degrees of success were achieved in each of the above scenarios.

The precision surveyed positions of the Building 202 test range benchmarks (using the same procedures described in Chapter 4) are presented in Table 5.1.1. On the basis of these data true horizontal distances between points were calculated. It is these true horizontal distances that are reported in subsequent tables comparing radar test data to the benchmark grid.

Table 5.1.1: Building 202 NLS Test Range

[all units are mm relative to the NIST site coordinate system]

North	East	Up	Station
Inside Stations			
4259404.	3636286.	25912.	"G"
4278244.	3617447.	25920.	"A"
4271776.	3623910.	25921.	"C"
4277593.	3629731.	25914.	"D"
4266469.	3629210.	25922.	"E"
4272280.	3635030.	25919.	"F"
4265231.	3642105.	25916.	"H"
4264717.	3616840.	25917.	"I"
4283874.	3623451.	25902.	"B"

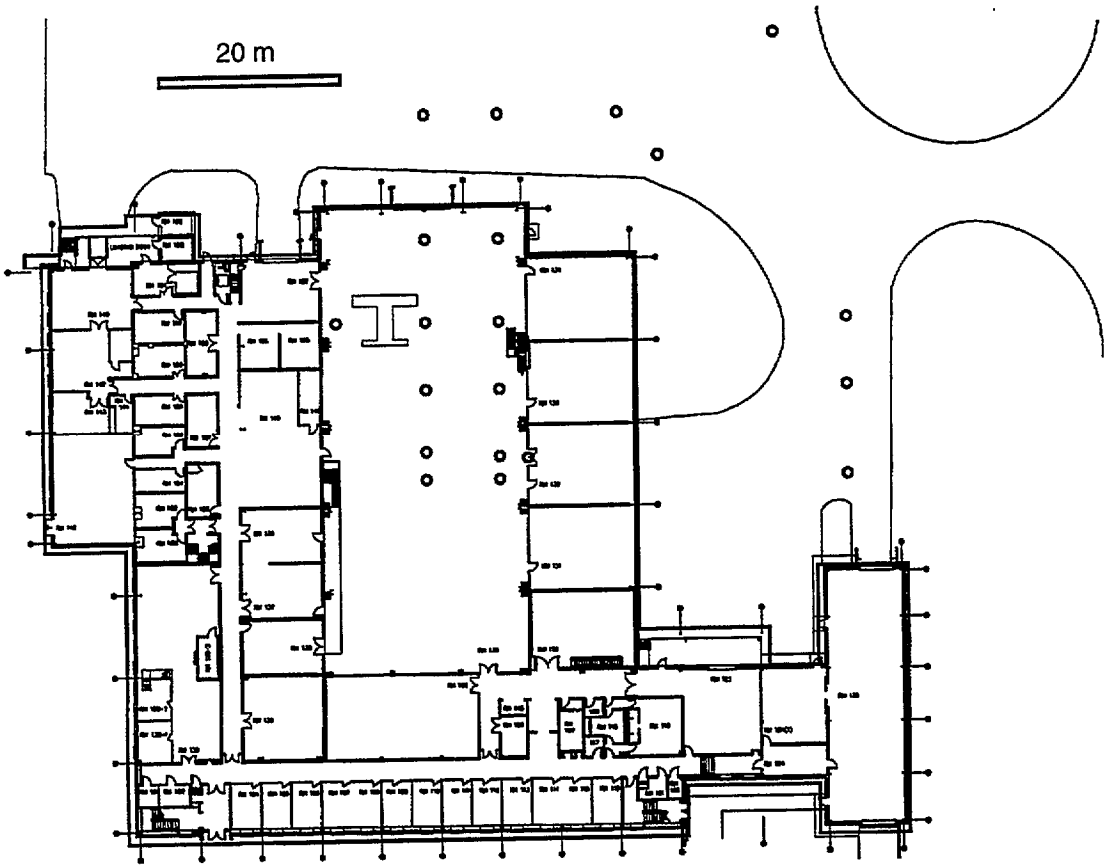

Figure 5.1.1: Plan view of the Building 202 NLS Test Range at NIST. Thick circles represent precision surveyed benchmarks. Those outside the building were used as radar transmission points while those inside were used to position roving receivers. Specific details are given in Figure 5.1.2.

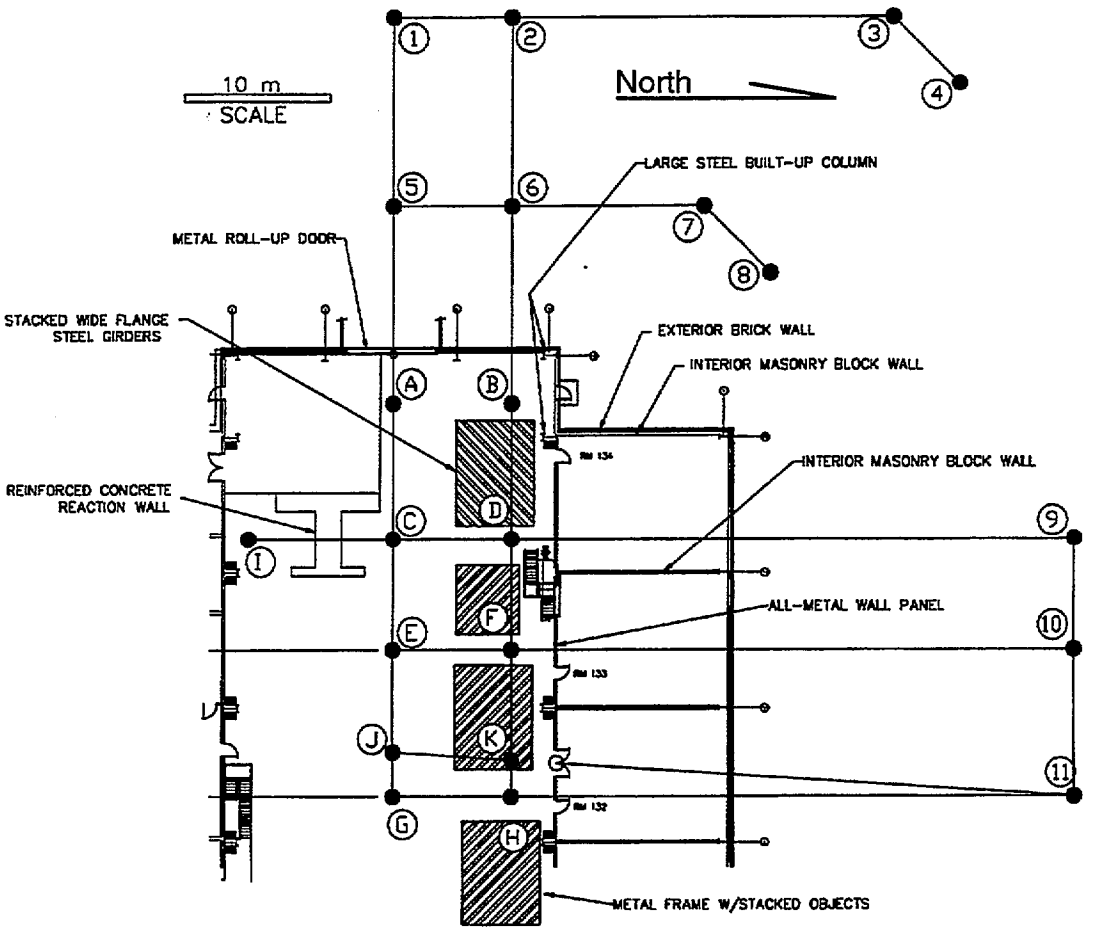

Figure 5.1.2: Detailed drawing of northwest corner of Building 202 at NIST. Numbered stations correspond to exterior benchmarks established in the building's west parking lot. These stations served as the radar transmission sites. Lettered stations correspond to interior benchmarks used to position the receiving antenna.

Outside Stations

4302687.	3604644.	25228.	"2"
4322032.	3623980.	25202.	"3"
4321310.	3629741.	25269.	"4"
4287681.	3608018.	25575.	"5"
4293494.	3613836.	25559.	"6"
4302937.	3623280.	25520.	"7"
4302938.	3629730.	25598.	"8"
4305001.	3657144.	25269.	"9"
4299698.	3662446.	25020.	"10"
4292629.	3669512.	24801.	"11"

5.2 Test Procedure

As with the building 226 wall penetration tests, free space calibrations were made at the onset of each day of experiments at the Building 202 test range. This measurement formed the basis for the $\tilde{A}$ vector in Figure 3.7.3, which is used to compensate for system and atmospheric response. The transmitting antenna was set up on one of the numbered exterior benchmarks (see Figures 5.2.1 and 5.2.2), leveled, and the elevation recorded. Similar steps were undertaken at the receiving antenna, set up on one of the interior (lettered) stations, as shown in Figures 5.2.3 and 5.2.4. These photos show the realistic nature of the testing (from a construction site clutter stand point) and the very serious obstacles (disabling from a line-of-sight surveying standpoint) presented by this test range. In particular in the case of Figures 5.2.3 and 5.2.4, it should be recognized that the orgin of the survey transmission is coming from outside the building and the signal must pass first through the exterior wall of the building and in some cases several interior walls, in addition to passing through and around the clutter seen in front of the receiving antenna in these photos. Sampling and processing procedures were identical to those discussed in Chapter 4.

5.3 Results

5.3.1 Masonry Block and Brick Wall Tests

A large number of tests were conducted in which the principle obstacles consisted of masonry block and brick. The masonry block were of a type common to U.S. construction measuring approximately 200 mm square by 400 mm long. The bricks measured 89 mm wide, 57 mm high, by 196 mm long. The exterior walls of

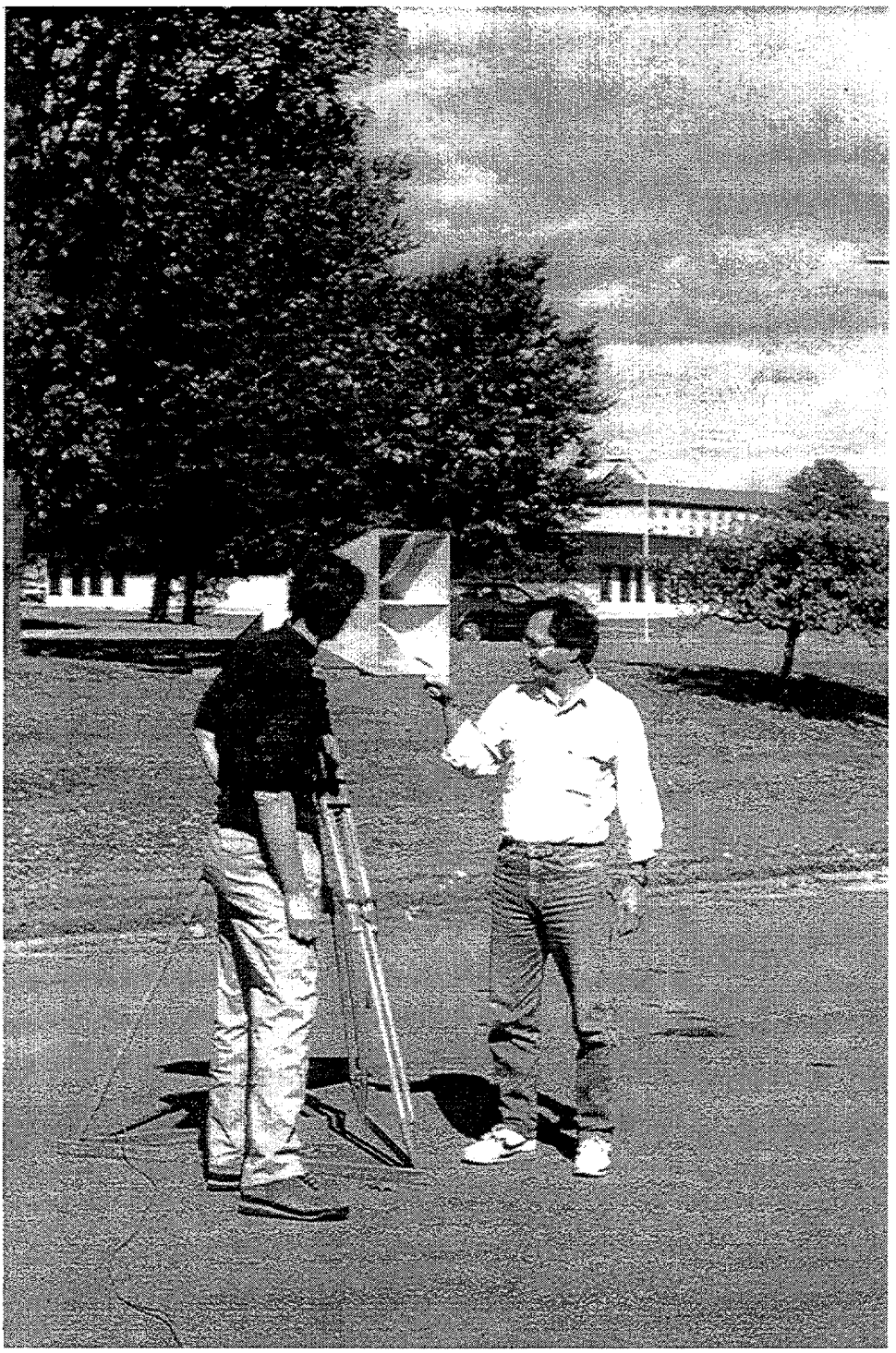

Figure 5.2.1: Setup of the quad-ridge radar transmitter antenna over Benchmark 11 at the NIST Building 202 NLS test range.

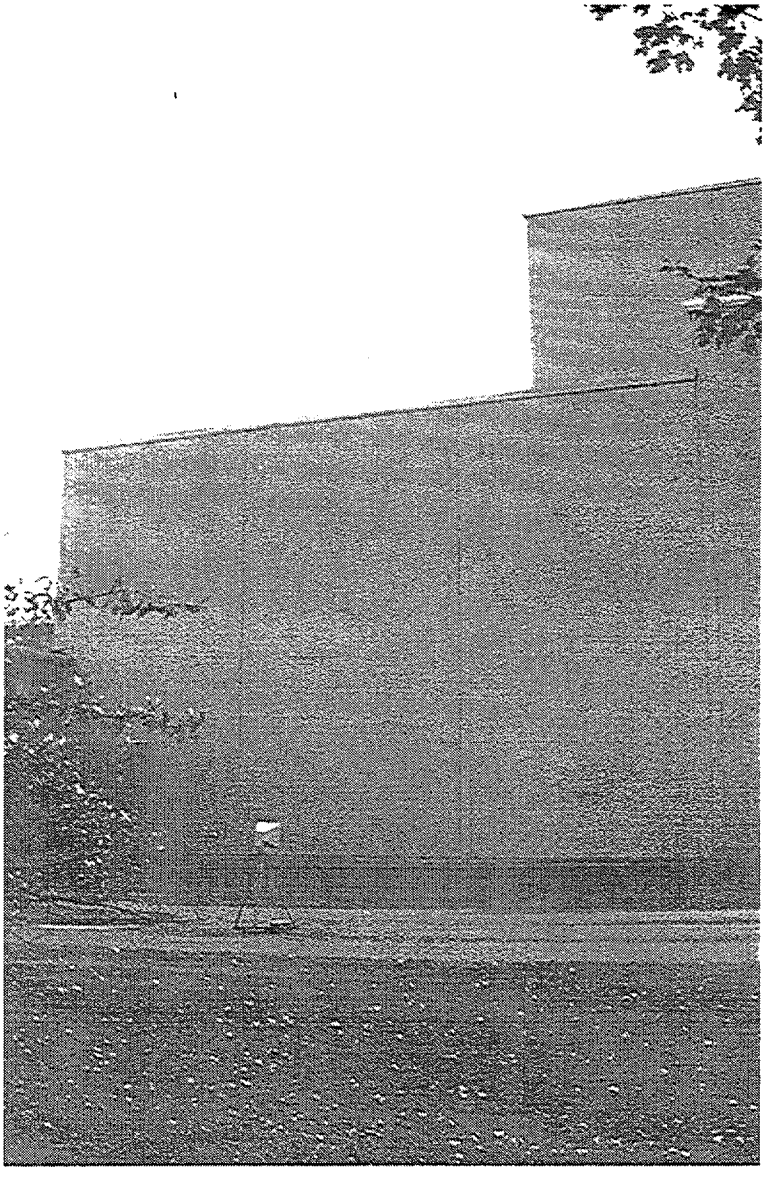

Figure 5.2.2: Setup of the quad-ridge radar transmitter antenna over Benchmark 11 at the NIST Building 202 NLS test range. The roving receivers were located at varying benchmarks inside building. The exterior walls consisted of a single layer of masonry block faced with a single layer of kiln fired brick. In some cases up to three tiers of this wall were penetrated.

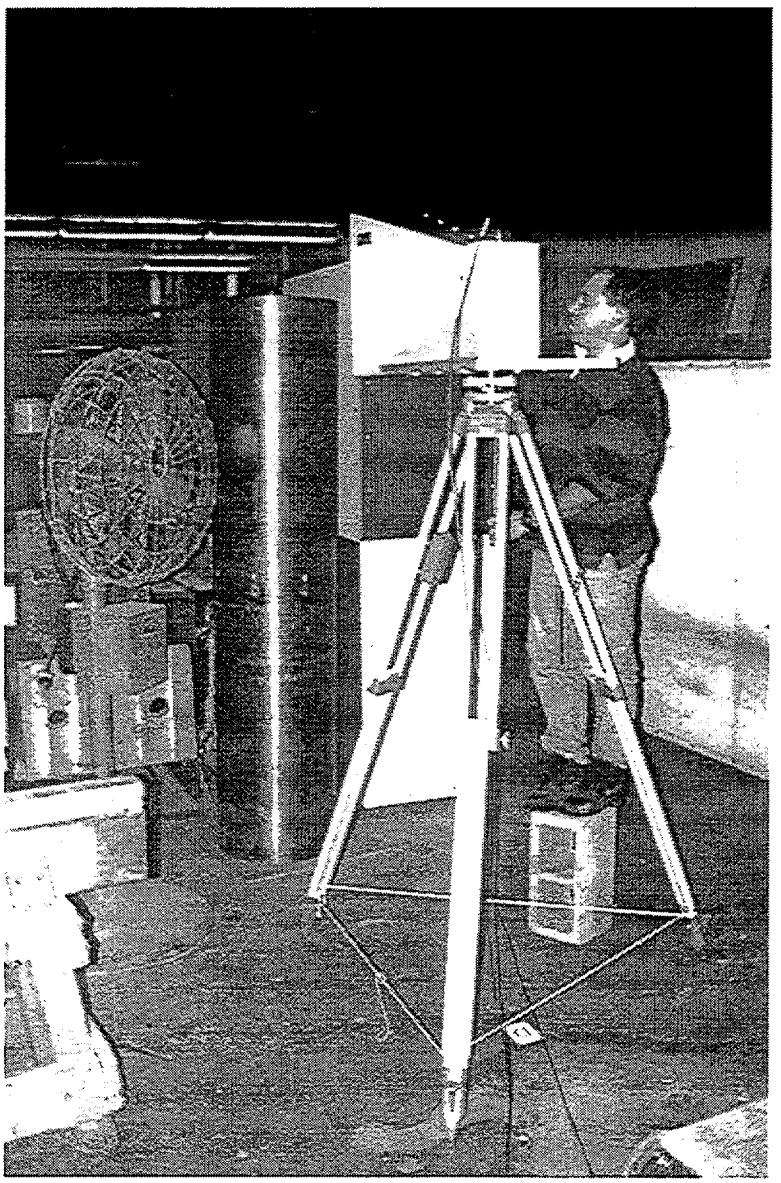

Figure 5.2.3: Roving receiver antenna set up at interior benchmark Station D. Note the presence of metal cylinder, piping, and other debris.

Building 202 consist of a single layer of brick facing and an interior single layer wall of masonry block for a combined thickness of 289 mm. The building was constructed in the early 1960s.

Point "B", inside the building, was selected as the primary target for the tests involving masonry block and brick penetration. A closeup plan view of this area is presented in Figure 5.1.2. Of particular interest are the presence of two large built-up columns which flank point B on the northwest corner of the building. These large steel obstacles appear to have played a role in blocking distance measurements from exterior transmission stations 3, 9, 10, and 11. Otherwise, as listed in Table 5.3.1 below, effective distance determination was able to be acquired from points 2, 4, 6,7,8, and 9. These test data were used as the basis for discussions concerning lag time and penetration distance presented in Chapter 6.

It is notable that, for transmissions from station 2, distances were able to be obtained at the interior stations D, F, and H, which were situated beyond a 2m stack of steel girders, and two metal frame racks stacked 2 m high with various test equipment and metal test samples. Data in Table 5.3.1 indicate that there is no significant difference between results obtained using horizontal or vertical polarization.

Table 5.3.1: Masonry Block and Brick Wall Tests

T-Pos = Benchmark position of transmitter
R-Pos = Benchmark position of receiver
T-Hgt = Height of transmitter (m)
R-Hgt = Height of receiver (m)
Survey = Separation distance as surveyed by NIST (m)
Radar = Separation distance as seen by radar (m)
Δ = Difference between survey and radar results (m)
N/D = no distance obtained using radar.

File	Polarity	T-Pos	R-Pos	T-Hgt	R-Hgt	Survey	Radar	Δ
Vertical-Vertical Polarization								
94092803	VV	#6	B	2.000	1.956	13.353	13.872	0.549
94092806	VV	#7	B	1.728	1.956	18.884	19.393	0.509
94092807	VV	#8	B	1.730	1.956	19.960	20.297	0.137
94092810	VV	#4	B	1.740	1.956	37.825	38.265	0.440
94092814	VV	#2	B	1.735	1.956	26.353	26.809	0.456
94092841	VV	#2	F	1.741	1.953	43.000	43.552	0.552
94092844	VV	#2	H	1.741	1.955	53.000	53.506	0.506
94092845	VV	#2	D	1.965	1.955	35.497	36.177	0.680
94092927	VV	#9	B	1.746	1.960	40.137	40.322	0.185

Horizonta-Horizontal Polarization								
94092804	HH	#6	B	2.000	1.956	13.353	13.894	0.541
94092805	HH	#7	B	1.728	1.956	18.884	19.493	0.609
94092808	HH	#8	B	1.730	1.956	19.960	20.728	0.151
94092809	HH	#4	B	1.740	1.956	37.825	38.293	0.468
94092813	HH	#2	B	1.735	1.956	26.353	26.809	0.456
94092842	HH	#2	F	1.741	1.953	43.000	43.481	0.481
94092846	HH	#2	D	1.965	1.955	35.497	36.054	0.557
94092926	HH	#9	B	1.746	1.960	40.137	40.332	0.195
No Viable Distance Detected								
94092843	HH	#2	H	1.741	1.955	53.000	N/D	N/D
94092811	VV	#3	B	1.740	1.956	37.269	N/D	N/D
94092812	HH	#3	B	1.740	1.956	37.269	N/D	N/D
94092919	VV	#11	B	1.754	1.960	47.127	N/D	N/D
94092920	HH	#11	B	1.754	1.960	47.127	N/D	N/D
94092921	HH	#11	B	1.754	1.960	47.127	N/D	N/D
94092922	VV	#11	B	1.754	1.960	47.127	N/D	N/D
94092923	VV	#10	B	1.746	1.960	42.286	N/D	N/D
94092924	VV	#10	B	1.746	1.960	42.286	N/D	N/D
94092925	HH	#10	B	1.746	1.960	42.286	N/D	N/D

5.3.2: Roll-up Metal Door Tests

It is well known that Maxwell's Laws of electromagnetism preclude the penetration of a perfect conductor by an electromagnetic wave (see Chapter 6). However, these equations do not preclude the ability of an electromagnetic wave to propagate through small openings in an otherwise seamless metallic structure, and thereby penetrate enclosed cavities. In such cases a distance, containing errors proportional to the scatter angle, could be determined. To test this hypothesis an all-metal roll up door, shown in Figure 5.3.1 and located between points 5 and A, was used as a test barrier. In successive increments this door was raised from its closed position to a fully open height of 3.3 m (and a width of 4.27 m). Transmission in all cases was from exterior station 1 to interior stations A, C, and G, respectively. Other than being placed further inside the high test bay, stations C, E, J, and G had no additional intervening obstacles in the transmission path.

The results, presented in Table 5.3.2., show, as expected, that no distance could be ascertained with a closed door. However, with as little as a 100 mm gap between the bottom of the roll-up door and the concrete foundation, strong first arrival peaks were detected which were useable for distance determination. Since we know that a direct transmission to the receiver through the metal door is not possible, this means that the beam is being defracted by the bottom edge of the roll-up door, the gap in effect serving as a diffraction grating slot, and it is the diffracted rays which are being

detected. The errors induced by this diffraction are proportional to both the height of the door opening as well as the distance to the receiving antenna. This can be deduced from elementary consideration of the geometry of the test setup in the vertical plane, as shown graphically in Figure 6.4.3. This suggests that it will be possible to btain "rough" distances inside a structure containing "all metal" walls, provided it has windows. It may be possible, furthermore, to develop compensation algorithms which seek to minimize such errors in recognition of the present geometry of the structure (which presumably will be tracked as part of construction automation efforts, and will be known from as-built drawings in the case of an existing building).

In these particular tests, the use of horizontal or vertical polarization appeared to have no significant effect: when obtaining distances between points 1 and A, the horizontal polarization yielded better results; yet for distances between points 1 and G the vertical polarization yielded the least error.

Table 5.3.2: Roll-up Metal Door Tests

T-Pos = Survey position of transmitter
R-Pos = Survey position of receiver
T-Hgt = Height of transmitter
R-Hgt = Height of receiver
Survey = Separation distance as surveyed by NIST (meters)
Radar = Separation distance as seen by Lincoln radar (meters)
Δ= Difference between survey and radar results (meters)
Gap Ht. = Open vertical gap distance from bottom of rollup door to floor (meters)
[0=closed;open=fully opened = 3.3m]
N/D = no distance obained using radar

File	Polarity	T-Pos	R-Pos	T-Hgt	R-Hgt	Survey (m)	Radar (m)	Δ (m)	Gap Ht. (m)
94092817A	VV	#1	A	1.736	1.957	26.353	N/D	N/D	0.0
94092824	VV	#1	A	1.736	1.957	26.353	26.832	0.479	0.1
94092820	VV	#1	A	1.736	1.957	26.353	26.620	0.267	0.5
94092819	VV	#1	A	1.736	1.957	26.353	26.469	0.088	1.0
94092815	VV	#1	A	1.736	1.956	26.353	26.265	0.088	3.3
94092817	HH	#1	A	1.736	1.957	26.353	N/D	N/D	0.0
94092823	HH	#1	A	1.736	1.957	26.353	N/D	N/D	0.1
94092821	HH	#1	A	1.736	1.957	26.353	26.738	0.385	0.5
94092818	HH	#1	A	1.736	1.957	26.353	26.552	0.199	1.0
94092822	HH	#1	A	1.736	1.957	26.353	26.545	0.192	1.0
94092816	HH	#1	A	1.736	1.957	26.353	26.286	0.067	3.3
94092832	VV	#1	C	1.736	1.957	35.497	35.632	0.135	0.1

94092829	VV	#1	C	1.736	1.957	35.497	35.579	0.082	0.5
94092828	VV	#1	C	1.736	1.957	35.497	35.567	0.070	1.0
94092825	VV	#1	C	1.736	1.957	35.497	35.485	0.012	3.3
94092831	HH	#1	C	1.736	1.957	35.497	N/D	N/D	0.1
94092830	HH	#1	C	1.736	1.957	35.497	35.666	0.169	0.5
94092827	HH	#1	C	1.736	1.957	35.497	35.606	0.109	1.0
94092826	HH	#1	C	1.736	1.957	35.497	N/D	N/D	3.3
94092840	VV	#1	G	1.736	1.973	53.000	53.079	0.079	0.1
94092837	VV	#1	G	1.736	1.973	53.000	53.049	0.049	0.5
94092836	VV	#1	G	1.736	1.973	53.000	53.067	0.067	1.0
94092833	VV	#1	G	1.736	1.973	53.000	53.024	0.024	1.973
94092839	HH	#1	G	1.736	1.973	53.000	53.192	0.192	0.1
94092838	HH	#1	G	1.736	1.973	53.000	53.107	0.107	0.5
94092835	HH	#1	G	1.736	1.973	53.000	53.086	0.086	1.0
94092834	HH	#1	G	1.736	1.973	53.000	53.030	0.030	1.973

5.3.3 Mixed Obstacle Tests

Exterior stations 9-11, and interior stations E-K, were used to test the more difficult proposition of penetrating first an exterior masonry block and brick wall, then interior masonry block separation walls, followed finally by an all-metal prefabricated two story high wall which separated offices and smaller test laboratories from the main high-bay structural test area in Building 202. The metal partition wall had doorways, both single and double, which were able to be opened, as shown in Figure 5.3.1

There are a number of interesting results from this test series. Of particular note are the tests from transmit station 11 to receive station K. The double doors in the all-metal wall depicted in Figure 5.3.1 were positioned in both the fully open and fully closed states for these tests. In *both* cases confirmed distances were obtained for vertical-vertical polarization, whereas both horizontal polarized transmissions were blocked. It can be seen from Table 5.3.3. that the result of closing the double doors, for the vertical polarization case, was to increase the error by approximately 165 mm. Another interesting case is 11 to F. In this case, the horizontal polarized transmission was received through a brick wall, two masonry block walls, and a single office doorway in an all-metal wall. The error in the measurement was 649 mm, but the majority of this can be accounted for by consideration of propagation delays through the various walls.

In those cases listed in Table 5.3.3 where positive determination of distance was achieved the diffraction angles, if any, involved with passage through the metal doorways were slight. For example, a distance was obtained between station 11 and station H, but only for vertical polarization. No distance, using either polarization,

could be obtained for transmission at station 11 and a receiver at station G. The doors in the metal wall were open in both cases. Further discussion of individual results are presented in Chapter 6.

Table 5.3.3: Mixed Obstacle Tests

T-Pos = Survey position of transmitter
R-Pos = Survey position of receiver
T-Hgt = Height of transmitter
R-Hgt = Height of receiver
Survey = Separation distance as surveyed by NIST (meters)
Radar = Separation distance as seen by Lincoln radar (meters)
Δ= Difference between survey and radar results (meters)
Gap Ht. = Open vertical gap distance from bottom of rollup door to floor (meters)
[0=closed;open=fully opened = 3.3m]
N/D = no distance obtained using radar

File	Polarity	T-Pos	R-Pos	T-Hgt	R-Hgt	Survey	Radar	Delta	Doors
94092912	HH	#10	K	1.763	1.955	39.489	39.672	0.183	open
94092911	VV	#10	K	1.763	1.955	39.489	39.697	0.208	open
94092910	VV	#11	K	1.750	1.955	38.852	38.946	0.094	open
94092909	VV	#11	K	1.750	1.955	38.852	39.111	0.259	closed
94092905	VV	#11	H	1.750	1.955	38.871	39.514	0.643	open
94092917	HH	#11	F	1.,754	1.964	40.030	40.679	0.649	open
94092913	HH	#10	G	1.763	1.958	40.136	N/D	N/D	open
94092914	VV	#10	G	1.763	1.958	40.136	N/D	N/D	open
94092915	VV	#10	F	1.763	1.964	38.871	N/D	N/D	open**
94092916	HH	#10	F	1.763	1.964	38.871	N/D	N/D	open**
94092918	VV	#11	F	1.754	1.964	40.030	N/D	N/D	open
94092903	HH	#11	G	1.750	1.950	47.000	N/D	N/D	open
94092904	VV	#11	G	1.750	1.950	47.000	N/D	N/D	open
94092906	HH	#11	H	1.750	1.955	38.871	N/D	N/D	open
94092907	HH	#11	K	1.750	1.955	38.852	N/D	N/D	open
94092908	HH	#11	K	1.750	1.955	38.852	N/D	N/D	closed

** Receiver blocked by steel shelving

5.3.4 Reaction Wall Penetration Tests

As a final test of the radar distancing system an attempt was made to obtain a point-to-point distance between stations C and I, situated on either side of a 1.829 m thick,

heavily reinforced reaction wall (Figure 5.3.1). In these tests the Watkins-Johnson Quad-Ridged Horn antennas (described in Chapter 3) were stationed at benchmarks C and I inside Building 202 at an elevation of 1.2 m. The results, shown in Figure 39, Appendix B, were inconclusive. Using the techniques derived in Chapter 6, one would expect to see a time domain peak at approximately 13.2 m, accounting for a straight line distance of 10 m between the two points and the propagation delay associated with penetrating through a 1.8 m thick reinforced concrete wall with a dielectric constant of 7.4 (see eq. 6.2.16). None of the time domain peaks shown in Figure 39, Appendix B suggest a detection peak at this distance. It can therefore be concluded that either the transmission power was insufficient, or the attenuation associated with passing through the reinforcement mesh and thickness of concrete precluded establishing a detectable signal.

Chapter 6: Electromagnetic Wave Propagation Through Engineering Materials

6.1 Introduction

In general, there are four cases which describe the behavior of electromagnetic waves when they interact with matter. These all depend on the nature of the target material, including good conductors, non-conductors, semi-conductors, and plasmas. The latter two situations are not of engineering importance to surveying technology, since the likelihood of them being present on a typical construction site is very small. Excellent derivations of the physics behind the interaction of electromagnetic waves with matter may be found in (Born and Wolf, 1959) and (Orear, 1979).

A good conductor reflects the impinging electromagnetic wave with nearly 100% efficiency. Only in situations involving exceedingly thin sheets of metal will any portion of the electromagnetic wave be re-radiated on the opposite side of the incident face, where it might then be detected by a receiving antenna. Most metal sheet that might be used in construction is far too thick to permit penetration. Instead a current is induced in the sheet which produces electromagnetic radiation itself, following Maxwell's Laws. A portion of this energy is re-radiated back towards the source of the impinging wave (thus appearing as a reflected wave with the limiting case of a perfectly conducting sheet producing 100% reflection. *Simply summarized, surveying through all-metal walls using electromagnetic radiation is not possible.* Fortunately, this does not pose a problem for the vast majority of residential and commercial structures.

In contrast to an all-metal wall, a perfect nonconductor (such as an inert gas), allows an electromagnetic wave to pass through without any attenuation; however, the wave appears to travel slower than the speed of light in a vacuum. Since a broad variety of construction materials -- including brick, masonry block, concrete, wood, glass, asphault, and plastics -- may be considered nonconductors, it will be useful to examine this class of materials from the viewpoint of electromagnetic wave propagation.

6.2 Propagation Through Nonconducting Materials

Figure 6.2.1 shows a section of an infinite (stretching without limit in the plane of the wall) nonconducting (or dielectric) slab into which an electromagnetic incident impulse, E^i, is launched. In figure 6.2.1 the *dielectric constant* for the wall is defined as follows:

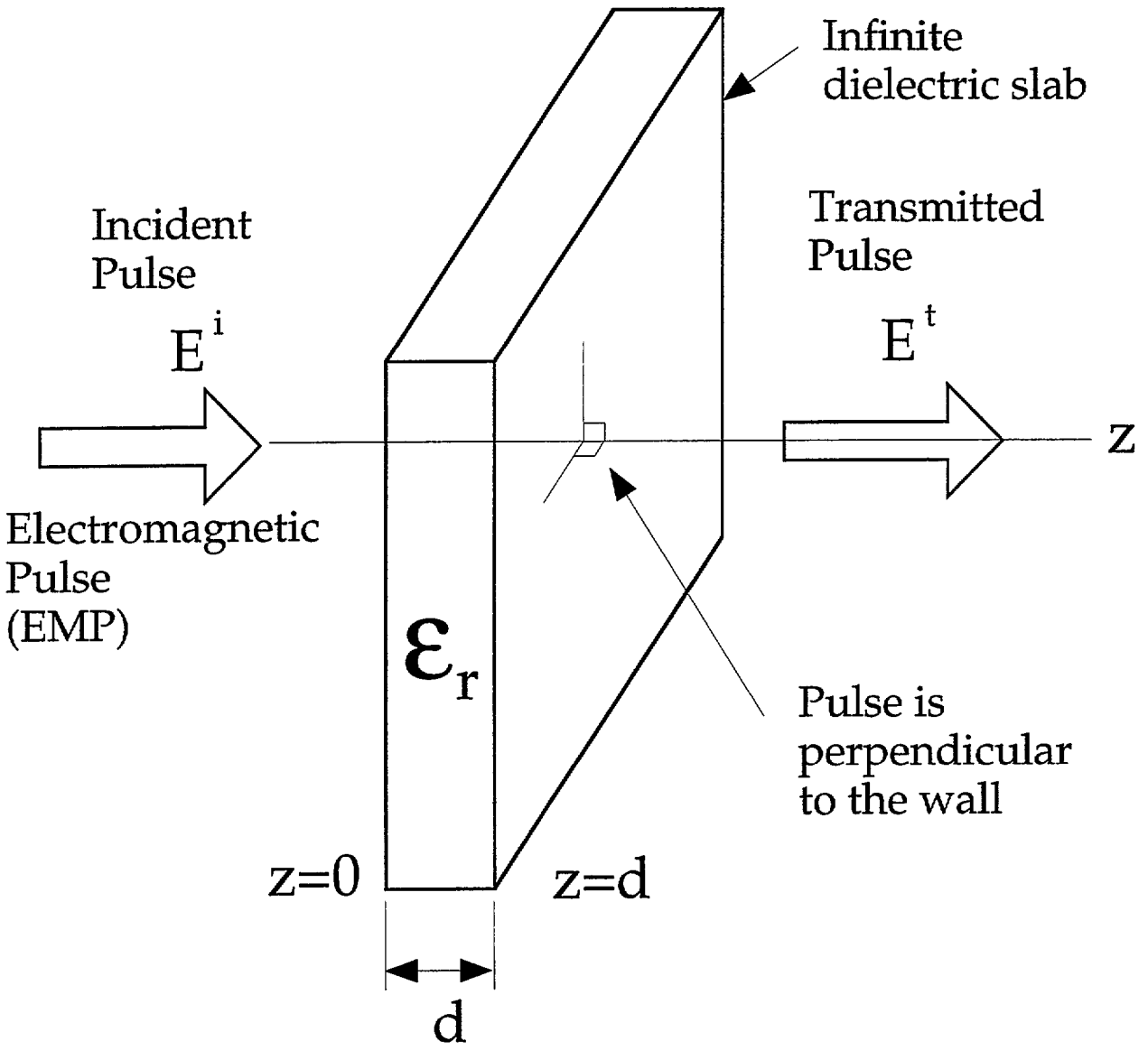

Figure 6.2.1: Electromagnetic transmission through a lossless dielectric wall (from Blejer, 1995).

$$\varepsilon = \varepsilon_r \varepsilon_\varphi \qquad \text{eq.(6.2.1)}$$

where:

ε_r = the relative dielectric constant
ε_0 = the permittivity of free space

When applied to optics within the visible spectrum the constant, ε_r , is more commonly known as the *index of refraction*, n. By definition, the propagation velocity of the electromagnetic wave through a material with an index of refraction, n, is given by:

$$v = c/n \qquad \text{eq.(6.2.2)}$$

It is important to recognize that eq.(6.2.1) applies to all materials. Two useful observations can be drawn this relationship:

1) The index of refraction is frequency-dependent, with higher frequencies (shorter wavelengths) leading to a higher index of refraction. Within the visible light spectrum, this is obvious to anyone who has ever observed the effects of white light passing through a glass prism.
2) Denser materials have higher indices of refraction at a given wavelength.

A simpler definition of the material dielectric constant, ε_r , may be derived from consideration of Figure 6.2.1 to determine the characteristics of the transmitted signal in the halfspace in which z>d, where d is the thickness of the slab being penetrated by the electromagnetic wave.

The incident electromagnetic field, E^i , is given by:

$$E^i = E_0(t - \frac{z}{c}) \qquad \text{eq.(6.2.3)}$$

where E^i is an arbitrary, time dependent signal that propagates in the positive z direction without dispersion. It is a plane wave pulse that propagates at the speed of light in a vacuum, c = $2.998(10)^8$ m/s, and where t is the propagation time in seconds, and E_0 is the amplitude of the signal.

The transmitted field may be represented as an infinite train of pulses of amplitude A_nE_0, and delay δ_n as:

$$E^t = \sum_{N=1}^{\infty} A_N E_0(t - \frac{z}{c} - \delta_N) \qquad \text{eq.(6.2.4)}$$

For a lossy dielectric, only the first pulse or two dominate the response and they may

be dispersed, meaning that their time dependence is different from the incident pulse and cannot be expressed as $E_0(\tau)$. The first transmitted pulse in the expression above is:

$$E_1^t = T_\uparrow T_\downarrow E_0(t - \frac{z-d}{c} - \frac{d\sqrt{\varepsilon_r}}{c}) \qquad \text{eq.(6.2.5)}$$

where the into-the-wall transmission coefficient is given by:

$$T_\uparrow = \frac{2}{1+\sqrt{\varepsilon_r}} \qquad \text{eq.(6.2.6)}$$

and the out-of-the-wall transmission coefficient is given by:

$$T_\downarrow = \frac{2\sqrt{\varepsilon_r}}{1+\sqrt{\varepsilon_r}} \qquad \text{eq.(6.2.7)}$$

Therefore, the loss in power due to transmission only (not attenuation inside the wall) is given by:

$$\left|T_\uparrow T_\downarrow\right|^2 = \frac{16\varepsilon_r}{(1+\sqrt{\varepsilon_r})^4} \qquad \text{eq.(6.2.8)}$$

As an example, if the dielectric constant, ε_r , is equal to 9 we find that:

$$\left|T_\downarrow T_\uparrow\right|^2 = \frac{9}{16} \qquad \text{eq.(6.2.9)}$$

or, expressed in dB:

$$10Log_{10}\left|T_\downarrow T_\uparrow\right|^2 = 10Log_{10}(\frac{9}{16}) = -2.5dB \qquad \text{eq.(6.2.10)}$$

However, loss is considered by convention to be a positive quantity, so the loss is 2.5 dB. Negative loss is gain, another positive quantity. This result proves that for the walls tested at NIST, most of the loss is due to absorbtive losses in the media (i.e. the wall), not transmission.

The delay in arrival time due to the presence of the wall is given by the argument in eq.(6.2.5) by solving for the signal peak when the argument equals zero:

$$t - \frac{z-d}{c} - \frac{d\sqrt{\varepsilon_r}}{c} = \phi \qquad \text{eq.(6.2.11)}$$

or

$$t = \frac{z-d}{c} + \frac{d\sqrt{\varepsilon_r}}{c} \qquad \text{eq.(6.2.12)}$$

at z=d we can solve for t:

$$z = d \Rightarrow t = \frac{d(\sqrt{\varepsilon_r} - 1}{c} \qquad \text{eq.(6.2.13)}$$

This represents a delay time of:

$$\frac{d\sqrt{\varepsilon_r}}{c} - \frac{d}{c} \qquad \text{eq.(6.2.14)}$$

rearranging yields:

$$\Delta t = \frac{d(\sqrt{\varepsilon_r} - 1)}{c} \qquad \text{eq.(6.2.15)}$$

where Δt represents the additional propagation time between transmission and receiving antennas over that which would be measured if the wall were not there. If we consider the tests conducted at Building 226 at NIST, in which a 500 mm thick reinforced concrete wall was between the transmitting and receiving antennas, and we assume, for now, an approximate dielectric constant of 9 for aged, reinforced concrete, we find the delay time to be:

$$\Delta t = \frac{d(\sqrt{\varepsilon_r} - 1)}{c} = \frac{1}{c} = 3.33ns \qquad \text{eq.(6.2.16)}$$

We can express this as an equivalent range-error as: $\Delta t * c = 3.33(10)^{-9} * 2.998(10)^{8} = 0.998$ m. Thus we would expect to see approximately one meter of error in the measured distance between the transmitter and receiver due to delays in traversing through the wall, providing our estimate of the dielectric constant for the wall is correct. It is interesting to note that loss related to the electrical conductivity of the wall (if the wall is not an ideal nonconductor, e.g. a reinforced concrete panel) will not change the above result significantly. If the conductivity is large (e.g. an all-metal wall panel) then the delay still is not largely affected, provided the wall is not *electrically* thick, i.e. there is insufficient time for the pulse to disperse during its passage through the material.

6.3 Discussion of Building 226 "Wall" Tests

The concept of NLS surveying was speculative at the inception of this study and therefore the tests were designed to investigate a wide variety of variables using existing infrastructure under conditions that were representative of situations that might arise at a construction site. In some cases, what appeared to be simple tests produced results which were quite complex. This was the situation with the Building 226 wall penetration tests. It will be illustrative to discuss four specific instances where geometry and the distances between the transmitter, receiver, wall, and other objects played an important role in the resulting time history response detected at the receiving antenna. On the basis of these observations, it is possible to draw some initial conclusions concerning the accuracy of the NLS metrology system in its present configuration.

Figure 6.3.1 shows the time domain response of a free space calibration from station R20 to station R5 (Figure 4.1.2.2) in which the transmitting and receiving antennas were spaced 14.905 m apart with no intervening obstacles other than air. The singular peak is known to be exactly at 14.905 m is part of the calibration, which accounts for propagation speed through the ambient atmosphere. It can be seen that the peak magnitude is approximately 20 dB above the background noise, indicating a strong received signal.

In contrast, Figure 6.3.2 shows a typical response for the transmitter at location T10 and the receiver at location R5, with the 500 mm thick reinforced concrete wall between the two as shown in Figure 4.1.2.2. The precision surveyed distance between those two points (from Table 4.1.3) is 16.003 m. We see in Figure 6.3.2 that the first peak is strong, and is delayed from the expected straight line signal by 16.160 m - 16.003 m = 0.157 m. This peak *does not* correspond to the radar distance through the wall.

Figures 4.1.2.1 and 6.3.3 will help to explain why. Signals emitted from the transmission antenna at point T10 radiate outward towards the target wall. Ray A follows the straight line path to receiver R5 through the wall. There are, however, other rays -- B, C, and D for example -- which also reach the receiver. Originally, we explained that the surveyed distance between T10 and R5 was based on time of flight measurements, that is the distance was calculated as the time of flight multiplied by the speed of light. However, since electromagnetic radiation travels slower in nonconducting engineering materials (such as a reinforced concrete wall), we know that the time of flight from T10 directly to R5 will produce an estimate of the distance which will exceed the true distance by an amount which is proportional to the dielectric constant for that material. If the time of flight from T10 via some alternate path, which does not go through the engineering material, to R5 is faster than the straight line route, then that signal will arrive first.

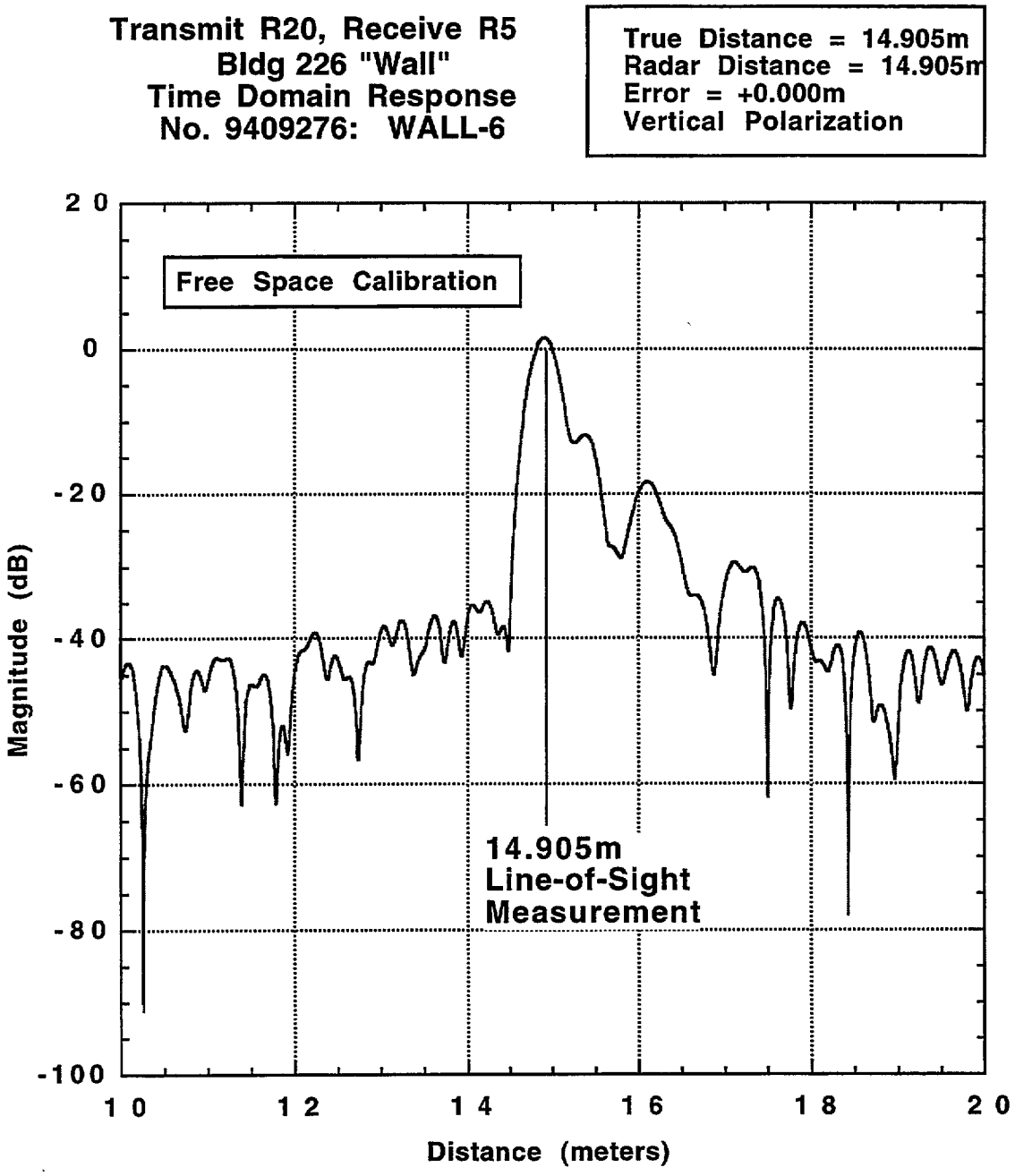

Figure 6.3.1: Time domain radar response for a free space calibration test. The transmission antenna was set atop benchmark R20 and the receiver atop R5. The raw frequency response spectra was converted to the time domain using Fourier techniques. For convenience the propagation delay time, T, was converted to distance, d, by the relation d=cT, where c is the speed of light in a vacuum. The peak shown is arbitrarily set to the precise surveyed distance between the two benchmarks. This calibration is then used to compensate for atmospheric effects on c for use in later measurements to a roving receiver at arbitrary location.

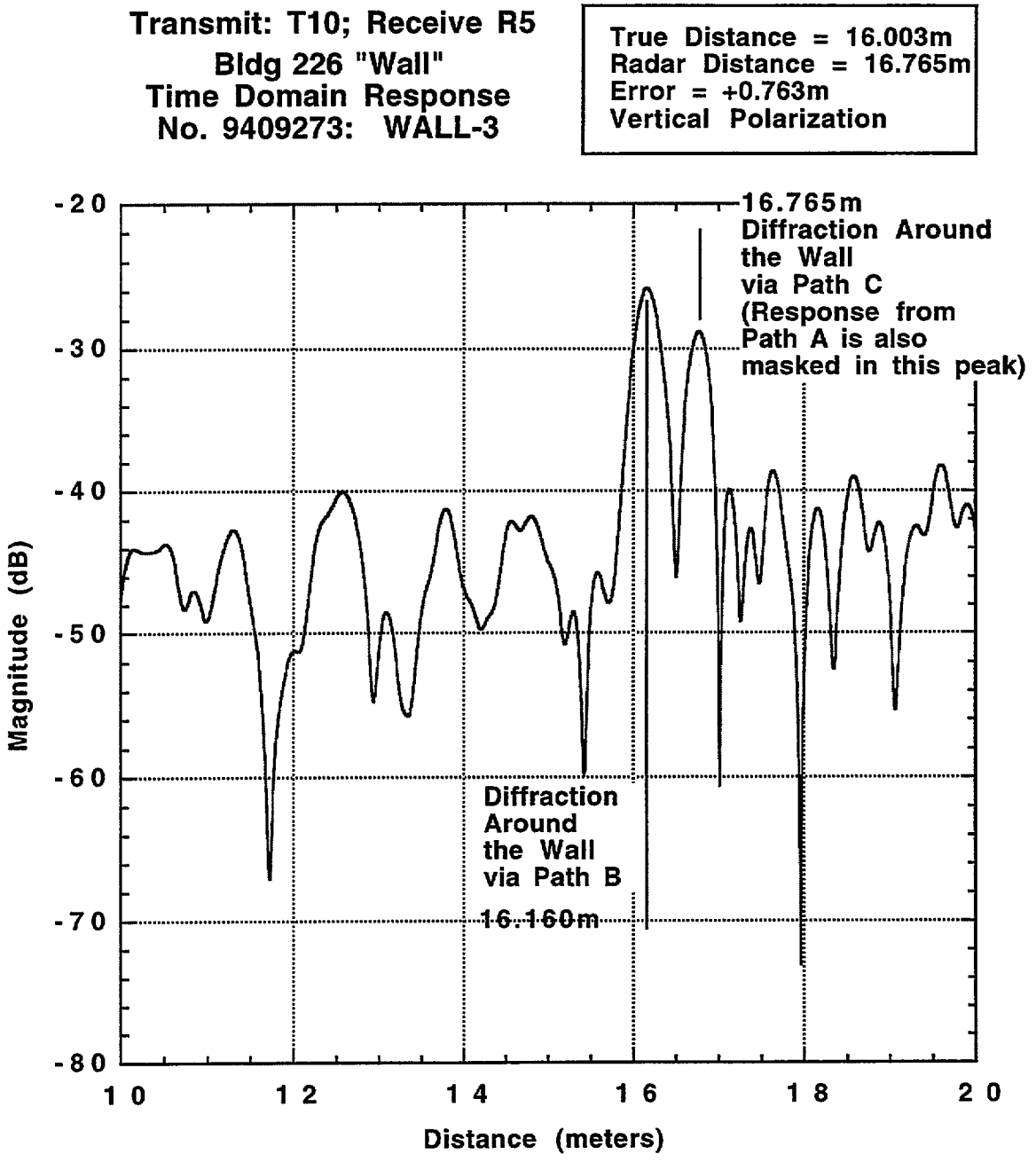

Figure 6.3.2: Time domain response for transmission at T10 and receipt at R5, through the 500 mm reinforced concrete wall. Multipath effects are present. Both of the two detected peaks represent false targets. The true (straight line response) signal is masked in the second peak.

In the case shown in Figure 6.3.3, there are three other paths which can reach the receiver located at R5. The first, path B, is permissable because of the geometry of the test wall (shown in Figure 4.1.2.1). The wall was constructed using available test slabs that had been cast for other experiments. The top tier measured 2 m wide while the bottom tier measured 4.5 m wide. Electromagnetic radiation has the property that it can be diffracted (bent and dispersed) by the presence of corners, edges, slots, and holes. Thus we can expect that a ray following path B will reach the inside corner at the base of the upper tier and be bent around that corner in such a fashion that a portion of it reaches the receiver at R5. In a similar fashion ray C can be diffracted around the end of the lower tier slab. Ray D shows yet another transmission path in which the signal is reflected off a temporary office structure adjacent to the parking lot where the tests were conducted. The calculated distances for each of these scenarios can be determined from three dimensional geometry as shown in Table 6.3.1.

Table 6.3.1: Calculated distances for rays shown in Figure 6.3.3 for transmission from T10 to R5.

Path	Distance (m)
A	16.003 + range delay due to slower propagation velocity through the wall.
B	16.152 (diffraction around upper tier)
C	16.722 (diffraction around lower tier)
D	25.214 (reflection off office structure)

From Table 6.3.1 we see that the first peak in Figure 6.3.2 corresponds closely to the calculated traverse distance of path B, meaning that the diffracted ray B arrived ahead of the straight-through component, marked by ray A.

The picture becomes further clouded since the *second* peak in Figure 6.3.2 corresponds closely to the distance traversed by ray C. Because of this the time domain response peak corresponding to the true distance, as defined by ray A, is not obvious from Figure 6.3.2. We conclude that it may be masked by one of the stronger peaks, or it could be one of the peaks lost in the noise to the right of the second peak. Path D does not show up in Figure 6.3.2 (the x-axis of which was turncated for clarity) and is therefore not a factor in determining the true distance.

One way in which the true distance peak could be masked would be if the delay due to propagation through the wall very nearly matched the delay associated with one of the alternate paths, for example, path C. We can test this hypothesis by examining the results for a different test, for example a transmission at T10 to a receiver located at R10, approximately five meters further away than for the results reported in Table 6.3.1. For this case we calculate the delays for the diffracted and reflected routes (known as "multipath" signals) as shown in Table 6.3.2. The actual field data obtained for this test are shown in Figure 6.3.4. The change in geometry has the effect of shifting the traverse distance for ray C closer to that for ray B. To the right of the second peak we now find that a third peak, approximately 8 dB down

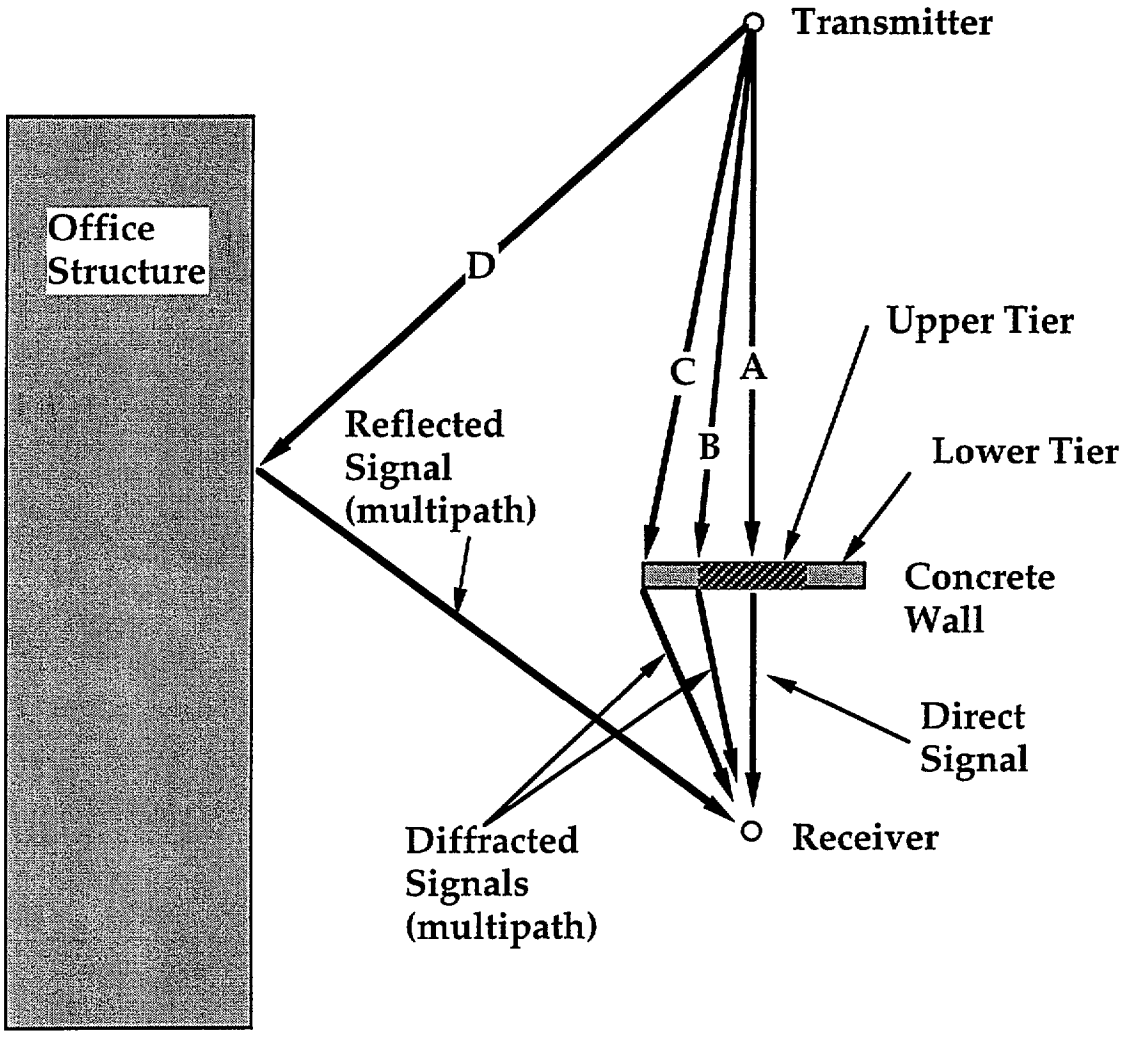

Figure 6.3.3: Multipath environment at the Building 226 NIST NLS test range. Path "A" represents the true straight-line signal, which would deliver the correct distance via time of flight measurement if propagation delays due to material dielectric characteristics were taken into account. Paths B and C represent geometry-dependent routes in which it is possible for a transmitted signal to diffract around the edges of the concrete wall (or around internal features) and still reach the receiver. Path D represents a different class of geometry dependent effects in which a transmitted signal is reflected from an adjacent structure in such a fashion that the reflected signal can reach the receiver. Paths B, C, and D, are referred to collectively as "multipath" effects.

from the first peak amplitude, has appeared. This third peak, as will be shown later (using Table 6.3.6 and eq.(6.2.16)), corresponds to the true straight-line path between the transmitter and receiver.

Table 6.3.2: Calculated distances for rays shown in Figure 6.3.3 for transmission from T10 to R10.

Path	Distance (m)	
A	20.911	(direct, no range delays)
B	21.009	(diffraction around upper tier)
C	21.415	(diffraction around lower tier)
A′	**21.765**	**Actual Path A signal**
D	29.139	(reflection off office structure)

We can take this line of discussion one step further by showing what happens as the baselines are extended. Figure 6.3.5 shows experimental time domain response for a test shot from R10 to T50, for an exact traverse length of 60.512 m. The calculated multipath distances for this configuration are shown in Table 6.3.3. In this case we see that the two diffracted paths, F and G (shown in Figure 6.3.6), are relatively close to one another and in fact their individual responses merge to create a broadened first peak. A much smaller peak at approximately 71.4 m corresponds, as shown in Table 6.3.3 to the direct path E.

Table 6.3.3: Calculated distances for Rays shown in Figure 6.3.6 for transmission from R10 to T50.

Path	Distance (m)	
E	60.512	(direct, no range delays)
F	60.612	(diffraction around upper tier)
G	60.857	(diffraction around lower tier)
H	63.857	(reflection off office structure)

In Tables 6.3.2 and 6.3.3 we have labeled **in bold** what we believe to be the straight line path distances A and E, respectively, as measured by the radar system, including delays due to propagation of the wave through the wall. Lacking a precise **apriori** value of ε_R for the target wall we proceeded to examine all of the test data, looking for correlations between peaks not within proximity of one of the calculated multipath peaks listed above, such as that illustrated by the differences between Figures 6.3.2 and 6.3.4. For completeness, the other calculated paths are given in Table 6.3.4.

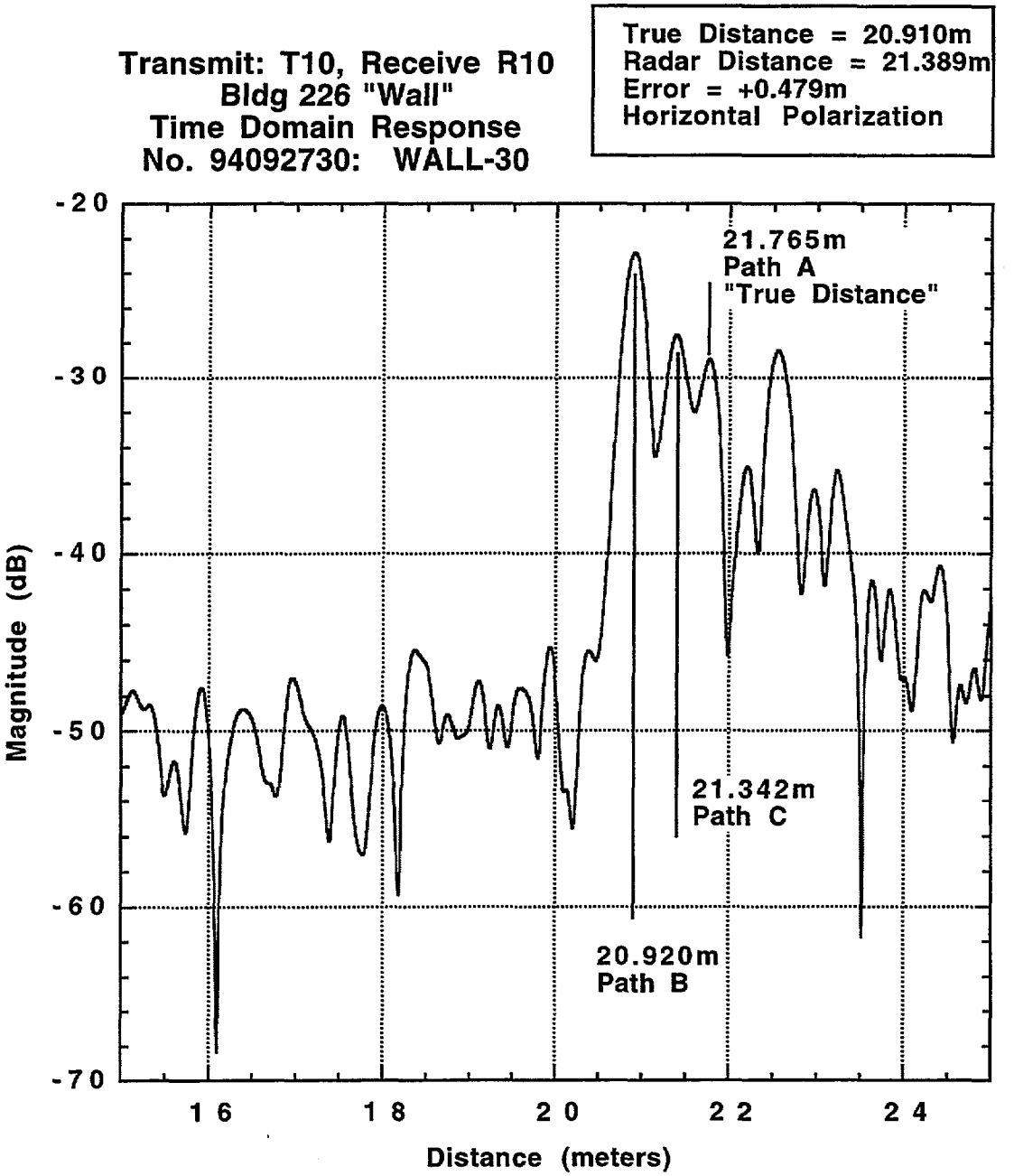

Figure 6.3.4: Time domain response for transmission from benchmark T10 to station R10 at the NIST Building 226 NLS test range. In this particular situation the propagation delay times associated with the various signal paths are sufficiently separated that the various peaks are clearly identified. Note that the straight "through-the-wall" response peak is the third detected, behind the multipath signals following the diffracted paths B and C (see Figure 6.3.3).

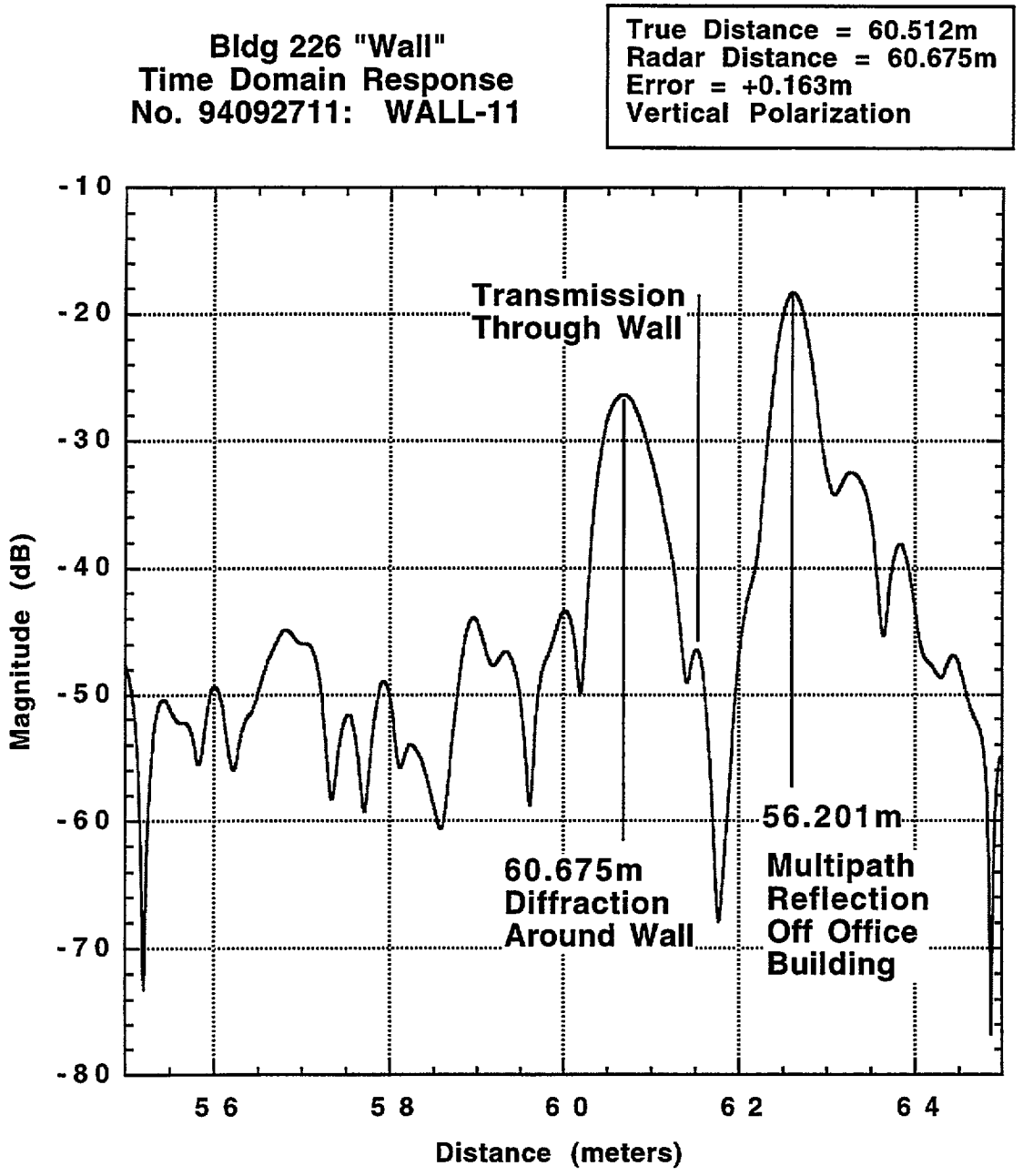

Figure 6.3.5: Time domain response for transmission from benchmark R10 to receive station T50 (see Figure 6.3.6 for multipath geometries).

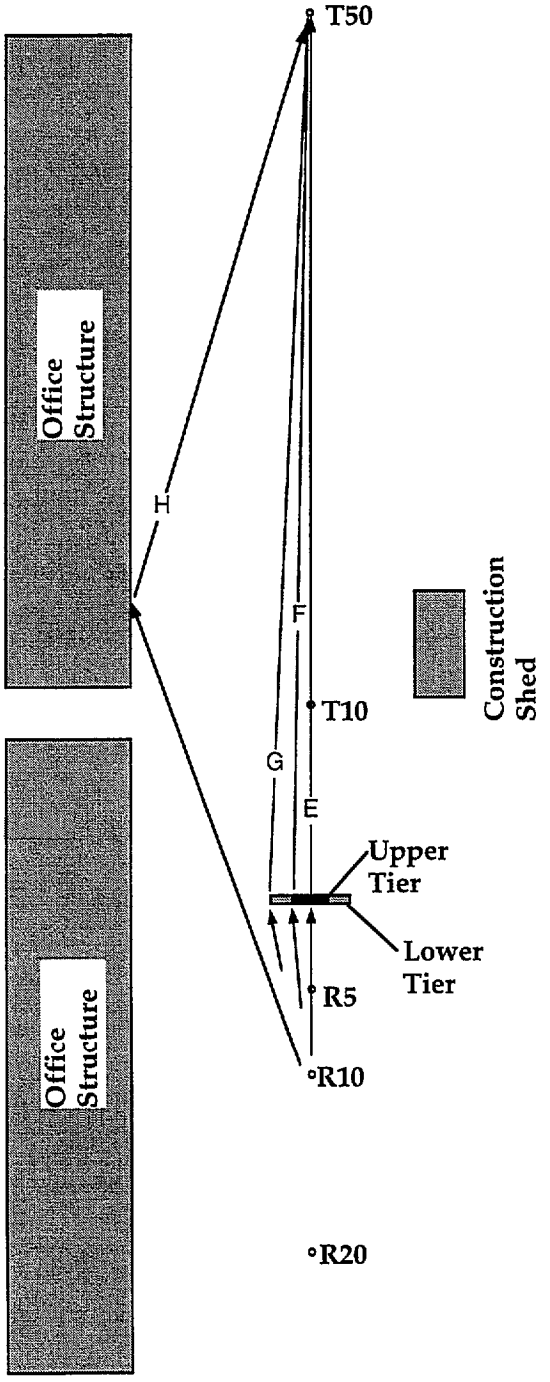

Figure 6.3.6: Test geometry for time domain response reported in Figure 6.3.5. Transmission is from benchmark R10 to a receiver located at station T50. Multipath signals dominate the response.

Table 6.3.4: Calculated distances for paths T10-R20, T50-R5, and T50-R10.

T10 to R20

Path	Distance (m)	
A	30.908	(direct, no range delays)
B	30.981	(diffraction around upper tier)
C	31.271	(diffraction around lower tier)
D	36.960	(reflection off office structure)

T50 to R5

Path	Distance (m)	
E	55.604	(direct, no range delays)
F	55.717	(diffraction around upper tier)
G	56.062	(diffraction around lower tier)
H	59.183	(reflection off office structure)

T50 to R20

Path	Distance (m)	
E	70.509	(direct, no range delays)
F	70.545	(diffraction around upper tier)
G	70.688	(diffraction around lower tier)
E′	71.420	Actual Path E signal
H	73.364	(reflection off office structure)

The results of these analyses are shown in Table 6.3.5 for both horizontal and vertically polarized signals. Two important observations can be made from these data:

- there appears to be a definite narrow range of error despite widely varying distances between the transmitter and receiver and for widely varying distance from the transmitter to the target wall and from the target wall to the receiver (see discussion and figures below) and
- the true signal was not always isolated and easy to detect; in some cases it was obscured by noise, or hidden in the response of a stronger multipath signal. As illustrated in Figure 6.3.5, there was as much as a 15dB reduction in signal magnitude between a reflected multipath signal and that for the ray which passed directly through the reinforced concrete wall, with the multipath signal being much stronger.

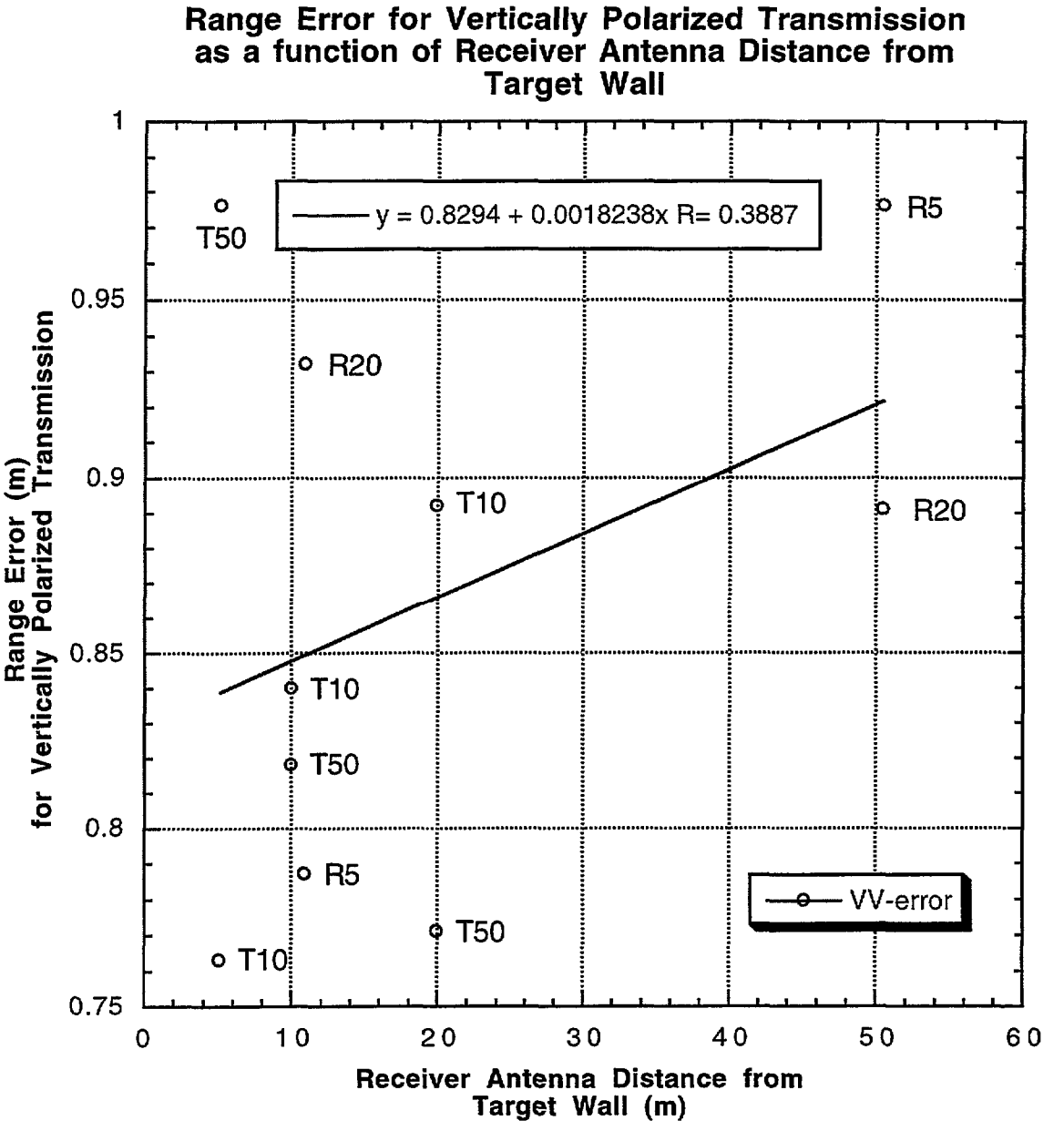

Figure 6.3.7a: Range error for vertically polarized transmissions as a function of receiver antenna distance from the target wall. Transmitter locations are labelled beside each data point. The straight line is an approximate global fit which assumes that there is no affect on range error resulting from the distance of the transmitting antenna from the target wall.

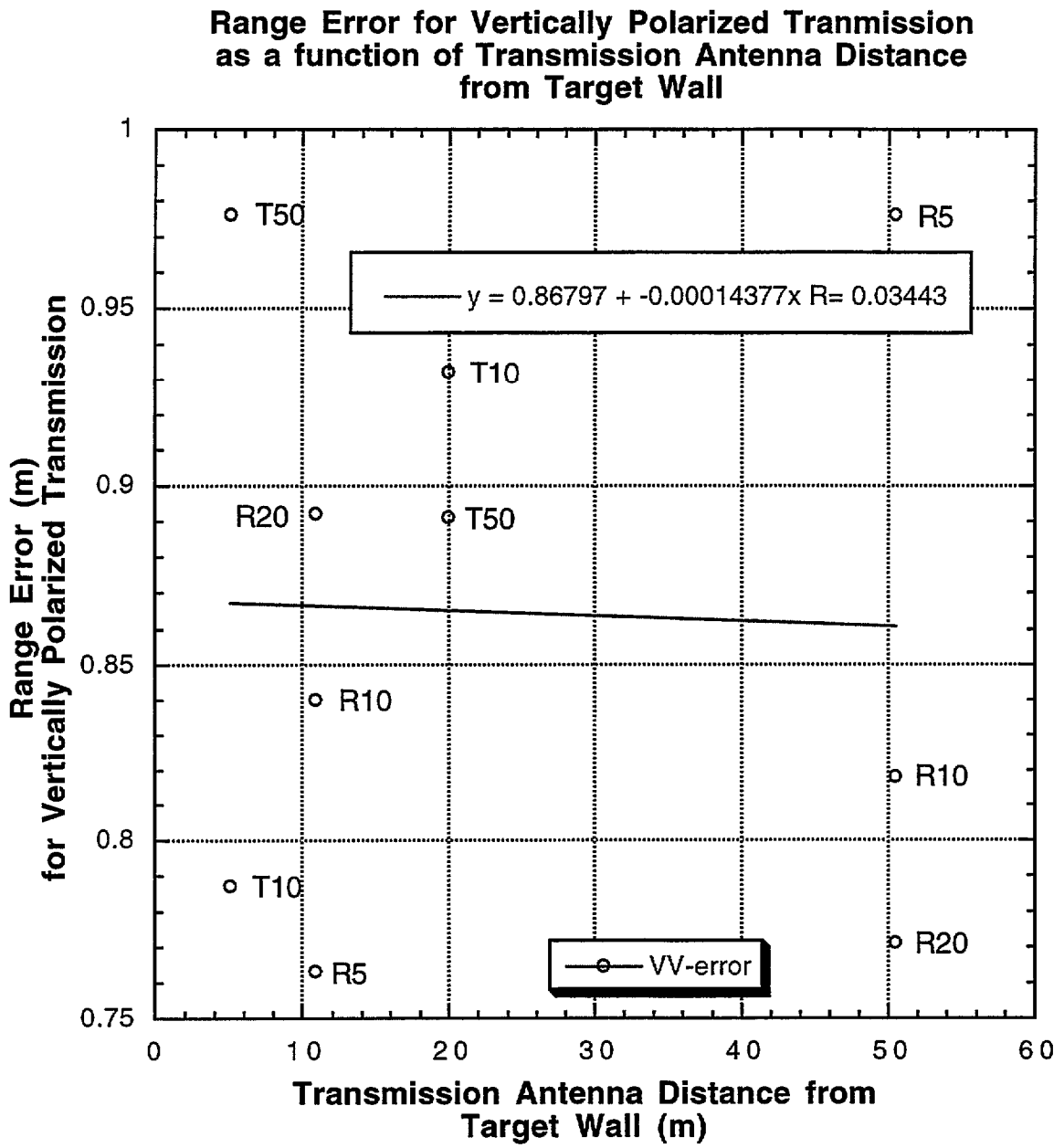

Figure 6.3.7b: Range error for vertically polarized transmissions as a function of transmission antenna distance from the target wall. Receiver locations are labelled beside each data point. The straight line is an approximate global fit which assumes that there is no affect on range error resulting from the distance of the receiving antenna from the target wall.

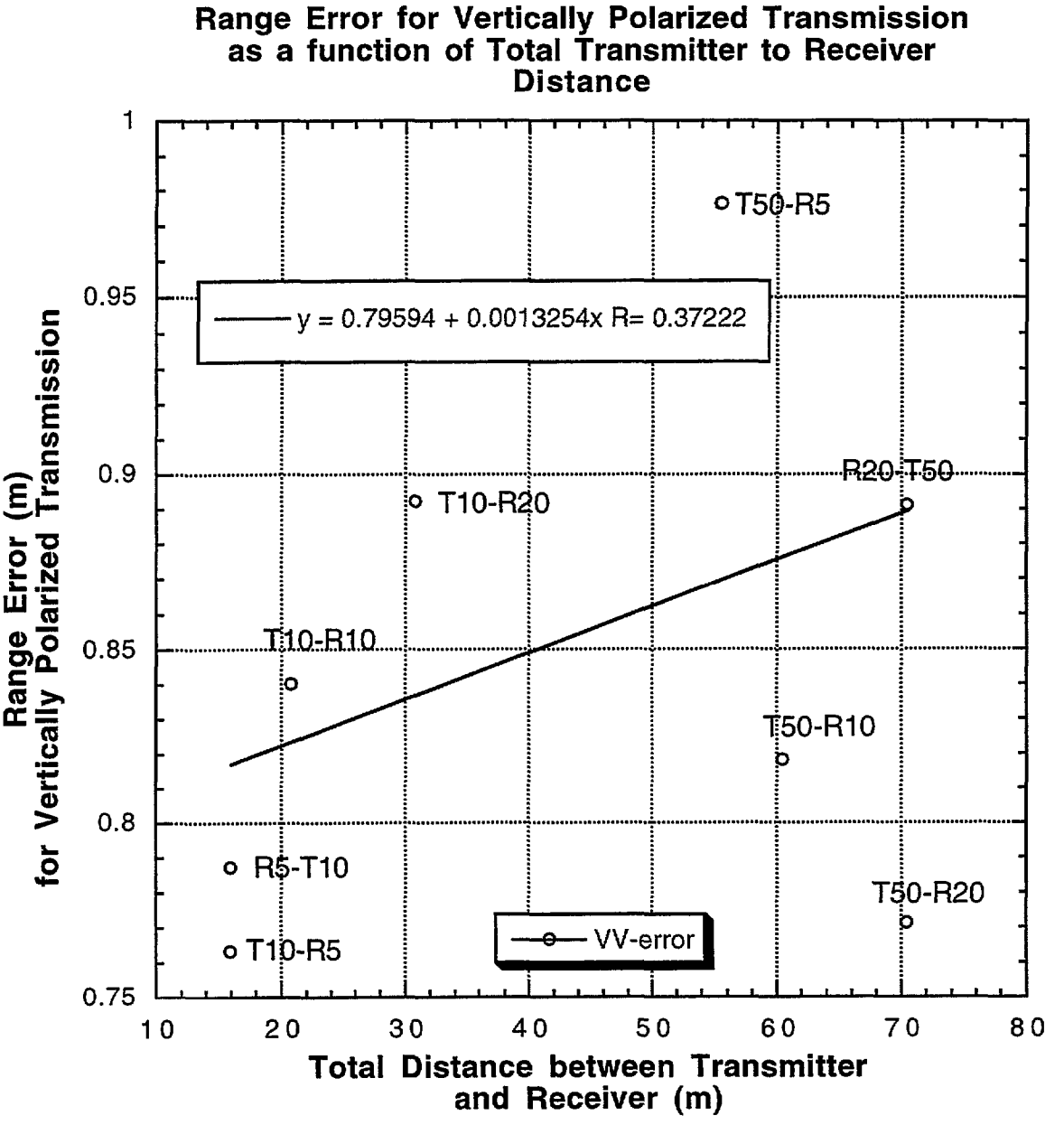

Figure 6.3.7c: Range error for vertically polarized transmission as a function of total transmitter to receiver distance. Individual test description is listed beside each point as (transmission station location - receiver station location).

Table 6.3.5: Direct Path Measurement Error

Path	Test	Polarization	Error	Notes:
T10-R10	wall-29	V V	0.840	ok, calibration offset required
R10-T50	wall-11	V V	ND	signal lost in noise
T50-R10	wall-24	V V	0.818	ok, partly merged with G peak
R20-T50	wall-14	V V	0.891	ok
R20-T10	wall-16	V V	0.932	ok
R5-T10	wall-19	V V	0.787	ok, merged with path C peak
R5-T50	wall-21	V V	0.976	ok
T50-R20	wall-25	V V	0.771	ok, partly merged with G peak
T10-R20	wall-28	V V	0.892	ok
T10-R5	wall-3	V V	0.763	ok, merged with path C peak
R10-T10	wall-18	V V	ND	signal lost in noise
T50-R5	wall-10	V V	0.976	ok
T10-R10	wall-30	HH	0.855	ok
R10-T50	wall-12	HH	0.762	ok partly merged with G peak
T50-R10	wall-23	HH	ND	signal lost in noise
R20-T50	wall-13	HH	0.911	ok
R20-T10	wall-15	HH	0.812	ok
R5-T10	wall-20	HH	0.937	ok
R5-T50	wall-22	HH	ND	signal lost in noise
T50-R20	wall-26	HH	0.821	ok, partly merged with G peak
T10-R20	wall-27	HH	0.932	ok
T10-R5	wall-4	HH	0.762	ok, merged with path C peak
R10-T10	wall-17	HH	0.870	ok
T50-R5	wall-9	HH	ND	signal lost in noise

We may further examine the data presented in Table 6.3.5 to determine if the above range error is correlated with three additional parameters: 1) the receiver distance from the target wall; 2) the transmitter distance from the target wall; and 3) the total distance between transmitter and receiver. Plots of range error versus these three variables are presented in Figures 6.3.7 and 6.3.8 for vertically and horizontally polarized transmissions, respectively.

Intuitively, one might expect that error would increase with range due to the greater distance the transmitted pulse must pass through the atmospheric air. However, previous discussions of EDM systems suggest that these errors can be expressed in the range of 5-10 ppm, well below the scatter shown in Figures 6.3.7 and 6.3.8. Although regression lines have been fitted to these data , and are labelled on the plots, the correlation between range and range error is slight at best. This implies that the scatter is associated with the penetration and re-transmission phenomenon as the wave passes through the wall. Some of this scatter may be attributable to the non-homogenous nature of the target wall itself. As shown in Figure 4.1.3, the slabs

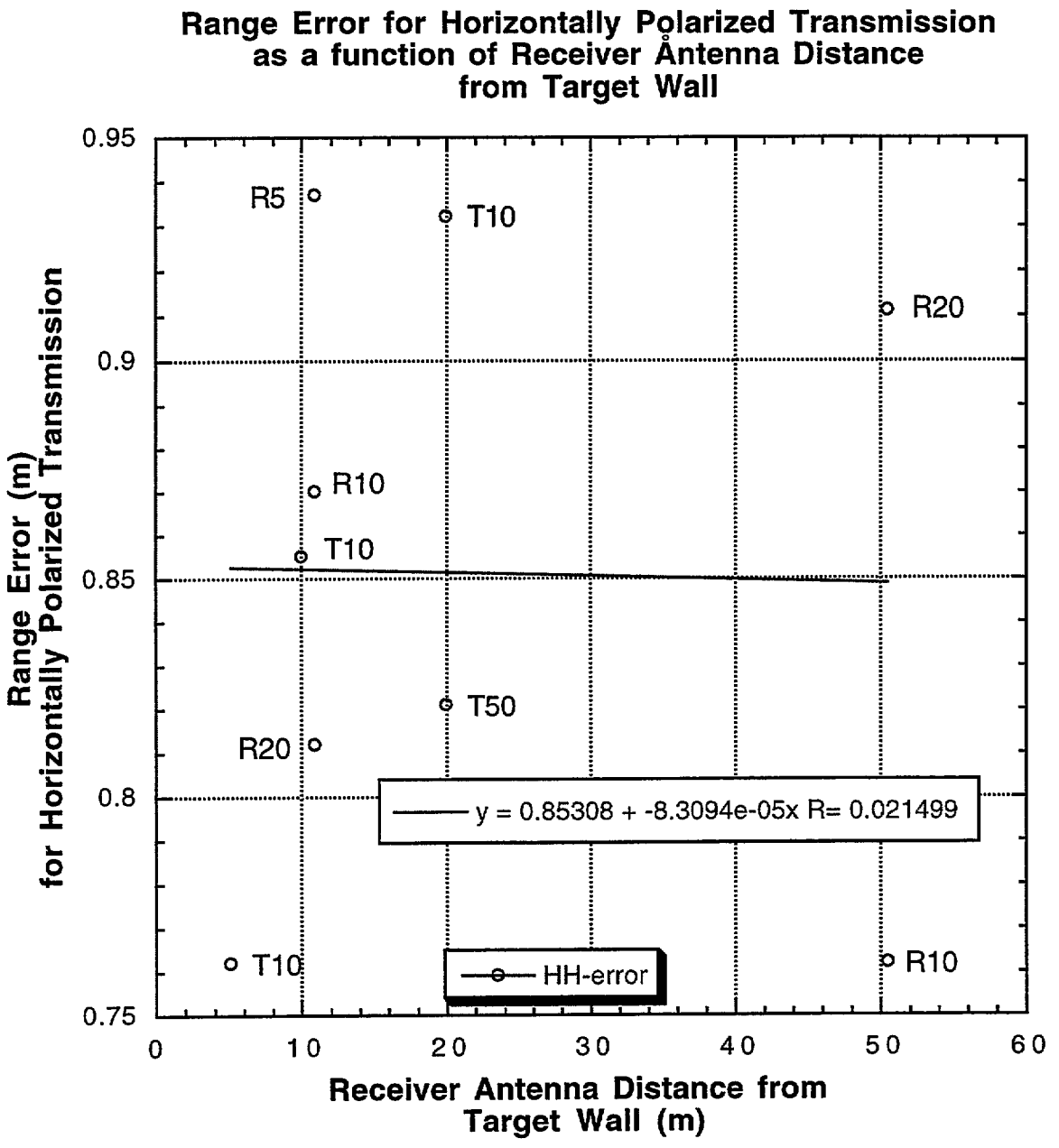

Figure 6.3.8a: Range error for horizontally polarized transmissions as a function of receiver antenna distance from the target wall. Transmitter locations are labelled beside each data point. The straight line is an approximate global fit which assumes that there is no affect on range error resulting from the distance of the transmitting antenna from the target wall.

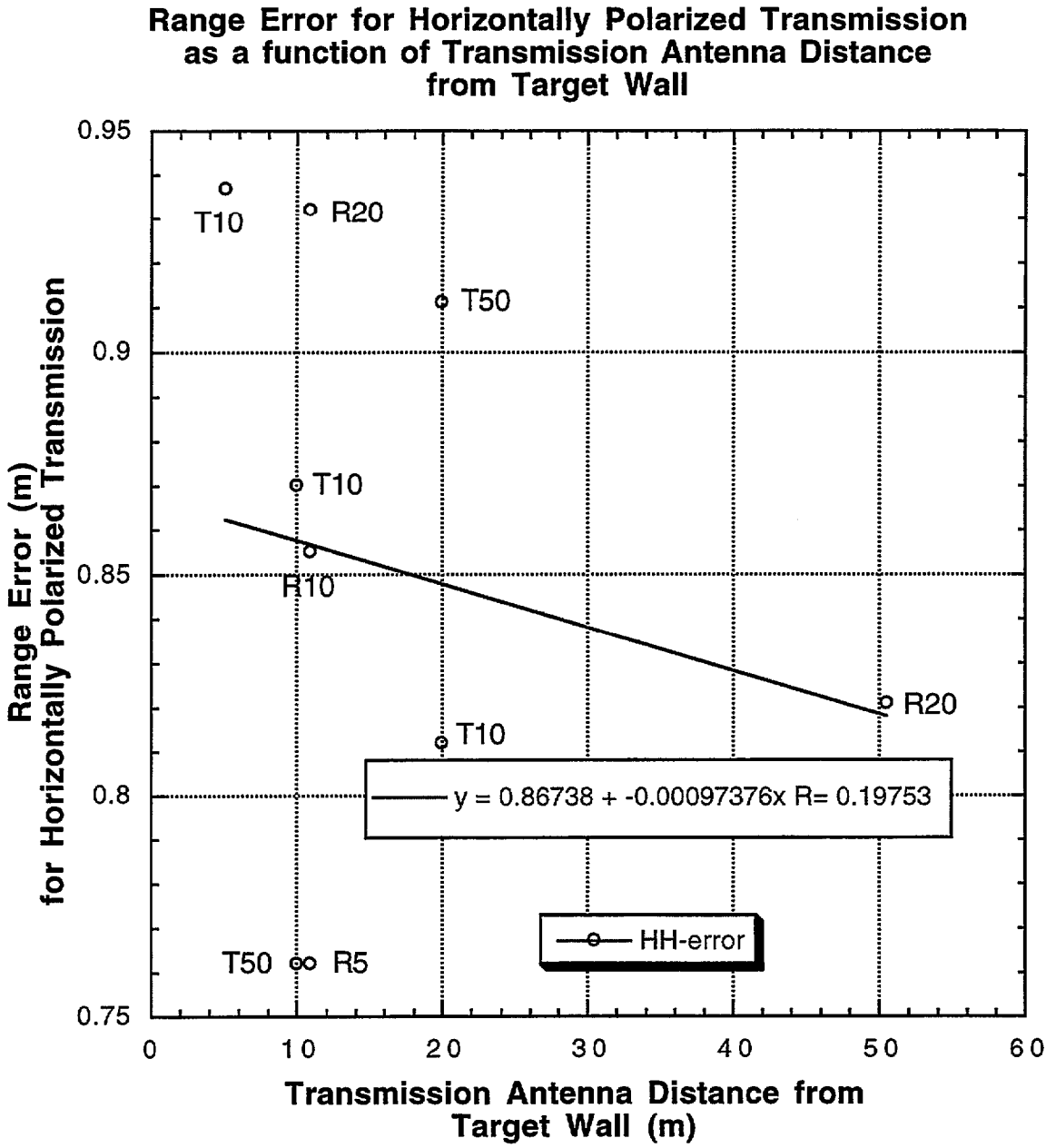

Figure 6.3.7b: Range error for horizontally polarized transmissions as a function of transmission antenna distance from the target wall. Receiver locations are labelled beside each data point. The straight line is an approximate global fit which assumes that there is no affect on range error resulting from the distance of the receiving antenna from the target wall.

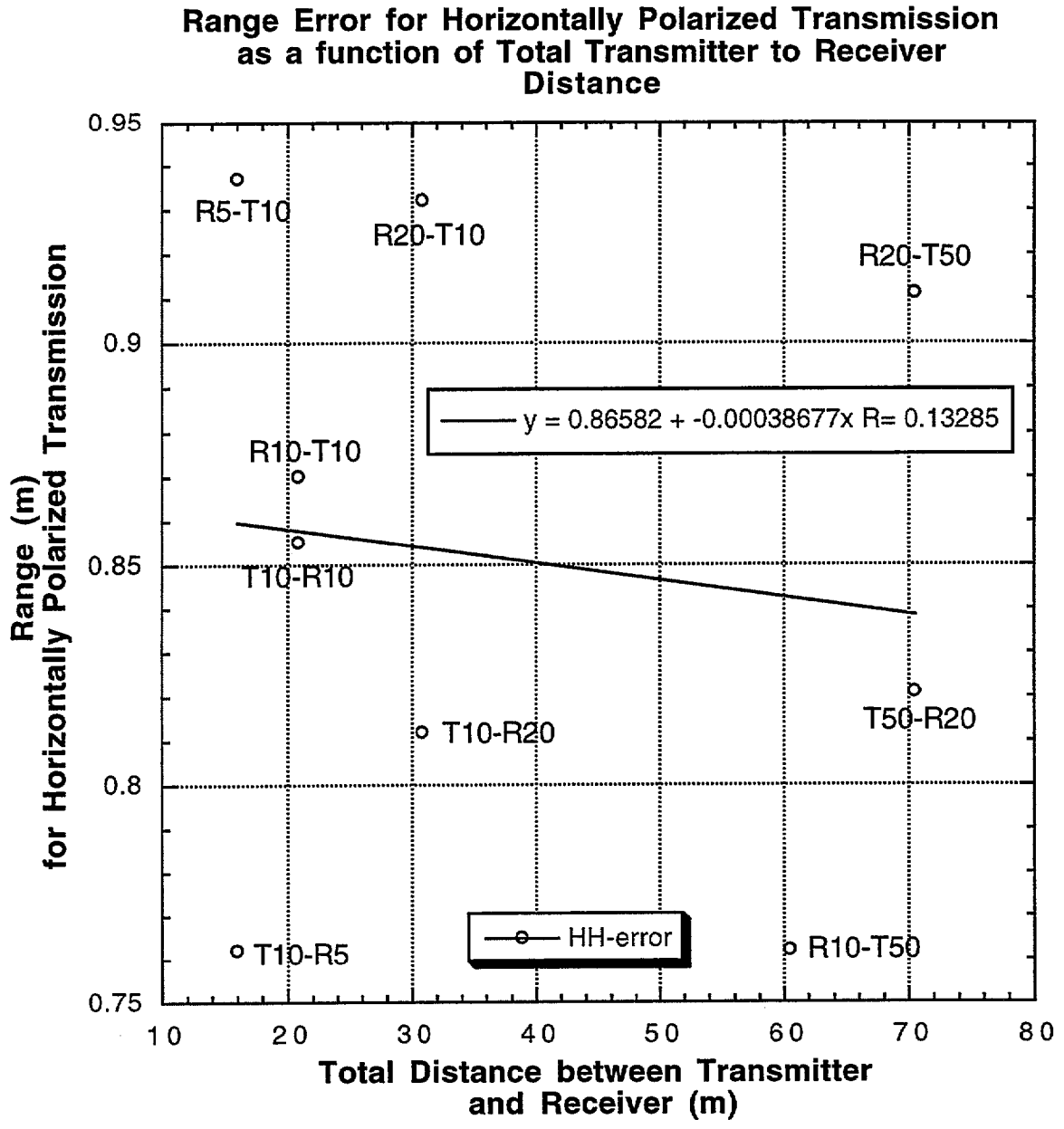

Figure 6.3.7c: Range error for horizontally polarized transmission as a function of total transmitter to receiver distance. Individual test description is listed beside each point as (transmission station location - receiver station location).

used to fabricate the target wall were previously used for non-destructive evaluation tests and contained embedded "flaws" in the form of styrofoam disks and rebar. Of course, actual construction sites will contain flaws (unplanned) and rebar (planned) within concrete walls.

Dielectric Constant for Concrete Target Wall

How much is the signal delayed, on average, as it penetrates directly through the 500 mm thick wall? Another means of stating this question is: "what is the dielectric constant for this engineering material?" Returning to Figure 6.3.4, we see an error between the known distance (20.910 m) and the Path A distance as seen by the radar (21.765 m) of 0.855 m. The error is positive, meaning that the arrival time was delayed due to propagation through the wall. Furthermore, the magnitude of the through-the-wall distance is approximately -8 dB down from the first peak, meaning the received power is less than 16% that of the first (diffracted) signal. By re-arranging eq.(6.2.16) we obtain the relationship for range error, ΔR, as a function of dielectric constant as:

$$\Delta R = \Delta t \cdot c = d(\sqrt{\varepsilon_r} - 1) \qquad \text{eq.(6.3.1)}$$

solving for ε_r, we obtain:

$$\varepsilon_r = \left(\frac{\Delta R}{d} + 1\right)^2 \qquad \text{eq.(6.3.2)}$$

for the case just described, where ΔR = 0.855 m and d = 0.500 m, we obtain an empirical estimate for the dielectric constant for the reinforced concrete wall as:

$$\varepsilon_r = \left(\frac{0.855}{0.500} + 1\right)^2 = 7.34 \qquad \text{eq.(6.3.3)}$$

Eq. (6.2.16) may be plotted, as shown in Figure 6.3.9, to illustrate the range error dependency on wall thickness and dielectric constant. As explained earlier, denser construction materials can be expected to have higher dielectric constants and produce greater range errors. A corrolary is that non-homogenous engineering materials (e.g. concrete with significant random voids) will produce random scattering in the results which serves to reduce the level of certainty associated with a measurement.

Examination of Table 6.3.5 and the use of eq.(6.3.2) allows for a statistical estimate to be made of both the range error, ΔR, and the dielectric constant, ε_R, for the target wall. These are presented below in Table 6.3.6. Results are presented for both vertically polarized transmissions (VV) and horizontally polarized transmissions (HH).

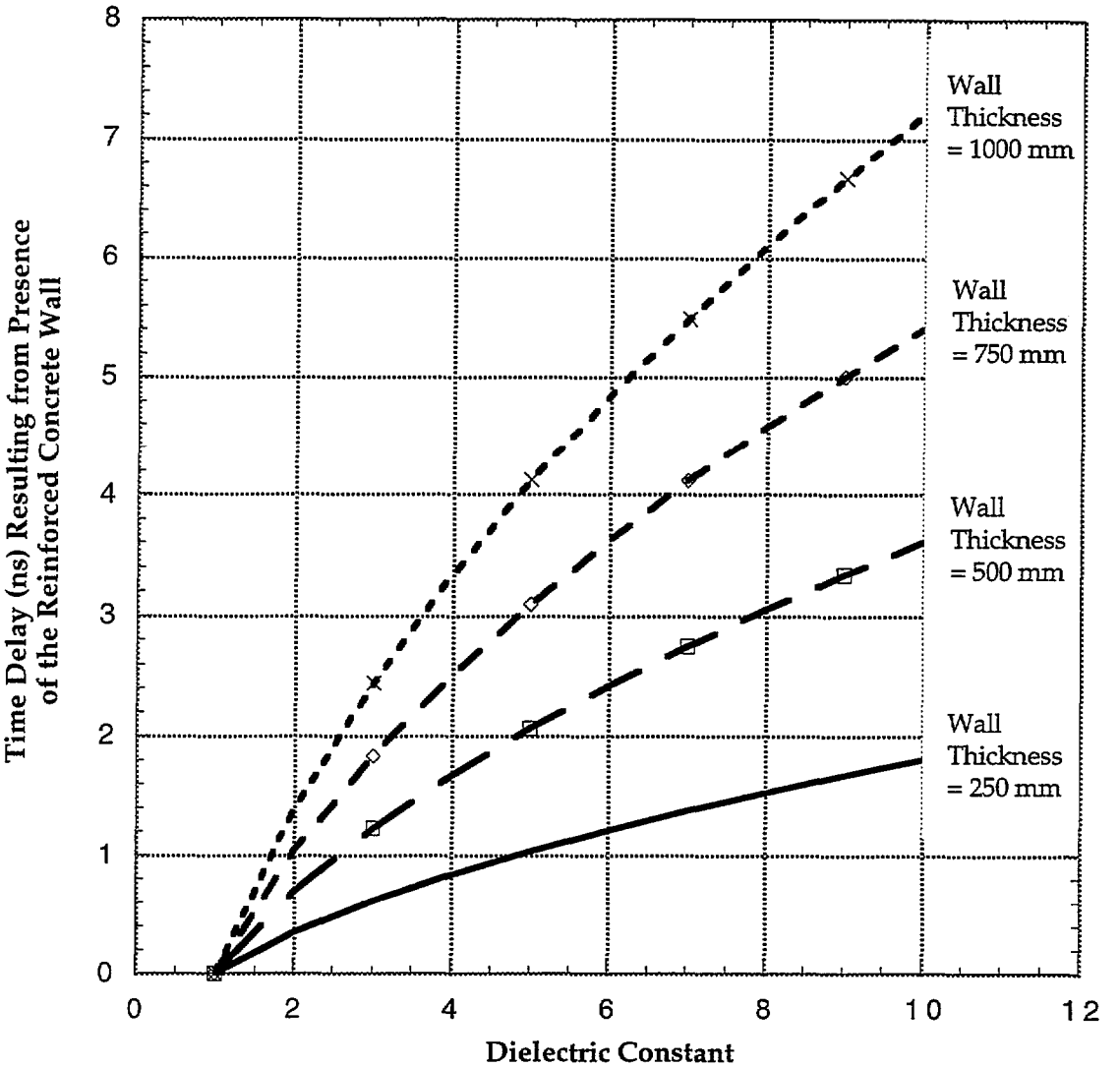

Figure 6.3.9: Time delay (in nanoseconds) as a function of dielectric constant for several non-metallic wall thicknesses.

There are two important observations relating to range error as observed during the Building 226 target wall tests. First, the mean value for range error is effectively insensitive to the polarization of the transmitted signal. In other words there appear to be no particular benefits in terms of precision associated with polarization.

Second, the mean range error is significant, on average about 860 mm. This error is independent of the absolute range. It is, however, proportional to the thickness and dielectric constant for the target wall. If we require a 95% confidence interval ($\pm 2\sigma$) on this measurement, then we must add the qualification ±156 mm for the vertical polarization figures and ±140 mm for the horizontally polarized tests. This latter term is likely related to the degree of homogeneity in the construction material.

The good news is that we were able to survey through 500 mm of reinforced concrete. The accuracies listed in Table 6.3.6 would, in fact , be quite sufficient for the purposes of keeping track of machines, individuals, and materials. The bad news is that the presently achieved accuracies are insufficient for vehicle control, automated placement of components, and for logging the as-built structural configuration. Accurate knowledge of the material propagation characteristics, e.g. as related to the dielectric constants given in Table 6.3.6, will allow development of compensation algorithms which will eliminate the bulk of the range error. If errors due to propagation delay were completely eliminated, we would still have a statistical distribution of uncertainty associated with propagation through a non-homogenous medium. It may be possible to shrink these errors by means of ambiguity resolution techniques and the use of many transmission stations.

Table 6.3.6: Range Error and Dielectric Constant Statistics for 500 mm Wall Tests

Statistic:	V V Range error (m)	HH Range error (m)	Dielectric Constant VV Polar.	Dielectric Constant HH Polar.
Minimum	0.763	0.762	6.381	6.371
Maximum	0.976	0.937	8.714	8.260
Sum	8.526	7.782	73.403	67.202
Points	10	9	10	9
Mean	**0.853**	**0.865**	**7.340**	**7.467**
Median	0.829	0.870	7.065	7.508
RMS	0.856	0.867	7.386	7.501
Std Deviation	**0.078**	**0.070**	**0.862**	**0.759**
Variance	0.006	0.005	0.744	0.577
Std Error	0.025	0.023	0.273	0.253
Skewness	0.537	-0.442	0.591	-0.404
Kurtosis	-1.051	-1.280	-1.001	-1.315

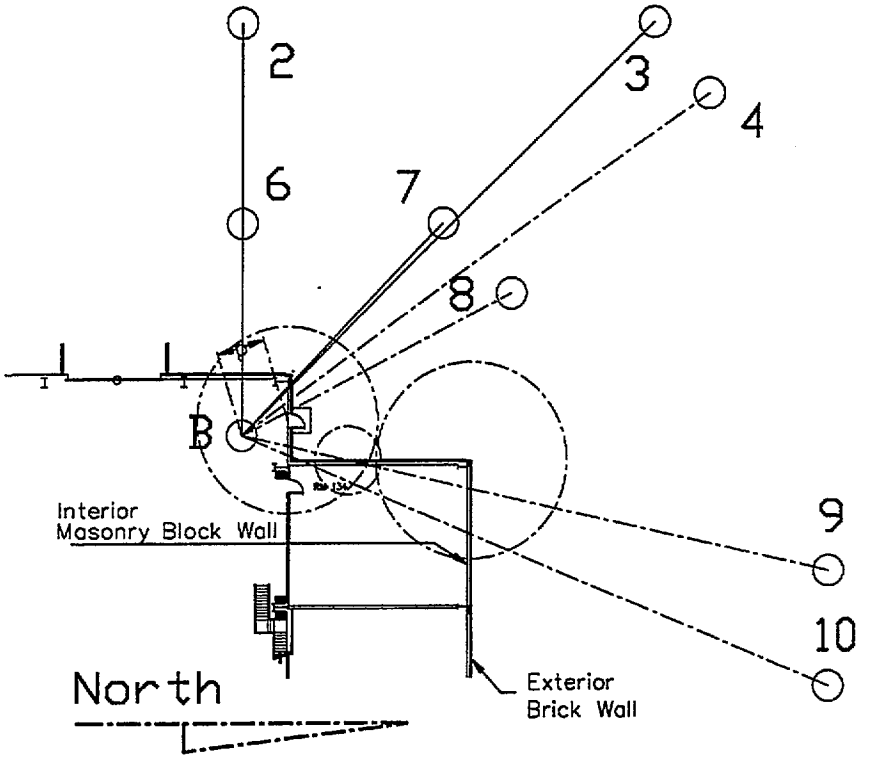

Figure 6.4.1: Building 202 NIST NLS test range showing locations of survey shots used for estimating dielectric constants for the exterior building wall and its components.

6.4 Discussion of Building 202 Tests

Table 6.4.1 summarizes data for all tests conducted at Building 202 for which the interior target was point "B." Figure 6.4.1 shows a schematic of the various tests. Also presented in Table 6.4.1 are the total wall penetration distances for the respective constituent materials. The wall structure at Building includes an exterior brick facing laid against an interior masonry block wall.

In all but two test configurations (2-to-B and 6-to-B) multipath routes existed which accounted for the first detected peak in the time history plots (See Appendix B). These multipath peaks relate to the presence of a door on the northwest corner of the building (Figure 6.4.1). Although the door was metal, it contained a large glass window through which electromagnetic radiation could pass. A typical multipath route exists, for example, for a ray eminating from a transmitter at Station 9 which diffracts around the northwest corner of the building, passes through the door window and arrives at the receiver at Station B. Such multipath distances can be calculated from CAD models of building 202 and the pre-defined survey grid established as part of the experiment. It can be shown that the multipath signal will always arrive first for these particular tests, owing to the delay in the arrival of the direct signal due to its slower passage through the various masonry block and brick walls. Table 6.4.1 lists both "true" (line-of-sight surveyed) direct and multipath distances between the various points as well as the radar measurements for the same station pairs.

Table 6.4.1: Summary of Brick and Masonry Block Penetration Tests

Transmit-Receive Station	Test ID	Pol.	Total Brick Pen. (m)	Total Mas. Block Pen. (m)	True MP Dist. (m)	Meas. MP Dist. (m)	True Dist. (m)	Meas. Radar Dist.	ΔR [Ra Err (m
			D1	**D2**					**ΔR**
2 to B	202-28-14T	V V	0.102	0.203	none	none	26.613	27.160	0.5
3 to B	202-28-11T	V V	0.142	0.284	38.536	38.562	38.173	38.925	0.7
4 to B	202-28-10T	V V	0.125	0.250	38.133	38.265	37.970	38.875	0.9
6 to B	202-28-03T	V V	0.102	0.203	none	none	13.605	13.872	0.2
7 to B	202-28-06T	V V	0.145	0.290	19.511	19.393	19.074	19.670	0.5
8 TO B	202-28-07T	V V	0.114	0.228	20.124	20.097	20.078	20.475	0.3
9 to B	202-29-27T	V V	0.651	1.303	40.268	40.322	39.778	43.220	3.4
10 to B	202-29-23T	V V	0.480	0.957	43.413	43.597	42.098	44.896	2.7
10 to B	202-29-24T	V V	0.480	0.957	43.413	43.415	42.098	44.775	2.6
11 to B	202-29-19T	V V	0.123	0.400	49.501	none	46.904	none	N/

2 to B	202-28-13T	HH	0.102	0.203	none	none	26.613	27.150	0.53
3 to B	202-28-12T	HH	0.142	0.284	38.536	38.563	38.173	38.915	0.74
4 to B	202-28-09T	HH	0.125	0.250	38.133	38.293	37.970	39.790	1.82
6 to B	202-28-04T	HH	0.102	0.203	none	none	13.605	13.894	0.28
7 to B	202-28-05T	HH	0.145	0.290	19.511	19.493	19.074	19.840	0.76
8 TO B	202-28-08T	HH	0.114	0.228	20.124	20.111	20.078	20.475	0.39
9 to B	202-29-26T	HH	0.651	1.303	40.268	40.322	39.778	42.975	3.19
10 to B	202-29-25T	HH	0.480	0.957	43.413	43.570	42.098	44.735	2.63
11 to B	202-29-20T	HH	0.123	0.400	49.501	none	46.904	none	N/A

The *anticipated* range error for the above tests is related to the material penetrations and respective dielectric constants using eq.(6.2.17) as:

$$\Delta R = D1(\sqrt{\varepsilon_{R1}} - 1) + D2(\sqrt{\varepsilon_{R2}} - 1) \qquad \text{eq.(6.4.1)}$$

From experiment we have ΔR, D1, and D2 , as given in the table. It is possible to obtain estimates for the dielectric constants ε_{R1} andε_{R2} by means of regression analysis. For the vertically polarized data (VV) listed in Table 6.4.1 it can be shown that an effective data fit can be achieved for ε_{R1} andε_{R2} equal to 5.2 and 9.5, respectively. This combination produces a residual standard deviation of 0.1973. However, the uncertainty associated with ε_{R1} andε_{R2} is high, meaning that other, significantly different combinations (e.g. ε_{R1}=9.7 and ε_{R2}=7.1 produce a residual standard deviation of 0.1971). The problem arises because D1 and D2 are linearly related, due to the construction technique of facing the masonry block walls with brick.

There is an important conclusion to be drawn from the above discussion. At a working construction site such situations involving interlaced materials and adjacent walls occur all the time. The dielectric constants for each material, if known ahead of time with robust statistical underpinning, can be used in real-time compensation systems which will effectively remove the delay time error due to propagation of the wave through the various material layers. This can be done provided a) a real-time CAD database is maintained for the as-built structure, b) a database of electromagnetic penetration characteristics exists for each material and c) a software algorithm can be developed which seeks to minimize spherical error probable (SEP). The development of statistical models for material dielectric constants requires more sophisticated experiments than those conducted at Building 202.

Metal Roll-up Door Tests

In Table 5.3.2 data were presented for a series of tests involving the presence of a metal roll-up door between the transmitting and receiving antennas. For these tests the transmitter was located at exterior station "1" while the receiver was located successively further inside the building at interior stations A, C, and G, respectively. We did not expect to observe detectable signals when the door was completely closed, and none were observed. As described earlier in Chapter 4, the transmitted signal is both reflected and dissipated within the metal panel in accordance with Maxwell's Laws. The intent of this series of tests was to investigate the effect of the presence of a gap between the base of the metal door and the concrete building foundation. Tests at the Building 226 concrete wall suggested that diffraction phenomena will produce multipath signals that can arrive ahead of the direct path signal, which may be delayed as it propagates through engineering materials. However good the correlation between the expected diffracted distances and those peaks which appeared on the time domain response, there was always the possibility that some alternative multipath route existed which might account for that peak. In other words, the close correlation in itself was not an absolute proof that the multipath signal due to diffraction was the one that caused that peak; it could have been caused by some other unidentified multipath route.

The Building 202 roll-up door tests provide the necessary proof that the diffraction multipath peaks are in fact the first arrival peaks. Figures 6.4.2 a,b, and c provide plots of range error as a function of the gap height between the base of the roll-up door and the concrete floor. As the door is raised the gap height increases until eventually the door is completely open and there is direct line-of-sight between the transmitter and receiver. Until the line-of-sight measurement becomes possible there exist only two possible detection paths: 1) diffraction around the bottom of the metal door and 2) ground bounce off the concrete floor beneath the metal door. These two transmission paths are shown graphically in Figure 6.4.4. The ground bounce error remains constant and is given by:

$$e_{GB} = \sqrt{(H_r - H_t)^2 + (D_t + D_r)^2} - \left(\sqrt{H_t^2 + D_t^2} + \sqrt{H_r^2 + D_r^2}\right) \qquad \text{eq.(6.4.2}$$

while the error in the multipath signal, which is diffracted around the bottom of the roll-up door, decreases as the door gap height increases:

$$e_{MP} = \sqrt{(H_r - H_t)^2 + (D_t + D_r)^2} - \left(\sqrt{(H_t - H_{gap})^2 + D_t^2} + \sqrt{(H_r - H_{gap})^2 + D_r^2}\right) \qquad \text{eq.(6.4.3)}$$

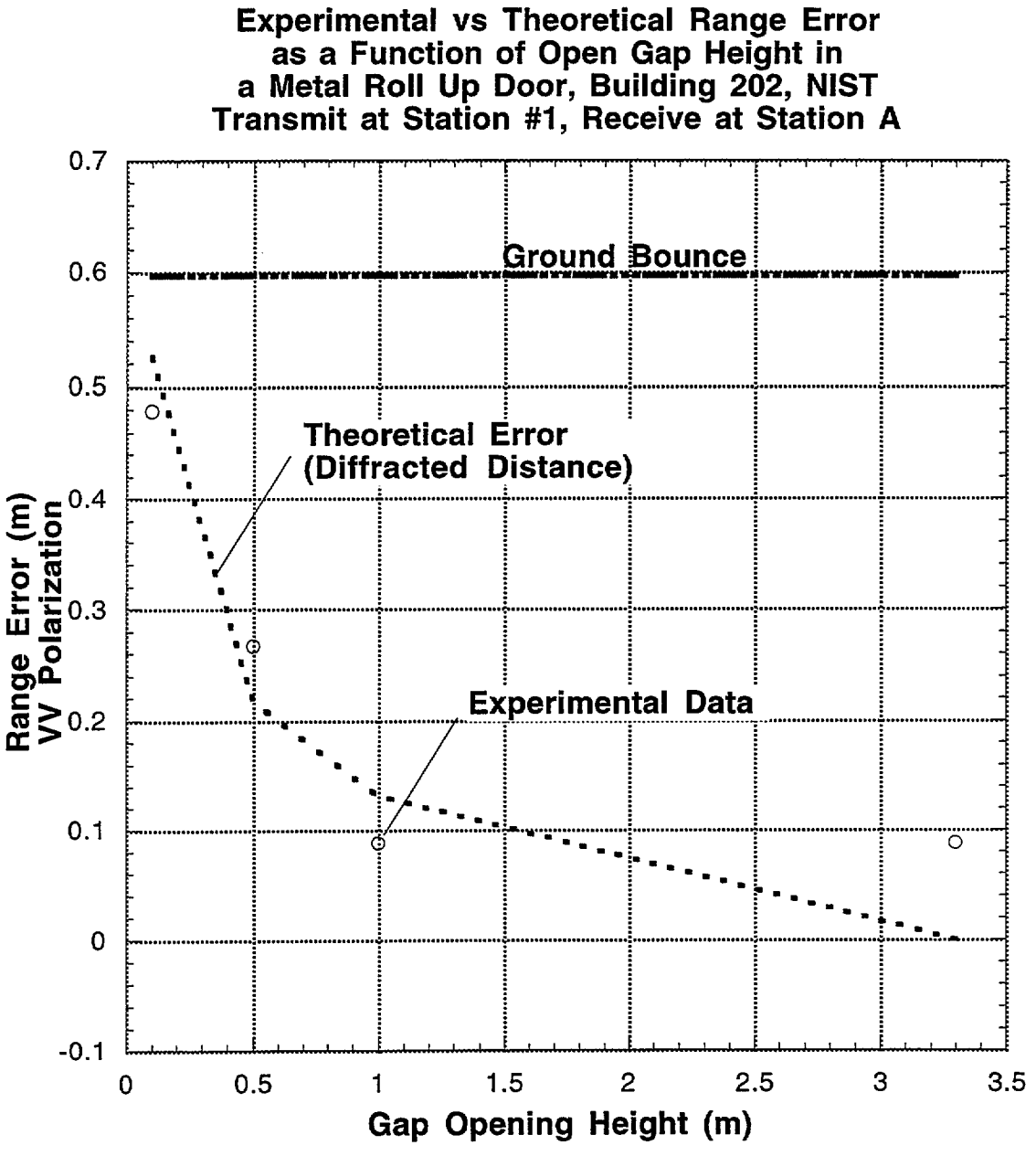

Figure 6.4.2a: Experimental and theoretical range error as a function of gap opening height in a metal roll up door at the NIST Building 202 NLS test range. Transmitter is located at exterior station #1 and the receiver is located at interior station A.

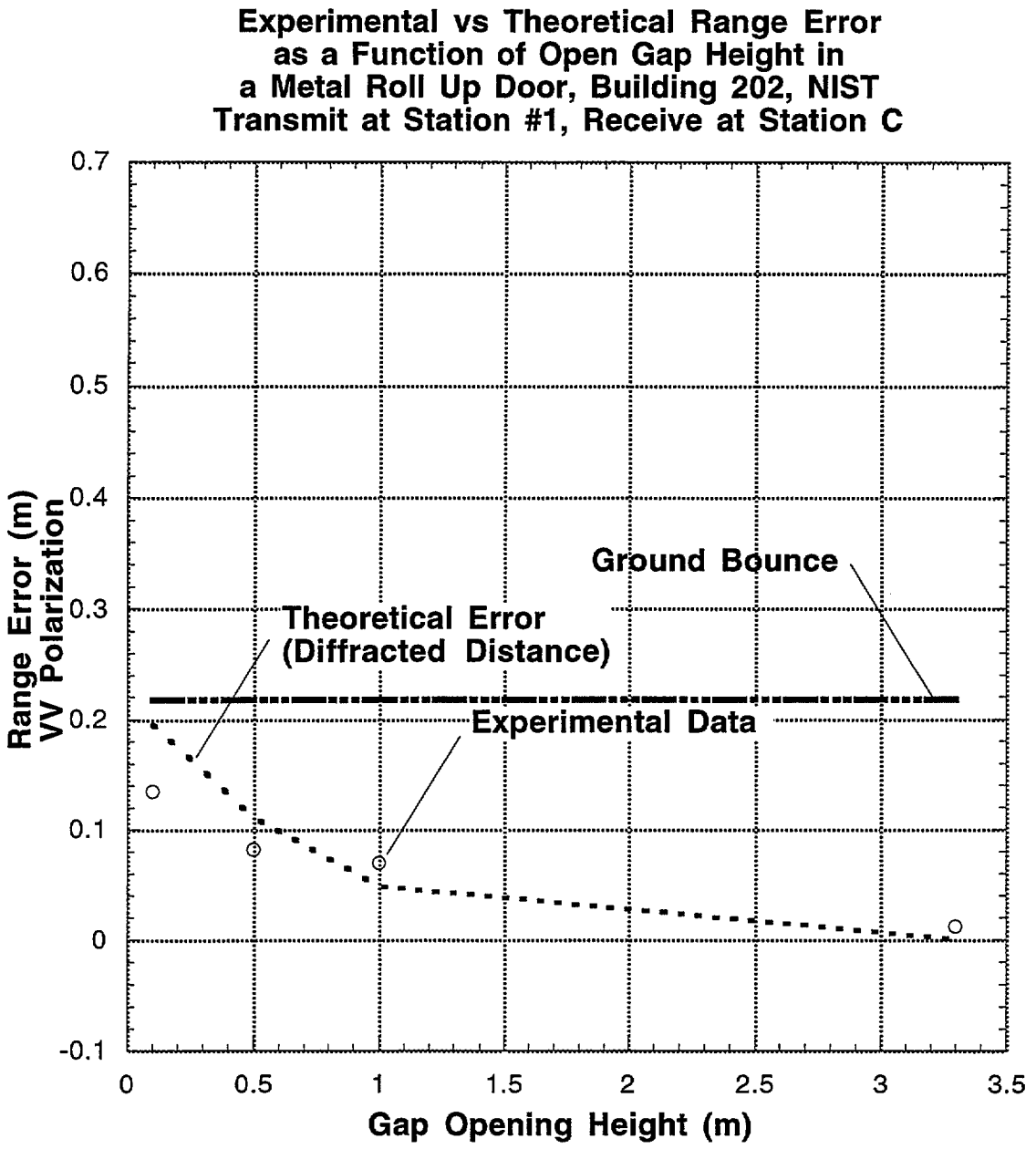

Figure 6.4.2b: Experimental and theoretical range error as a function of gap opening height in a metal roll up door at the NIST Building 202 NLS test range. Transmitter is located at exterior station #1 and the receiver is located at interior station C.

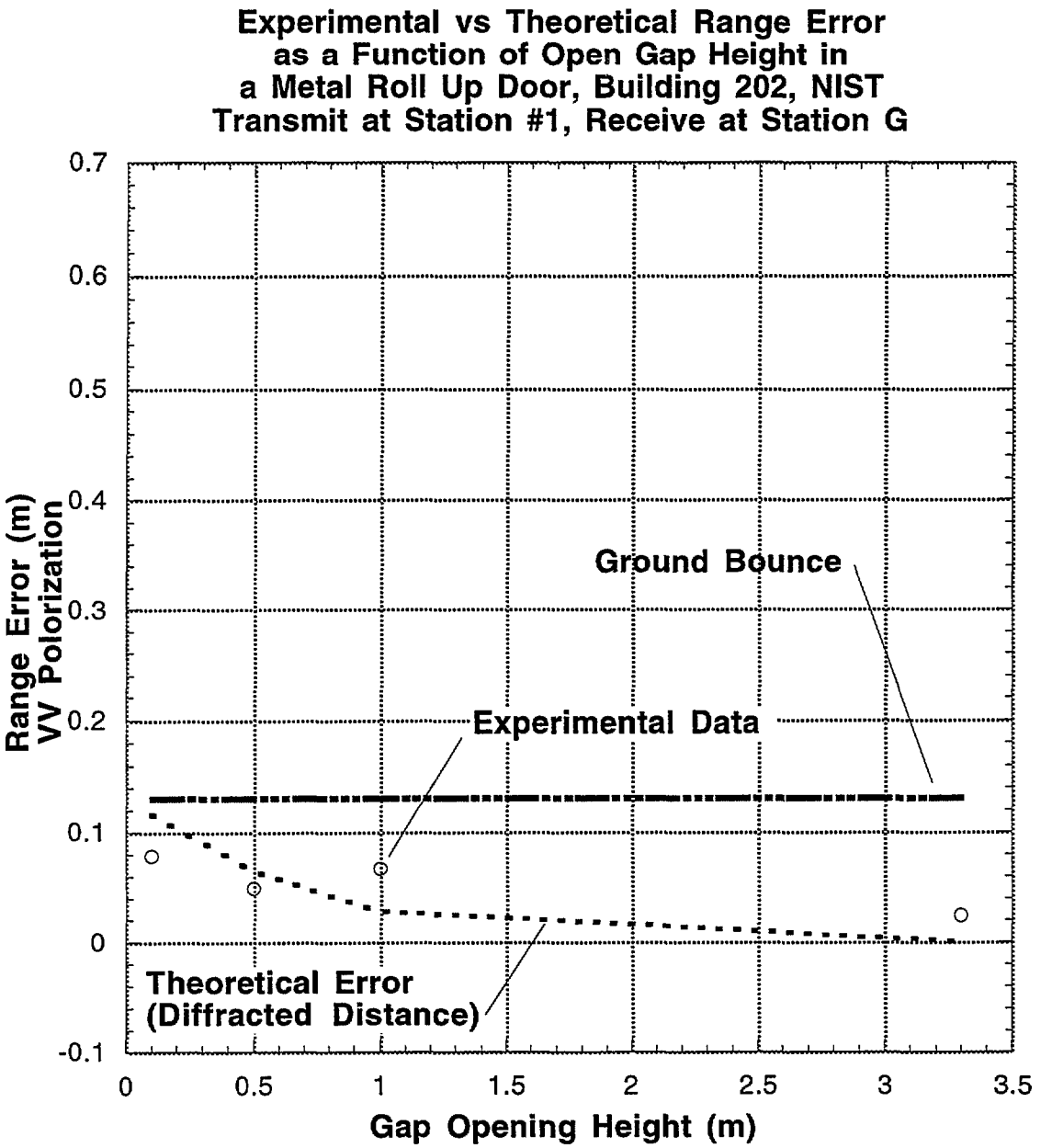

Figure 6.4.2c: Experimental and theoretical range error as a function of gap opening height in a metal roll up door at the NIST Building 202 NLS test range. Transmitter is located at exterior station #1 and the receiver is located at interior station G.

These predicted error quantities, e_{GB} and e_{MP}, are plotted against the experimentally measured range error in Figures 6.4.3 a, b, and c. Clearly the experimental range error associated with the first detected peak in the time domain response tracks the predicted multipath error associated with a diffracted ray which bends around the base edge of the roll-up door.

Table 6.4.2: Range Error vs Roll-Up Door Gap Opening Height for Station 1 to A:

Gap Height (m)	Direct Range (m)	Predicted Range Error Due to Diffraction (m)	Predicted Range Error Due to Ground Bounce (m)	Experiment First Arrival Range Error (m)
0.100	26.339	0.526	0.597	0.479
0.500	26.339	0.218	0.597	0.267
1.000	26.339	0.132	0.597	0.088
3.300	26.339	0.000	0.597	0.088

Table 6.4.3: Range Error vs Roll-Up Door Gap Opening Height for Station 1 to C:

Gap Height (m)	Direct Range (m)	Predicted Range Error Due to Diffraction (m)	Predicted Range Error Due to Ground Bounce (m)	Experiment First Arrival Range Error (m)
0.100	35.484	0.195	0.218	0.135
0.500	35.484	0.111	0.218	0.082
1.000	35.484	0.048	0.218	0.070
3.300	35.484	0.000	0.218	0.012

Table 6.4.4: Range Error vs Roll-Up Door Gap Opening Height for Station 1 to G:

Gap Height (m)	Direct Range (m)	Predicted Range Error Due to Diffraction (m)	Predicted Range Error Due to Ground Bounce (m)	Experiment First Arrival Range Error (m)
0.100	52.983	0.117	0.130	0.079
0.500	52.983	0.065	0.130	0.049
1.000	52.983	0.028	0.130	0.067
3.300	52.983	0.000	0.130	0.024

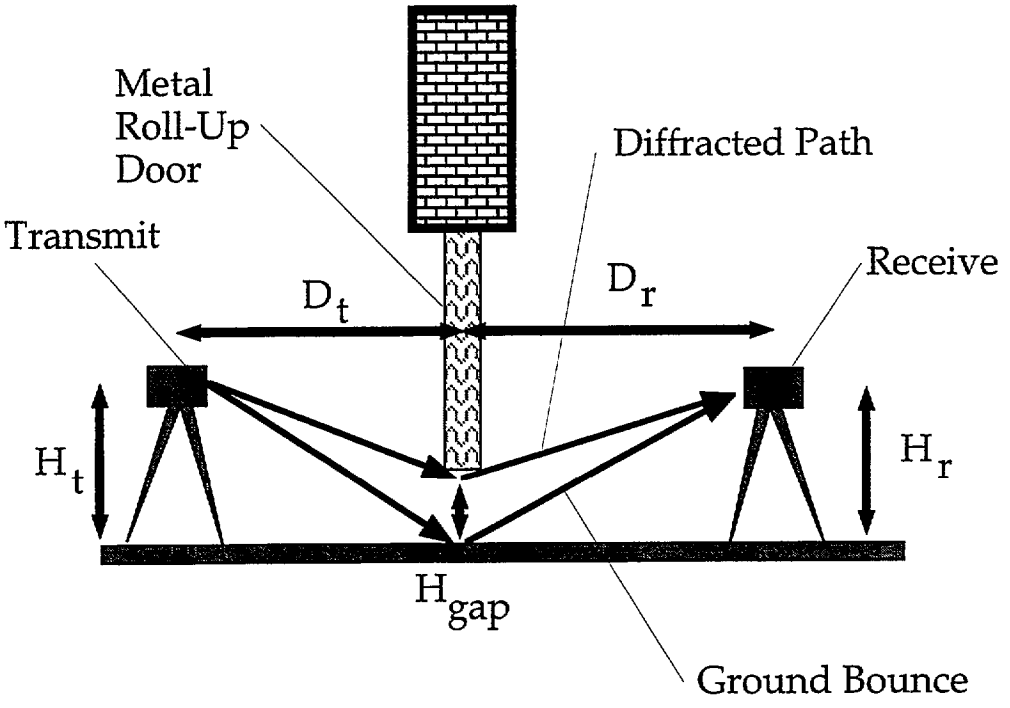

Figure 6.4.3: Transmission through a horizontal gap
in a metal roll up door at the NIST Building 202
NLS test range.

Several observations can be made from these tests:

- Multipath range errors can be predicted from as-built geometry. This implies that automated correction algorithms could be developed to provide on-the-fly compensation for such effects for kinematic position tracking at a construction site.
- Even a small gap in an otherwise impenetrable metal wall will permit entry of the transmitted electromagnetic wave. This gap need not be an open-air pathway. The previously described masonry block and brick wall penetration tests showed that a relatively small glass window within an all-metal door provides sufficient pathway to receive the transmitted signal within the building. Other tests, e.g. those described in Table 5.3.3, provide similar data to this effect.

6.5 Recommended Future Research

The experiments described in this report may be considered a tentative first step towards the realization of non-line-of-sight construction metrology. Many obstacles remain along the path to developing a commercially viable real-time positioning system based on this technology. The major impediments include:

- *Determination of Dielectric Constants as a function of power, material, thickness, angle of incidence, frequency, and signal processing technique.*

  Range error due to propagation delays in the transmitted signal as it passes through engineering materials represents the single largest source of error in NLS metrology. Compensation algorithms will of necessity have to predict the delay time for a given transmitted signal along any geometric path. Material characterization (dielectric and permitivity constants) presents the first major task. Not only is a standard database of electromagnetic penetration characteristics required for all engineering materials, so too are statistical models which relate the degrees of confidence associated with each property. These data will be essential to providing on-the-fly determination (and eventual minimization of) of spherical error probable at the roving receiver. Some common engineering materials, reinforced concrete being the best example, change properties with age. Following the casting of concrete, compressive and tensile strength increase with age until reaching an asymtotic value which represents the final achievable value. Electromagnetic penetration properties of these same materials also change with age and may change with the sustained application of stress over time. Concrete, for example, undergoes creep and shrinkage with time, both of which affect the geometry of the completed component. Likewise, density changes with curing time. In the case of these materials, special efforts will need to be made to characterize electromagnetic

penetration and propagation characteristics. NIST has identified research in this area as having top priority in construction metrology research and laboratory tests to determine these properties are set to commence in early 1996.

- *Clutter & Multipath discrimination (ray tracing)*

The second largest source of error in NLS metrology arises from the classic radar problem of clutter and multipath signal discrimination, i.e. the selection of the "true" target distance from alternative peaks. As was demonstrated at both Building 226 and Building 202, the transmission antenna effectively broadcasts a wide fan of electromagnetic radiation at the building and at the target receiver located behind the wall, or inside the building. This radiation fan is much like that from a visible spectrum floodlight. Like visible light, the radar transmission can be reflected , diffracted, and scattered. In the development of an automated position acquisition system, all of these possible paths must be considered and all but the direct, or "true," path rejected. One possible means for achieving this is to apply techniques originally developed for computer graphics rendering known as "ray tracing." In the construction automation scenario, a CAD model which represents the as-built structure must be maintained in near real-time. This means that, as various components are constructed, their presence and location must be made known to a global construction site database. With this information, and the absolute positions of the NLS transmission systems (which presumably would be arrayed around the construction to ensure coverage by at least three transmitters at all times) it is possible to solve mathematically for all possible detectable peaks in the time domain reponse function at the receiver. These can then be used in conjunction with a discrimination algorithm, likely based on expert systems theory, to reject the multipath signals, extract the propagation delay error, and assign a statistical error quantity to the expected direct signal distance. The transmission array will be designed such that each transmission antenna is pulsed in sequence with the delay times set so that no ambiguity will arise as to which is the source for the present signal. The development of this on-the-fly compensation algorithm, as well as appropriate computational hardware to run it on (keeping in mind the constraints of a backpack-born positioning system) will represent a major undertaking.

- *Resolution/Accuracy Enhancement (super resolution algorithms)*

The present limiting resolution for spread spectrum NLS technology is defined by eq.(3.3.3) indicates that the achievable accuracy is inversely proportional to bandwidth and signal-to-noise ratio. The use of wider bandwidths can be investigated as part of the 1996 construction automation laboratory program at NIST. The signal-to-noise ratio, however, might be dramatically improved through the use of existing image enhancement algorithms developed for the processing of deep space probe images as well as through the use of so-called

"super resolution" algorithms under development at various laboratories, including MIT Lincoln Lab.

- *Compensation Contour Field*

It may be appreciated that with sufficiently robust field data and material properties for the as-built structure it should be possible to calculate position-dependent compensation constants for every point in three dimensional space within a construction jobsite which would serve to characterize the anticipated frequency response waveform at a given position for each transmitter. This task could be performed remotely via massively parallel processing. A compressed, encoded packet of compensation constants could then be omnidirectionally broadcast at the site using off-shelf RF transmitters arrayed in such a fashion so as to insure complete coverage at any point on site. The roving NLS positioning system would receive these values, compare its presently perceived position state vector (which may contain errors) with those transmitted from the off-site system by means of rapid access look up tables, and if a match is found, the roving system requests, and receives the fully corrected present position, with accompanying uncertainty band. The advantage to this approach is that the roving receiver need only have sufficient computational power to determine a crude approximation of its present position (state vector). It is presumed (though not yet proven) that each such state vector will be unique and thus capable of being compared with similar data sets generated at the off site real-time computation system. Look up searches are ideally suited for smaller, lower-power portable embedded microcontrollers. The primary advantage is that the field units -- for which there will ultimately be a need for not one or two, but thousands -- could be made small, cheap, and reliable while only requiring one high speed computing system to handle all the digital signal processing. This is a long-range task expected to be addressed after completion of the more fundamental research.

Chapter 7: Conclusions

This research project addressed the subject of automated metrology (surveying) for use on construction sites. Specifically, the experimental program has been directed towards the practical development of a novel Non-Line-of-Sight (NLS) survey system with which the real-time position and orientation (attitude) of any object on a construction jobsite may be determined, irrespective of the presence of intervening obstacles that would otherwise render optical, electro-optical, and other short wavelength electromagnetic distancing techniques useless.

Tests were conducted using a specially configured broad band low frequency spread spectrum radar operating between 50 MHz and 2 GHz. The transmission and receiving antennae, which in normal radar are typically one and the same, were physically separated so as to create a system with a fixed broadcast unit and a "roving" receiver, whose range was to be determined relative to the transmission antenna by means of time-of-arrival measurements.

Time domain response was synthesized by means of chirp-z Fourier theory from a broad spectrum of data sampled in the frequency domain. Numerous field experiments were performed in which typical construction site obstacles were placed between the transmitter and receiver with separation distances of up to 70 meters. The obstacles included a half-meter thick, heavily reinforced concrete wall , varying combinations of masonry block and brick up to more than a meter in thickness and at varying angle-of-incidence orientations relative to the transmission path, and metal pre-fabricated wall panels. In all but the latter case, repeatable distance measurements were obtained. Range detection was lost in the presence of extensive metal panels which contained no windows. However, the presence of even small openings (on the order of several centimeters) permitted range acquisition.

Several types of problems which are well known to the radar community were observed during the tests. These included "clutter" (reflections of the transmitted beam off false "targets") and "multipath" (diffracted and scattered elements of the original signal which may, under certain conditions, arrive ahead of the desired signal and which, as a matter of course, may obscure or cast doubt upon which detected signal in the time domain response represents the true transmitter-to-target distance). Another phenomena that was observed is well known to the optics industry: electromagnetic radiation which propagates through a medium other than a vacuum travels through that medium with a velocity less than the speed of light in a vacuum. Thus, any signal transmitted through an engineering material -- e.g. brick, masonry block, or concrete walls -- will appear to have been *delayed* from its expected arrival time at the receiver. In some cases this delay was sufficient that multipath signals arrived ahead of the "true" signal representing the straight line distance from transmitter to receiver. The delay is directly proportional to the dielectric constant of the engineering material penetrated. Where long distances are

involved between the transmitter and receiver the characteristics of the air (including temperature, humidity, and barometric pressure) must be accounted for as well; during the NIST tests this was accomplished by means of a "free space" calibration with no intervening obstacles between the transmitter and receiver at the start of each test series.

Typical errors observed due to propagation delays were significant. Penetration of a half-meter thick reinforced concrete wall induced a range error mean of approximately 800 mm. For combined masonry block walls faced with brick, range errors of three meters were observed for a wall thickness of two meters and a half meter error for a wall thickness of 300 mm. Plots made with the limited data available indicate that these range errors are linearly proportional to the penetration depth (wall thickness) and the dielectric constant for the material.

While three meters of range error over a 70 m survey shot is unacceptable for modern construction surveying, it is important to recognize that nearly all of the error is related to propagation delay. This suggests that real-time compensation techniques can be developed which will be capable of eliminating this portion of the error. A method for doing this appears feasible:

- Construct a three dimensional database for the project which reflects the as-built geometry in real-time and which includes propagation characteristics and statistical variances for the various materials.
- Employ a ray tracing approach (borrowed from computer graphics technology) to follow each transmitted signal.
- A discrimination algorithm will need to be developed which will then, based on statistical analysis of the multiple time histories generated via alternate transmission stations, determine which is the true target and calculate its location and expected SEP (spherical error probable).

Data developed as a result of analyzing the Building 202 data suggest that residual errors that will remain after propagation delays are compensated will be on the order of 200 mm. It is anticipated that this number can be substantially reduced through a) the use of larger bandwidths in the transmitted signal and b) the use of super resolution (image enhancement) algorithms which will improve the signal to noise ratio in the received signal.

The results presented herein are both novel and encouraging. Confirmed distances (target detection) were obtained through a 500 mm thick reinforced concrete wall and through nearly two meters of brick and masonry block. The transmission power for all tests was only 1 milliwatt, a very modest signal power.

Appendix A

Frequency and Time Domain Response for Spread Spectrum Radar Signals Transmitted through a 500 mm Thick Reinforced Concrete Wall (NIST Building 226 NLS Test Facility)

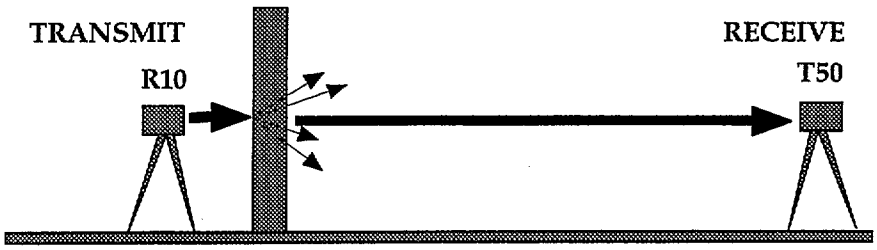

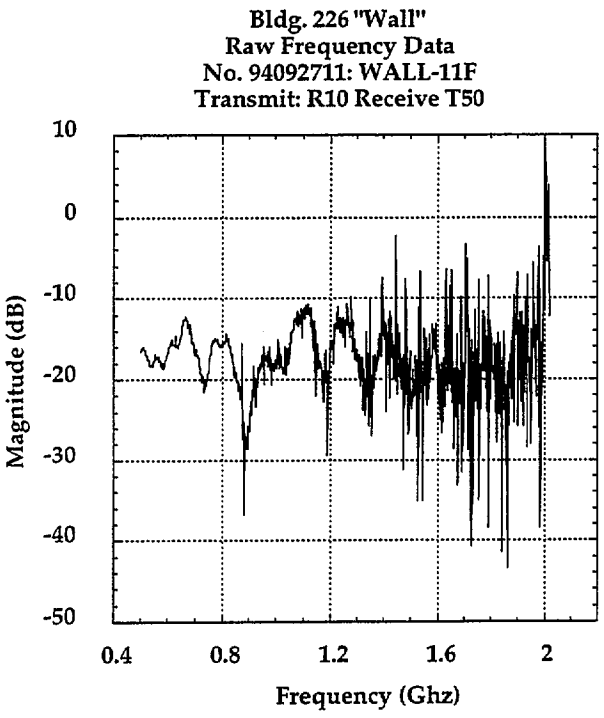

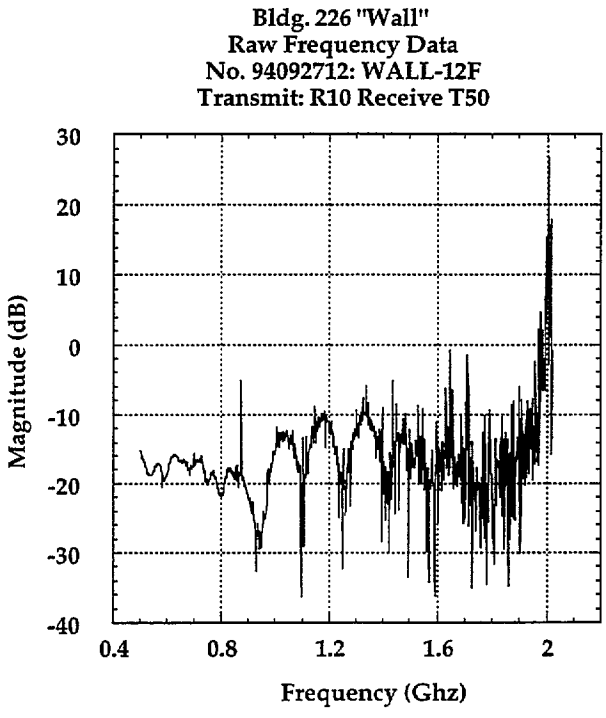

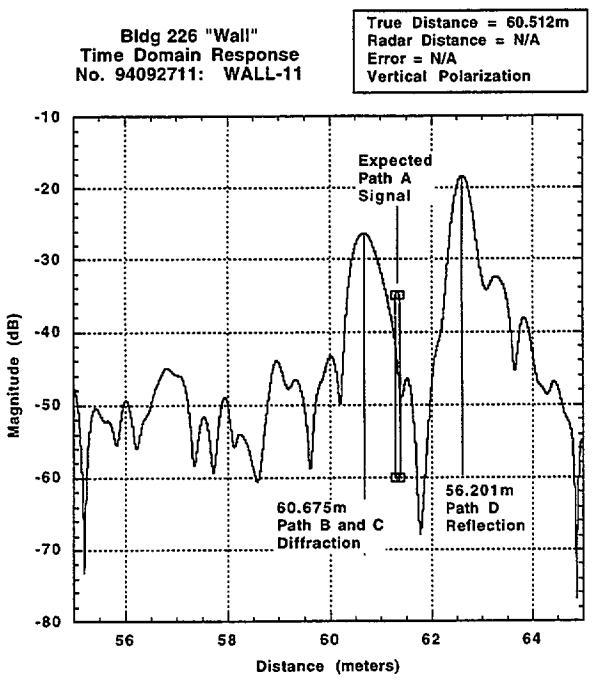

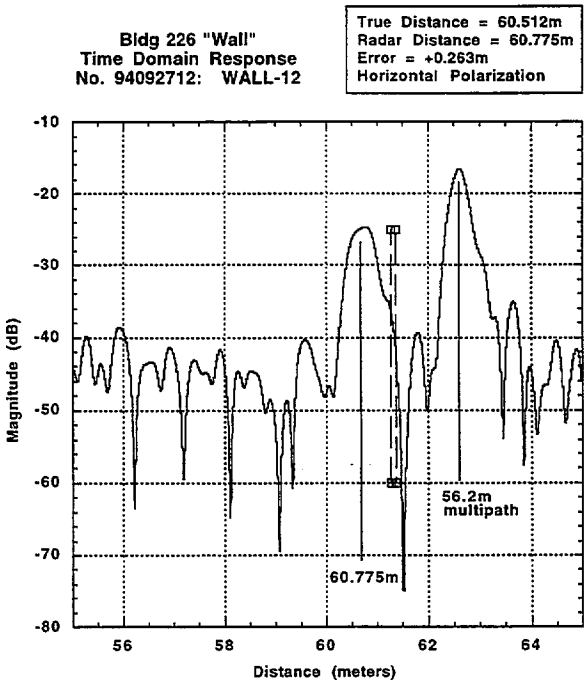

Fig 1a: Transmission at Station R10 to Receive Station T50. Vertical Polarization.

Fig 1b: Transmission at Station R10 to Receive Station T50. Horizontal Polarization.

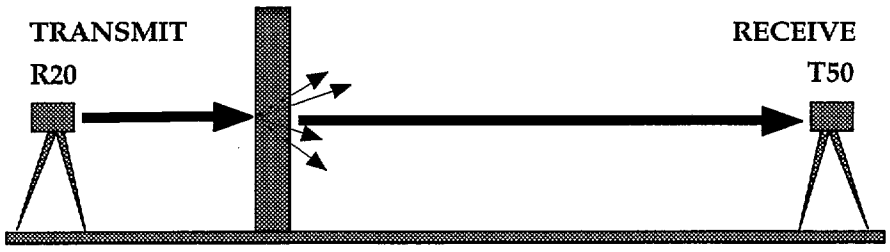

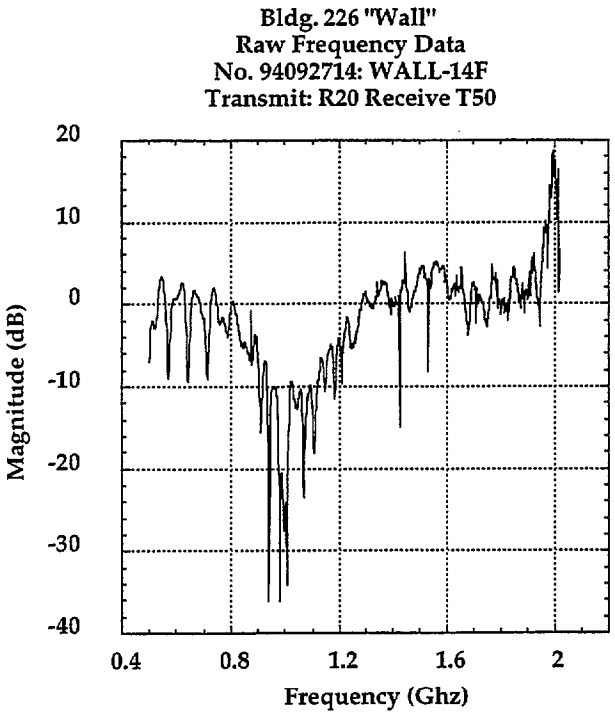

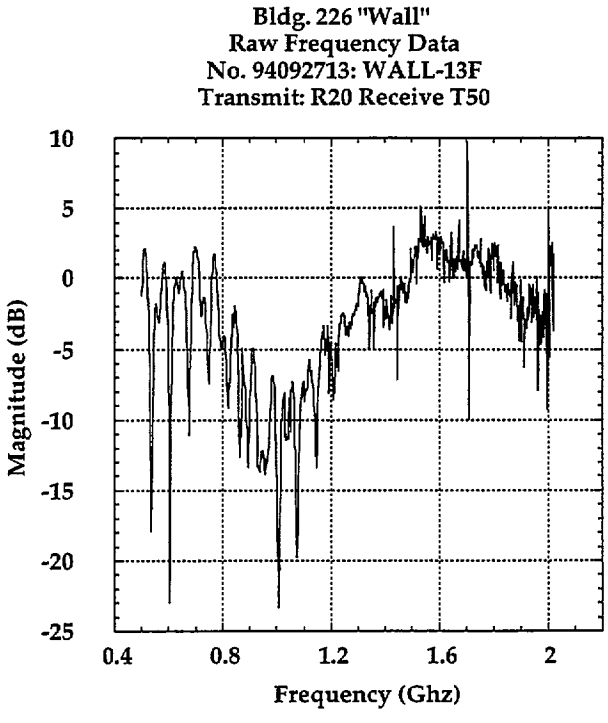

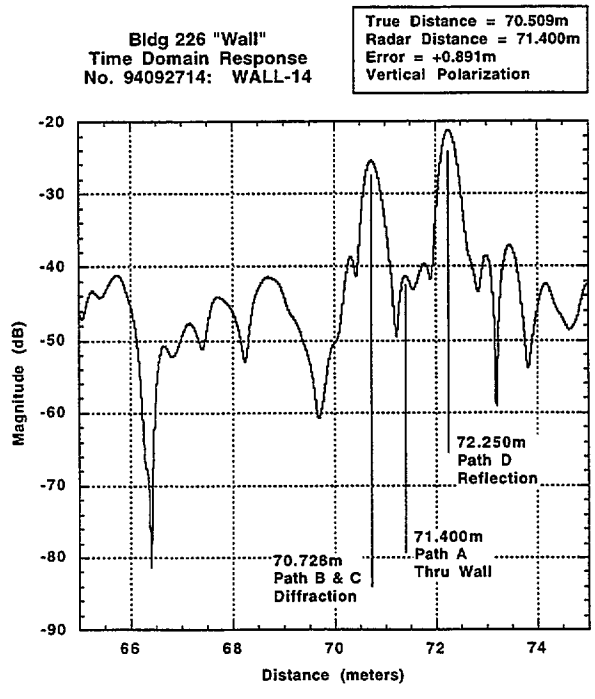

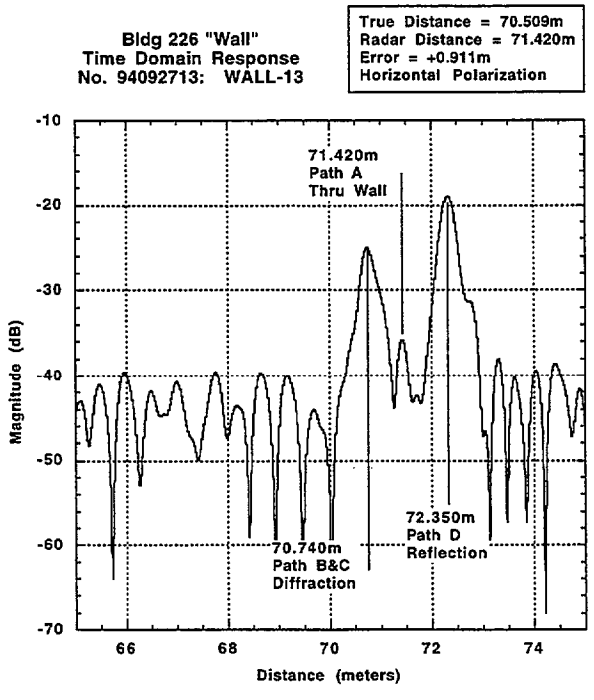

Fig 2a: Transmission at Station R20 to Receive Station T50. Vertical Polarization.

Fig 2b: Transmission at Station R20 to Receive Station T50. Horizontal Polarization.

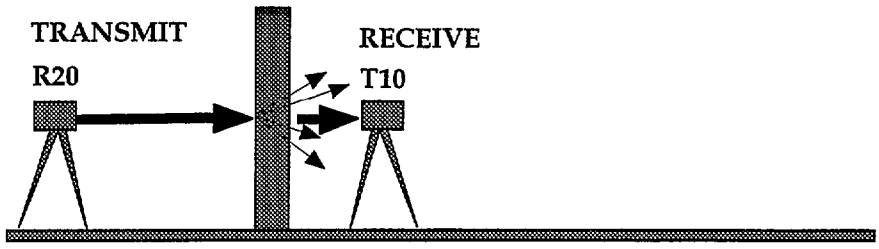

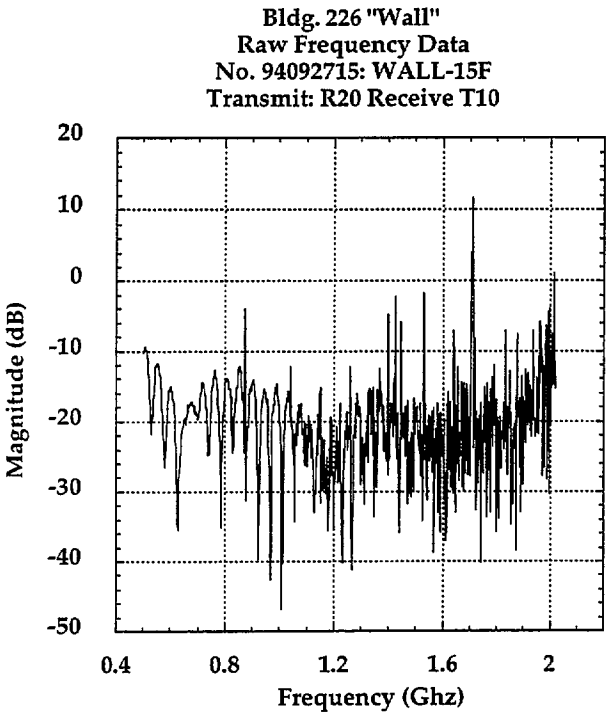

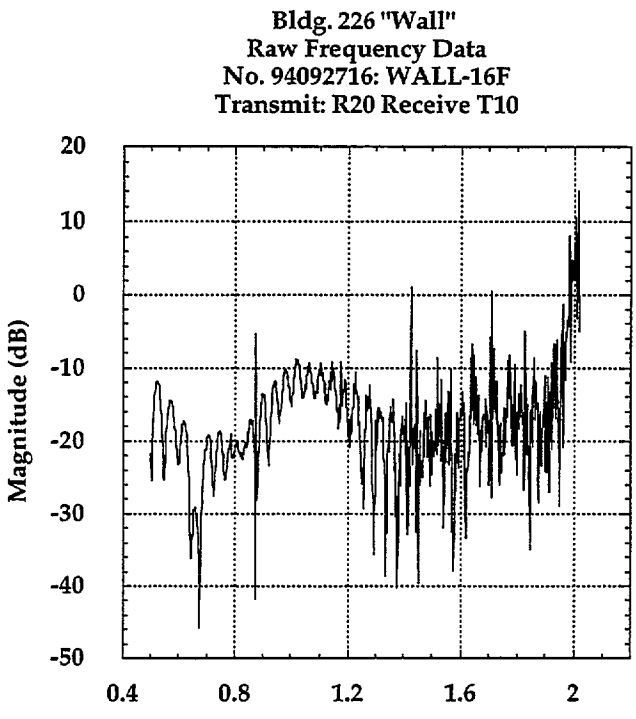

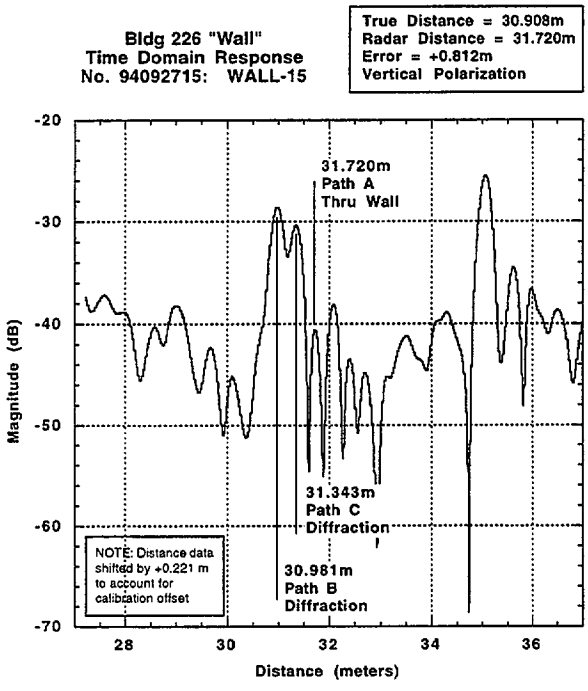

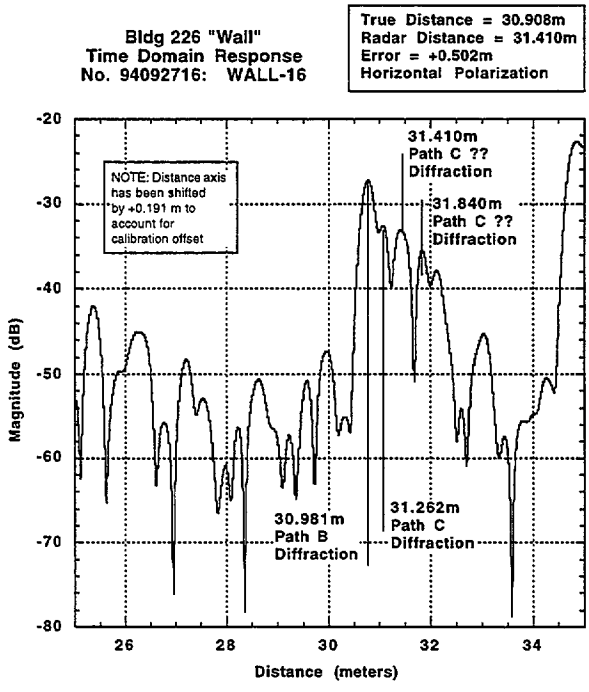

Fig 3a: Transmission at Station R20 to Receive Station T10. Vertical Polarization.

Fig 3b: Transmission at Station R20 to Receive Station T10. Horizontal Polarization.

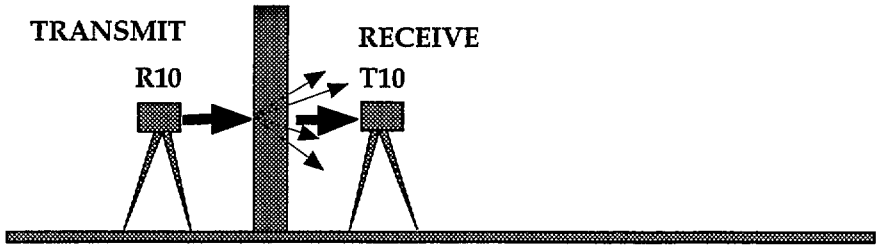

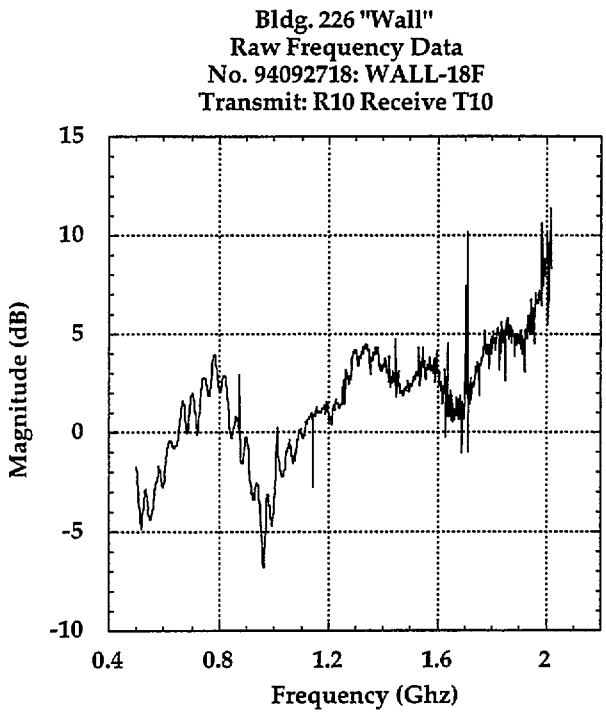

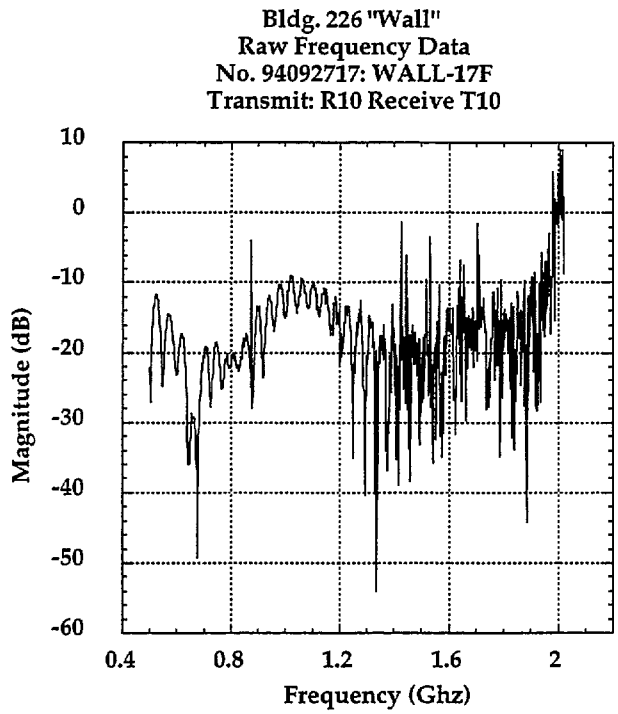

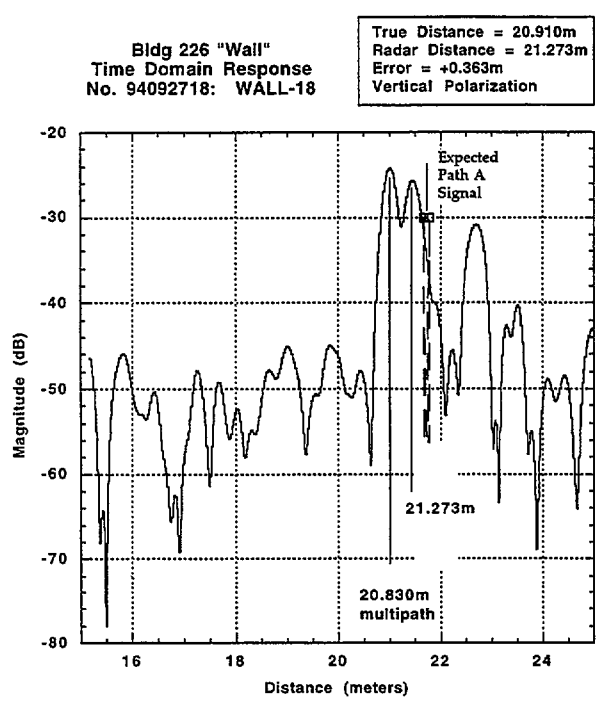

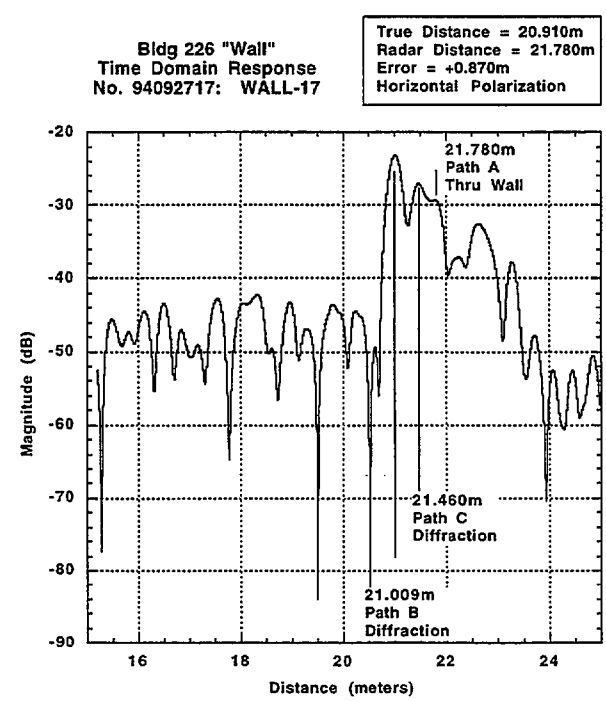

Fig 4a: Transmission at Station R10 to Receive Station T10. Vertical Polarization.

Fig 4b: Transmission at Station R10 to Receive Station T10. Horizontal Polarization.

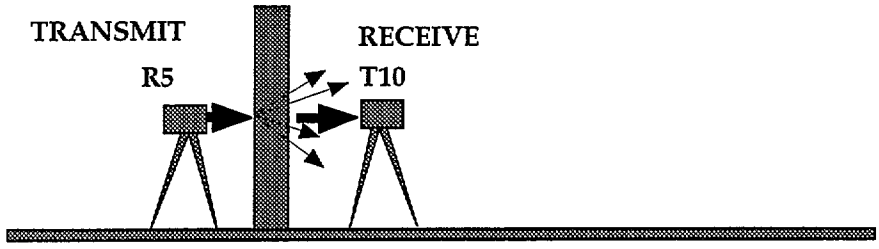

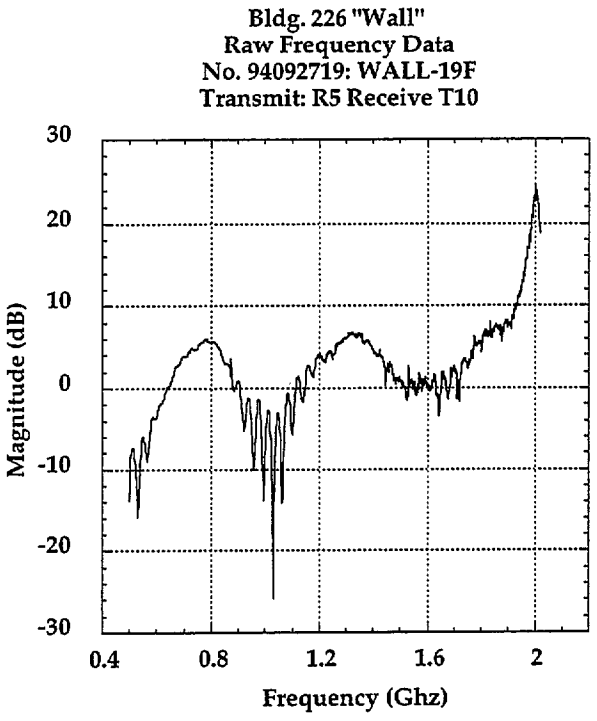

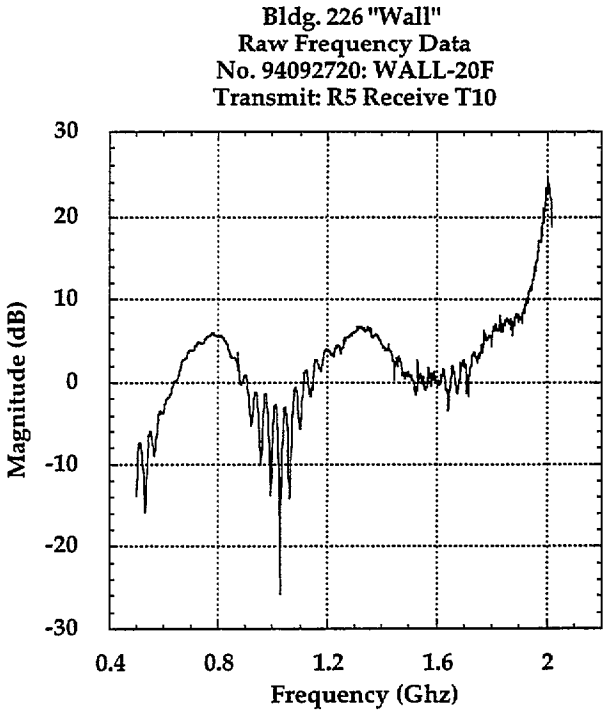

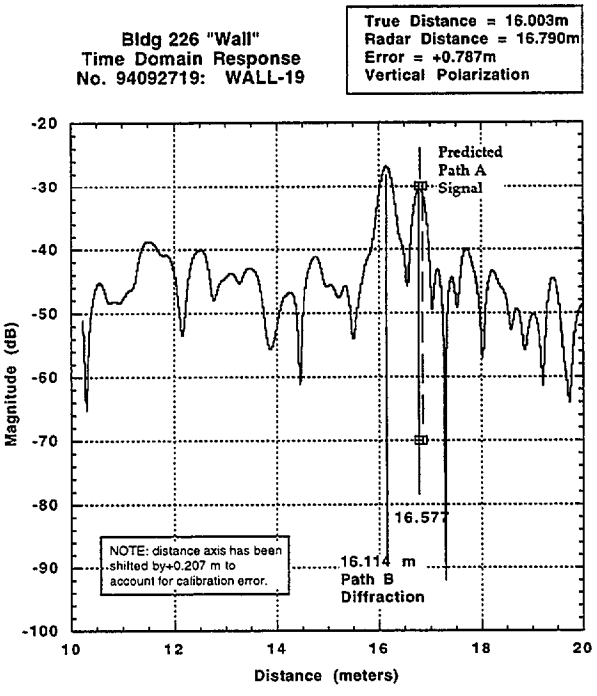

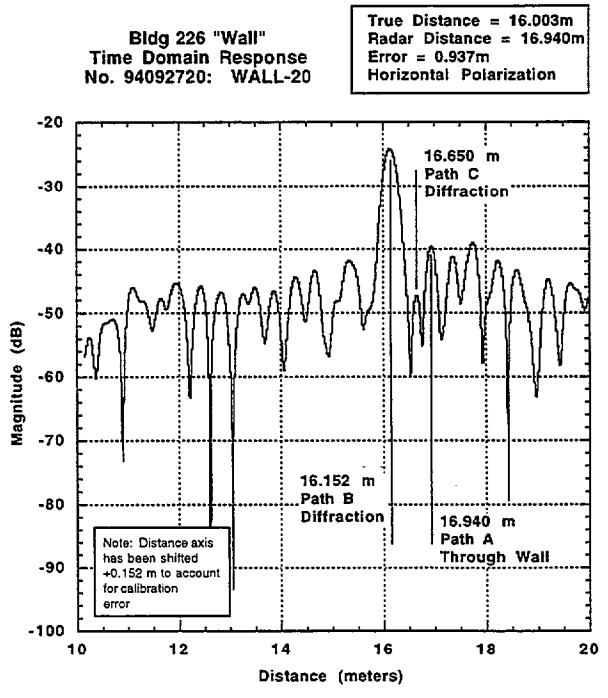

Fig 5a: Transmission at Station R5 to Receive Station at T10. Vertical Polarization.

Fig 5b: Transmission at Station R5 to Receive Station at T10. Horizontal Polarization.

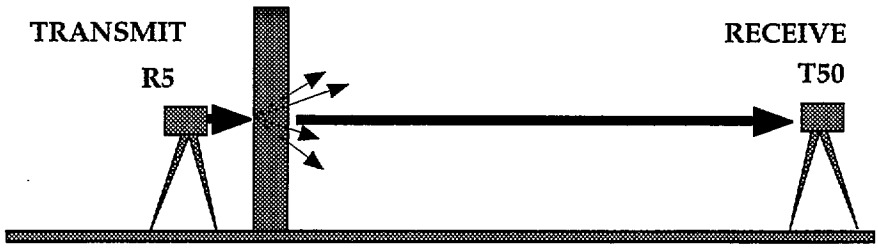

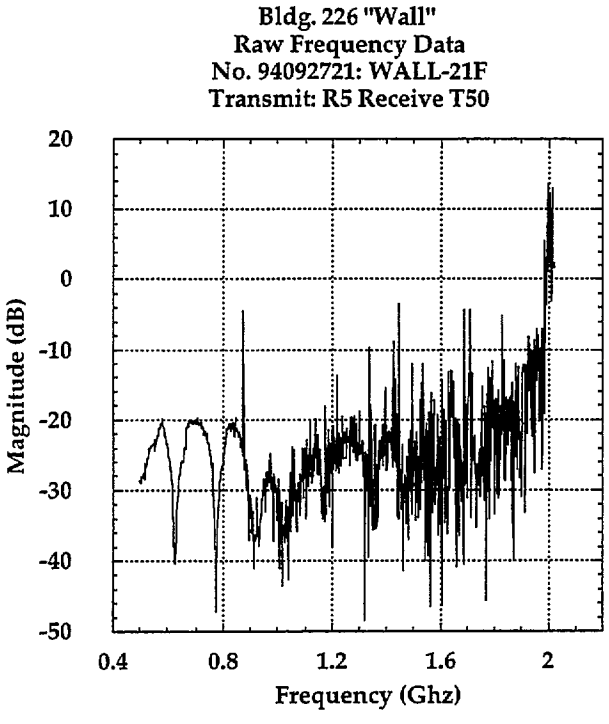

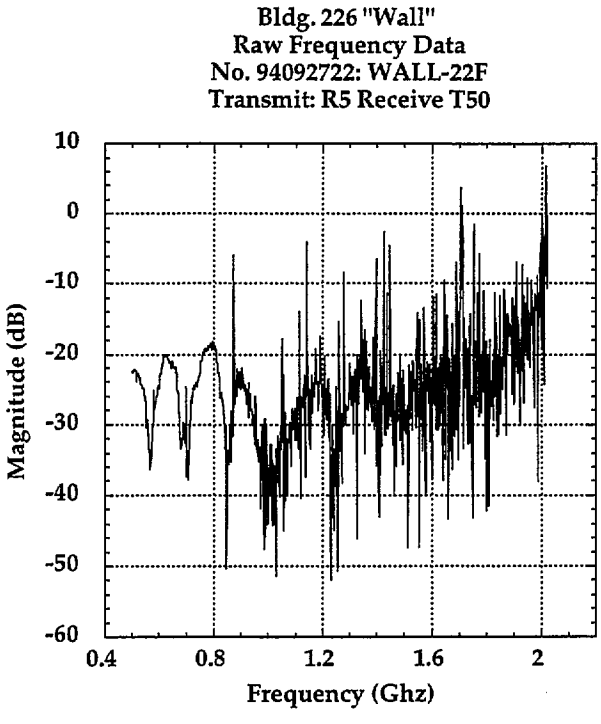

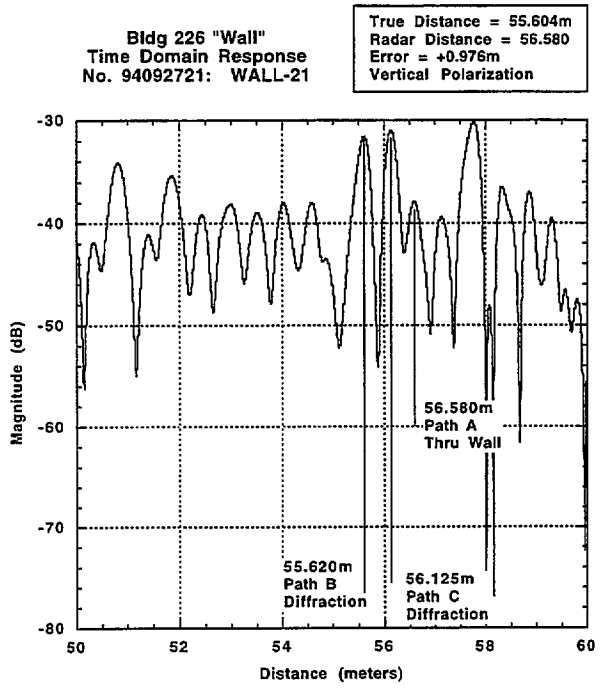

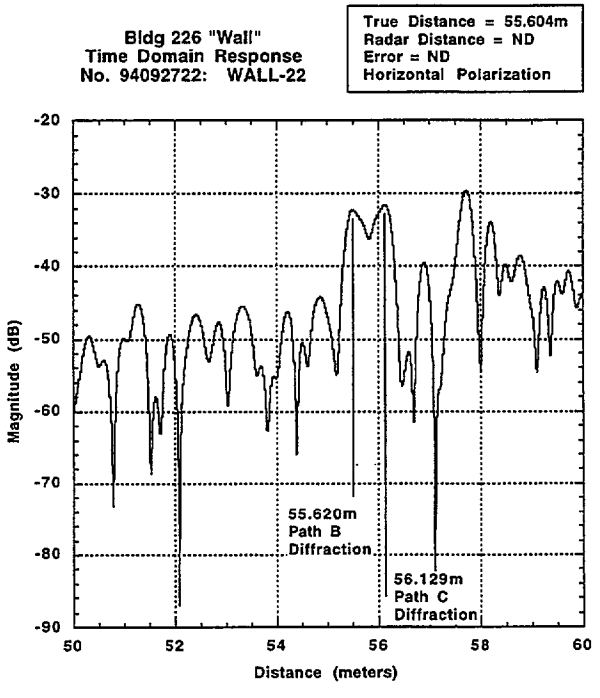

Fig 6a: Transmission at Station R5 to Receive Station T50. Vertical Polarization.

Fig 6b: Transmission at Station R5 to Receive Station T50. Horizontal Polarization.

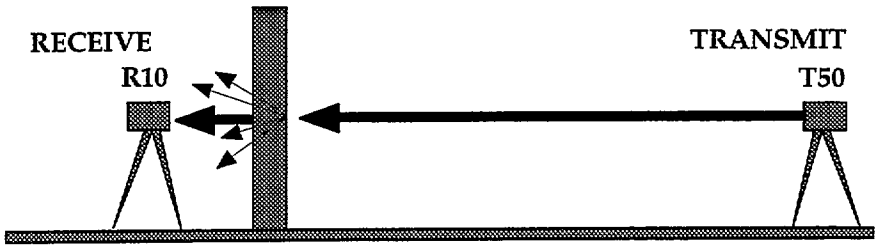

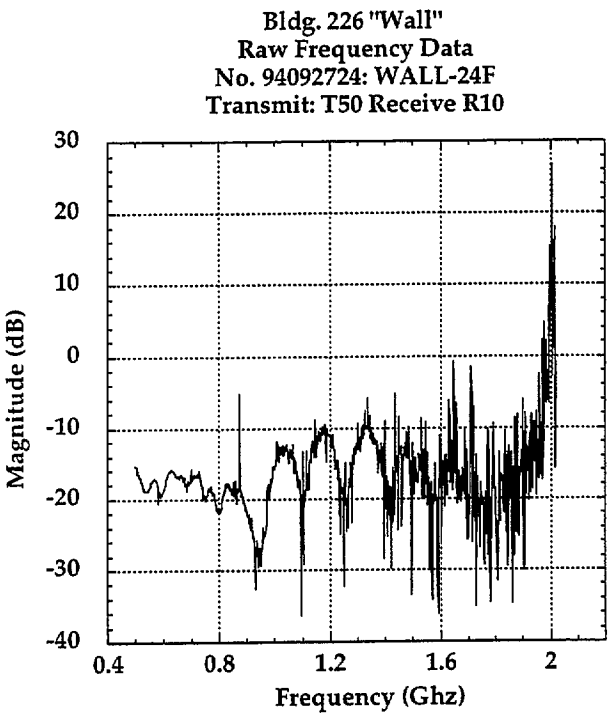

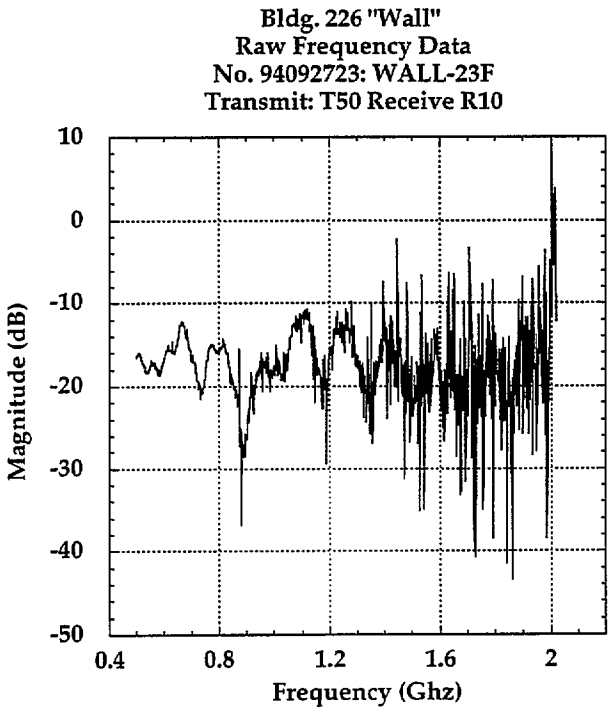

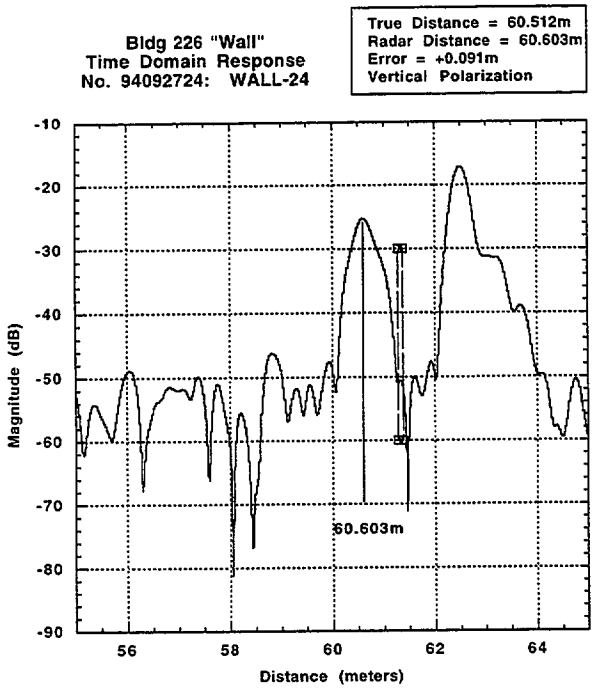

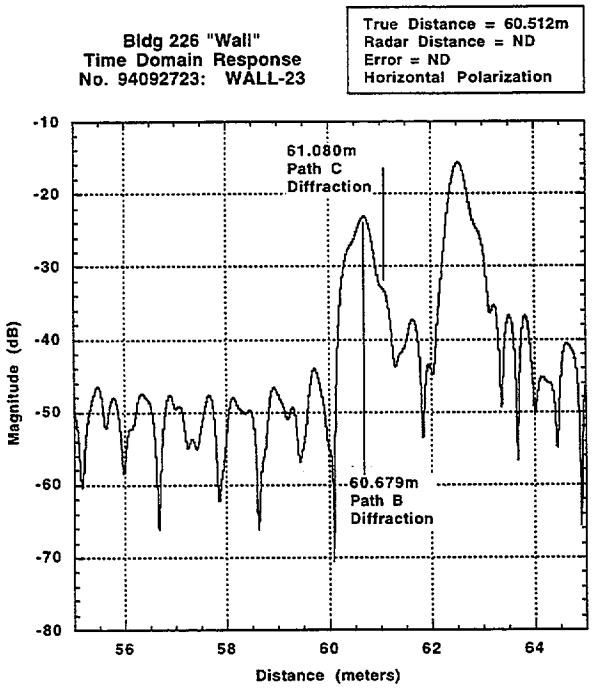

Fig 7a: Transmission at Station T50 to Receive Station R10. Vertical Polarization.

Fig 7b: Transmission at Station T50 to Receive Station R10. Horizontal Polarization.

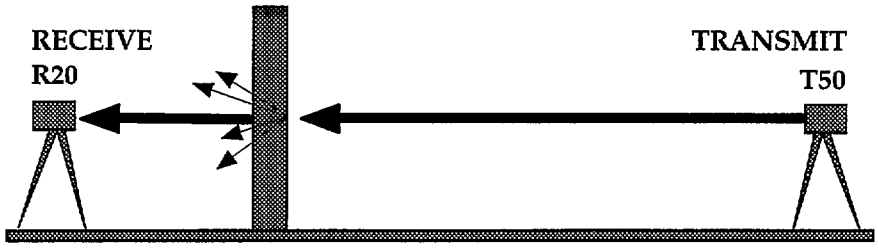

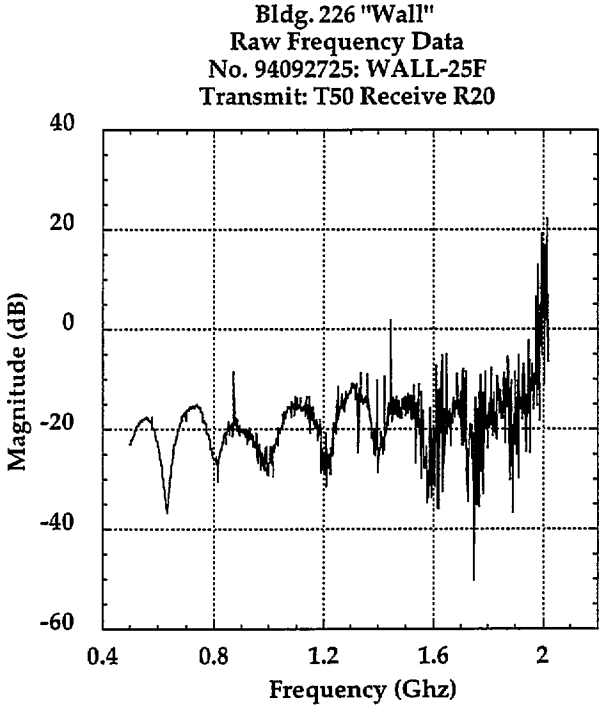

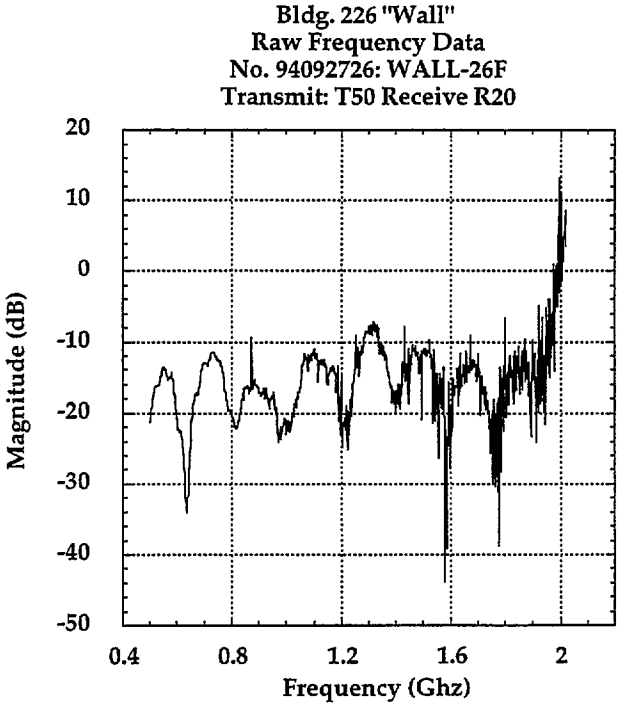

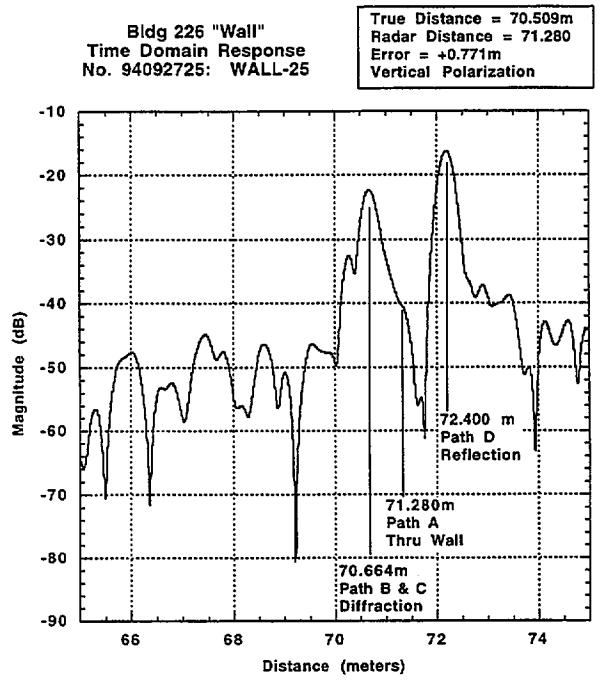

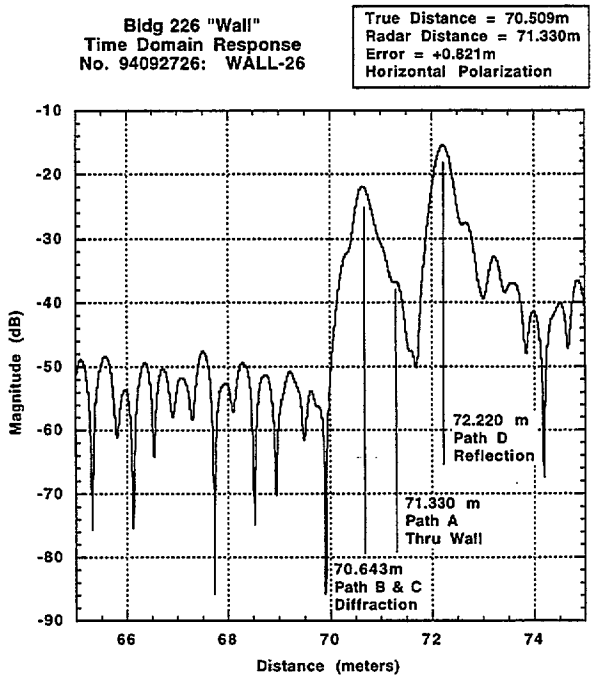

Fig 8a:Transmission at Station T50 to Receive Station R20. Vertical Polarization.

Fig 8b: Transmission at Station T50 to Receive Station R20. Horizontal Polarization.

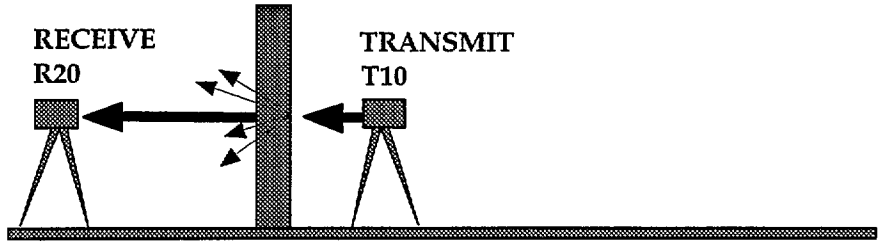

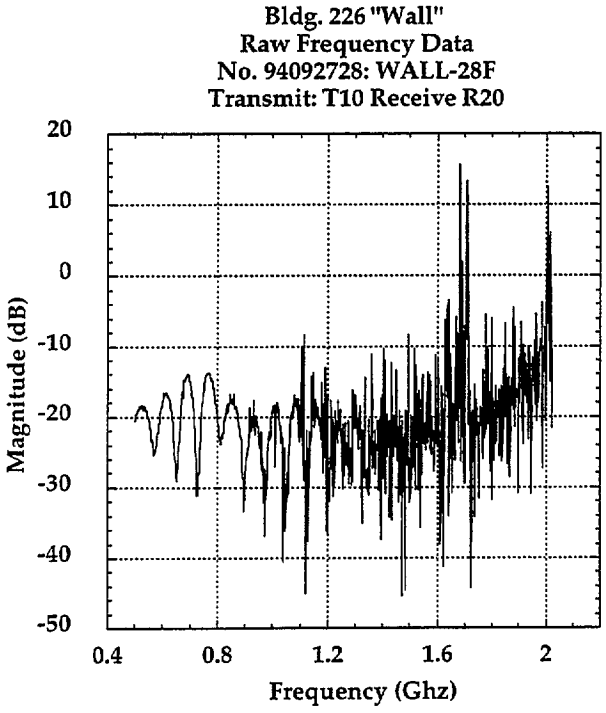

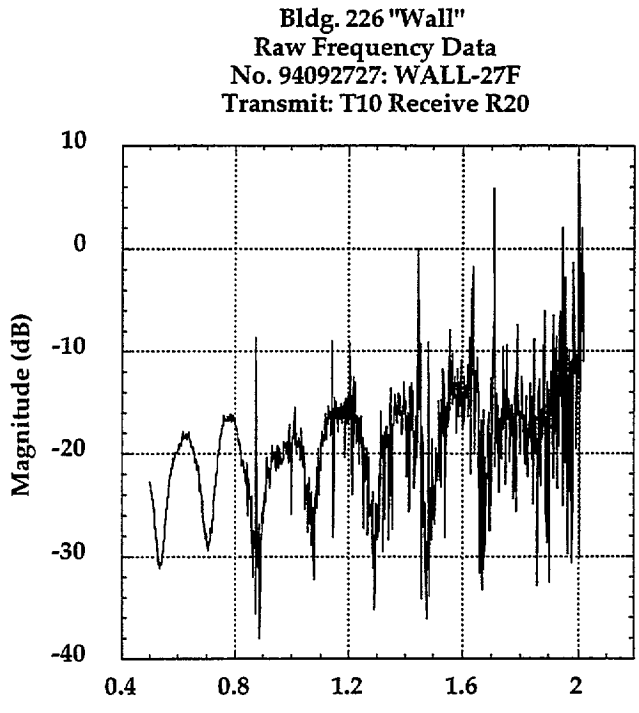

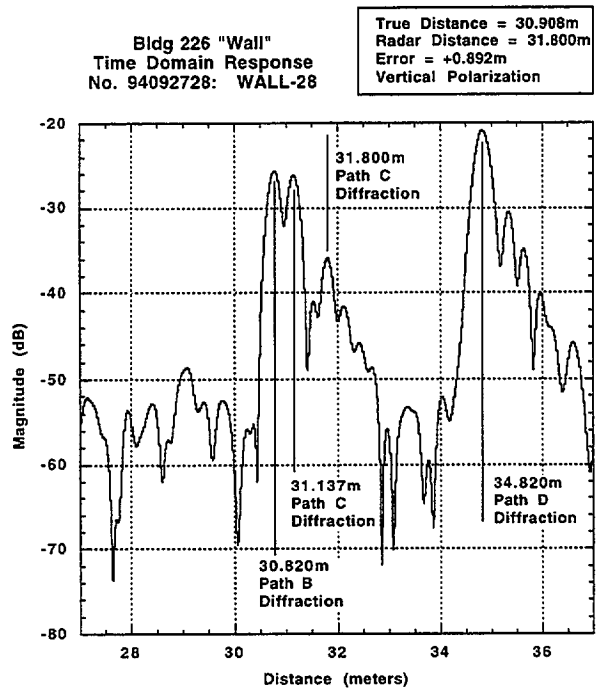

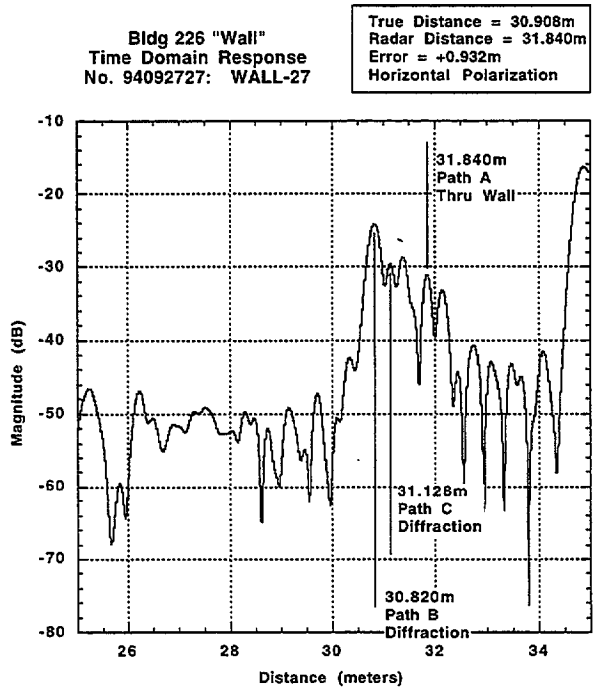

Fig 9a: Transmission at Station T10 to Receive Station R20. Vertical Polarization.

Fig 9b: Transmission at Station T10 to receive Station R20. Horizontal Polarization.

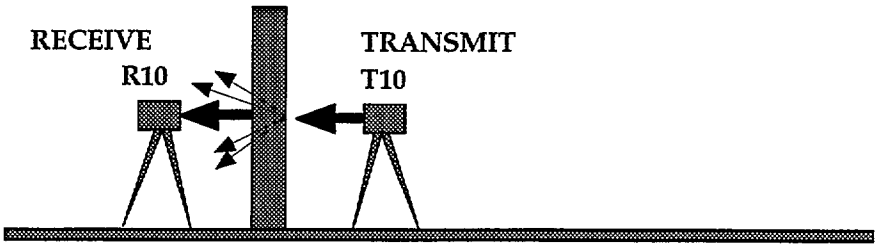

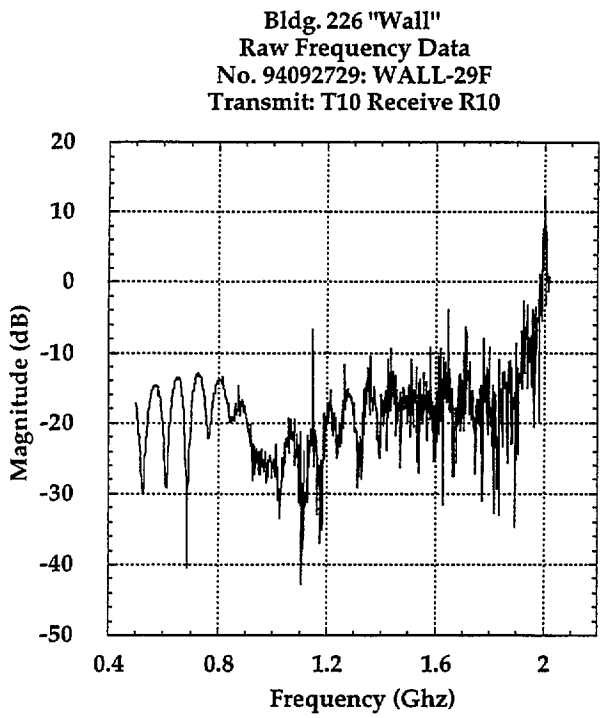

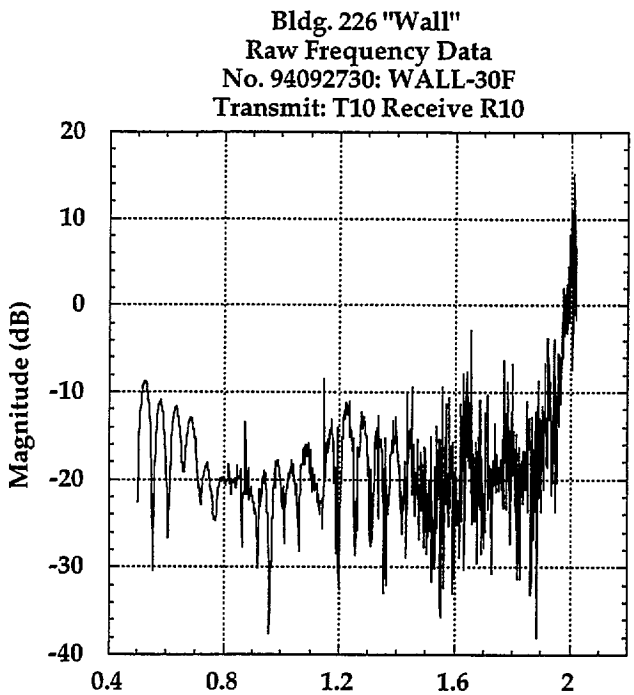

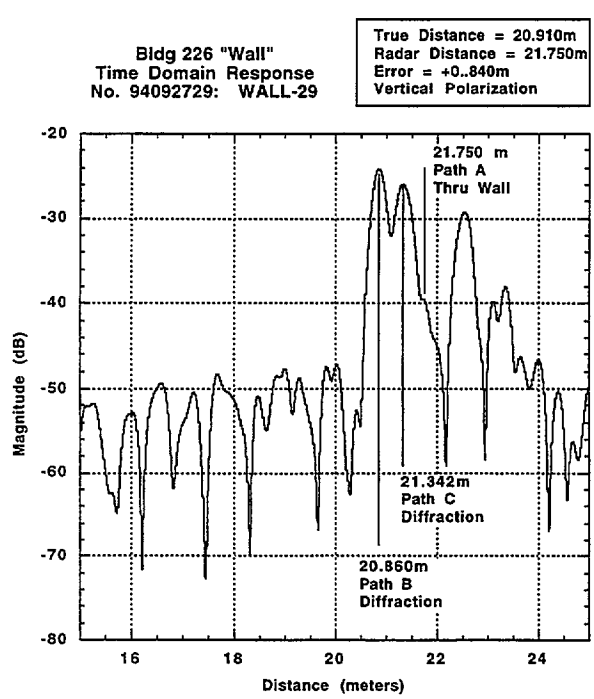

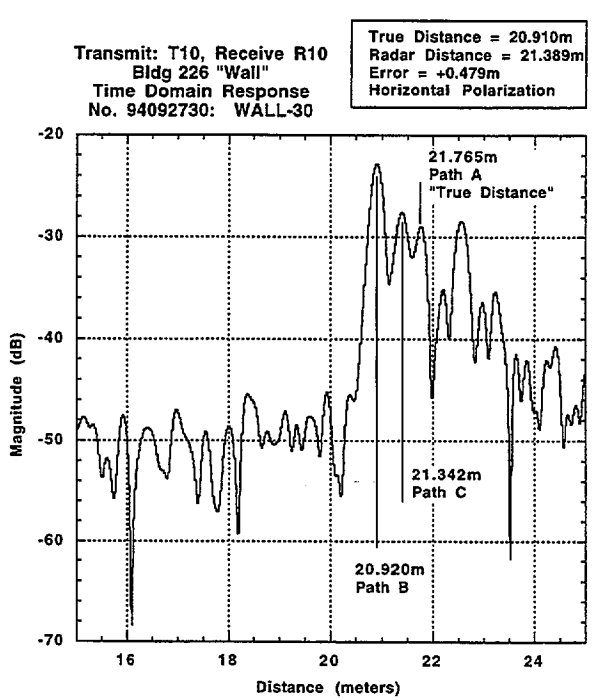

Fig 10a: Transmission at Station T10 to Receive Station R10. Vertical Polarization.

Fig 10b: Transmission at Station T10 to Receive Station R10. Horizontal Polarization,

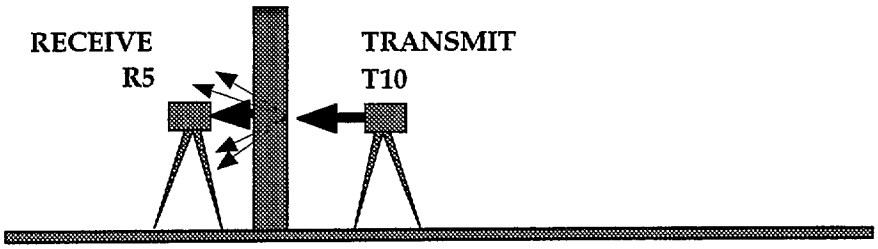

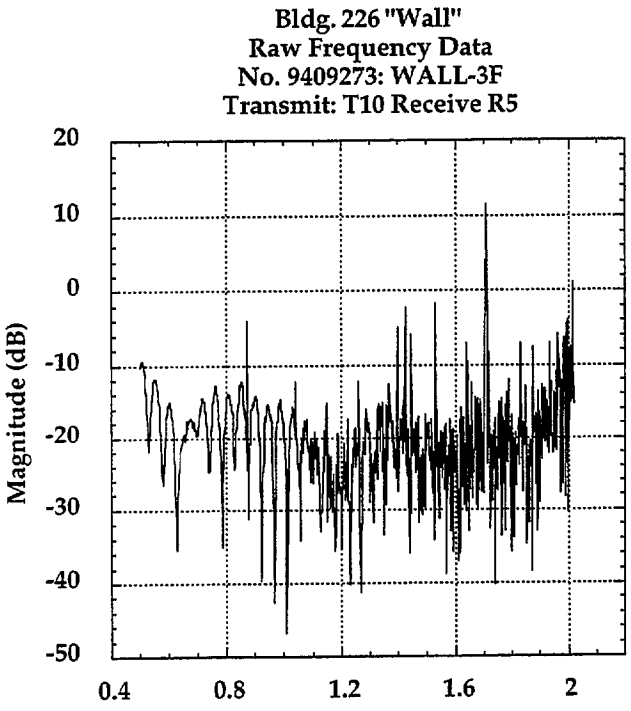

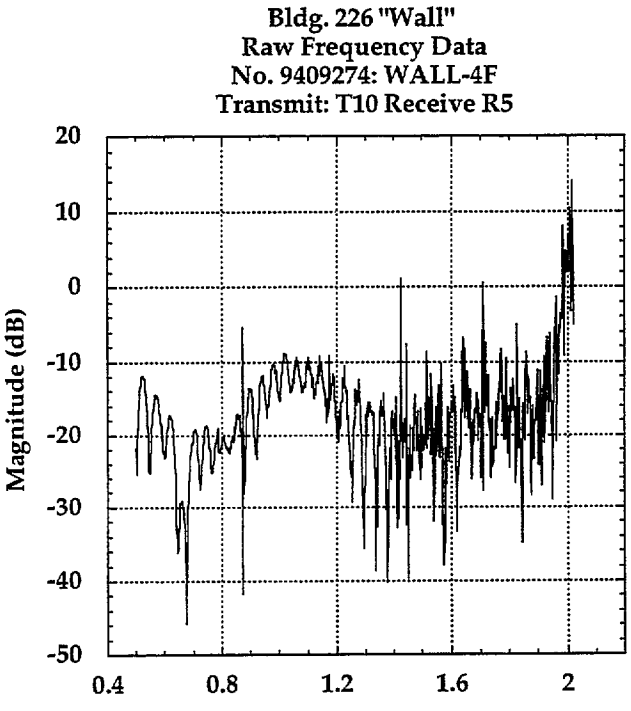

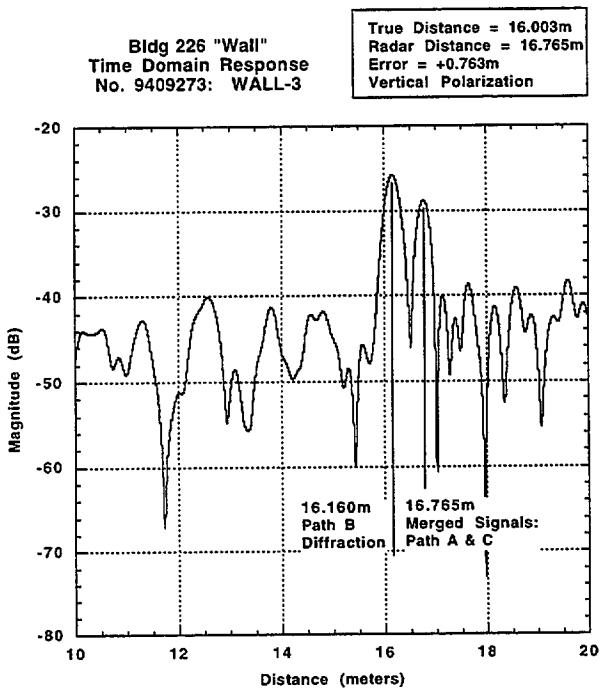

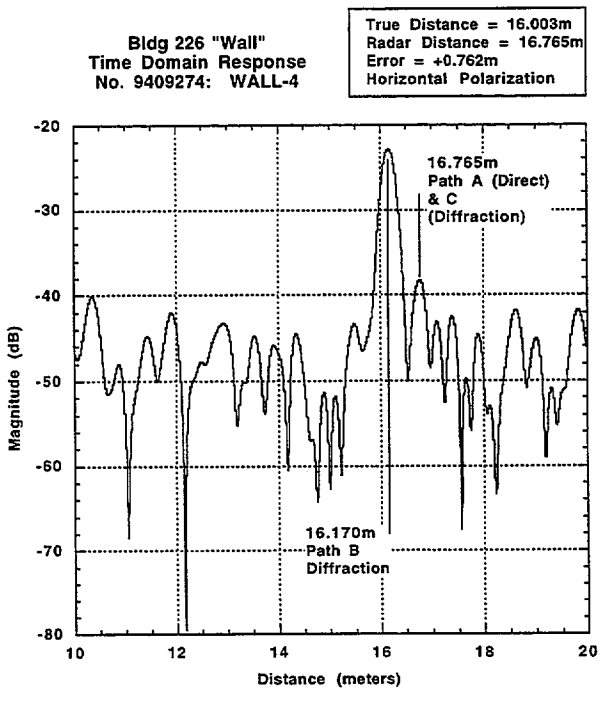

Fig 11a: Transmission at Station T10 to Receive Station R5. Vertical Polarization.

Fig 11b: Transmission at Station T10 to Receive Station at R5. Horizontal Polarization.

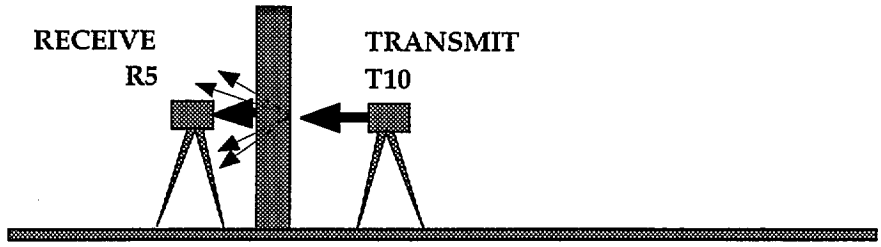

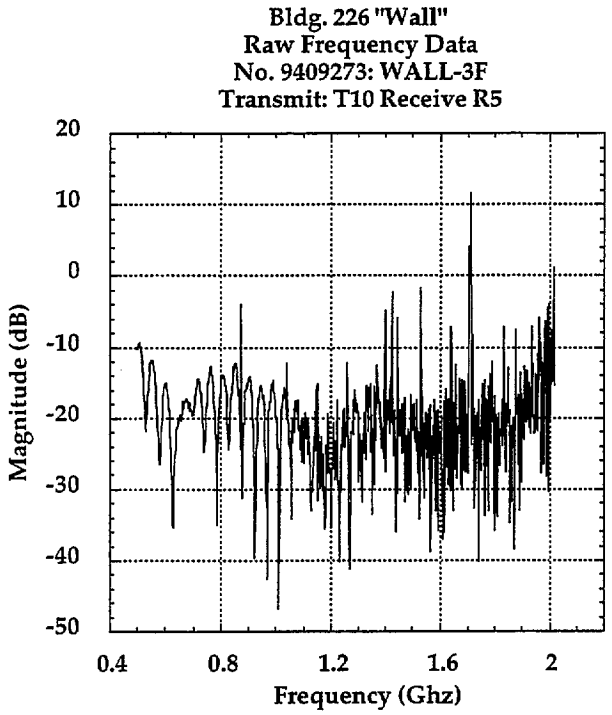

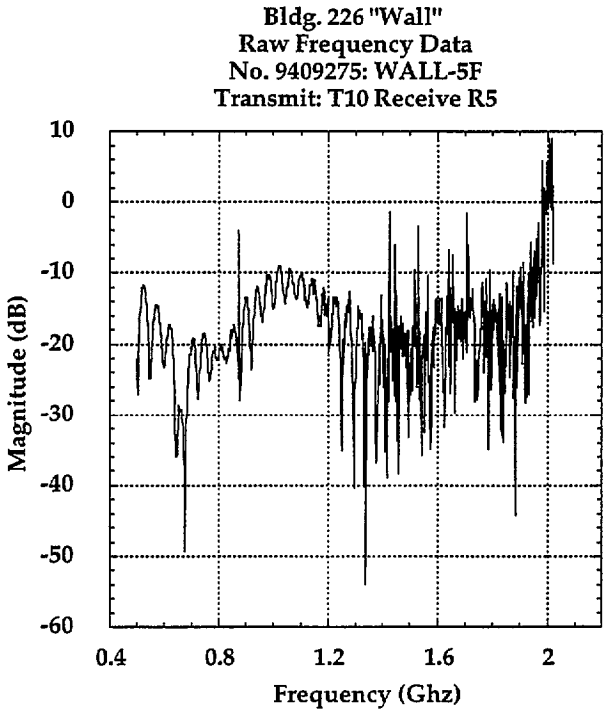

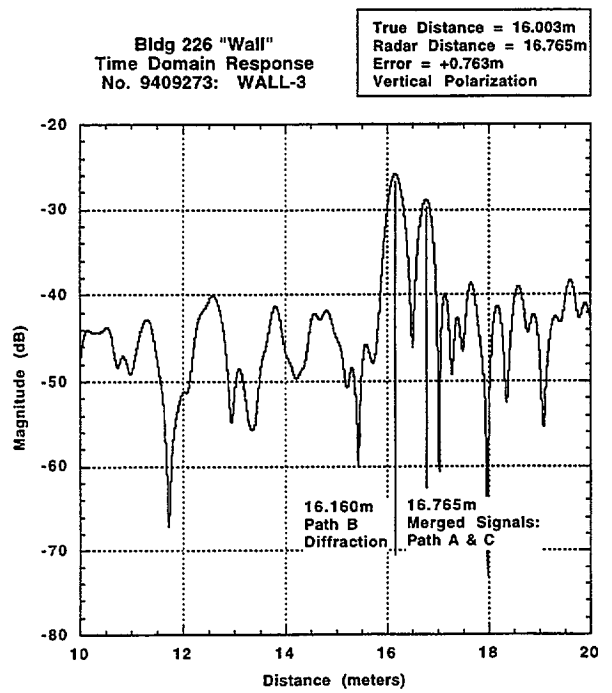

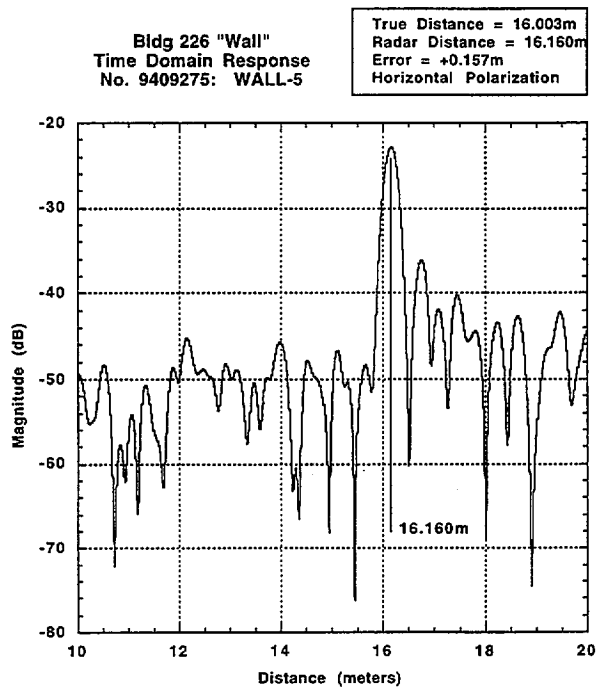

Fig 12a: Transmission at Station T10 to Receive Station R5. Vertical Polarization.

Fig 12b: Transmission at Station T10 to Receive Station R5. Horizontal Polarization.

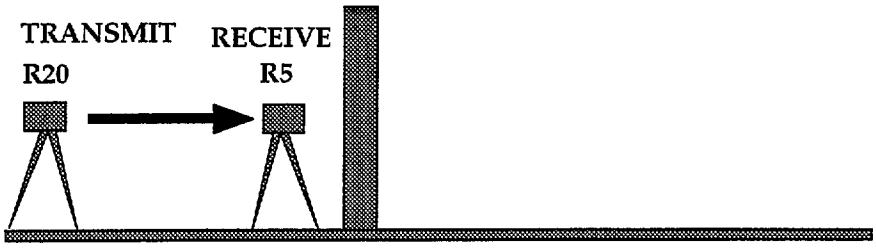

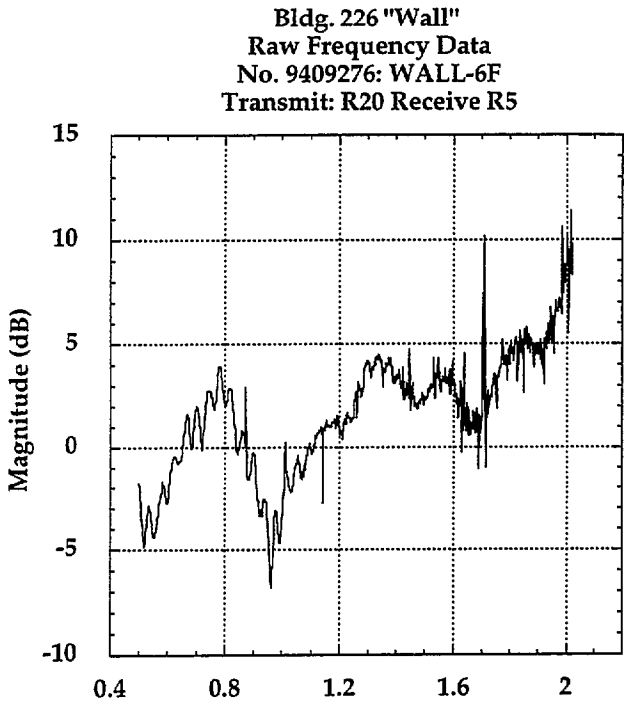

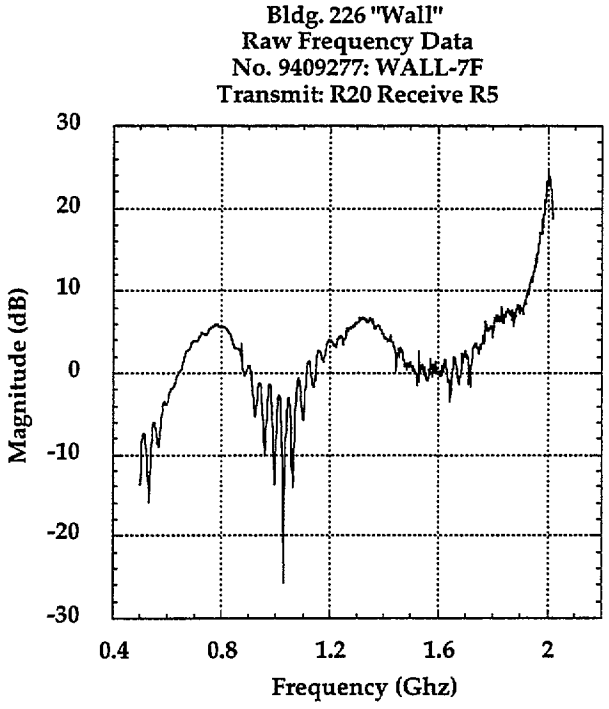

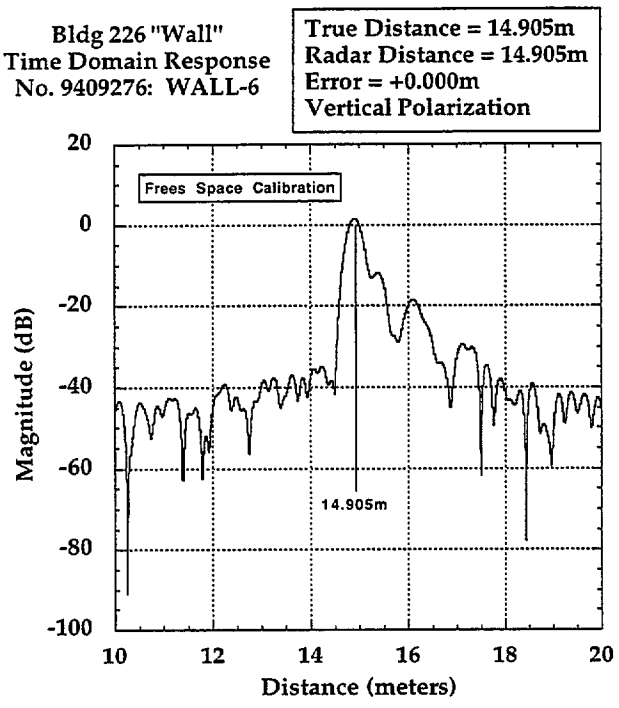

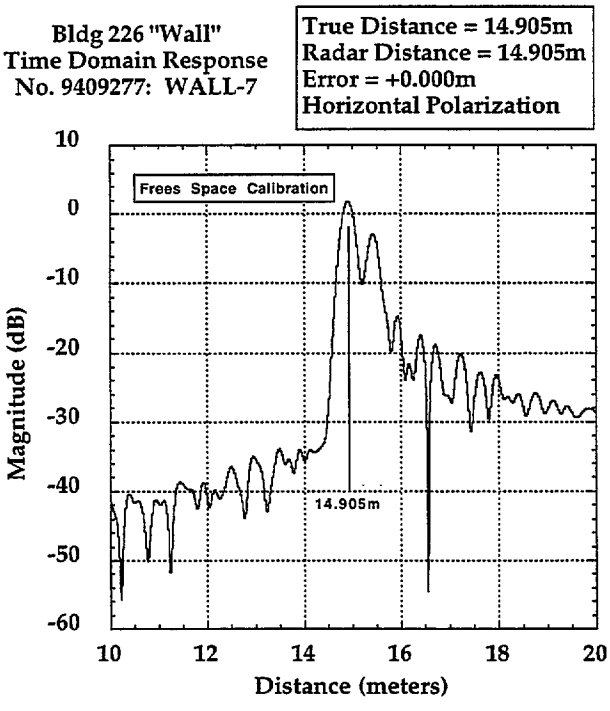

Fig 13a: Transmission at Station R20 to Receive Station R5. Vertical Polarization.

Fig 13b: Transmission at Station R20 to Receive Station R5. Horizontal Polarization.

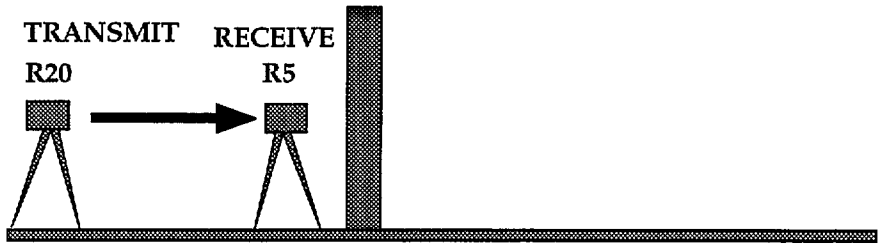

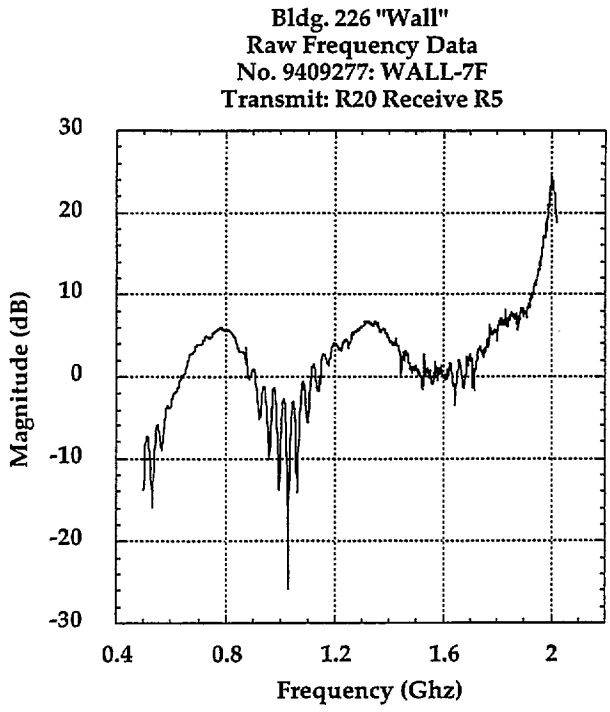

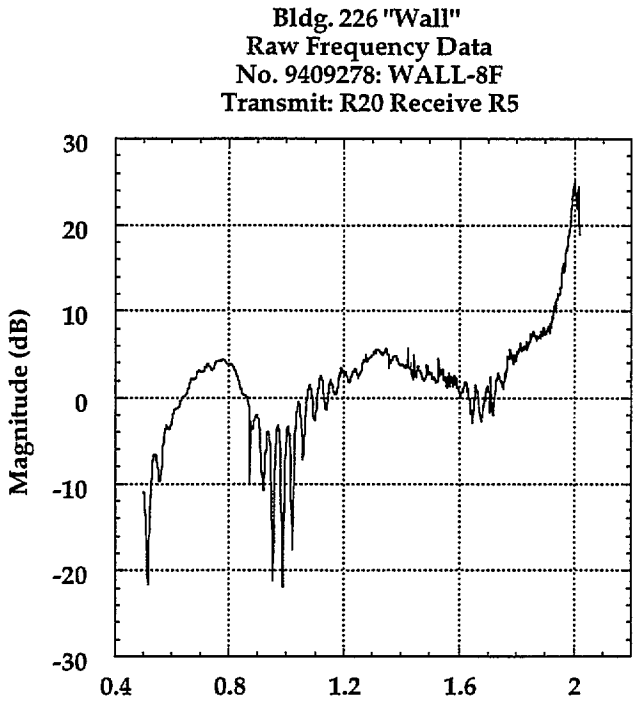

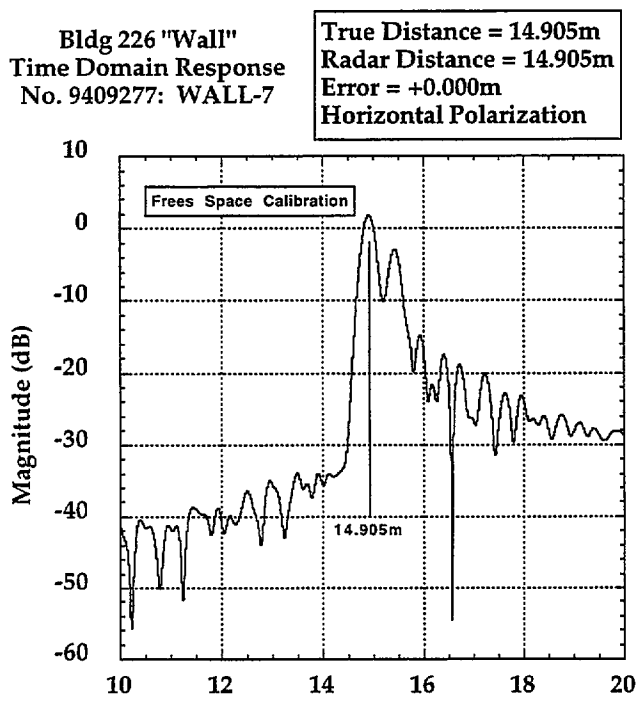

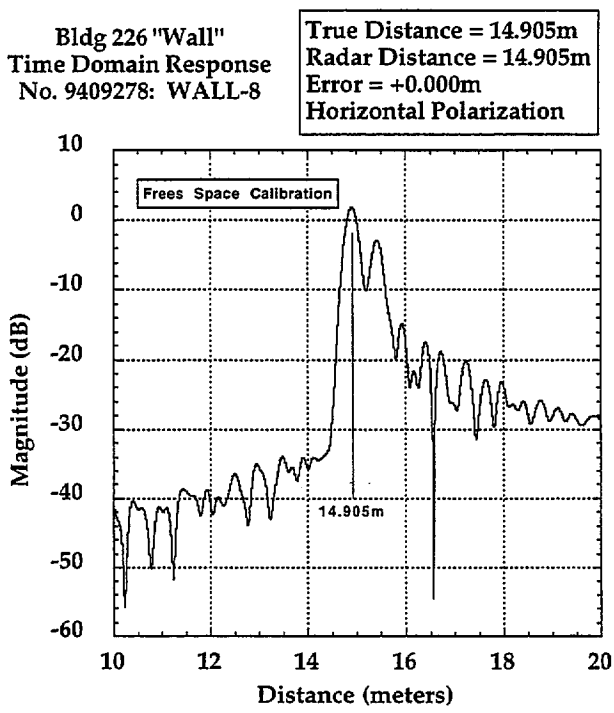

Fig 14a: Transmission at Station R20 to Receive Station R5. Horizontal Polarization.

14b: Transmission st Station R20 to Receive Station R5. Horizontal Polarization.

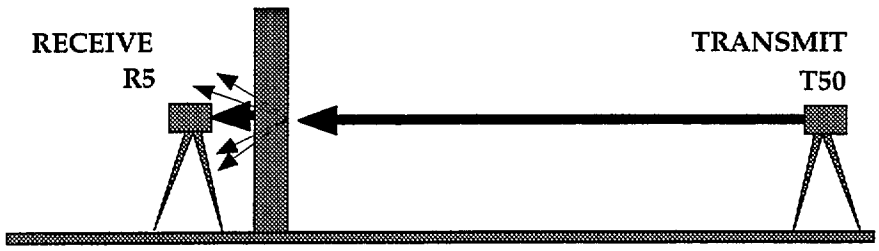

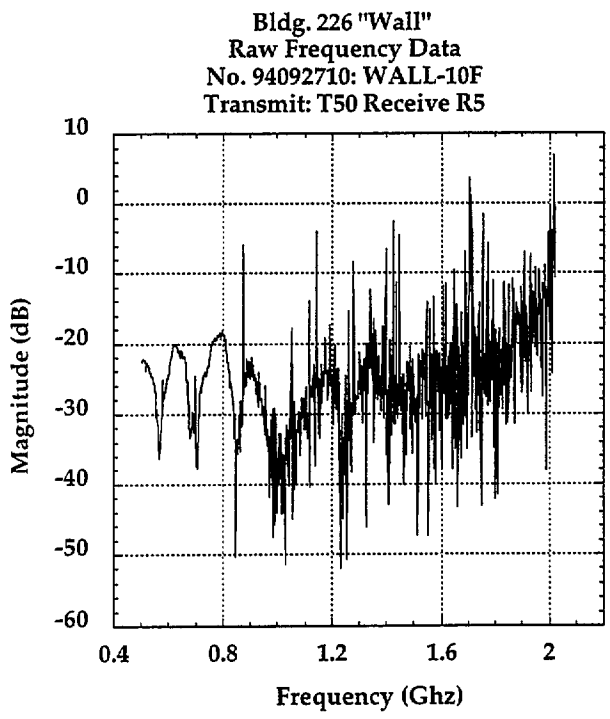

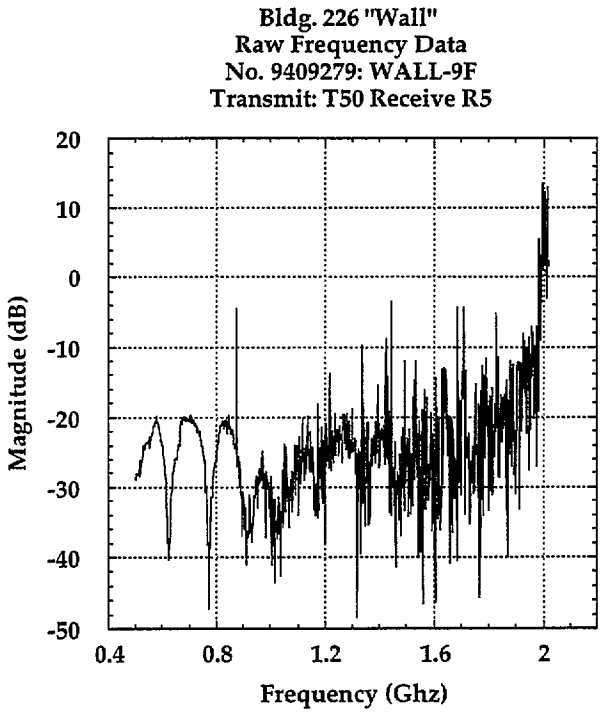

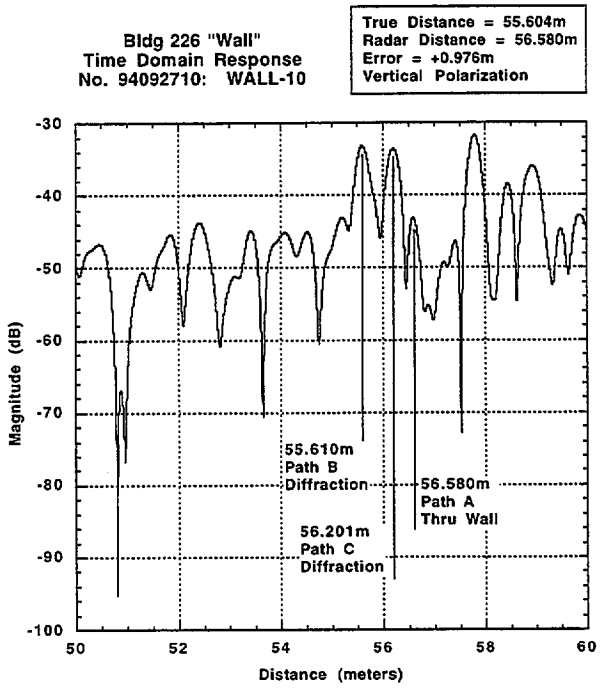

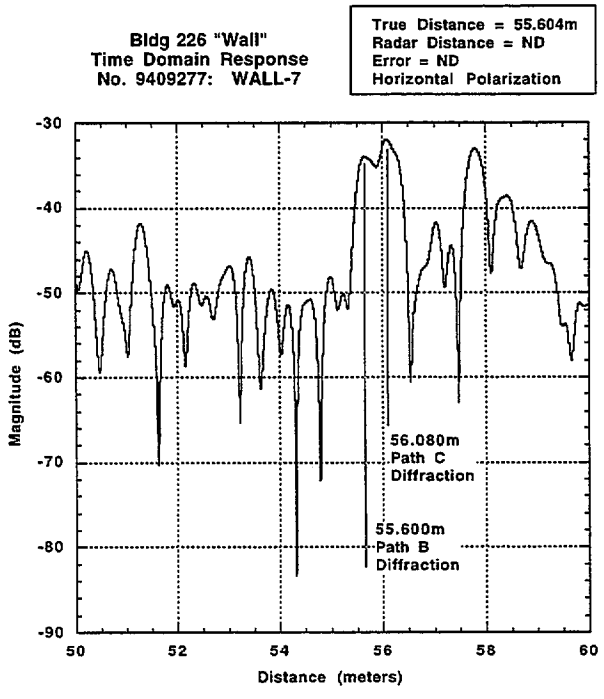

Fig 15a: Transmission at Station T50 to Receive Station R5. Vertical Polarization

Fig 15b: Transmission at Station T50 to Receive Station R5. Horizontal Polarization.

Appendix B

Frequency and Time Domain Response for Spread Spectrum Radar Signals Transmitted through a Brick- and Masonry-Block-clad Building (NIST Building 202 NLS Test Facility)

Free Space Calibration

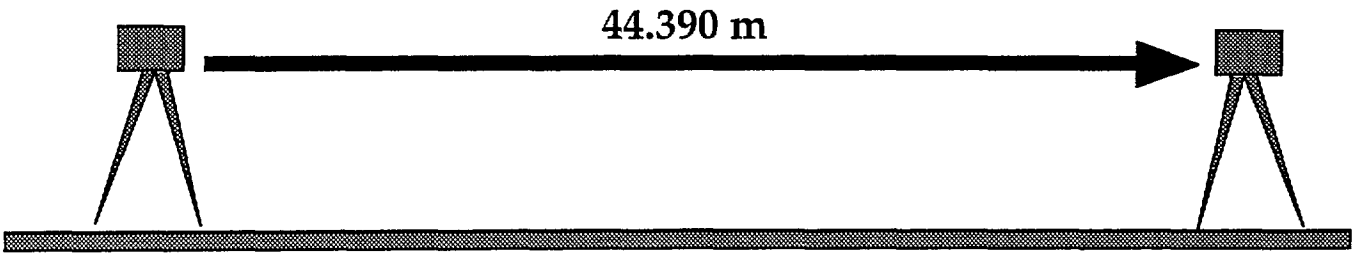

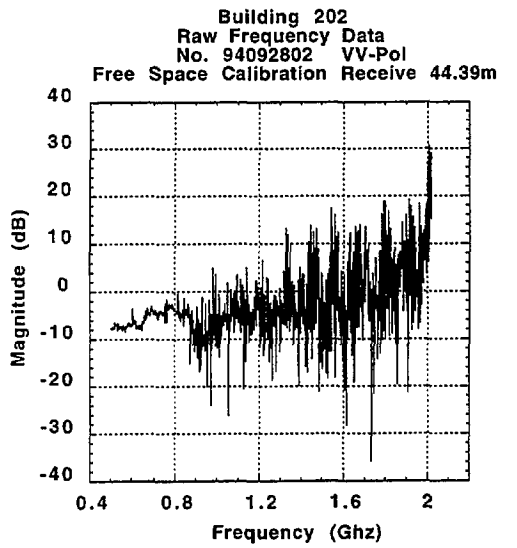

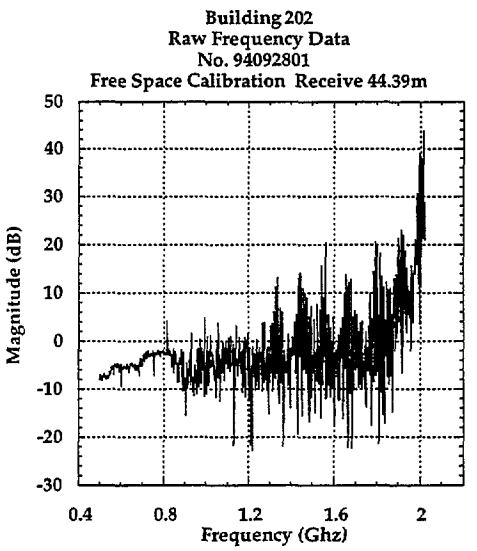

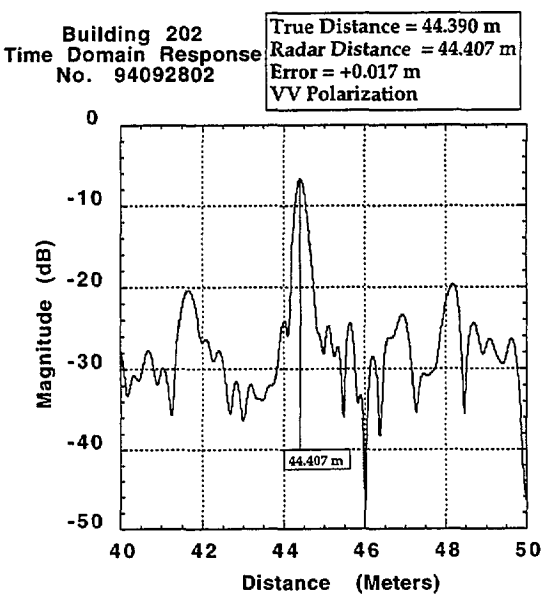

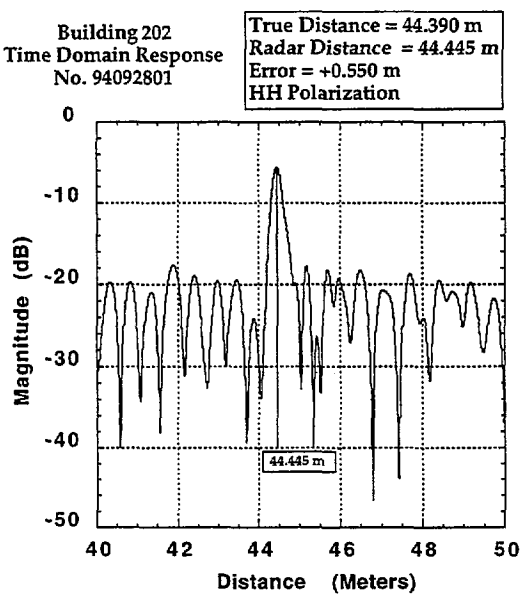

Fig 1a: Free Space Measurement. Vertical Polarization.

Fig 1b: Free Space Measurement. Horizontal Polarization.

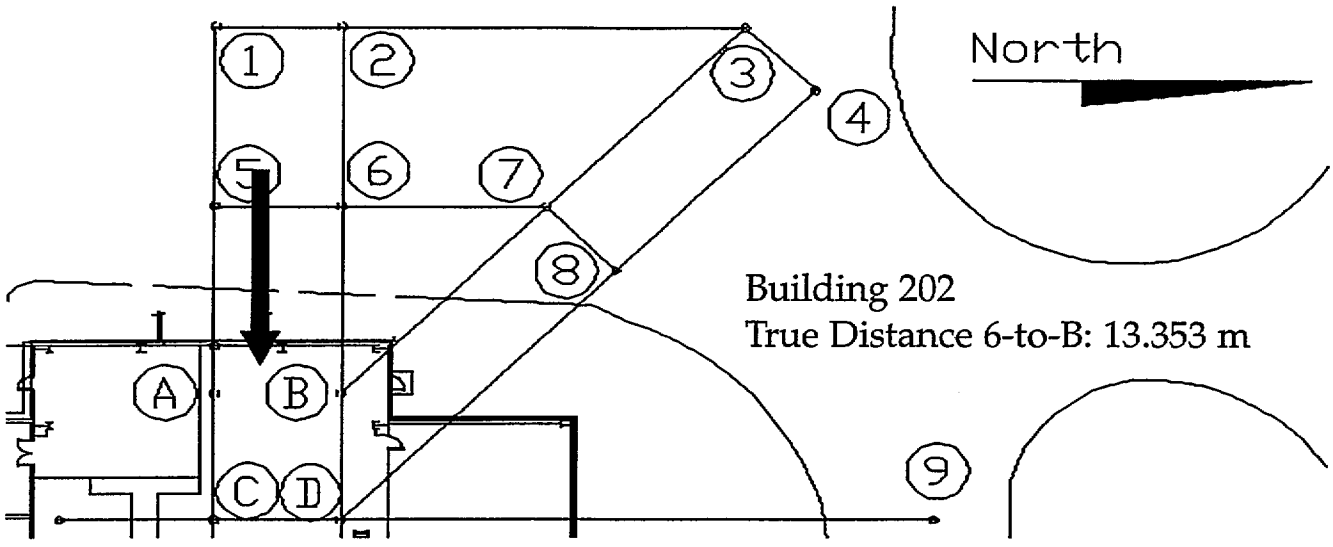

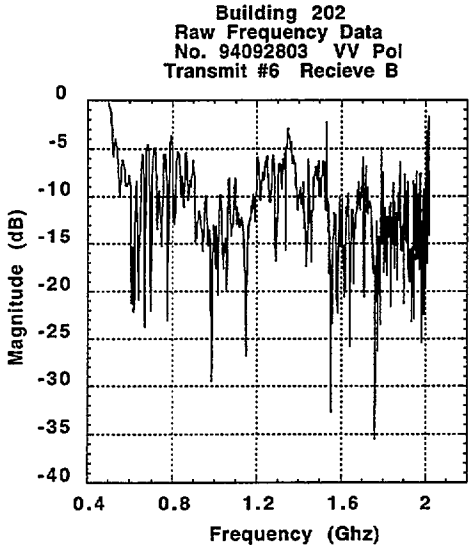

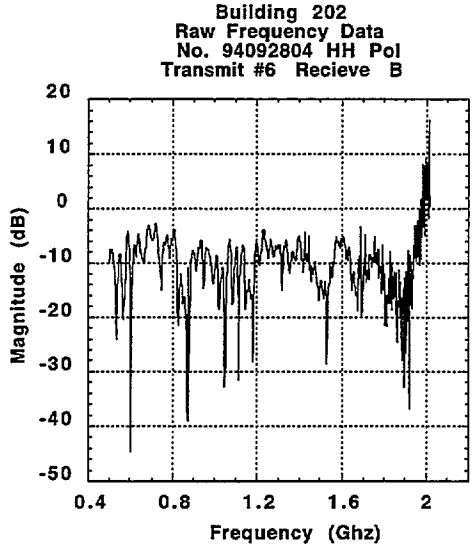

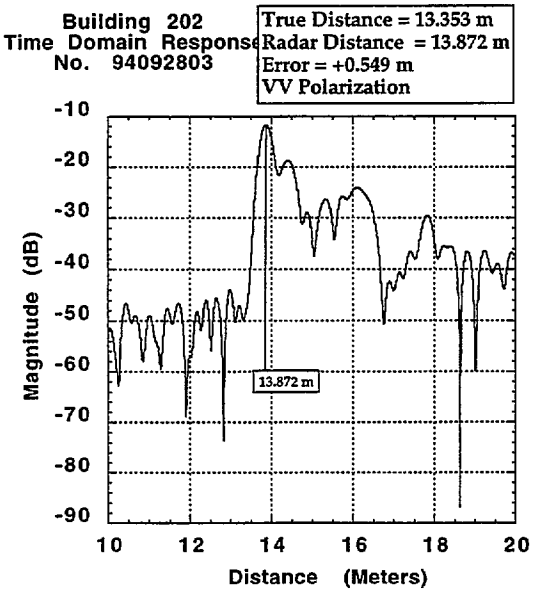

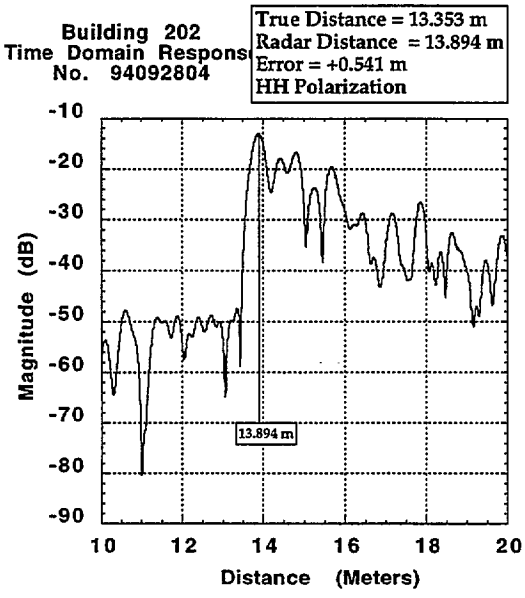

Fig 2a: Transmission at Station #6 to Receive Station B. Vertical Polarization.

Fig 2b: Tranmission at Station #6 to Receive Station B. Horizontal Polarization.

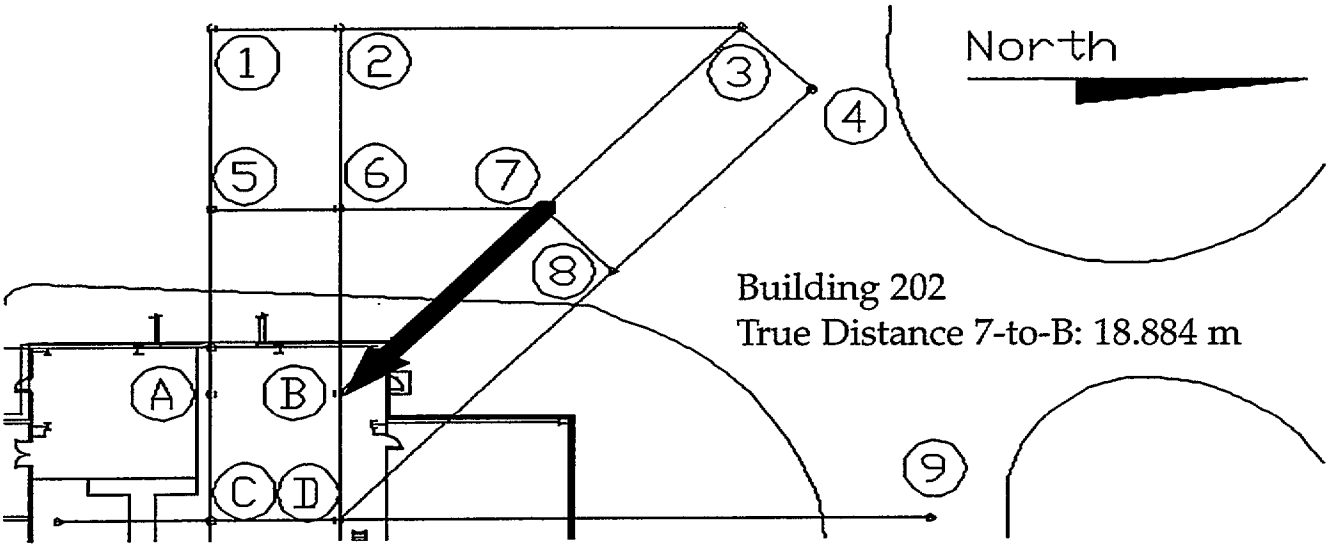

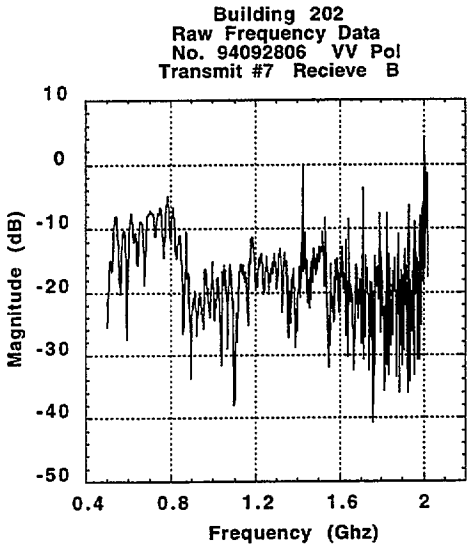

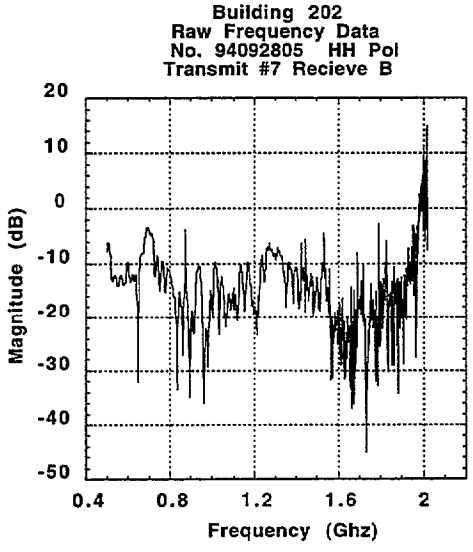

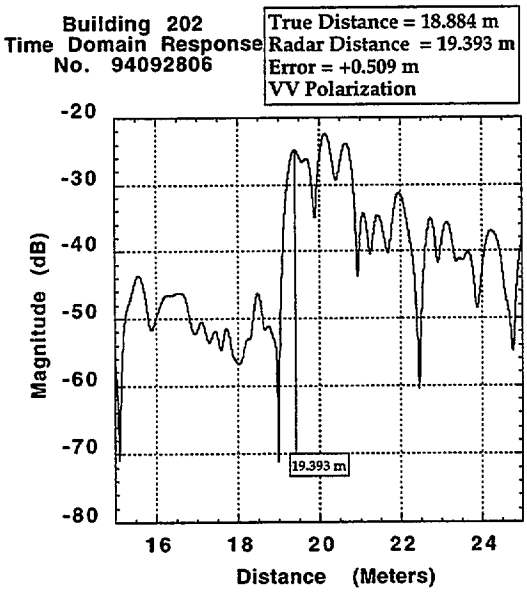

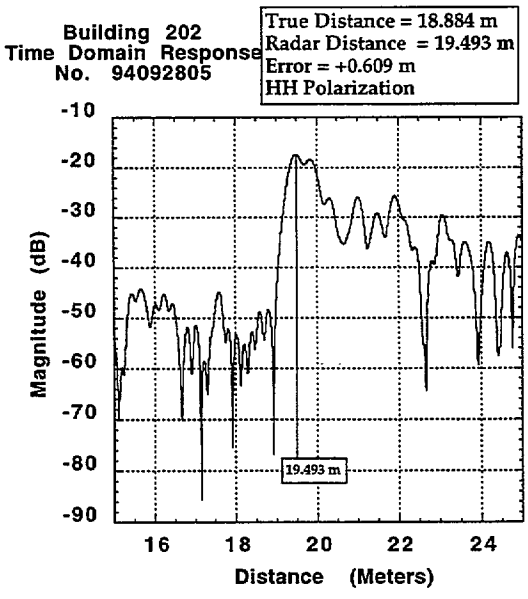

Fig 3a: Transmission at Station #7 to Receive Station B. Vertical Polarization.

Fig3b: Transmission at Station #7 to Receive station B. Horization Polarization.

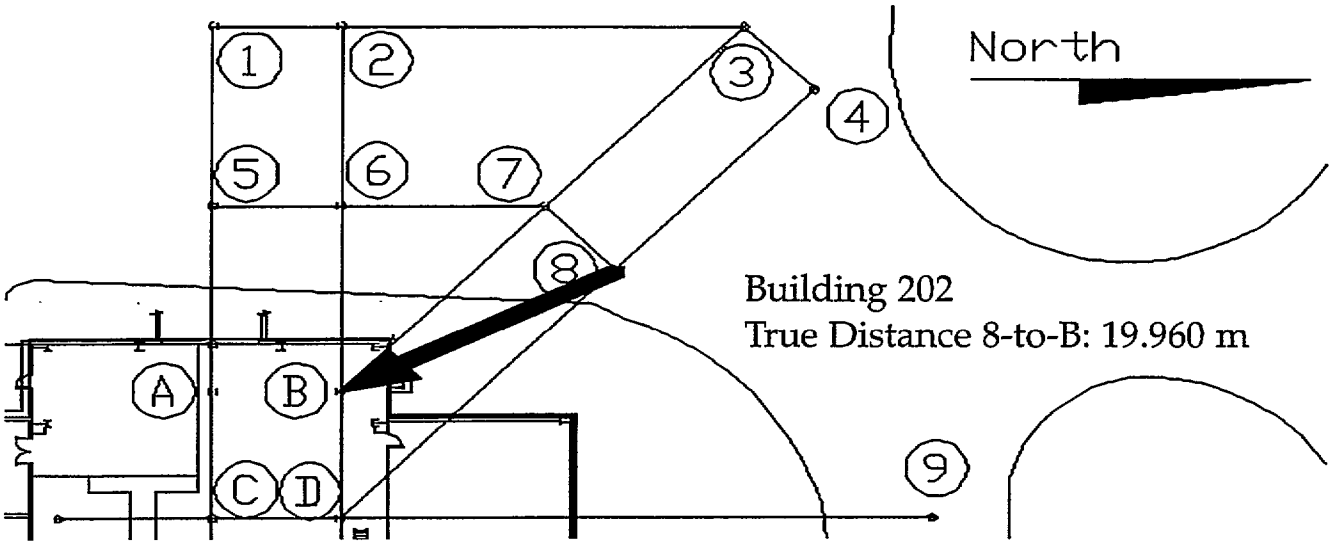

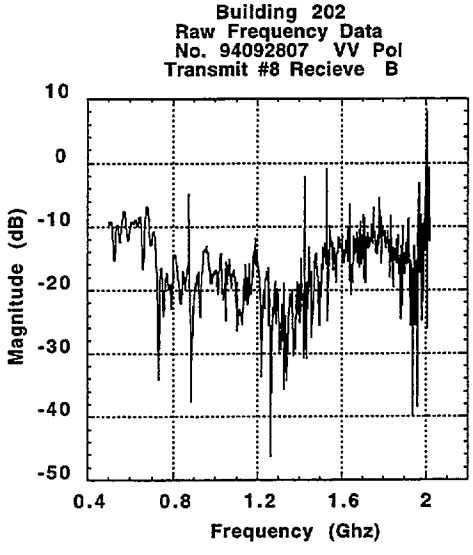

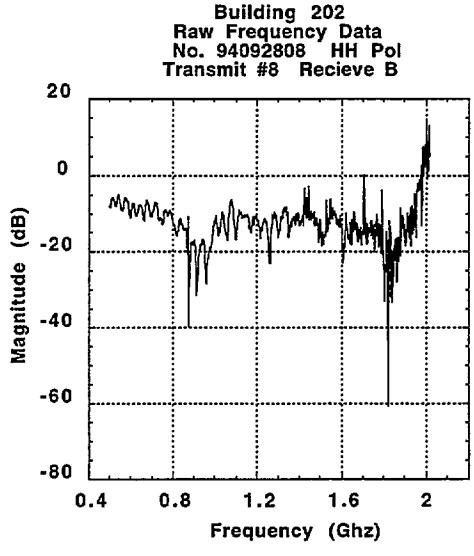

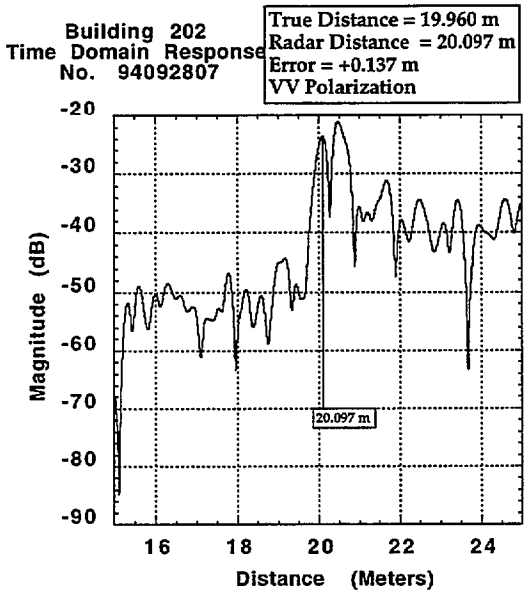

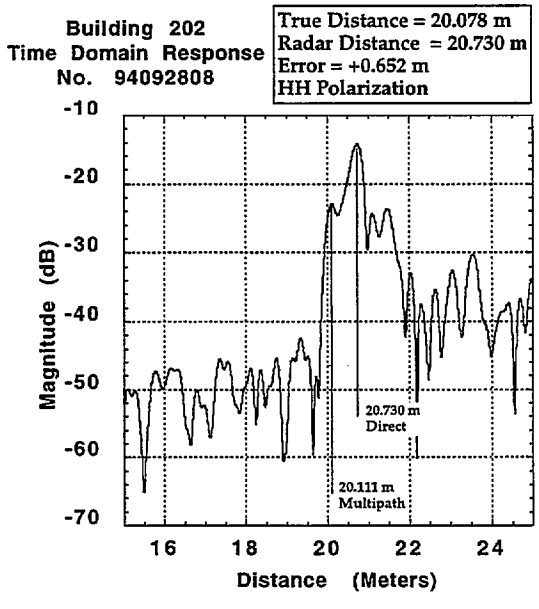

Fig 4a: Transmission at Station #8 to Receive Station B. Vertical Polarization.

Fig 4b: Transmission at Station #8 to Receive Station B. Horizontal Polarization.

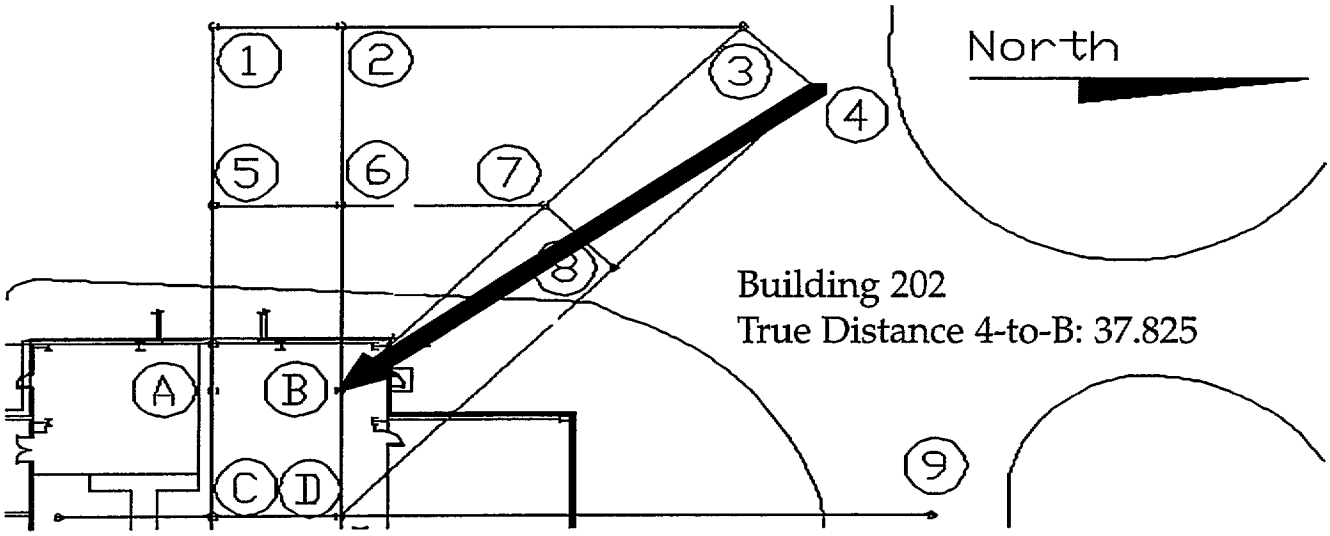

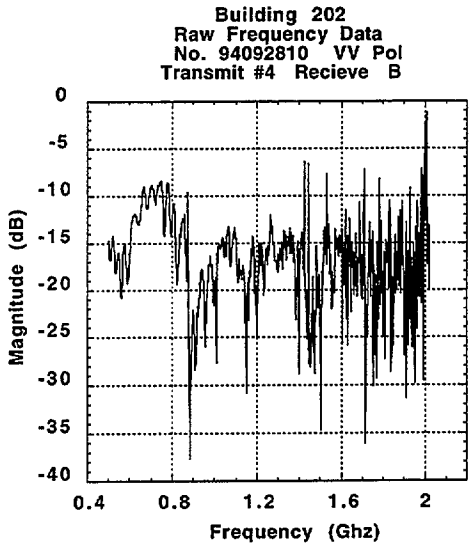

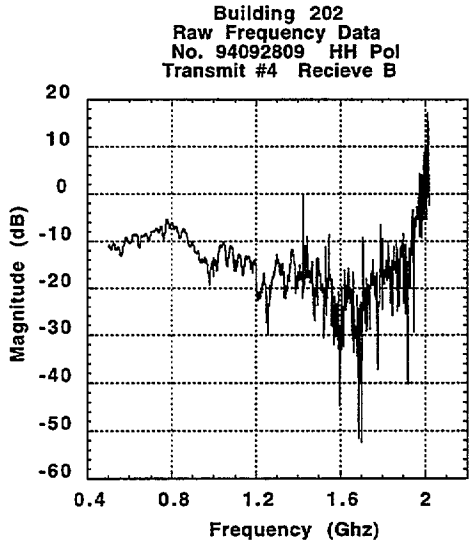

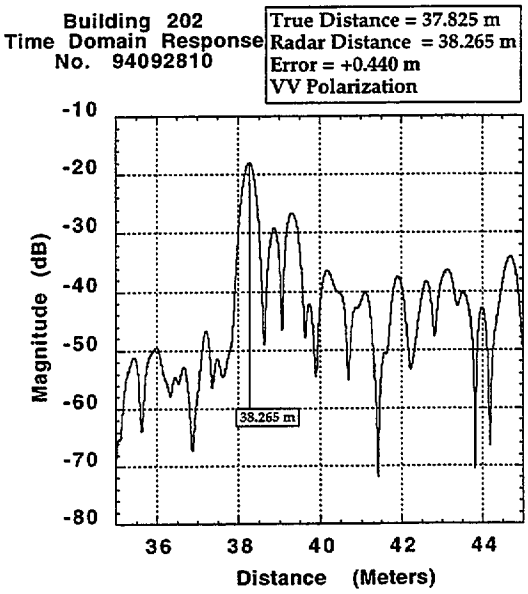

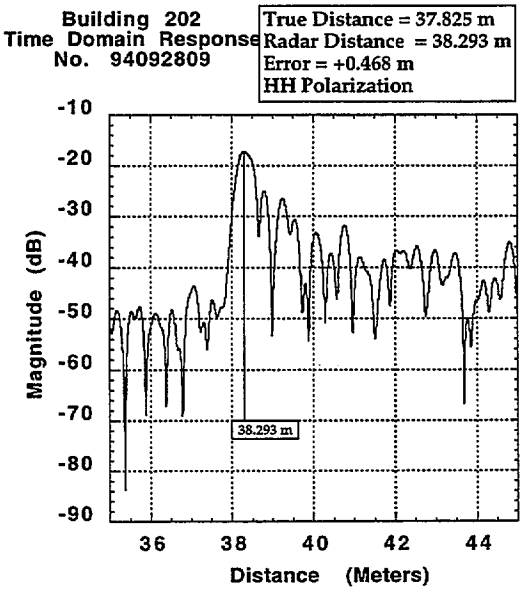

Fig 5a: Transmission at Station #4 to Receive Station B. Vertical Polarization.

Fig 5b: Transmission at Station #4 to Receive Station B. Horizontal Polarization.

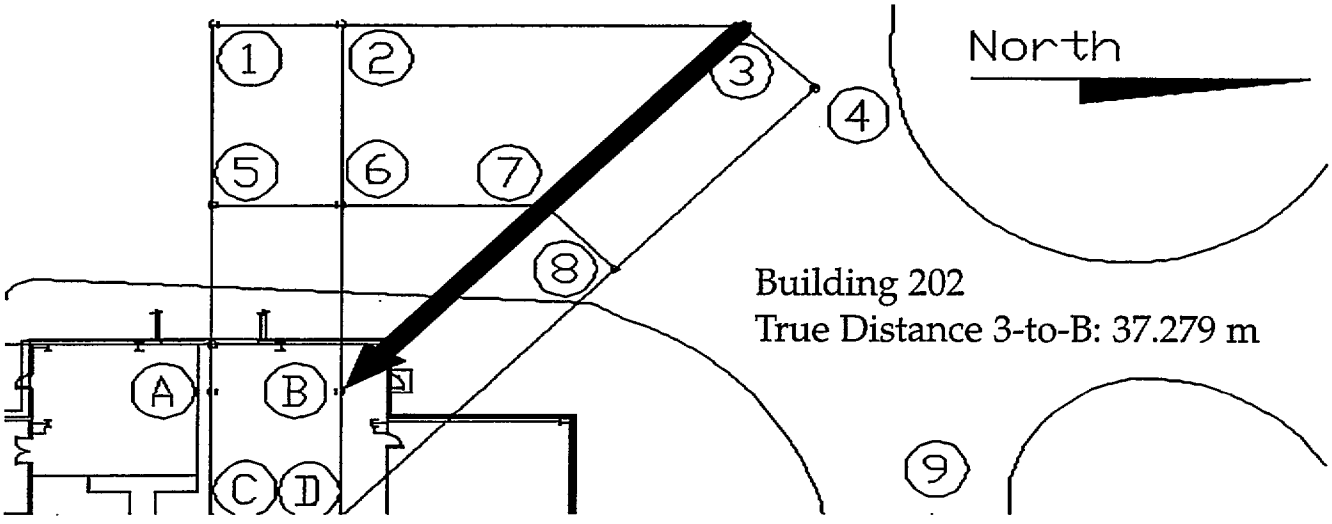

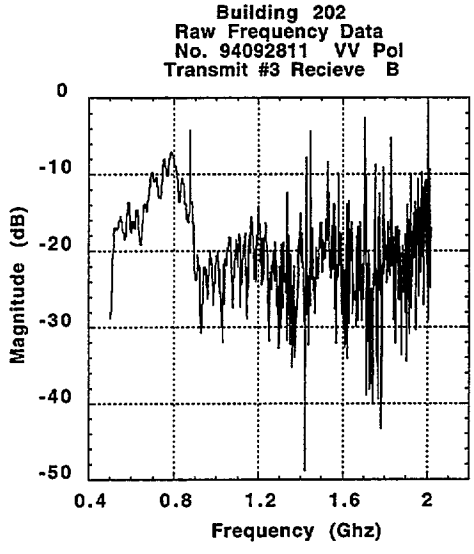

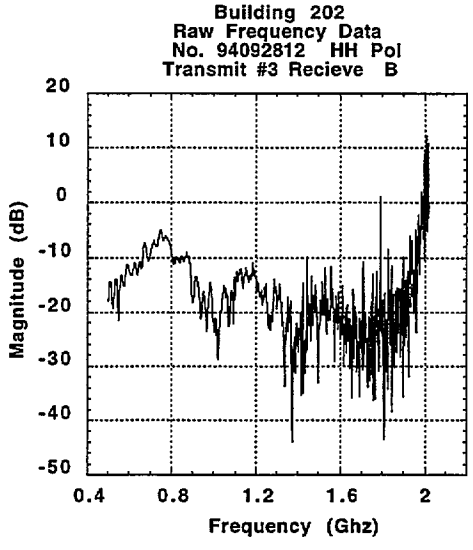

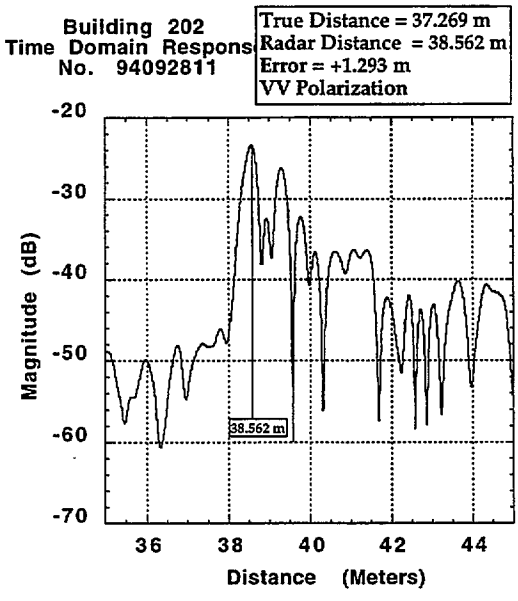

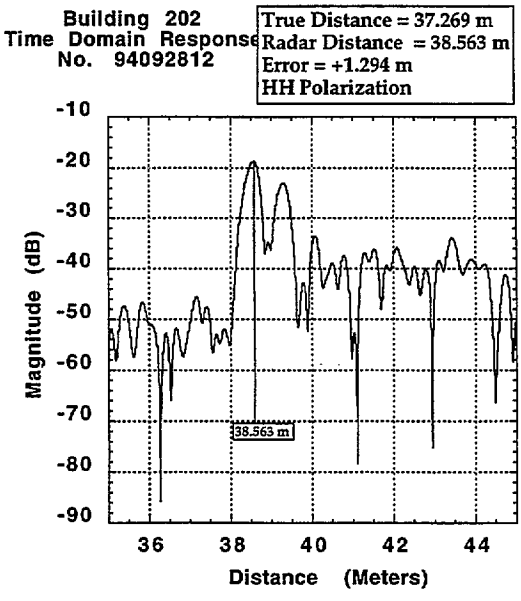

Fig 6a: Transmission at Station #3 to Receive Station B. Vertical Polarization.

Fig 6b: Transmission at Station #3 to Receive Station B. Horizontal Polarization.

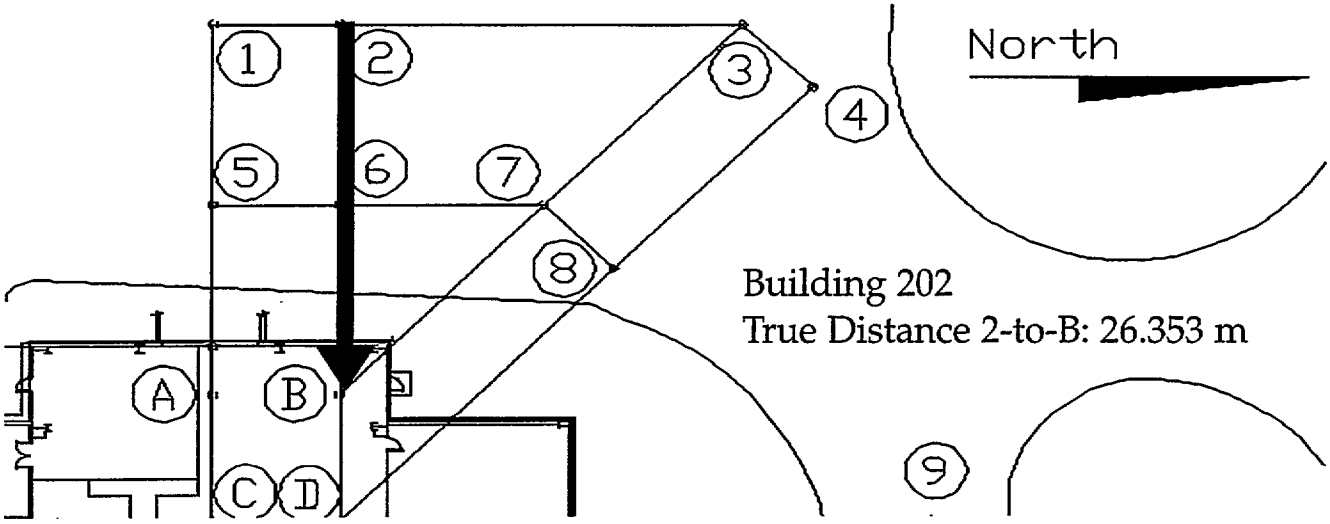

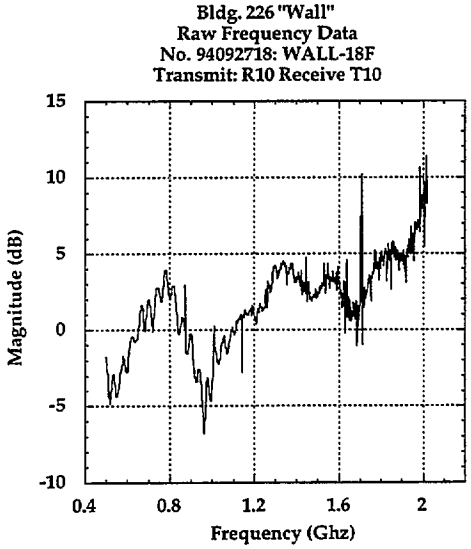

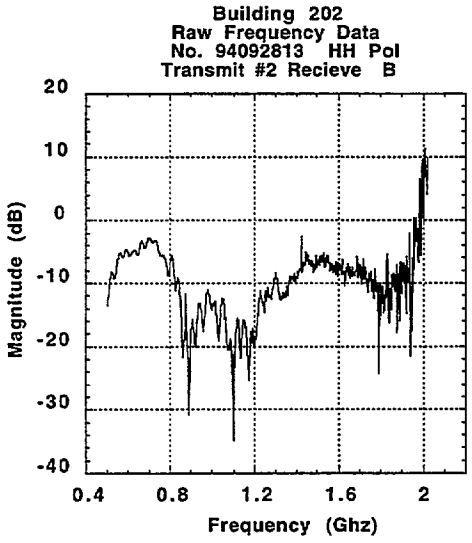

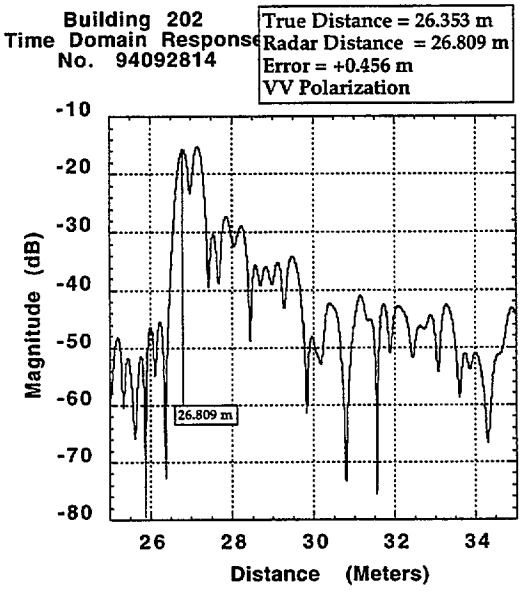

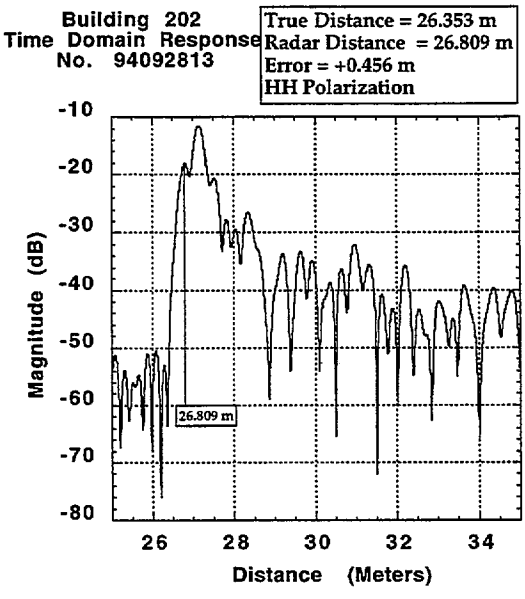

Fig 7a: Transmission at Station #2 to Receive Station B. Vertical Polarization.

Fig 7b: Transmission at Station #2 to Receive Station B. Horizontal Polarization.

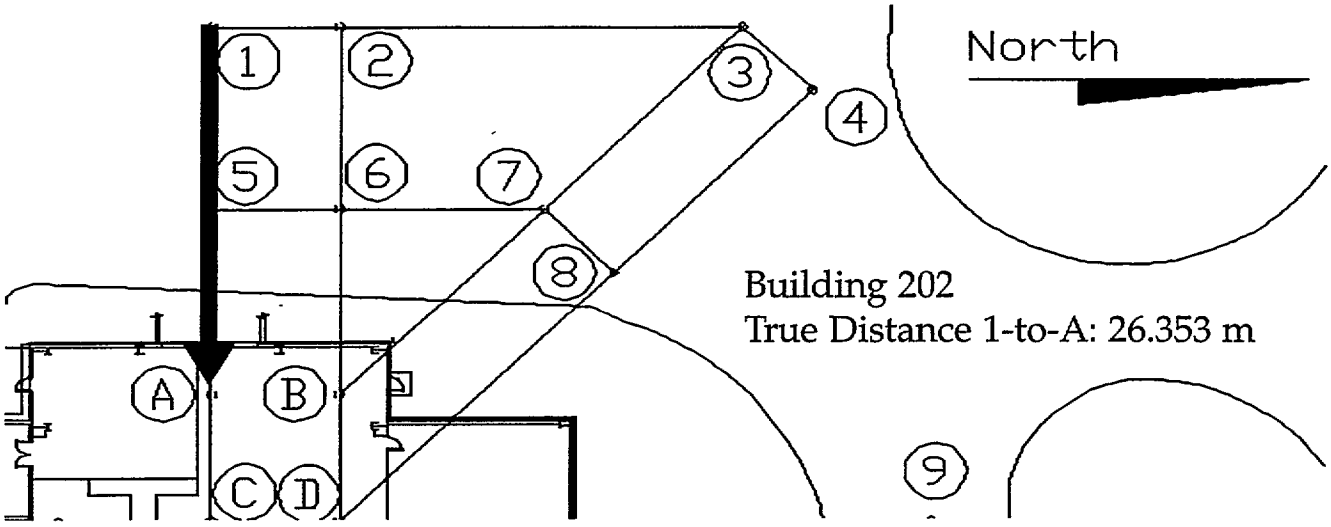

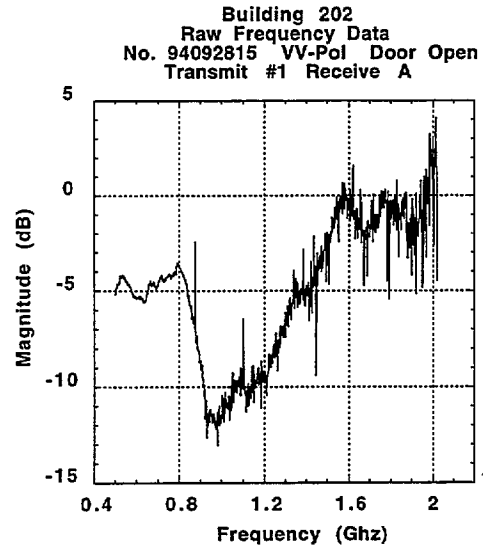

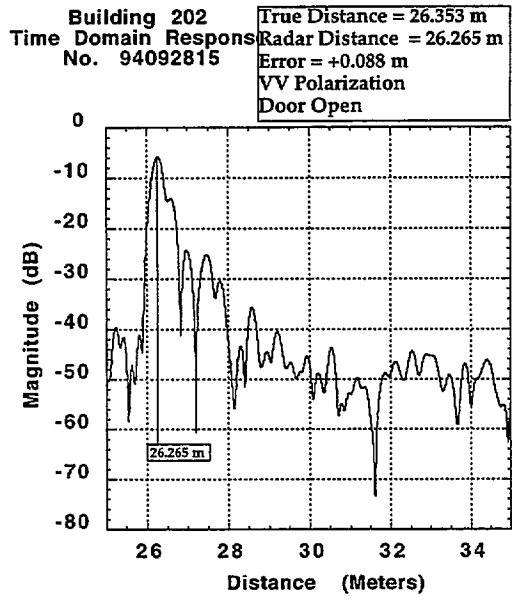

Fig 8a: Transmission at Station #1 to Receive Station at A. Vertical Polarization.

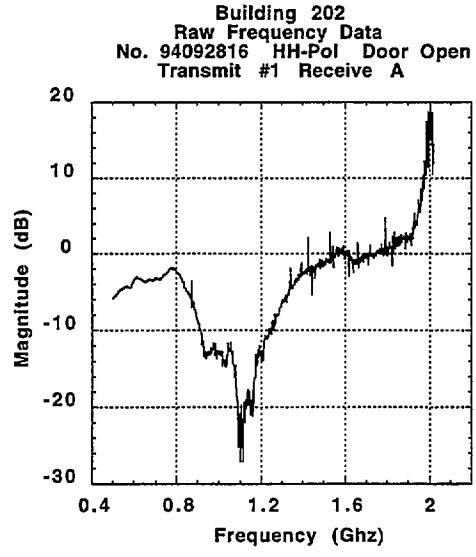

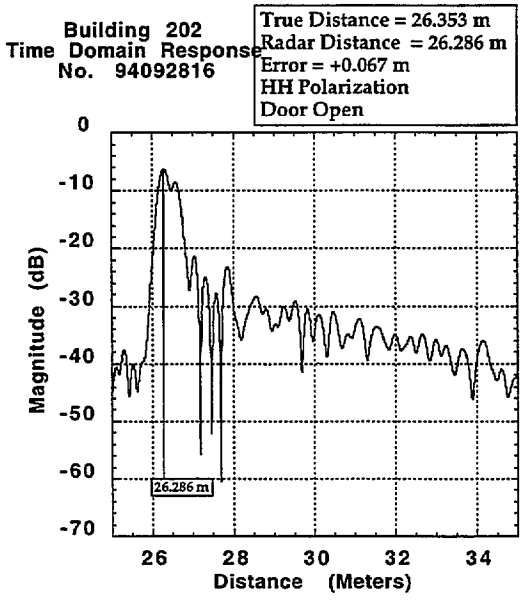

Fig 8b: Transmission at Station #1 to Receive Station at A. Horizontal Polarization.

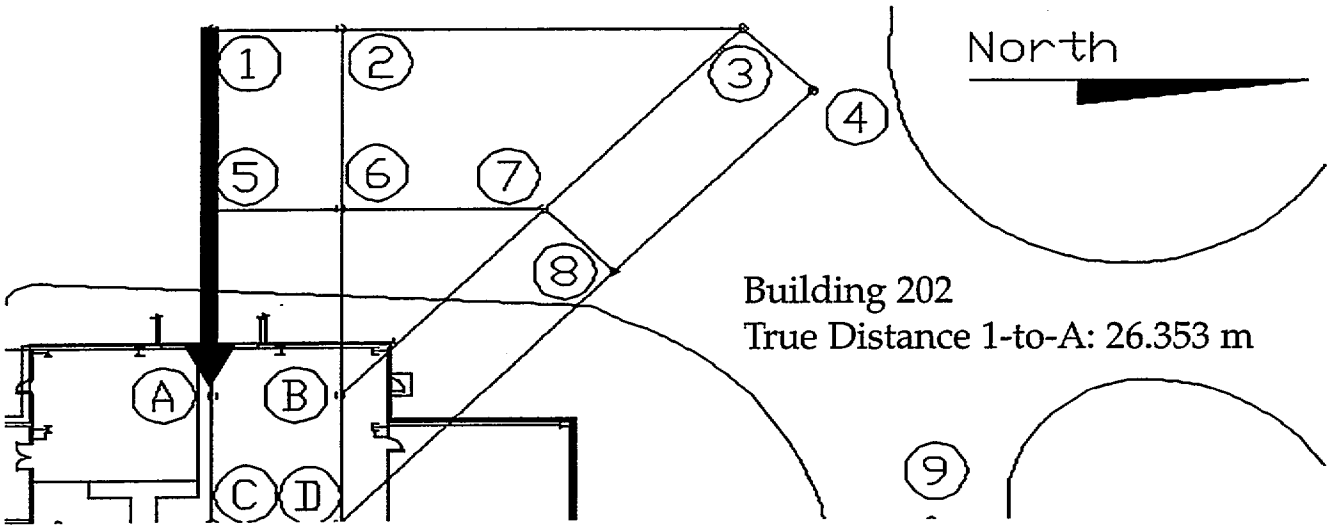

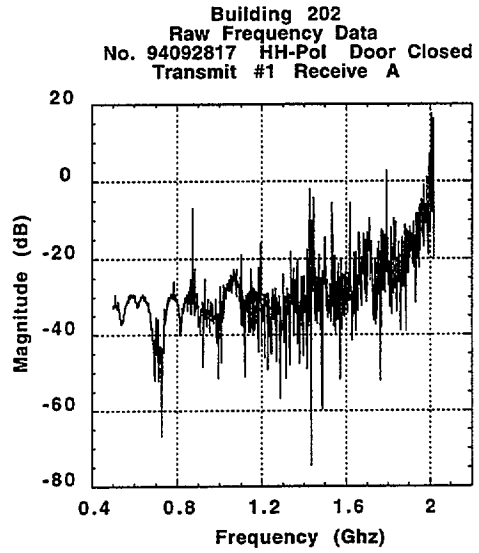

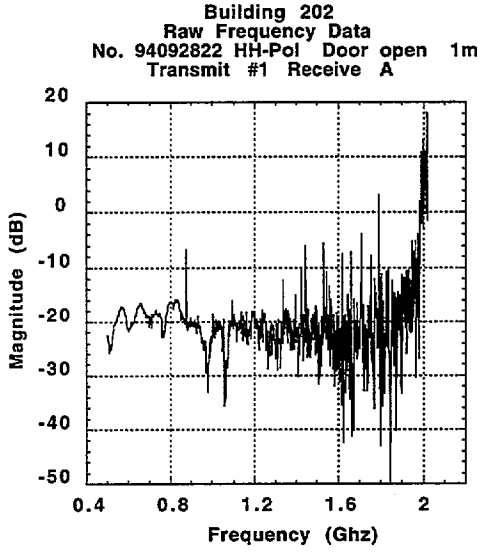

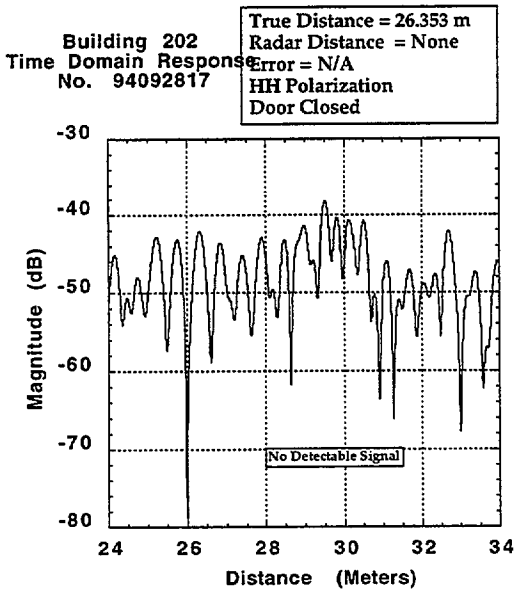

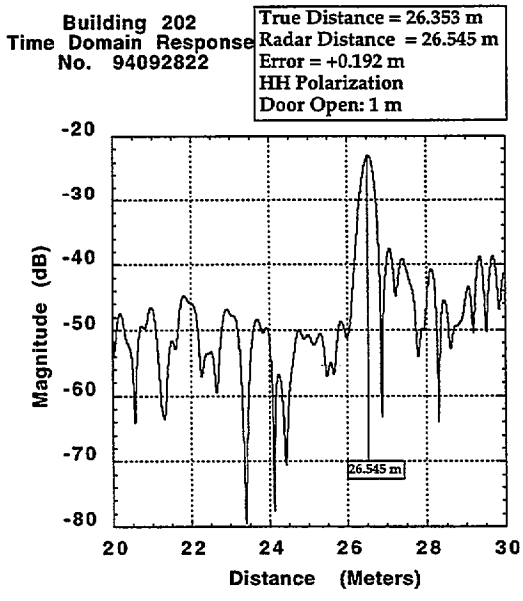

Fig 9a: Transmission at Station #1 to Receive Station A. Vertical Polarization.

Fig 9b: Transmission at Station #1 to Receive Station A. Horizontal Polarization.

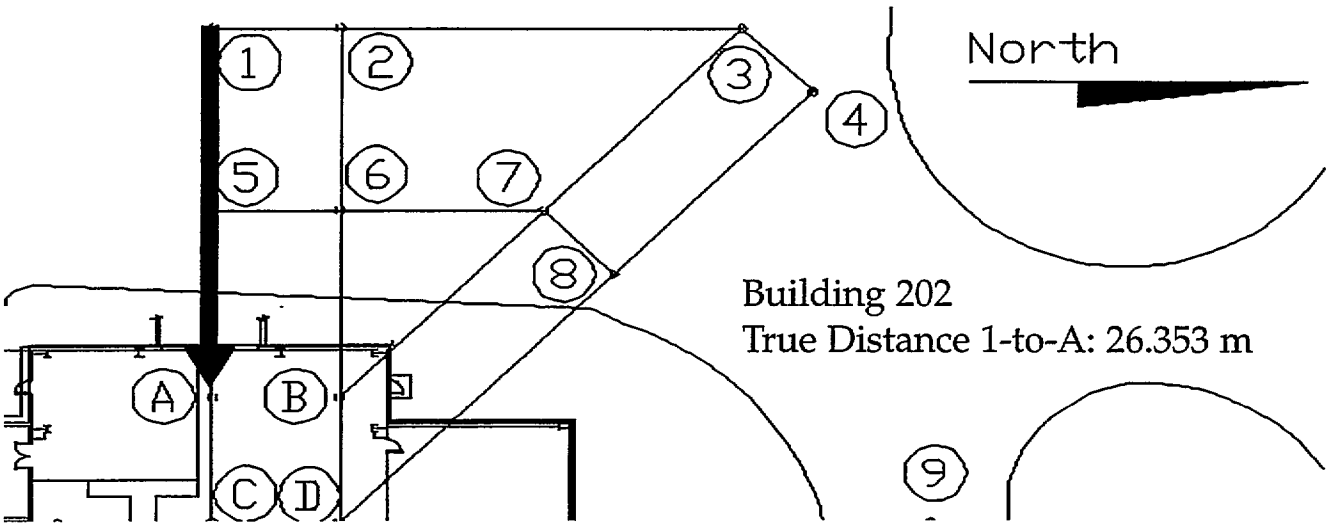

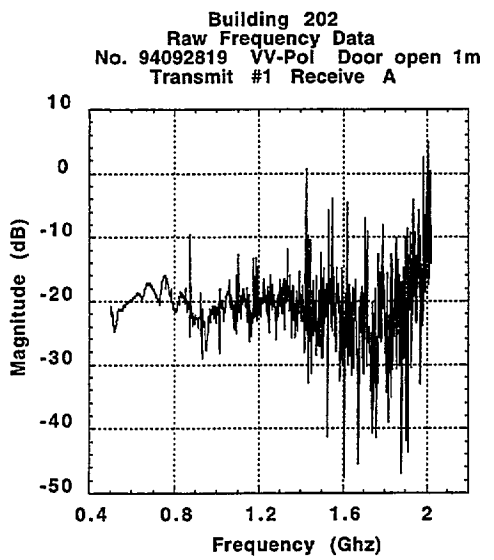

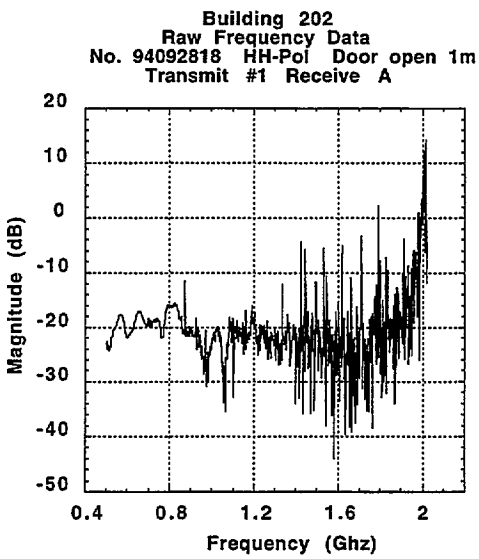

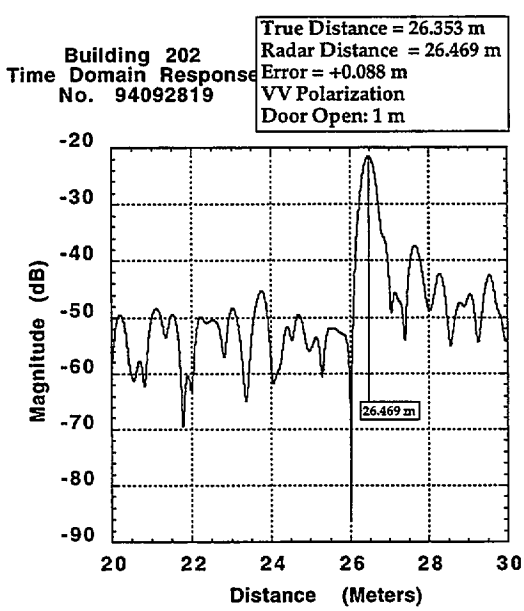

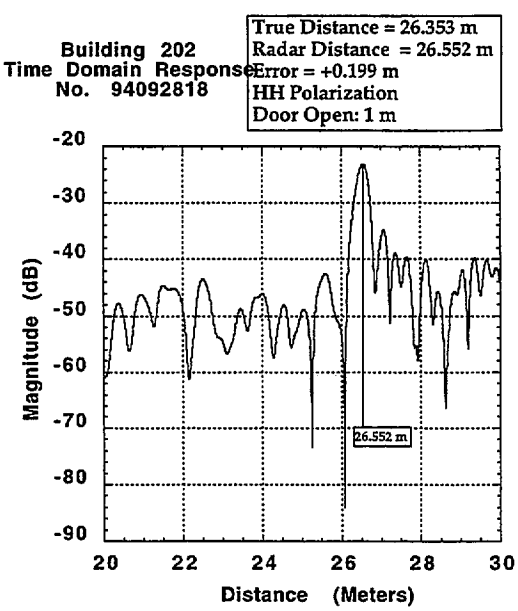

Fig 10a: Transmission at Station #1 to Receive Station A. Vertical Polarization.

Fig 10b: Transmission at Station #1 to Receive Station A. Horizontal Polarization.

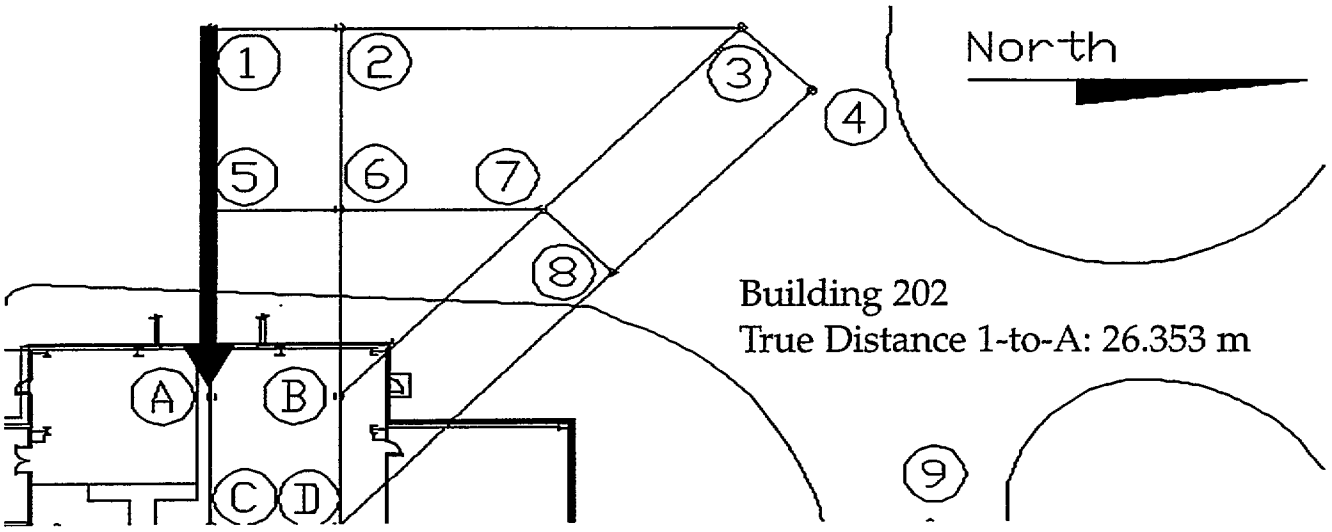

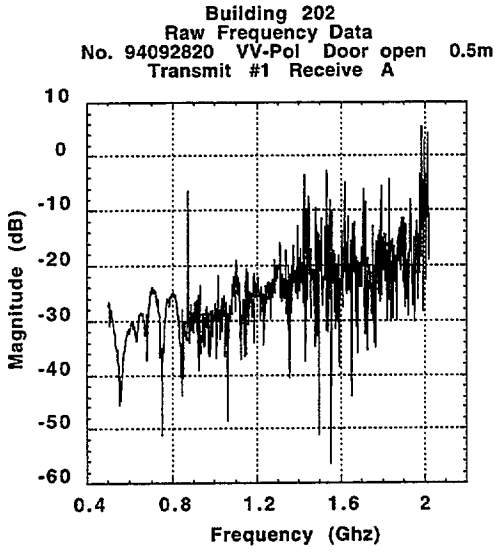

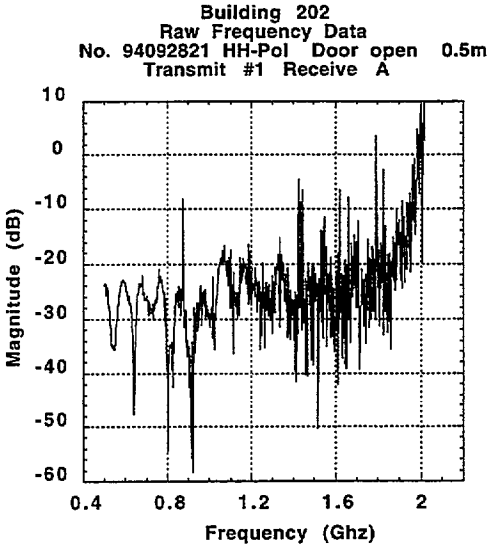

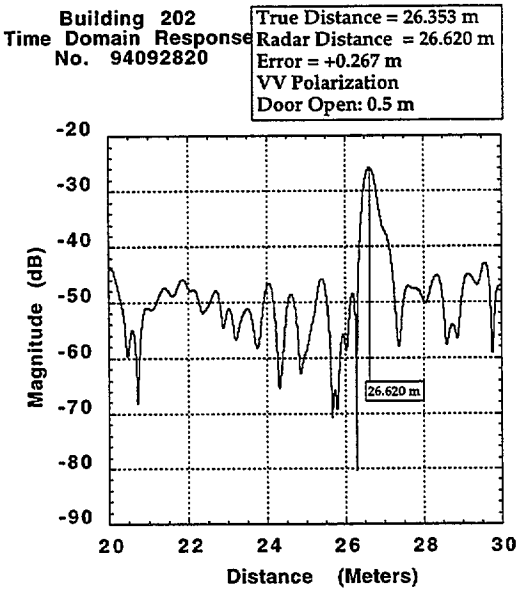

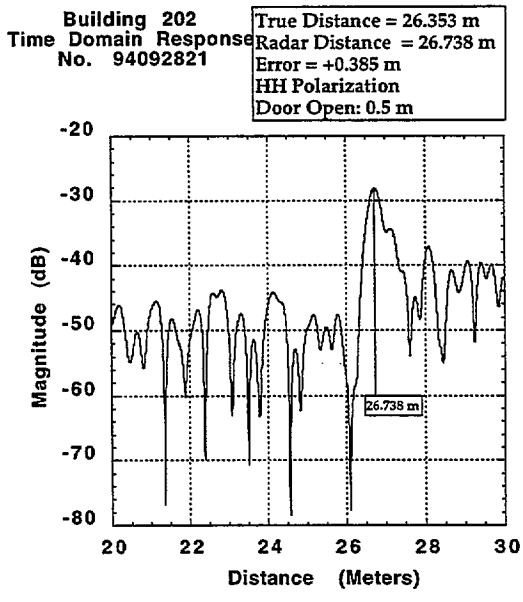

Fig 11a:Transmission at Station #1 to Receive Station A. Vertical Polarization.

Fig 11b: Transmission at Station #1 to Receive Station A. Horizontal Polarization.

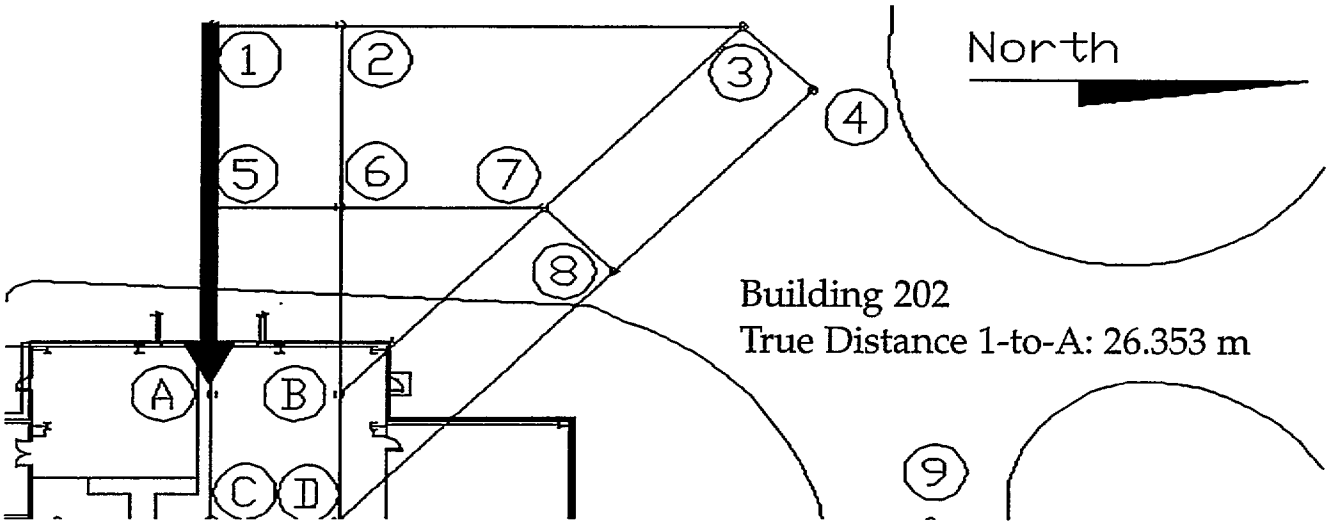

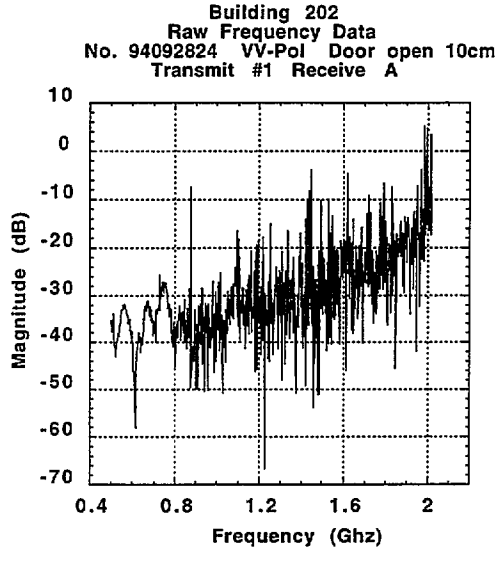

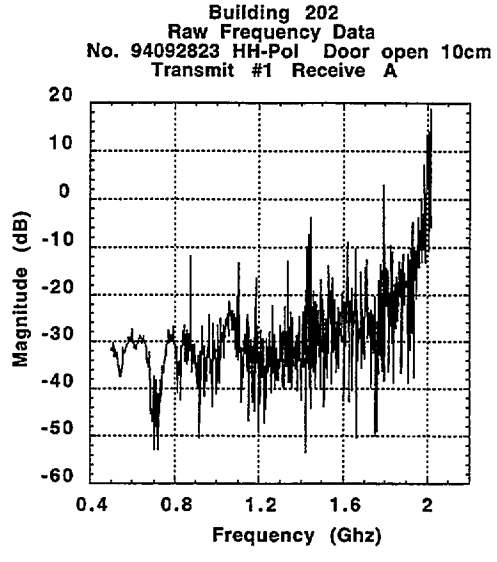

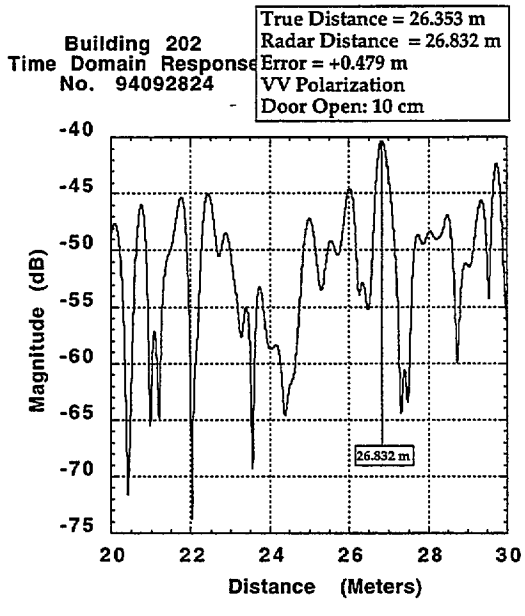

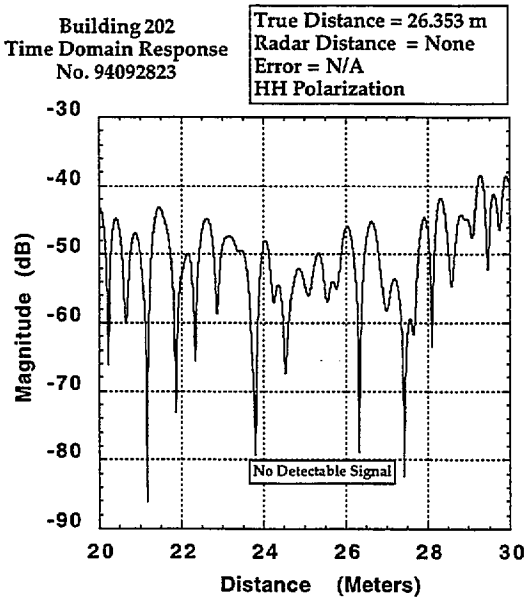

Fig 12a: Transmission at Station #1 to Receive Station A. Vertical Polarization.

Fig 12b: Transmission at Station #1 to receive Station A. Horizontal Polarization.

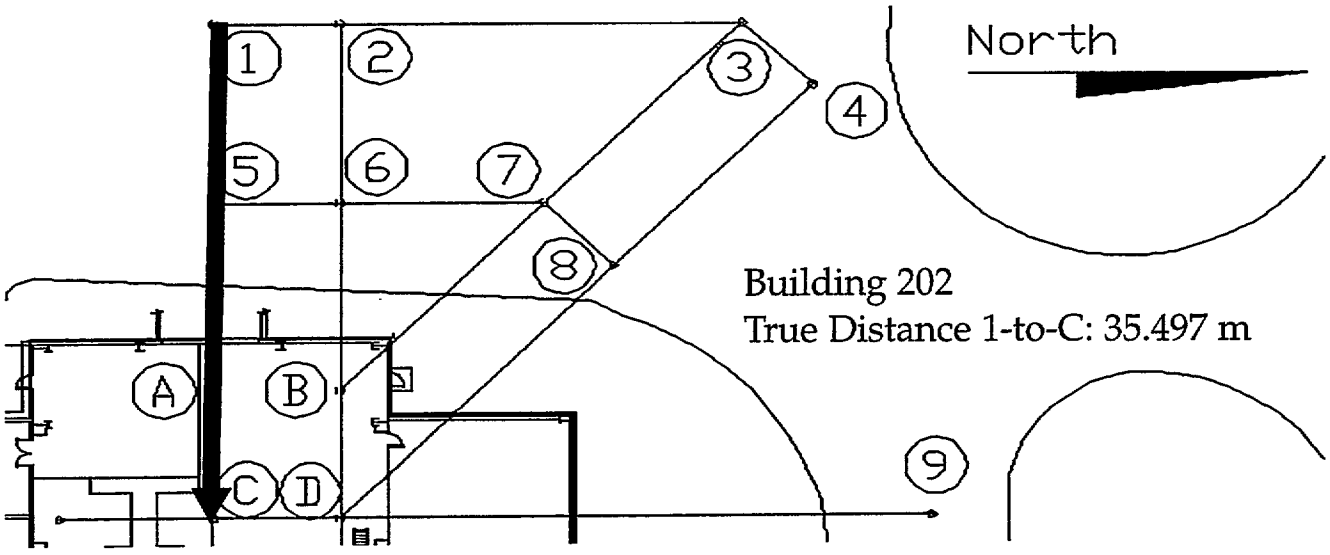

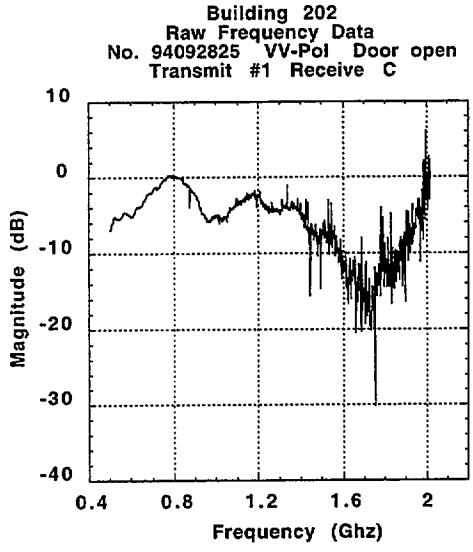

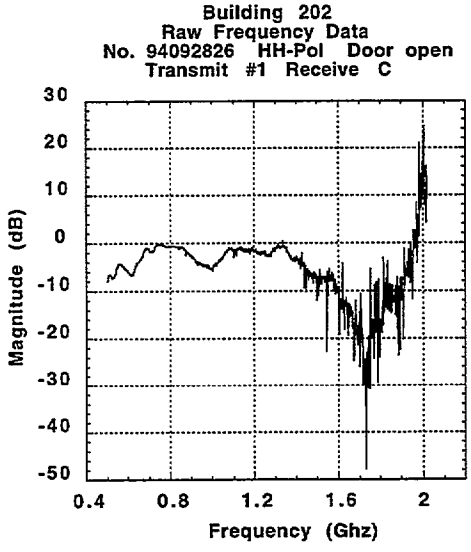

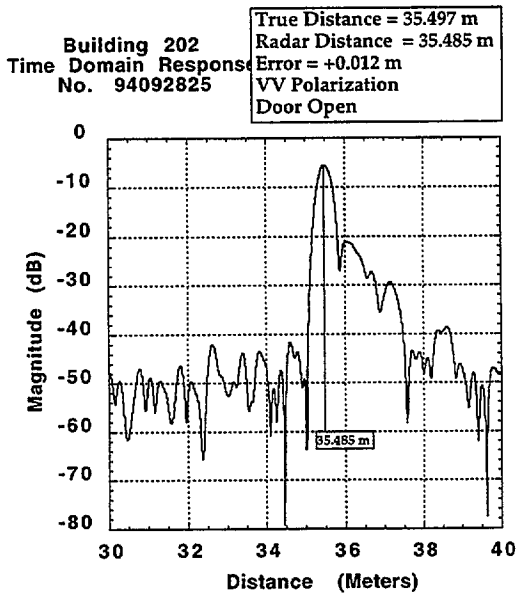

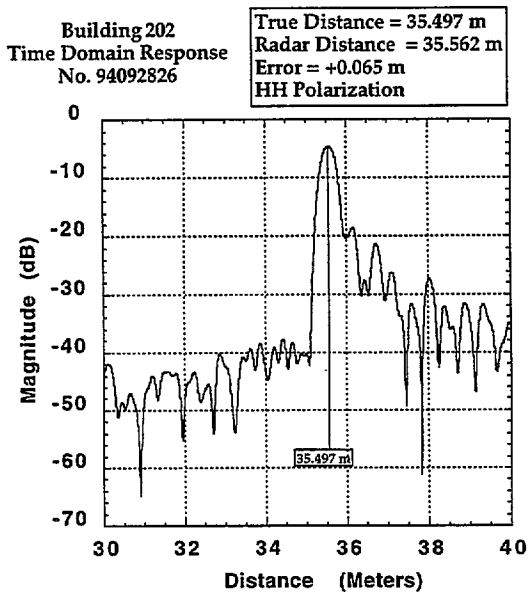

Fig 13a: Transmission at Station #1 to Receive Station C. Vertical Polarization.

Fig 13b: Transmission at Station #1 to Receive Station C. Horizontal Polarization,

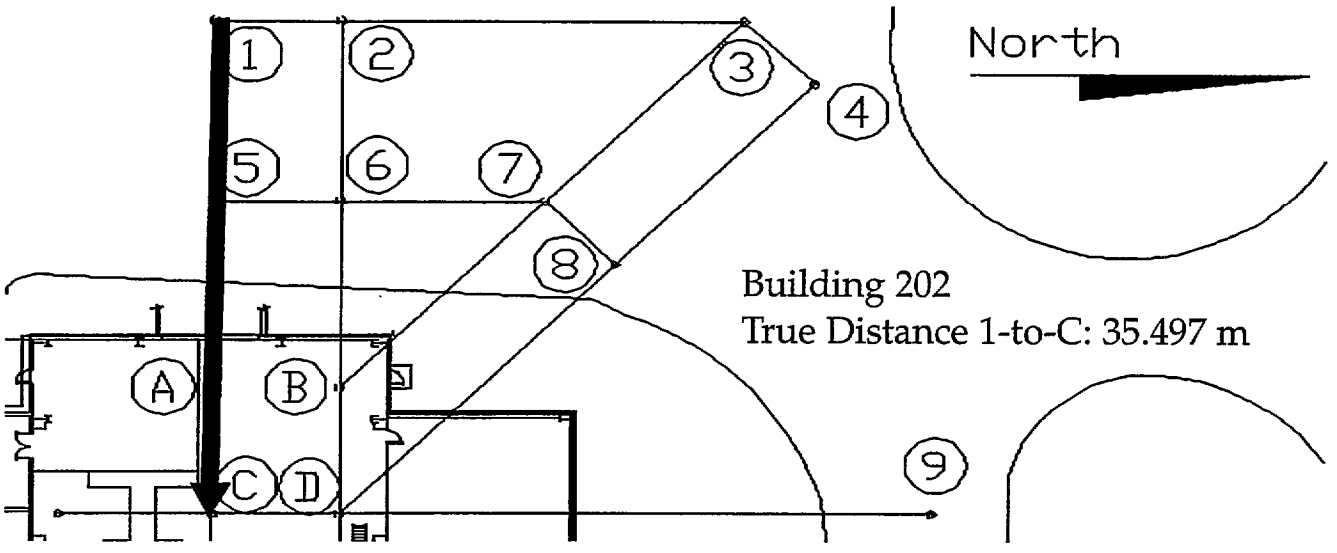

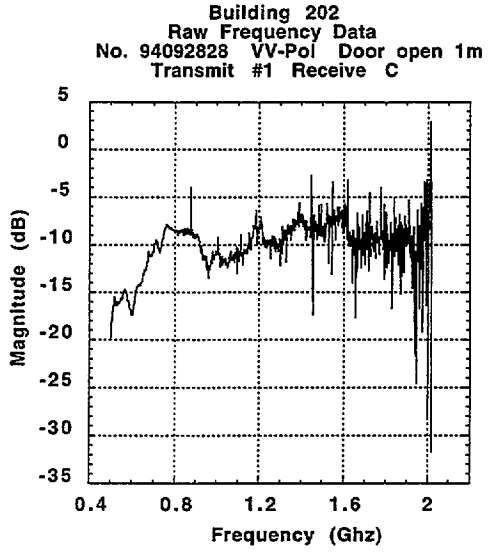

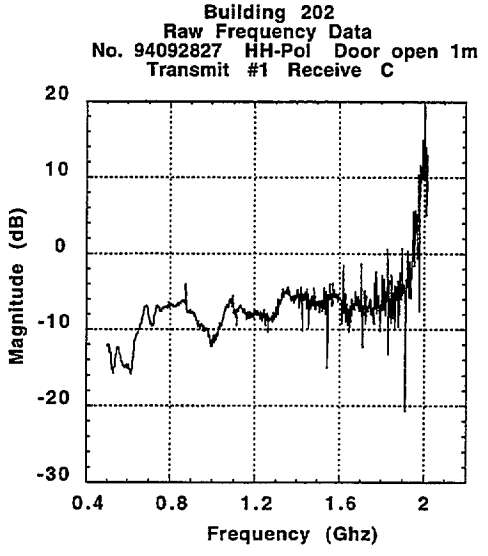

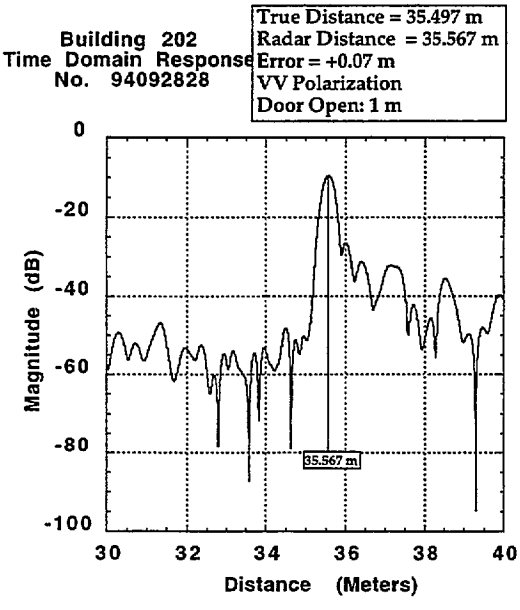

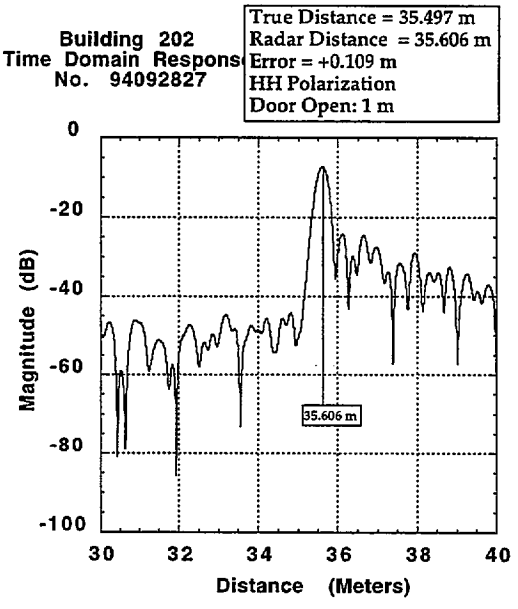

Fig 14a: Transmission at Station #1 to Receive Station C. Vertical Polarization.

Fig 14b: Transmission at Station #1 to Receive Station at C. Horizontal Polarization.

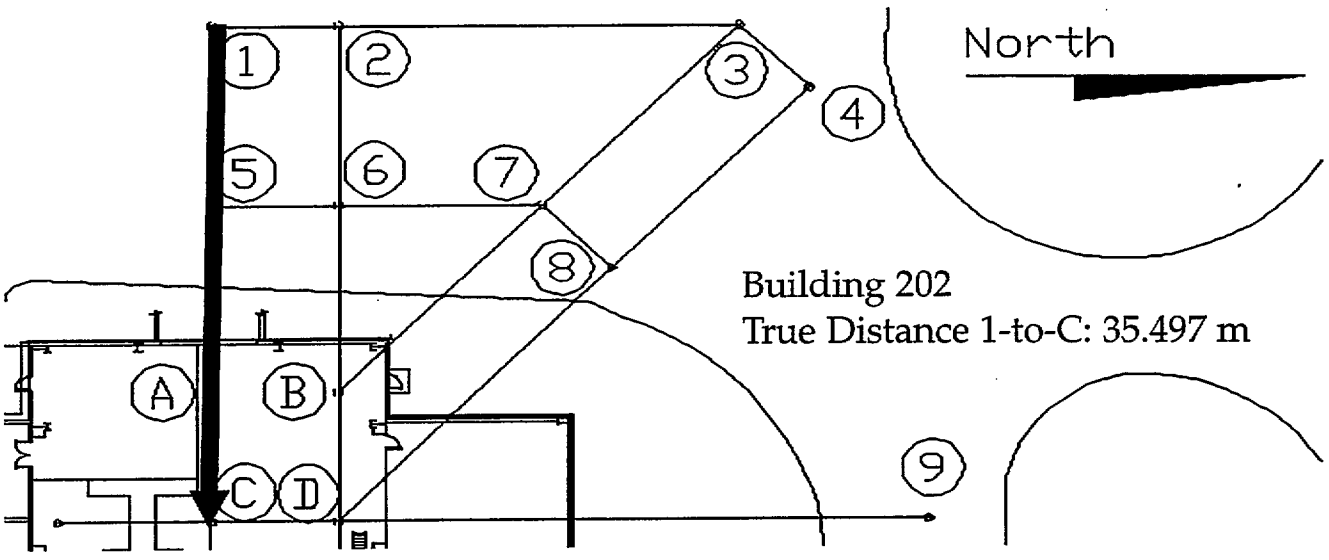

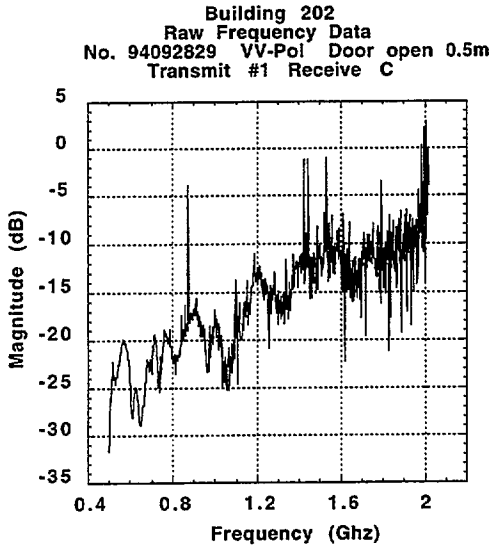

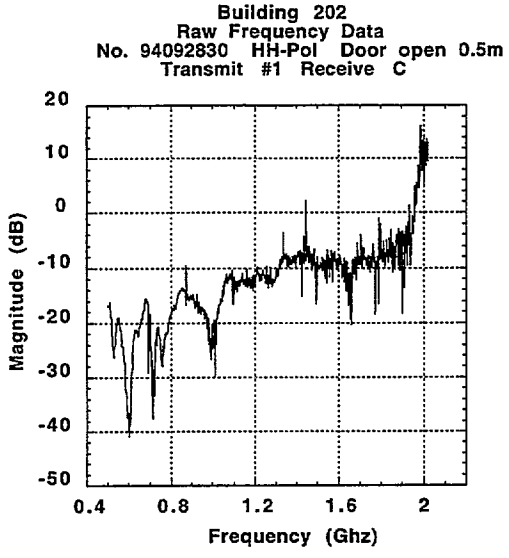

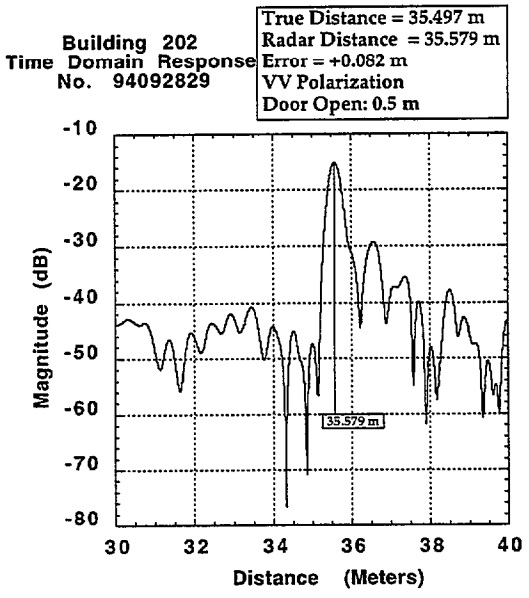

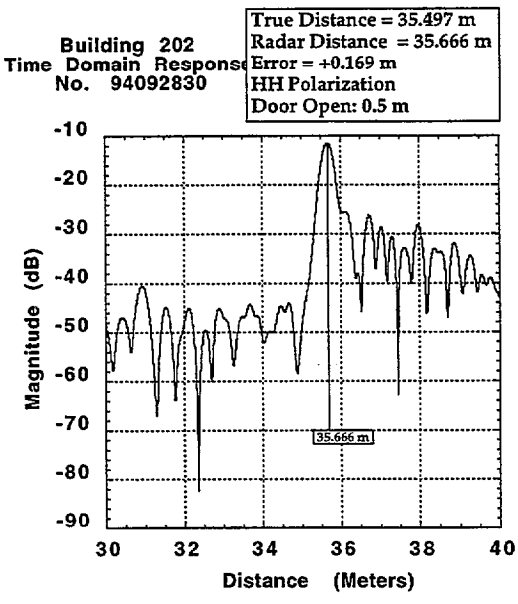

Fig 15a: Transmission at Station #1 to Receive Station C. Vertical Polarization.

Fig 15b: Transmission at Station #1 to Receive Station C. Horizontal Polarization.

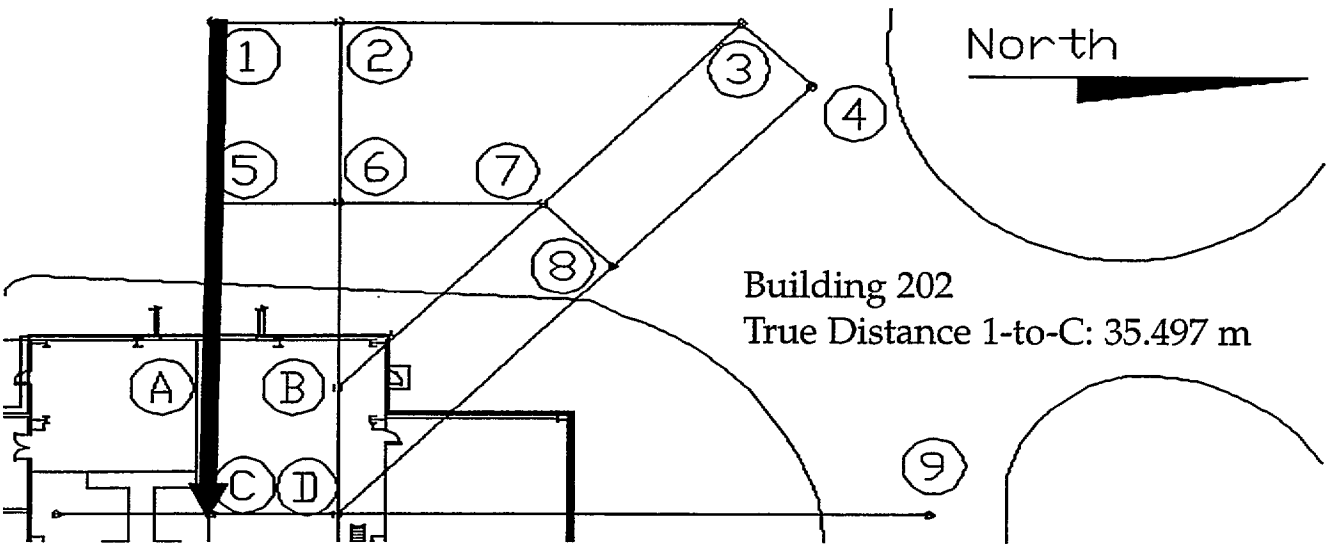

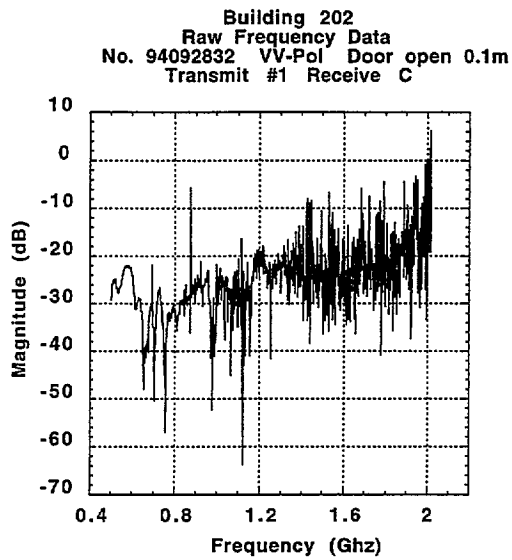

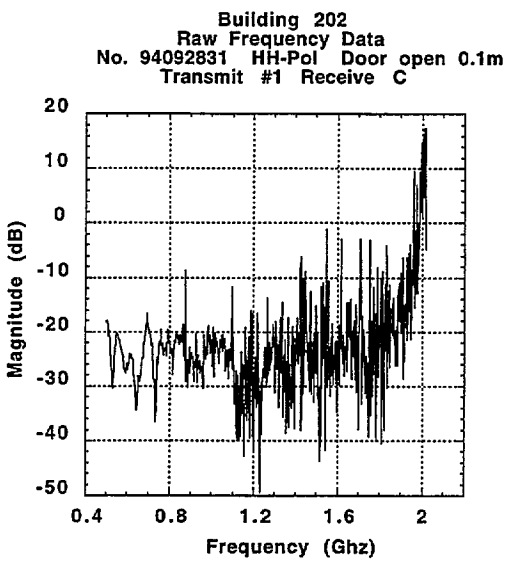

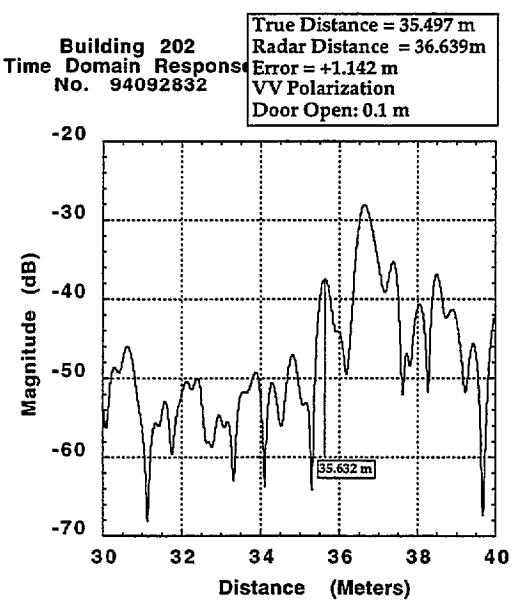

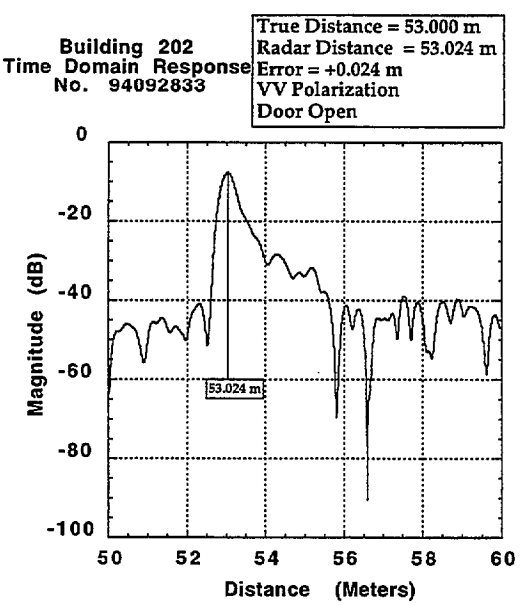

Fig 16a: Transmission at Station #1 to Receive Station C. Vertical Polarization.

Fig 16b: Transmission at Station #1 to Receive Station C. Horizontal Polarization.

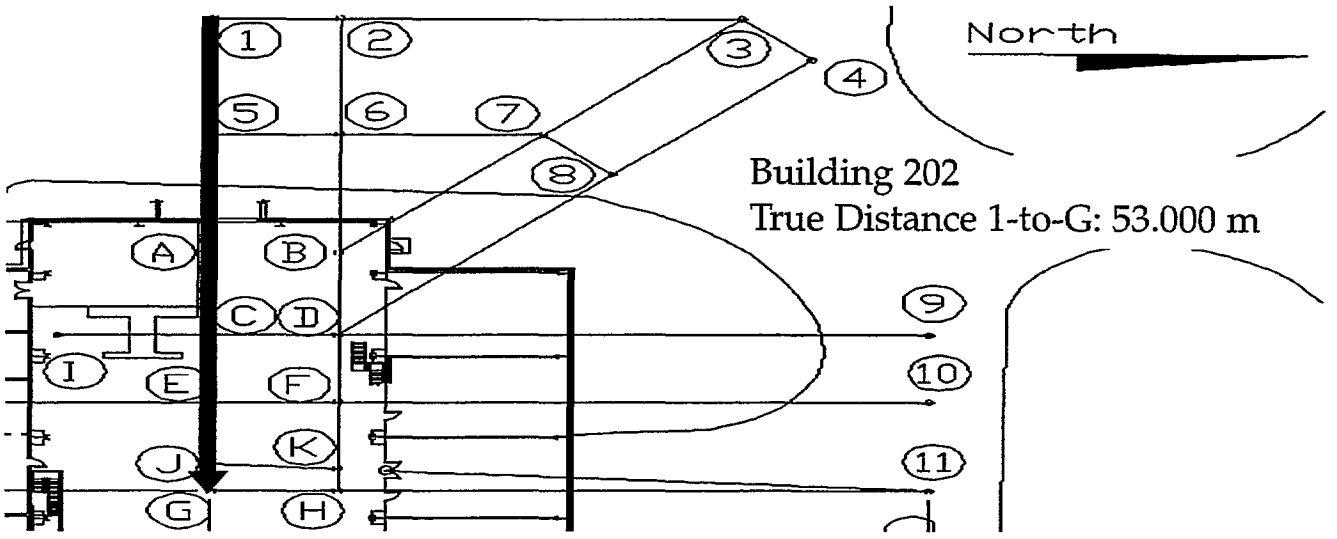

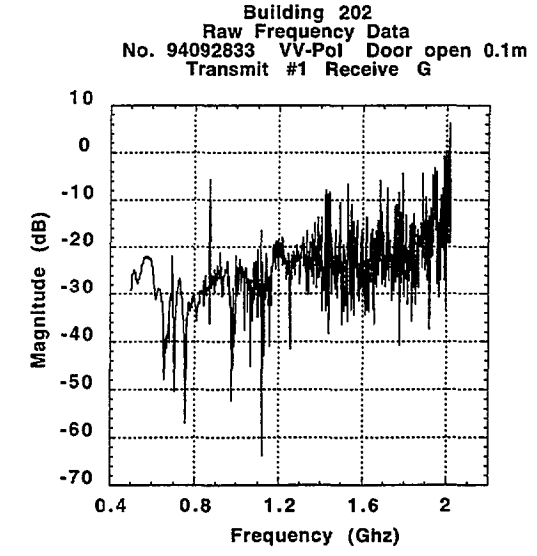

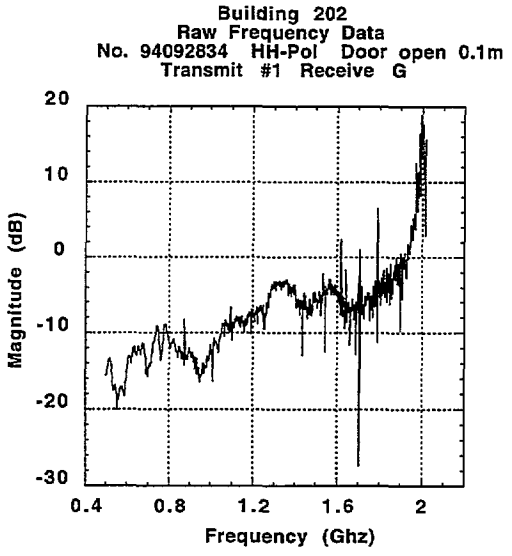

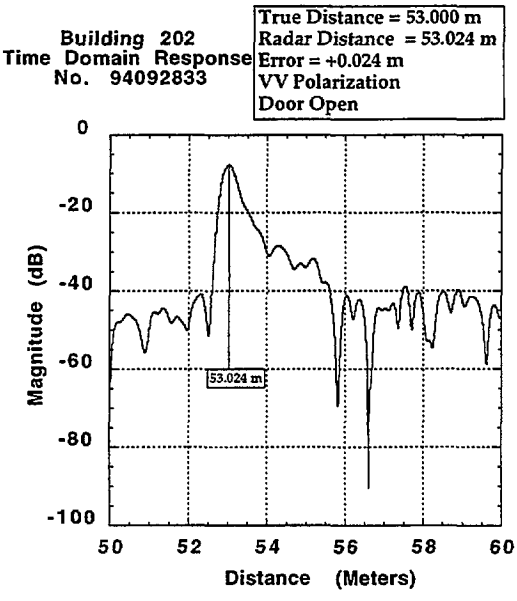

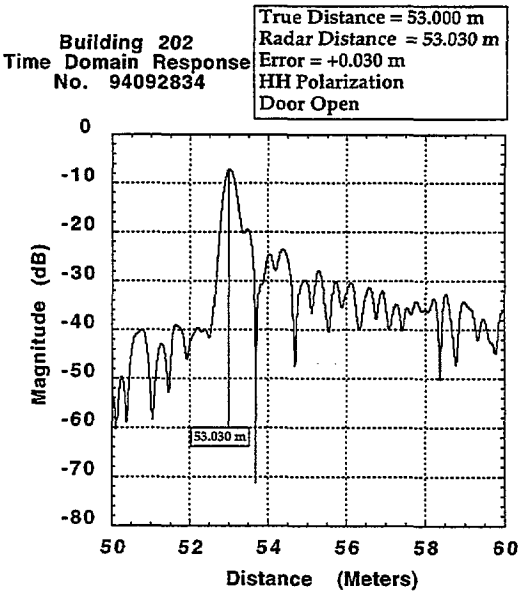

Fig 17a: Transmission at Station #1 to Receive Station G. Horizontal Polarization.

Fig 17b: Transmission st Station #1 to Receive Station G. Horizontal Polarization.

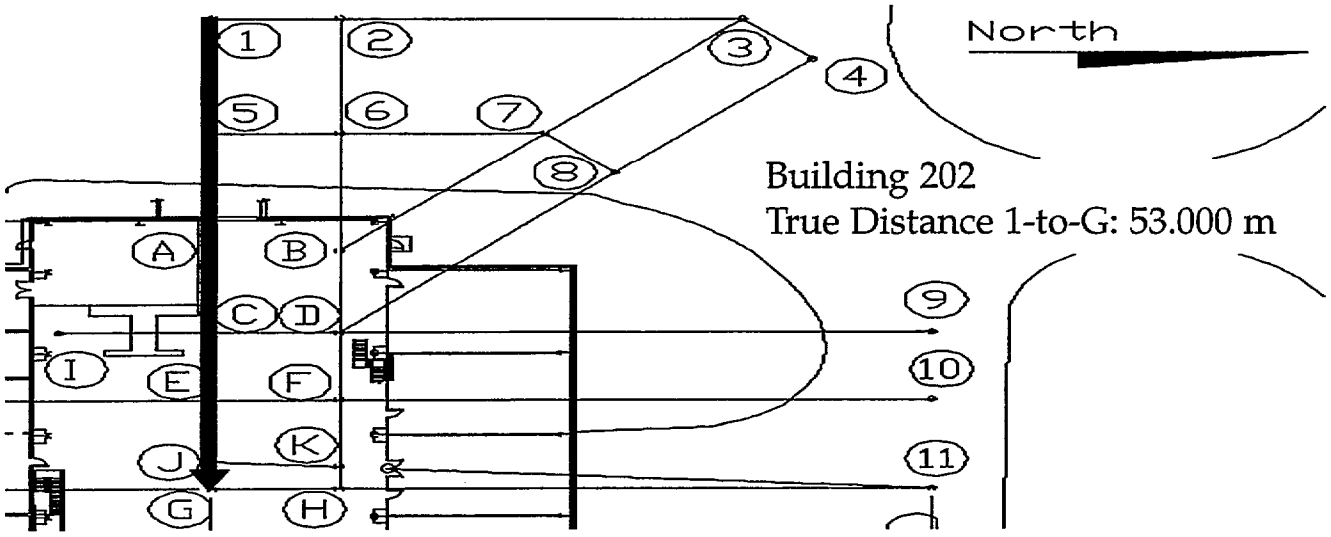

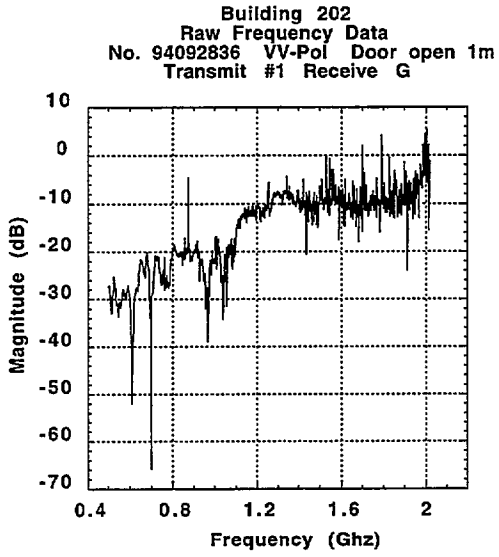

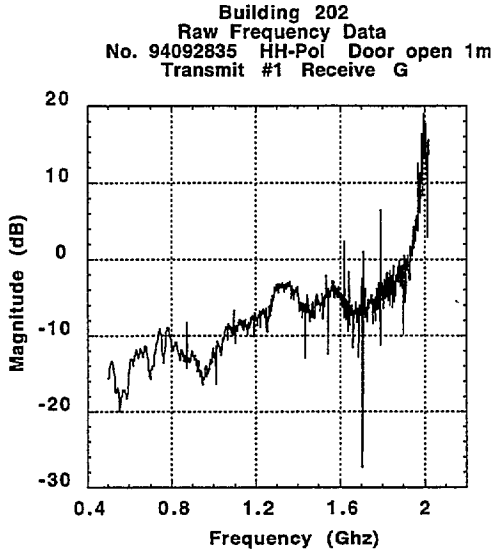

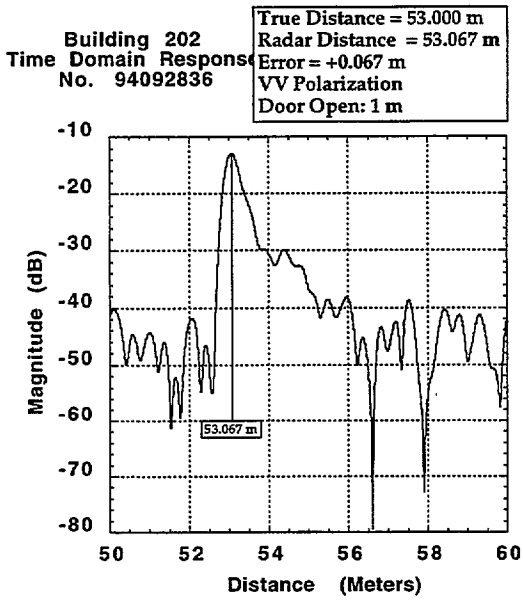

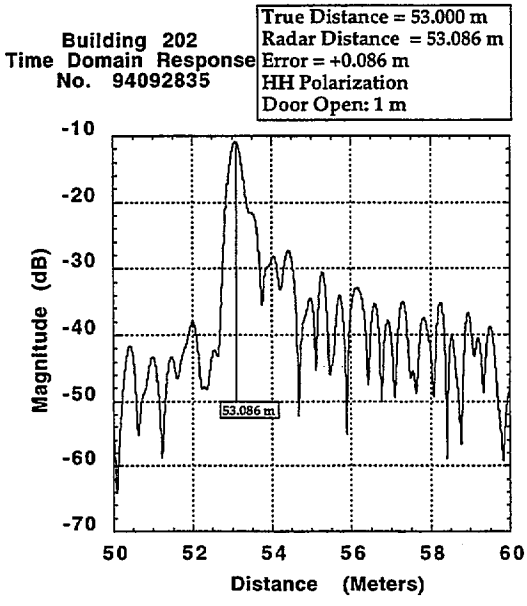

Fig 18a: Transmission at Station #1 to Receive Station G. Vertical Polarization

Fig 18b: Transmission at Station #1 to Receive Station G. Horizontal Polarization.

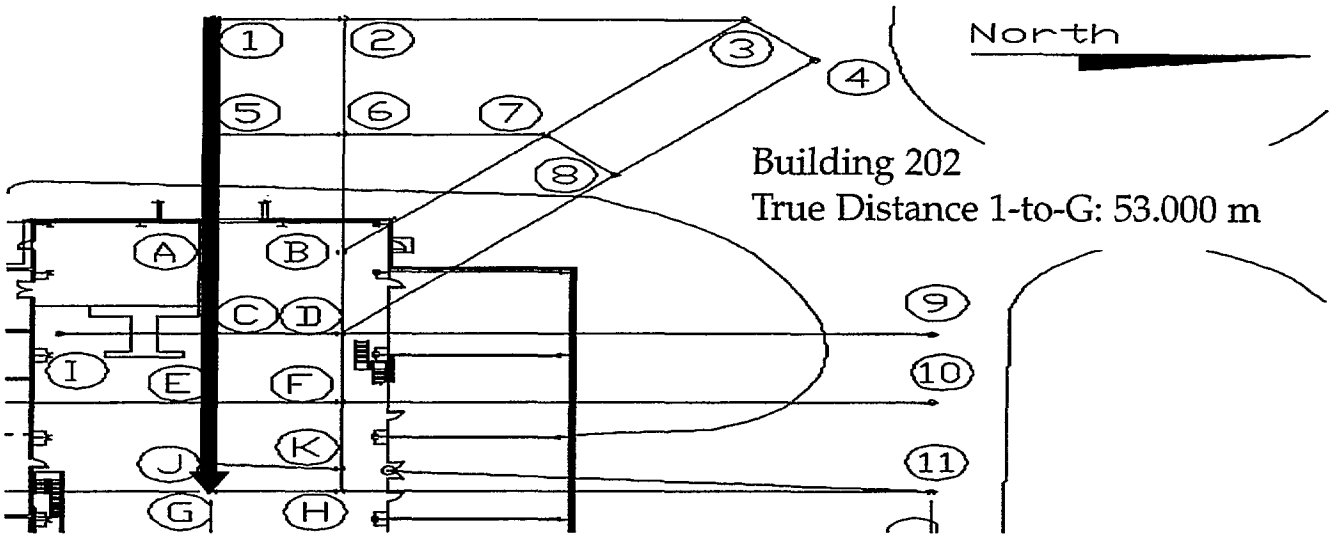

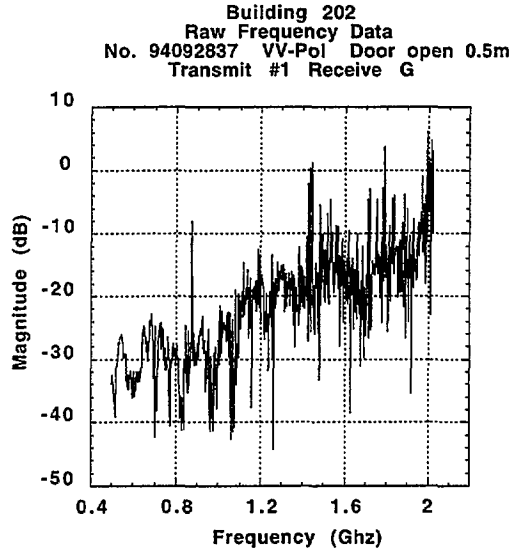

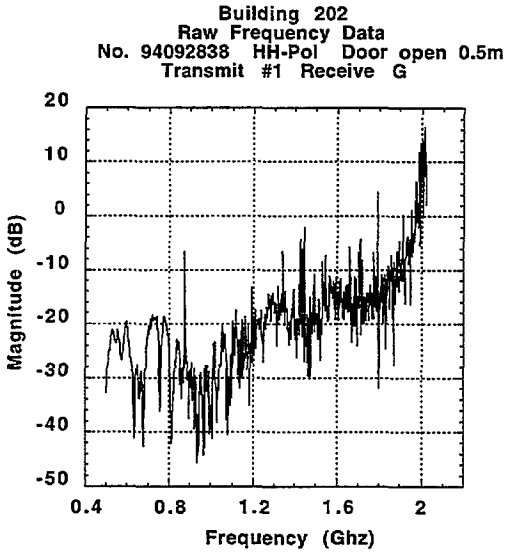

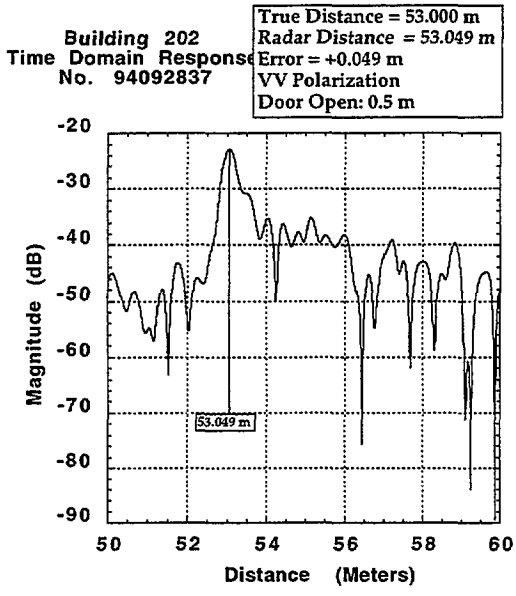

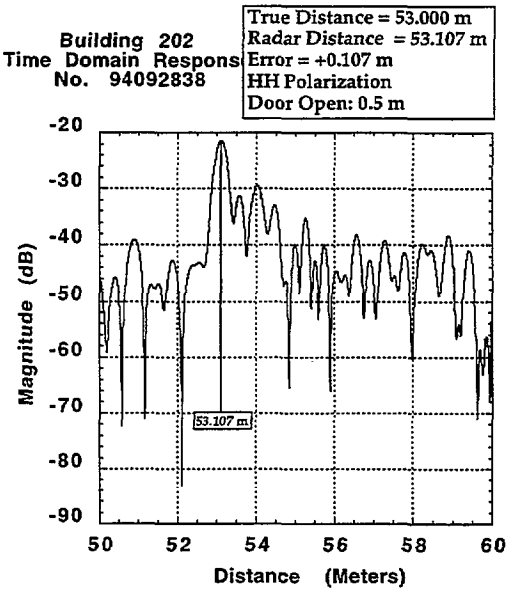

Fig 19a: Transmission at Station #1 to Receive Station G. Vertical polarization.

Fig 19b: Transmission at Station #1 to Receive Station G. Horizontal Polarization.

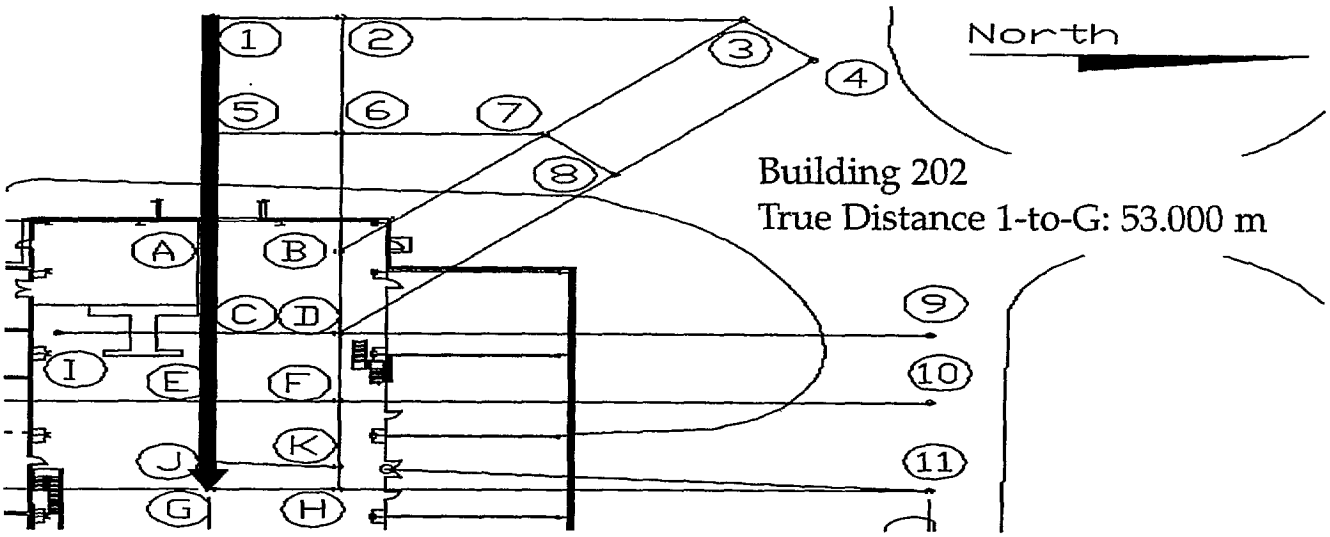

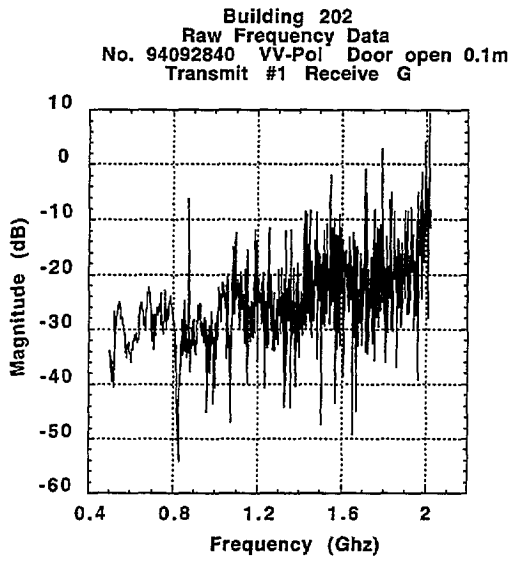

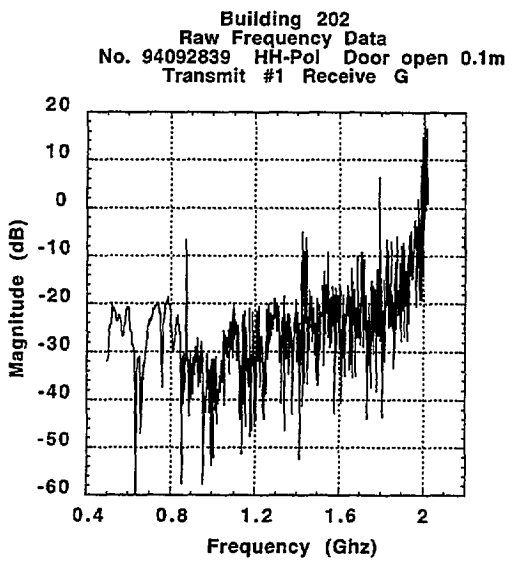

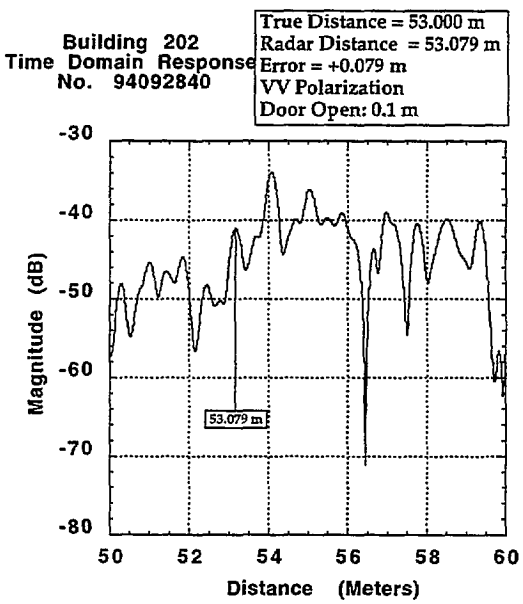

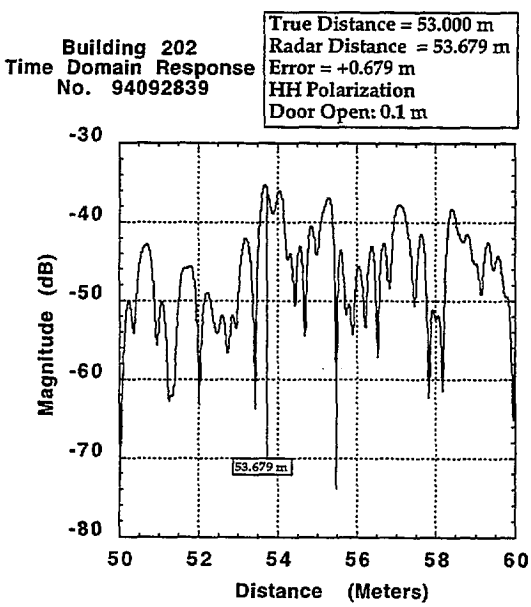

Fig 20a: Transmission at Station #1 to Receive Station G. Vertical Polarization.

Fig 20b: Transmission at Station #1 to Receive Station G. Horizontal Polarization.

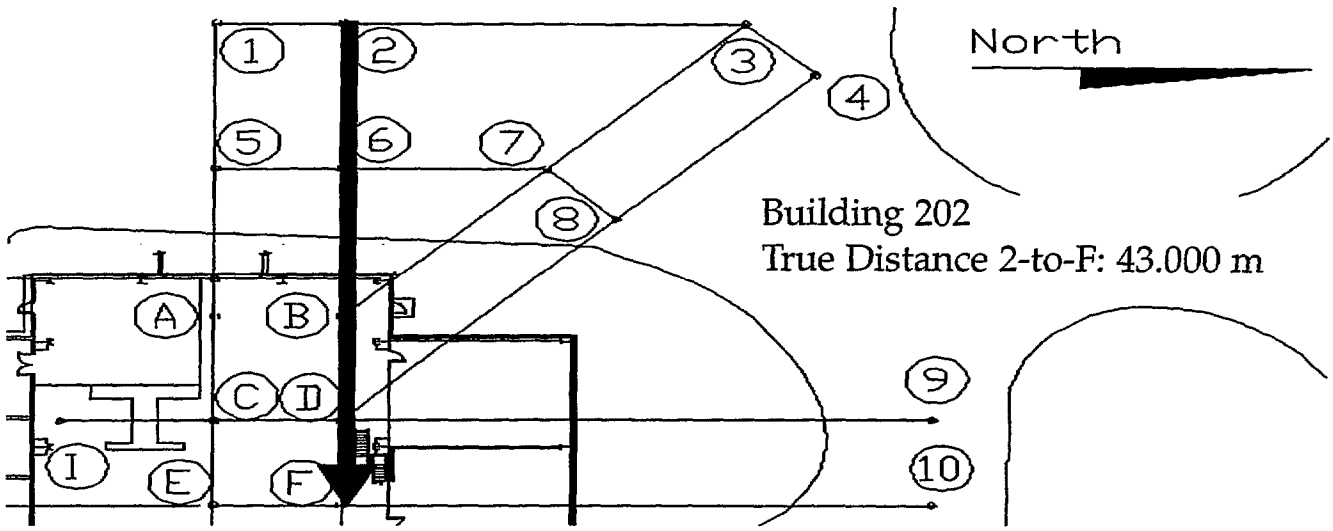

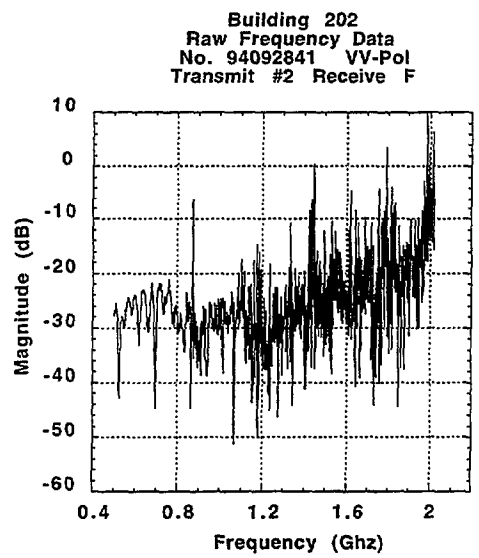

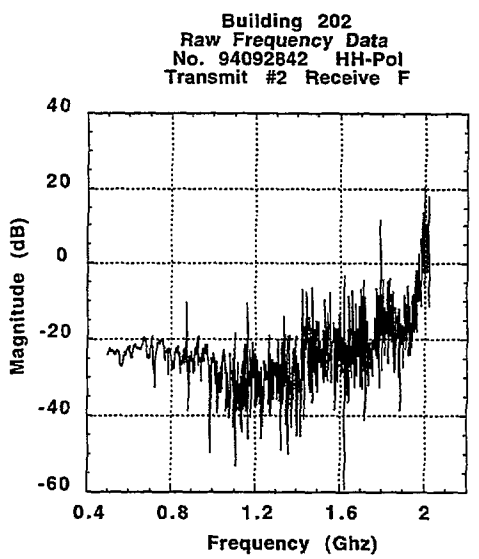

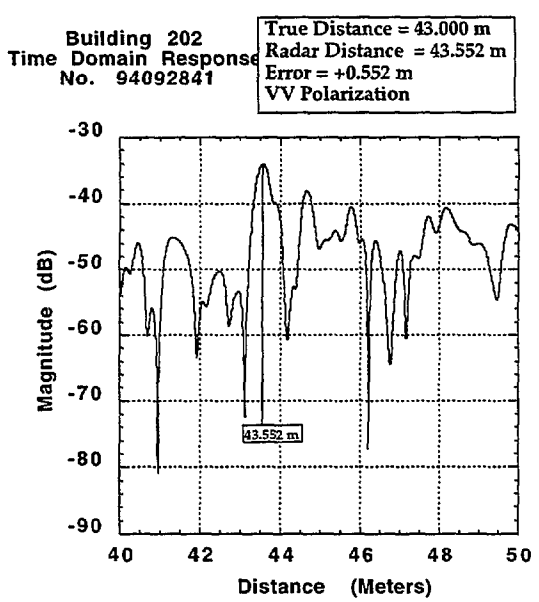

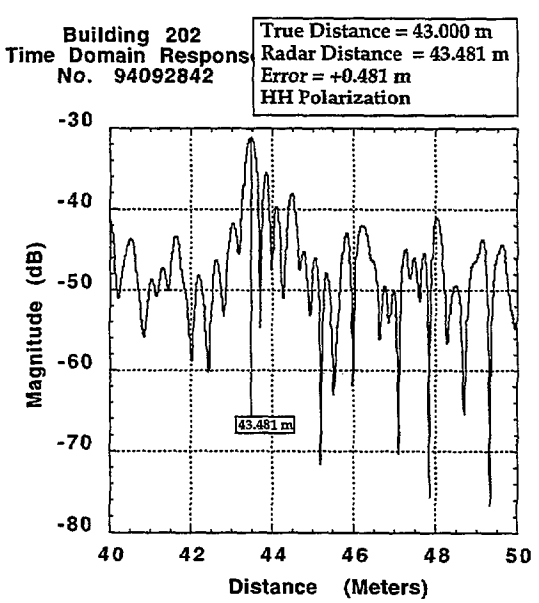

Fig 21a: Transmission at Station #2 to Receive Station F. Vertical Polarization.

Fig 21b: Transmission at Station #2 to Receive Station F. Horizontal Polarization.

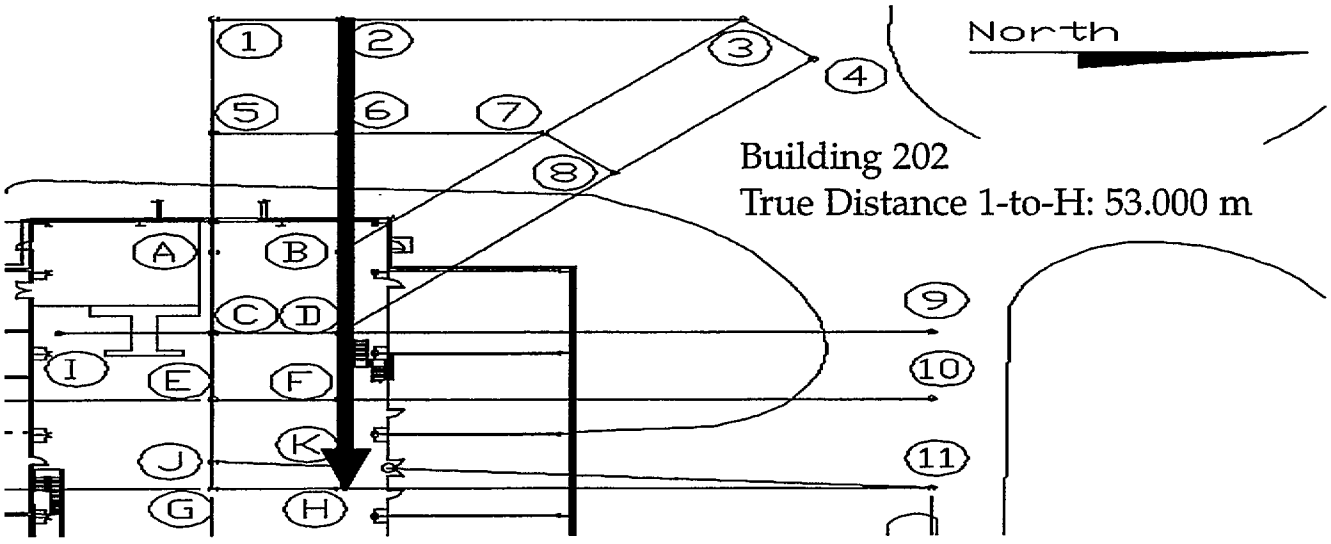

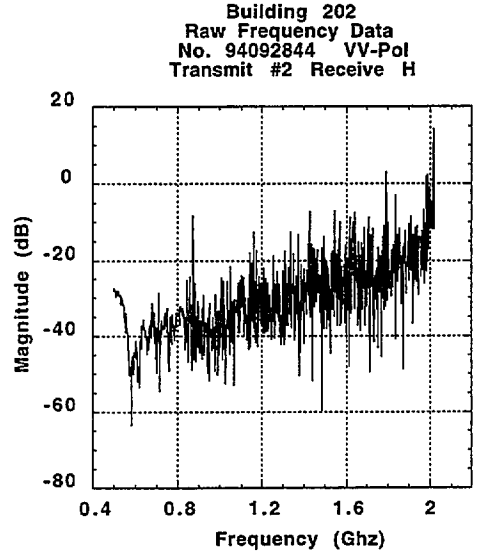

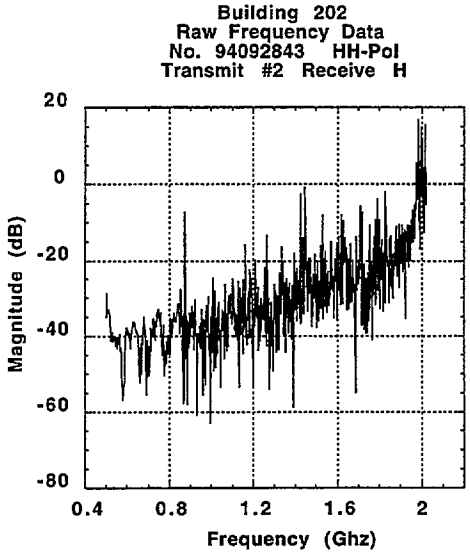

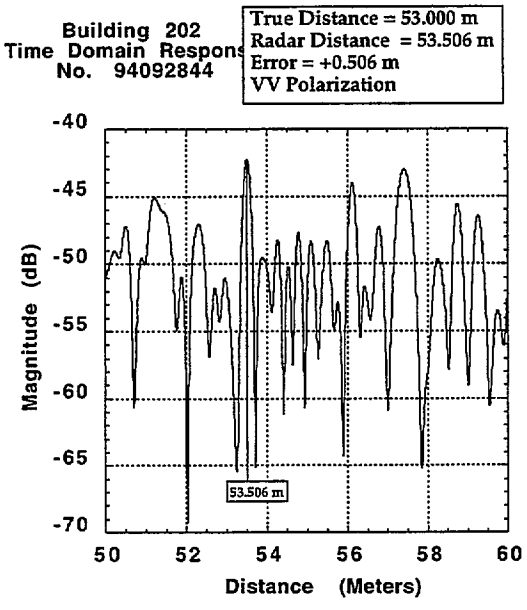

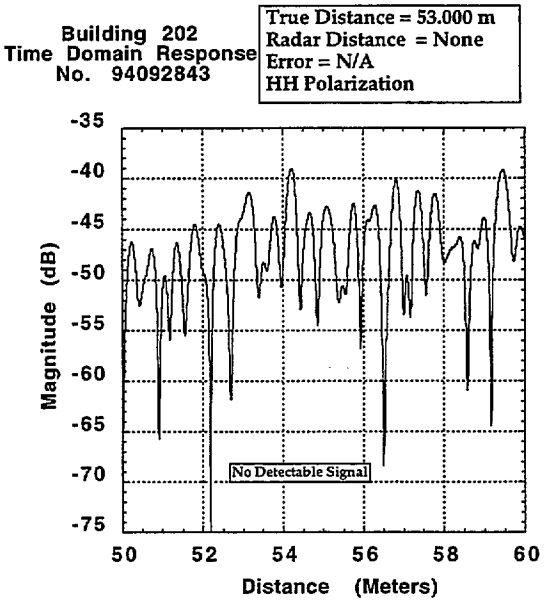

Fig 22a: Transmission at Station #2 toReceive Station H. Vertical Polarization.

Fig 22b: Transmission at Station #2 to Receive Station H. Horizontal Polarization.

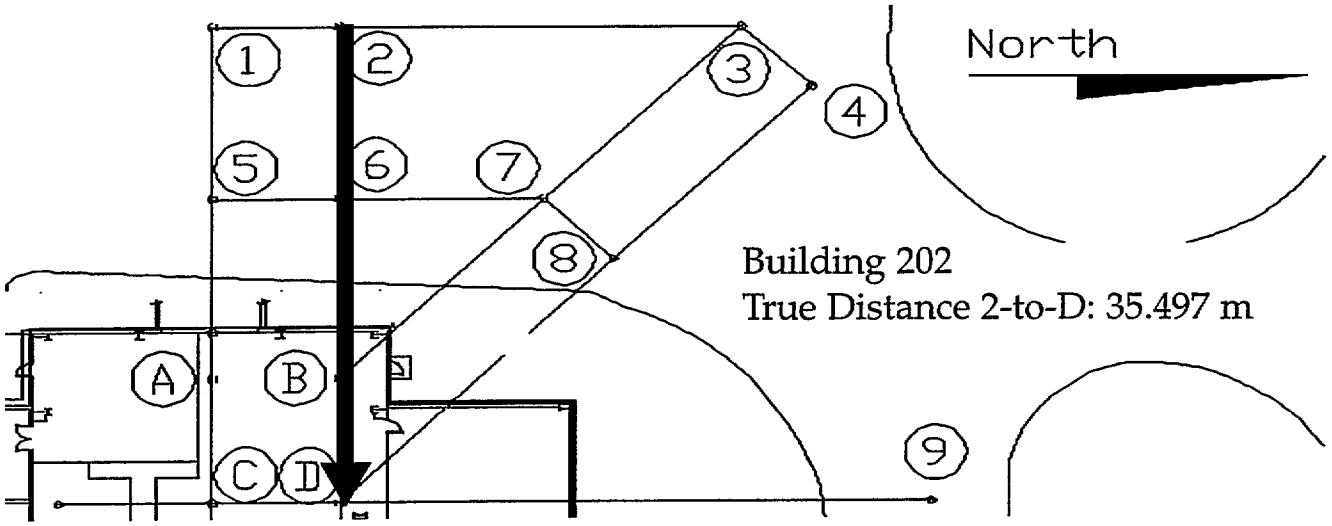

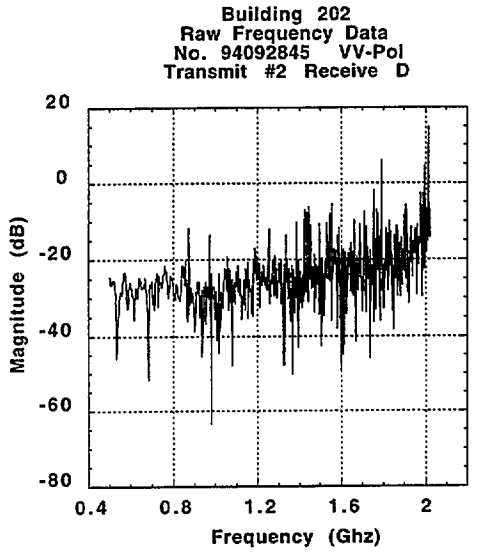

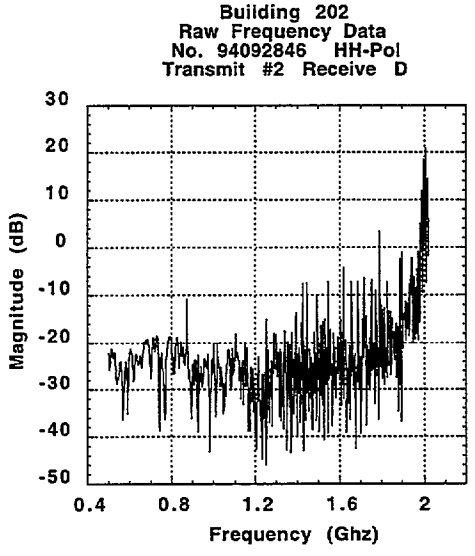

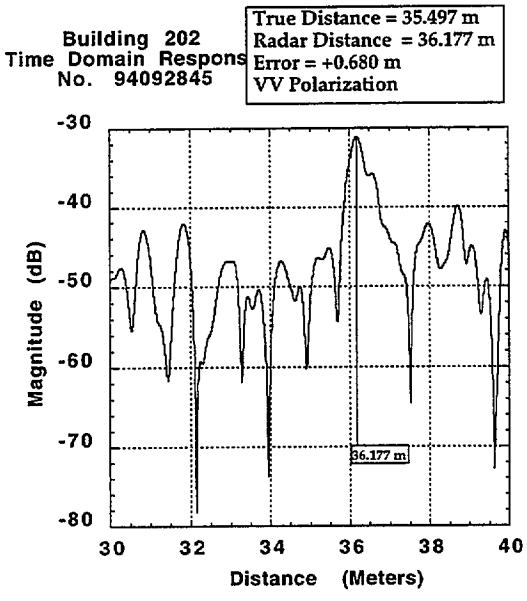

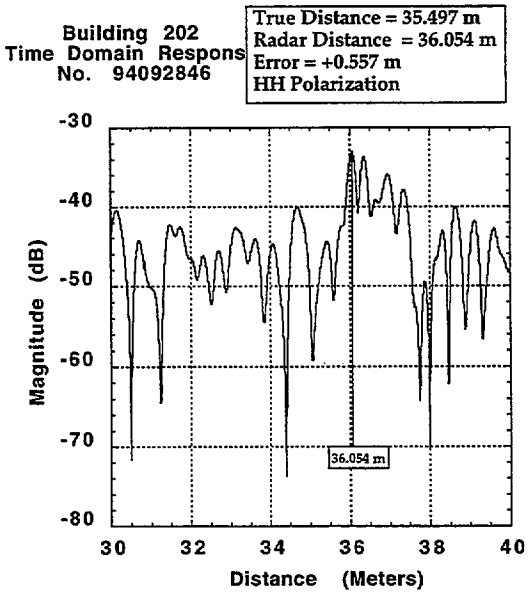

Fig 23a: Transmission at Station #2 toReceive Station D. Vertical Polarization.

Fig 23b: Transmission at Station #2 to Receive Station D. Horizontal Polarization.

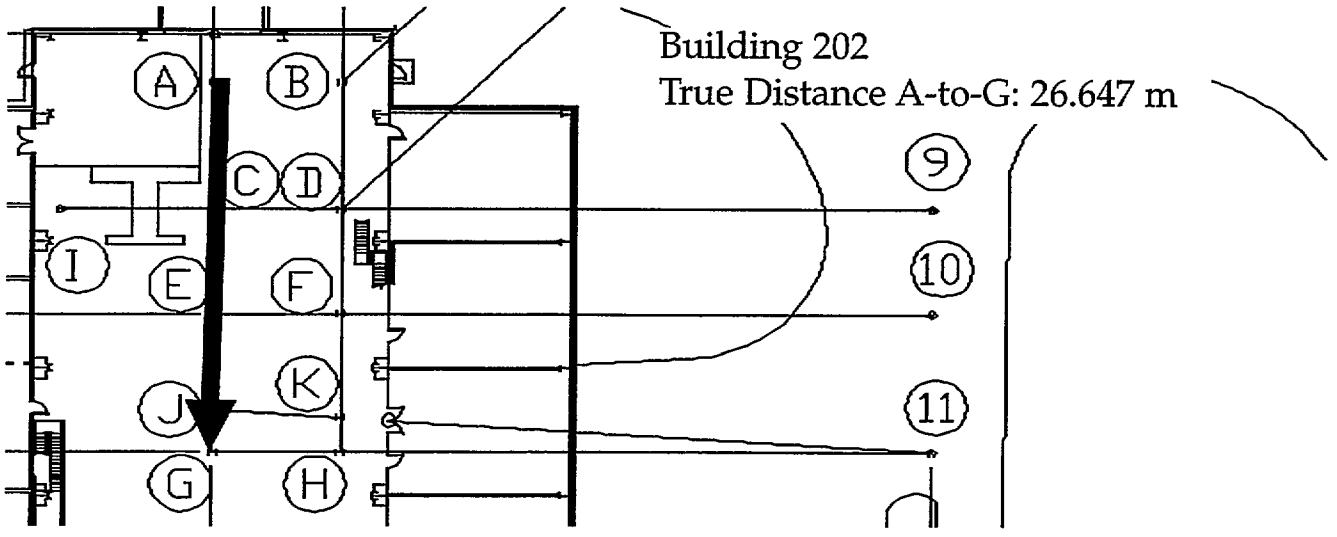

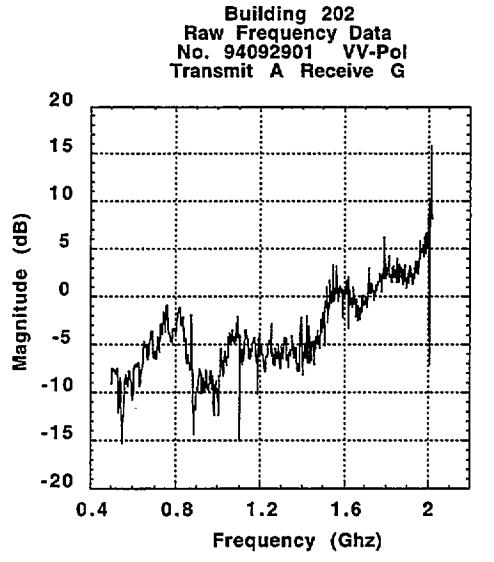

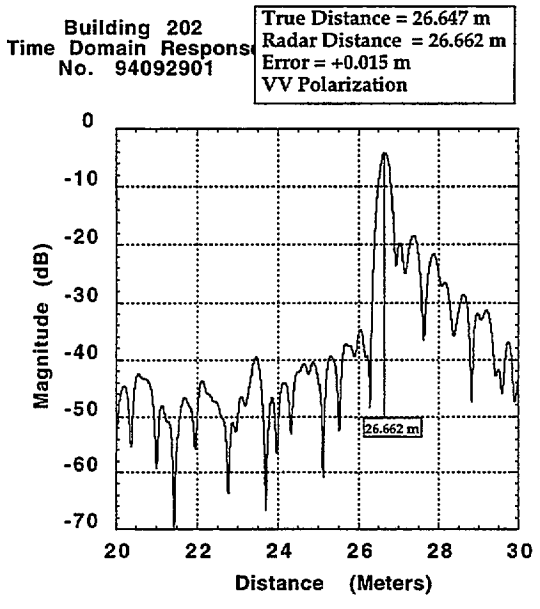

Fig 24a: Transmission at Station A to Receive Station G. Vertical Polarization.

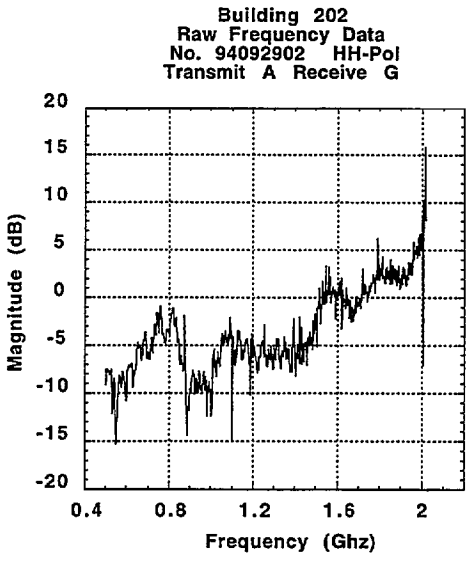

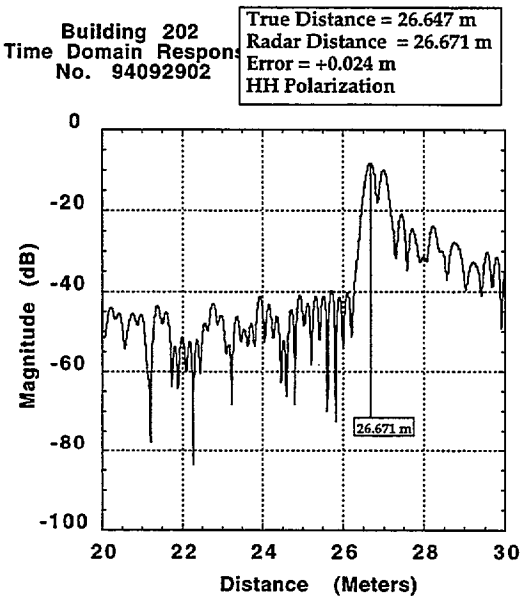

Fig 24b: Transmission at Station A to Receive Station G. Horizontal Polarization.

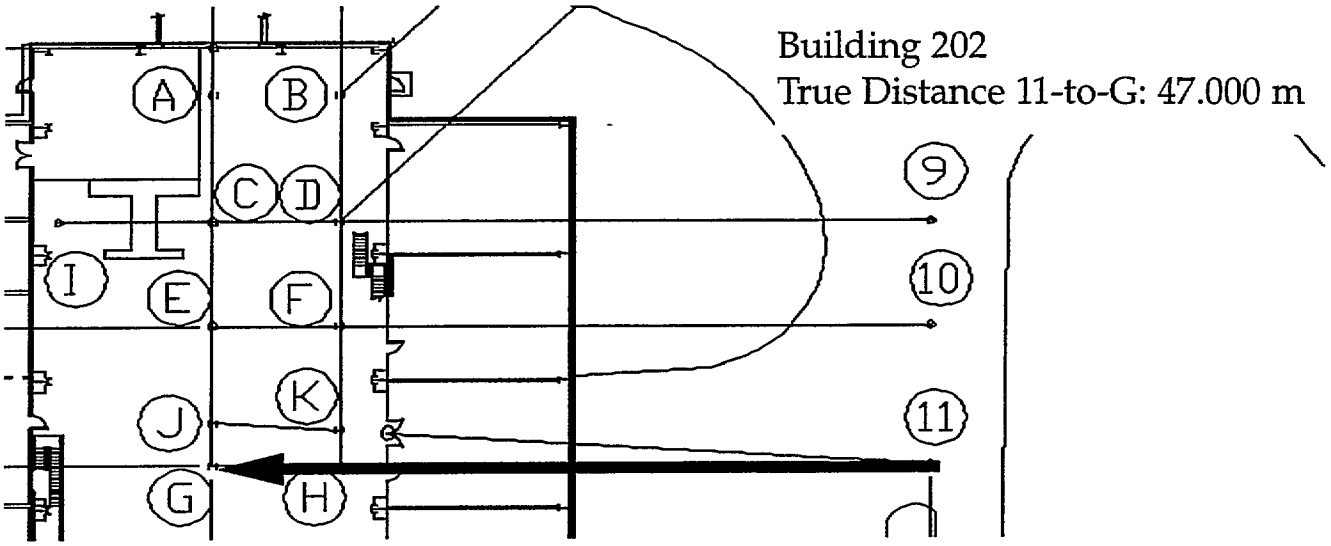

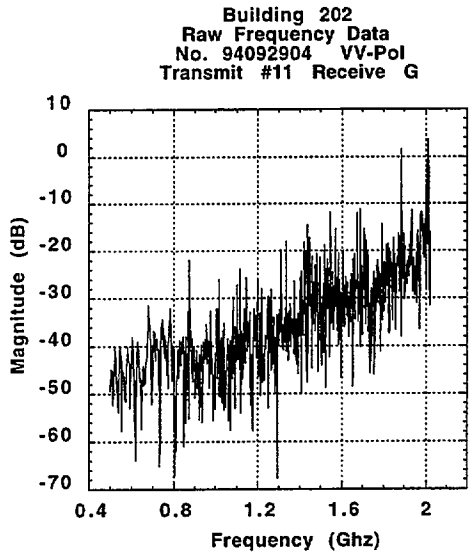

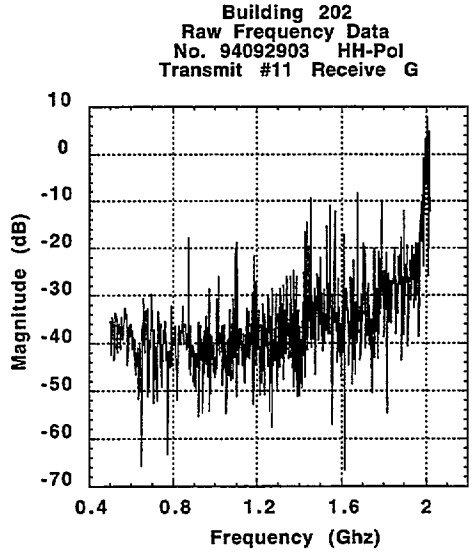

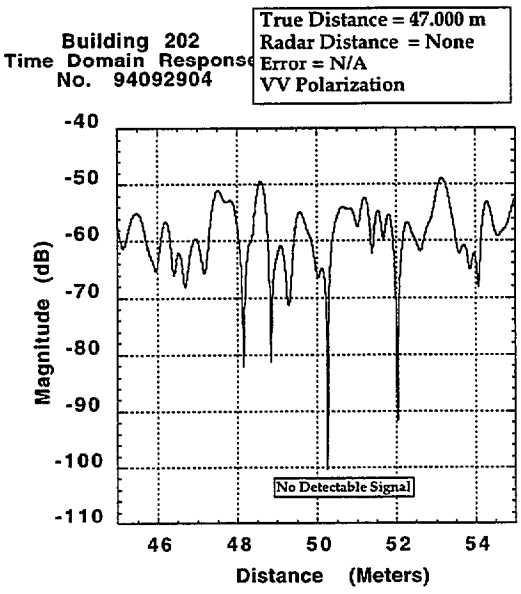

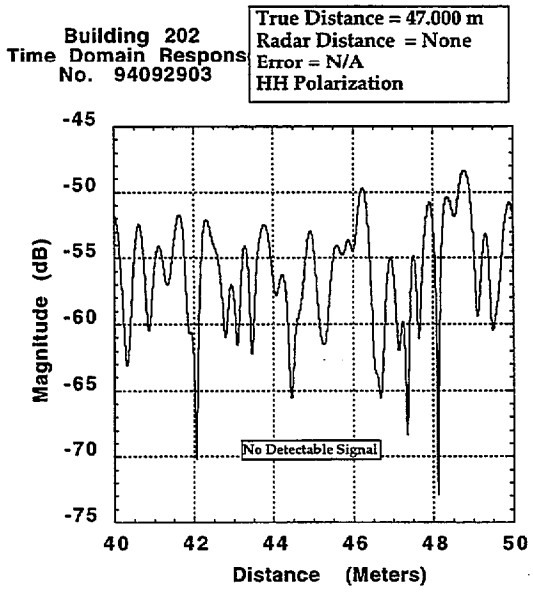

Fig 25a: Transmission at Station #11 to Receive Station G. Vertical Polarization.

Fig 25b: Transmission at Station #11 to Receive Station G. Horizontal Polarization.

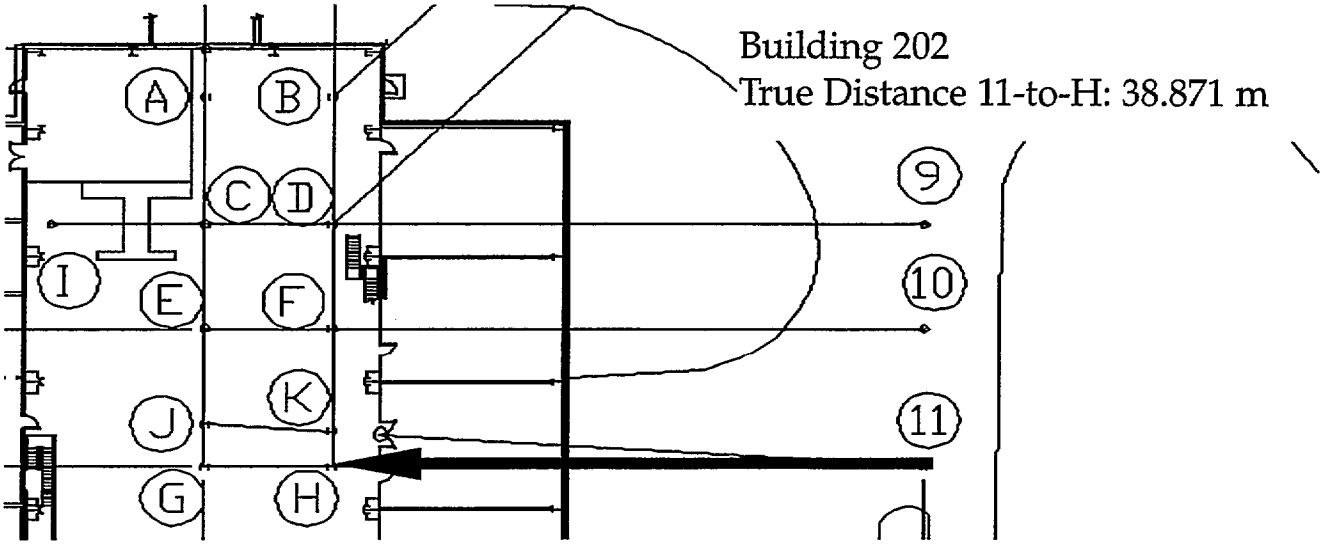

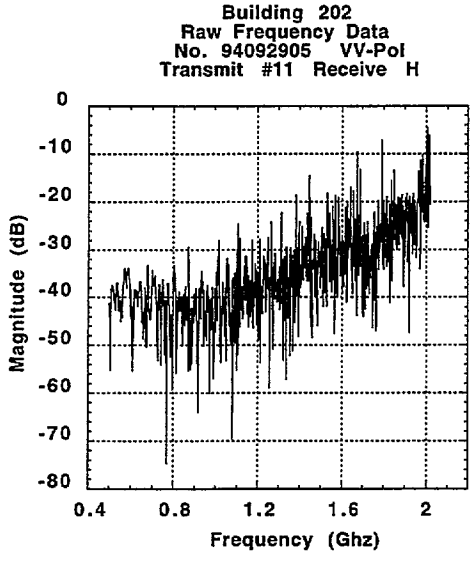

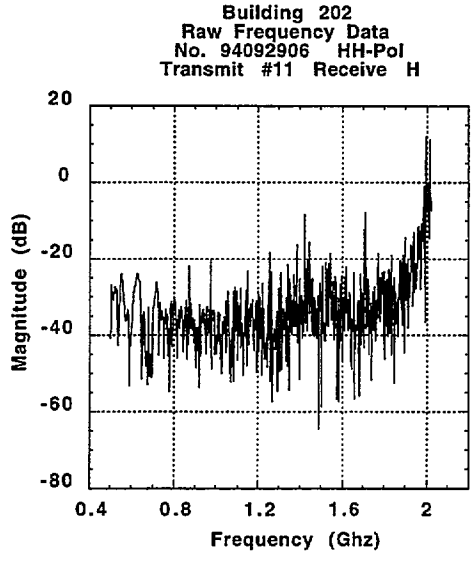

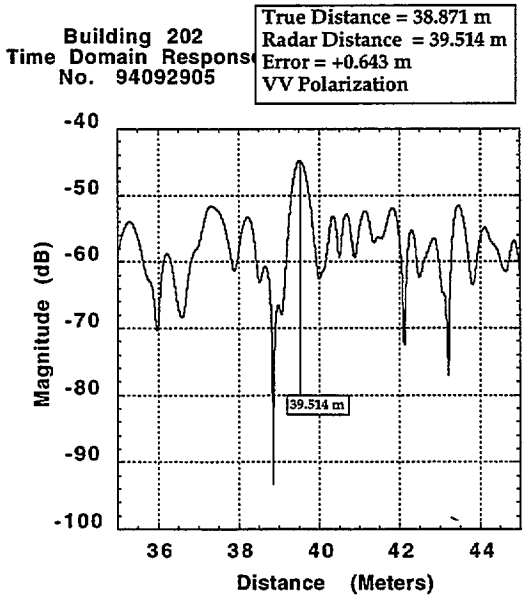

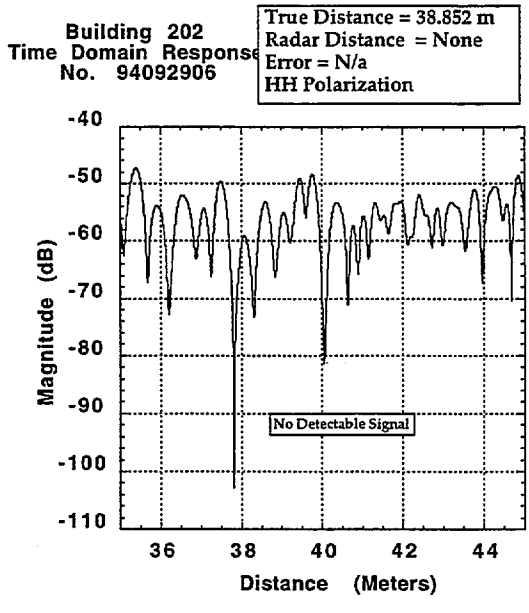

Fig 26a: Transmission at Station #11 to Receive Station H. Vertical Polarization.

Fig 26b: Transmission at Station #11 toReceive Station H. Horizontal Polarization.

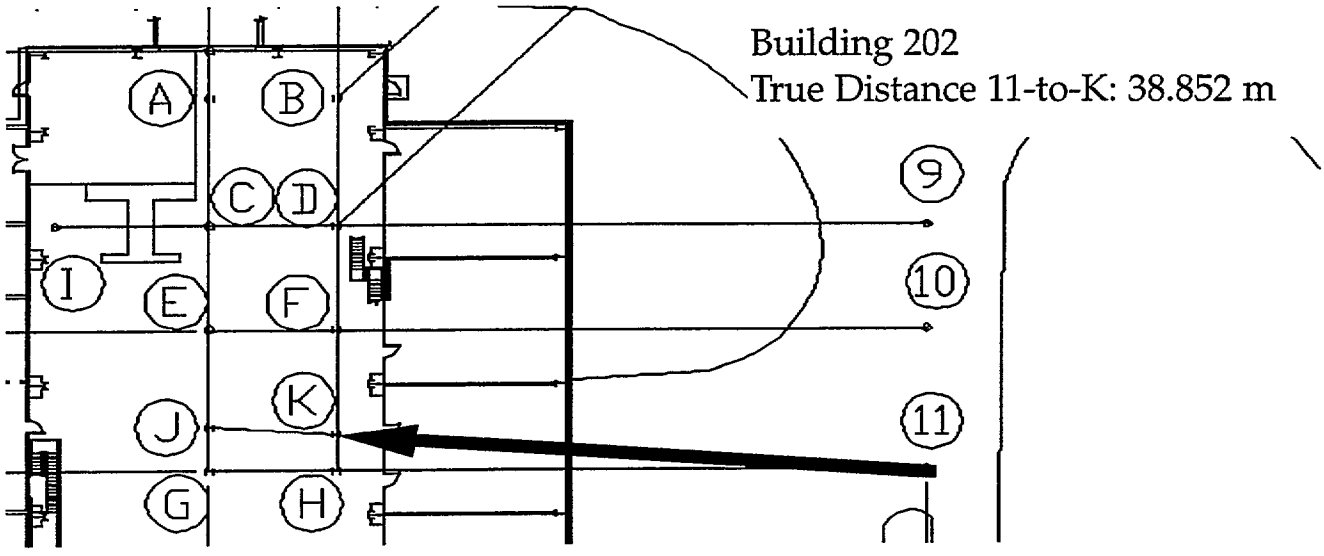

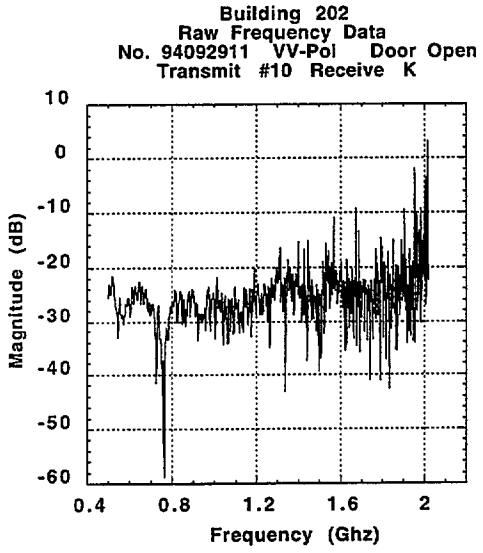

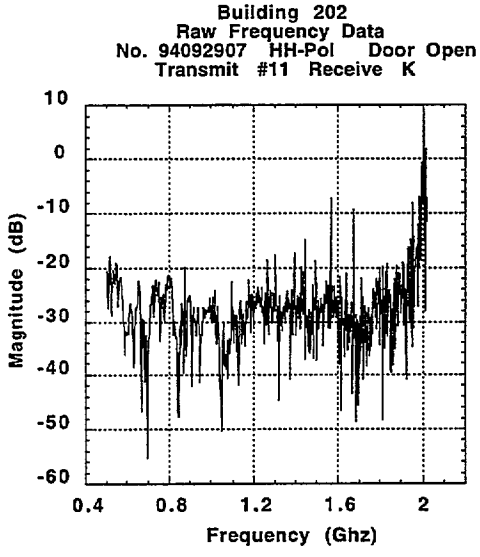

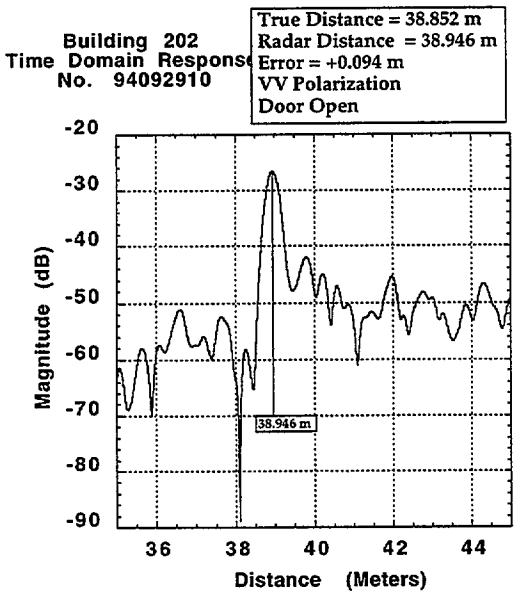

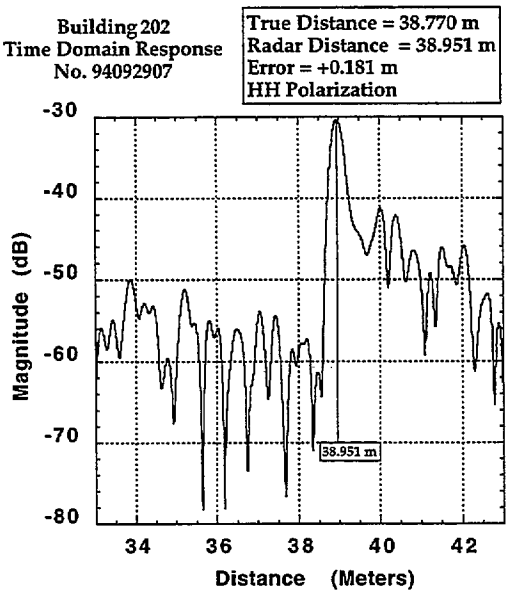

Fig 27a: Transmission at Station #11 to Receive Station K. Vertical Polarization.

Fig 26b: Transmission at Station #11 to Receive Station K. Horizontal Polarization.

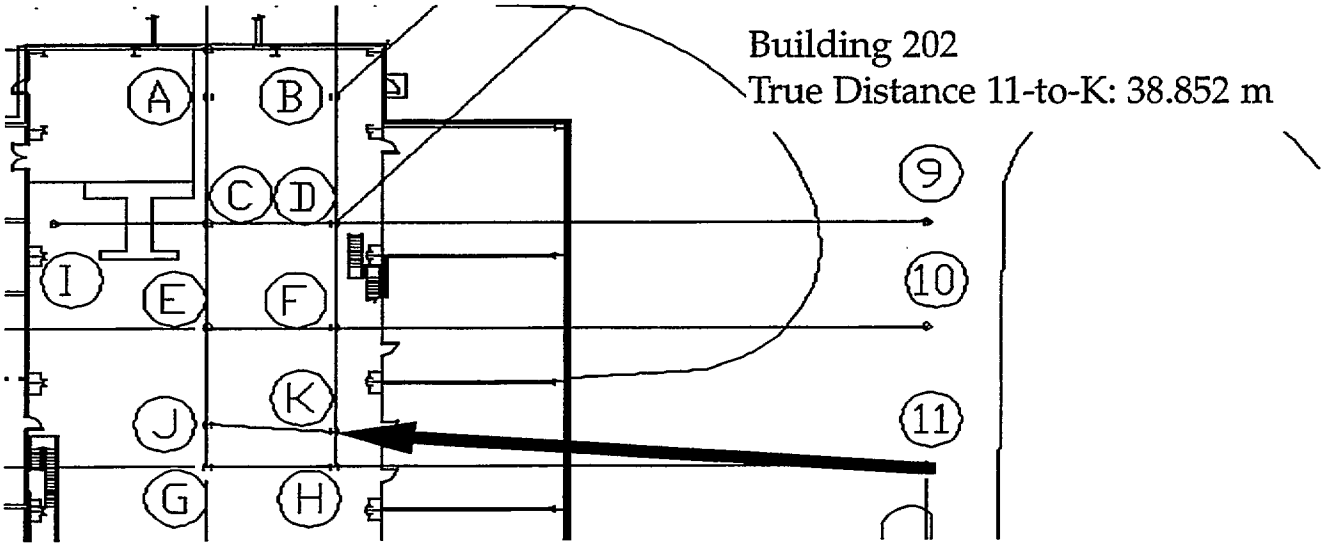

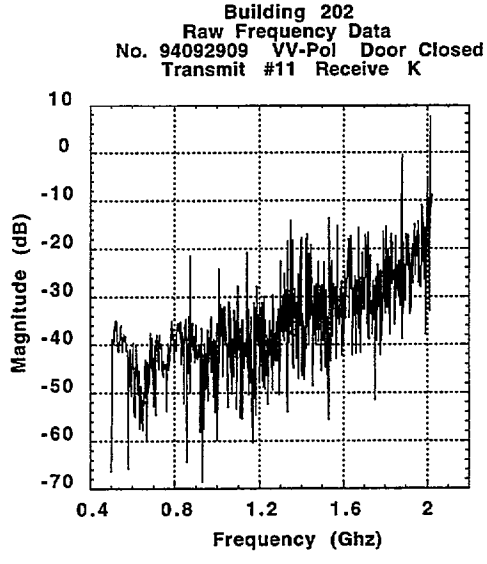

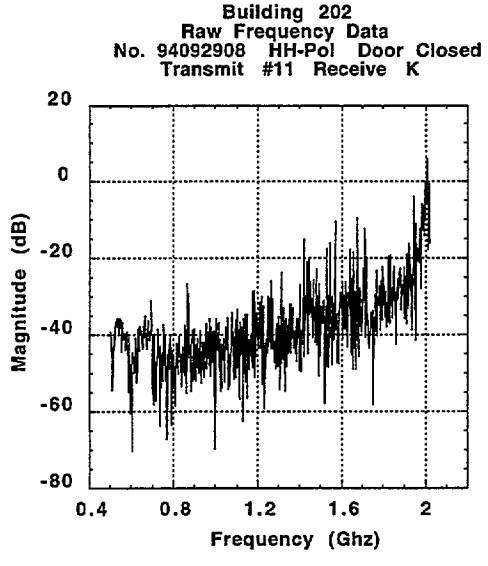

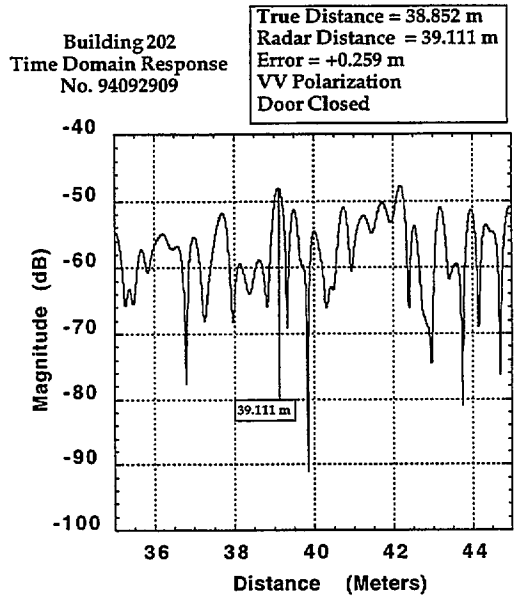

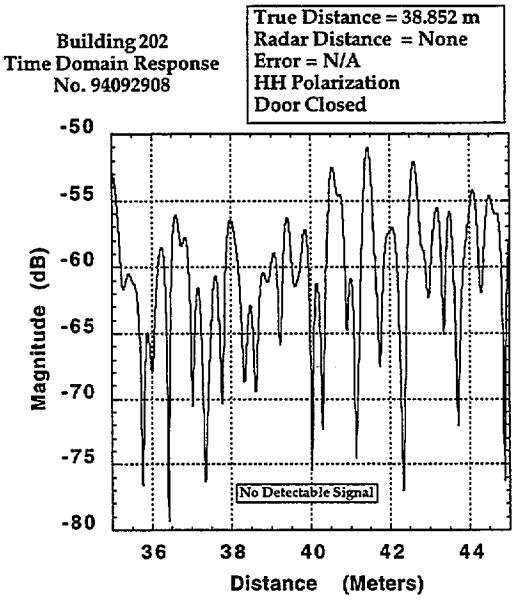

Fig 28a: Transmission at Station #11 to Receive Station K. Vertical Polarization.

Fig 28b: Transmission at Station #11 to Receive Station K. Horizontal Polarization.

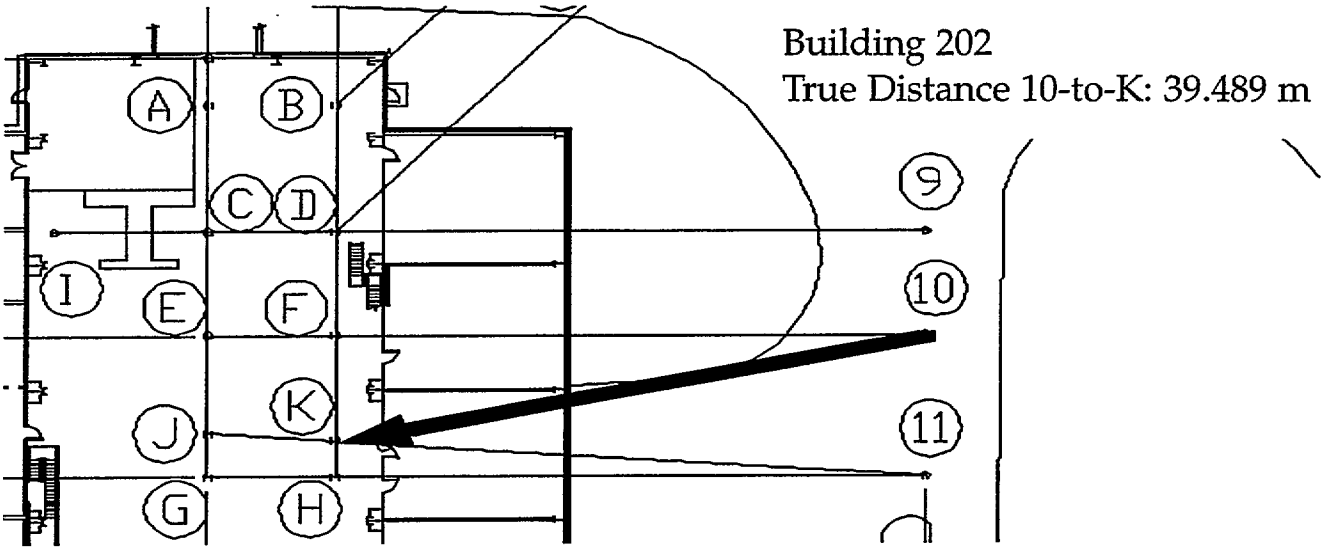

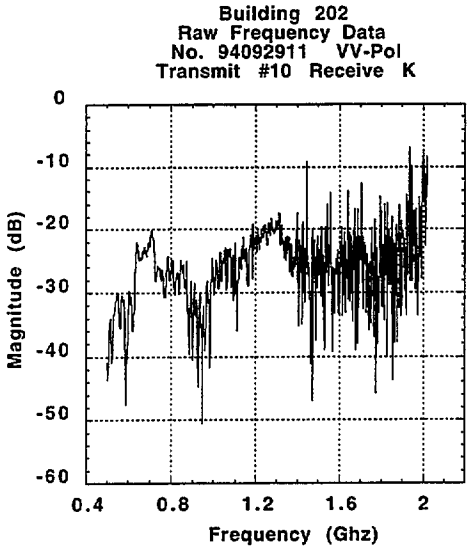

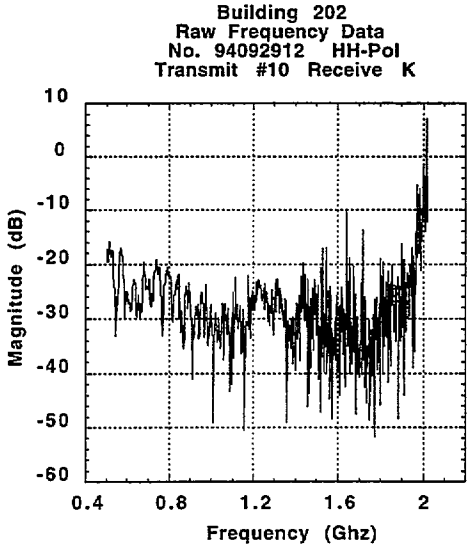

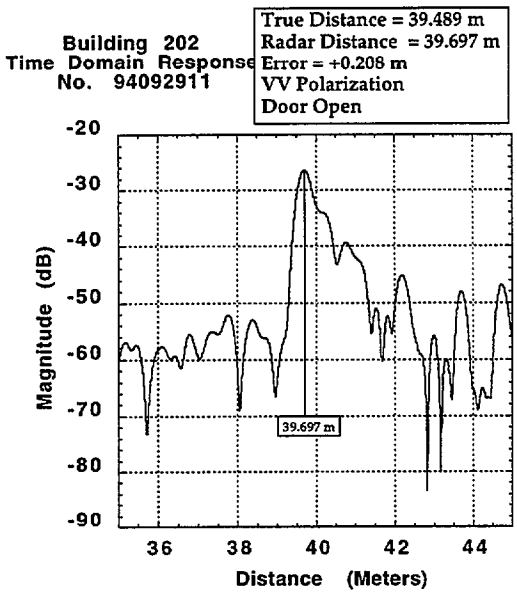

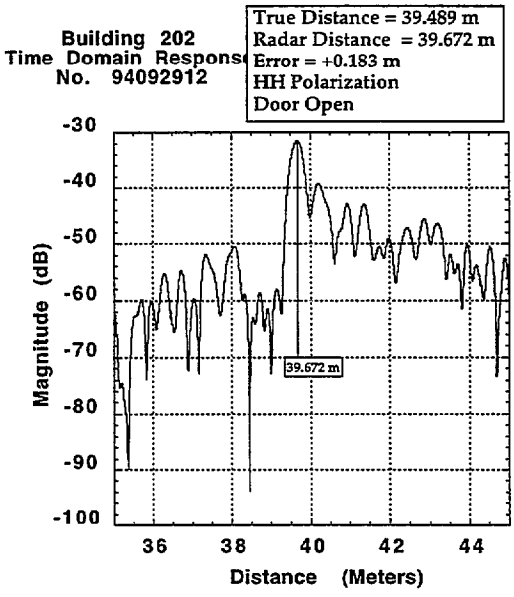

Fig 29a: Transmission at Station #10 to Receive Station K. Vertical Polarization.

Fig 29b: Transmission at Station #10 to Receive Station K. Horizontal Polarization.

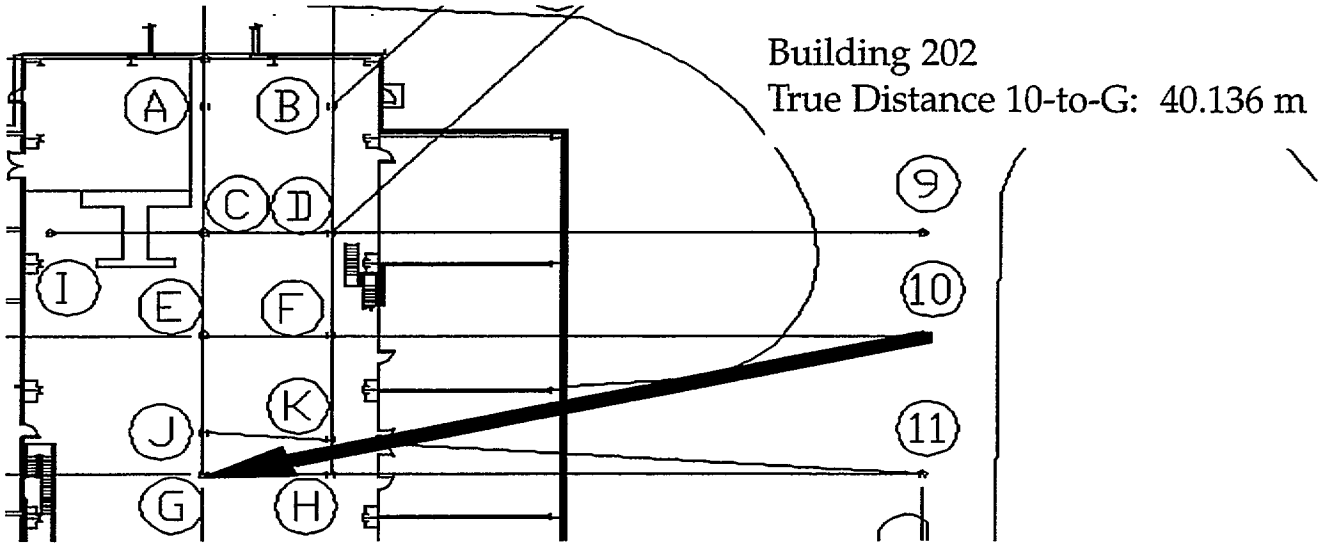

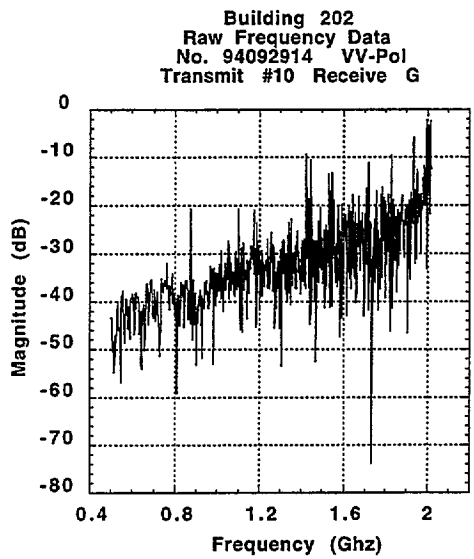

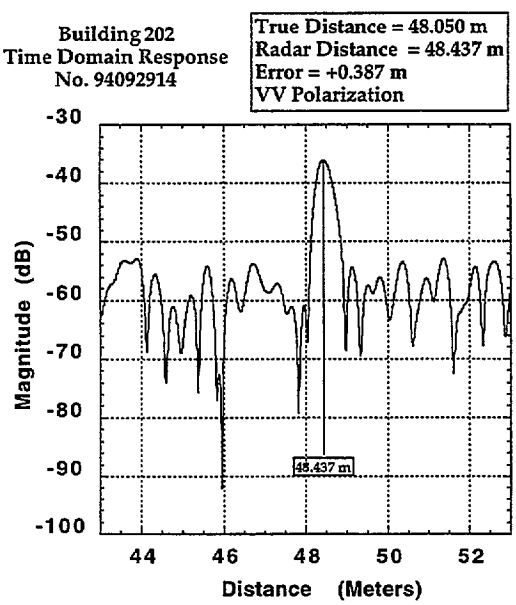

Fig 30a: Transmission at Station #10 to Receive Station G. Vertical Polarization.

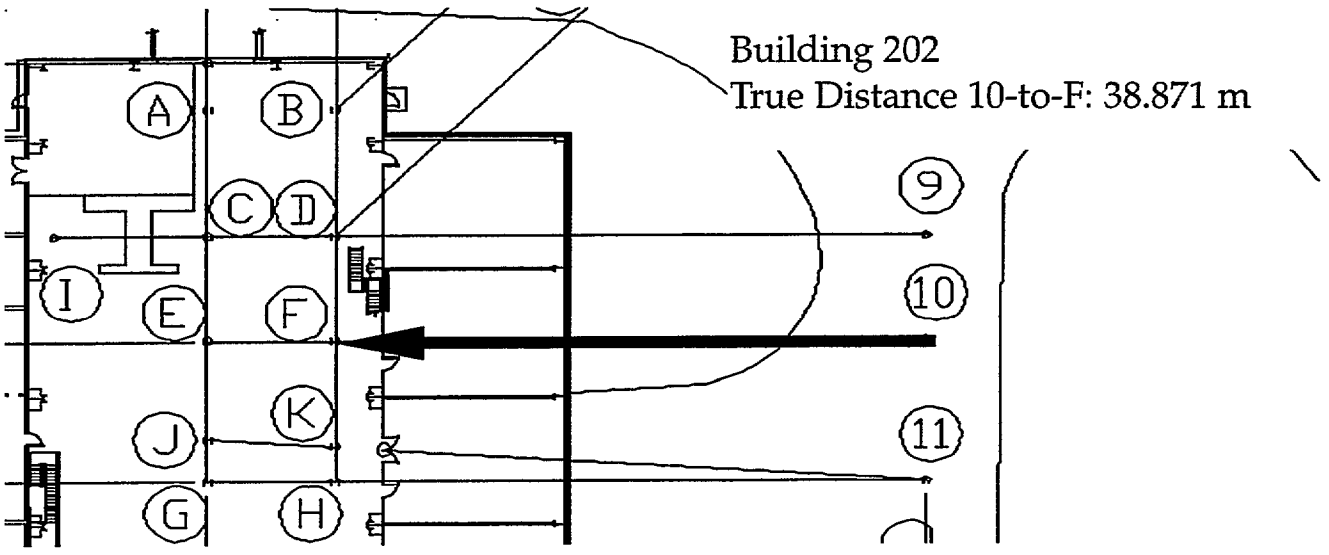

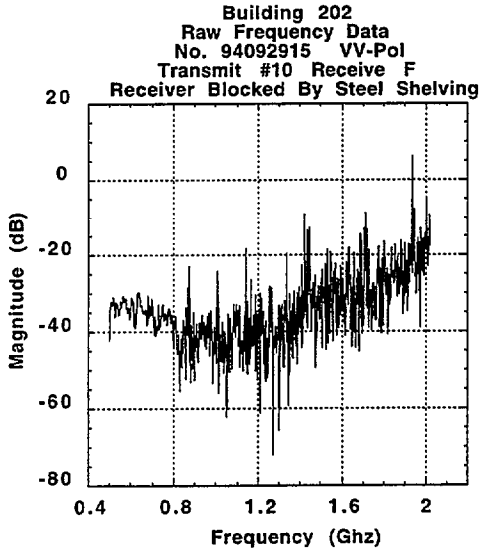

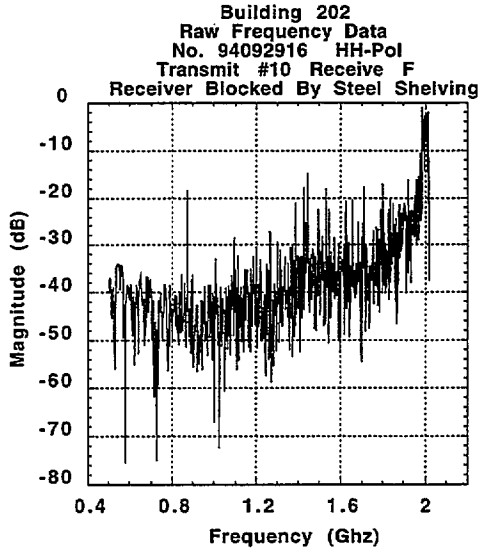

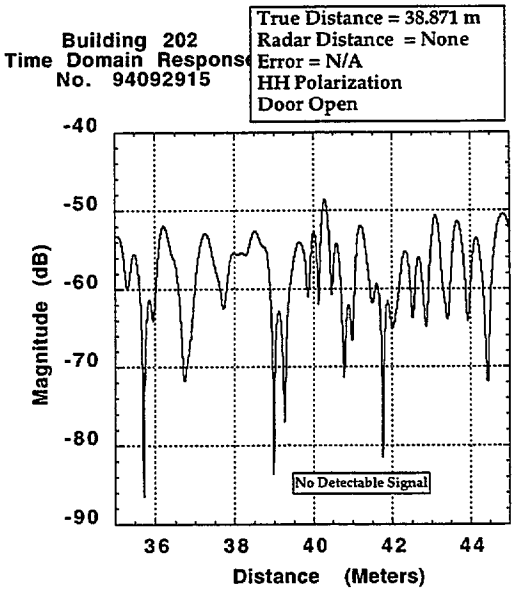

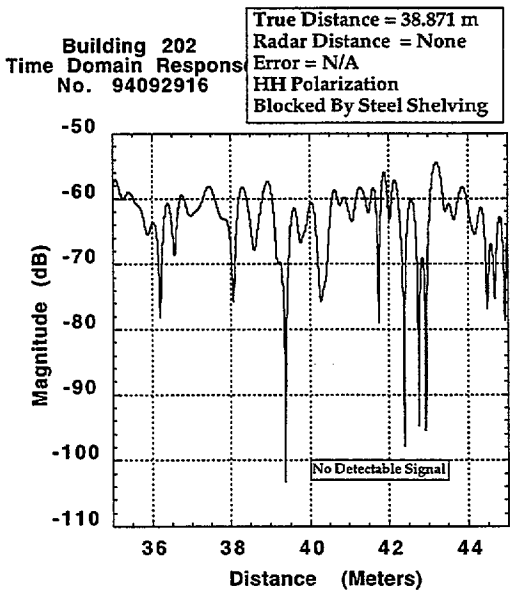

Fig 31a: Transmission at Station #10 to Receive Station F. Vertical Polarization.

Fig 32b: Transmission at Station #10 to Receive Station F. Horizontal Polarization.

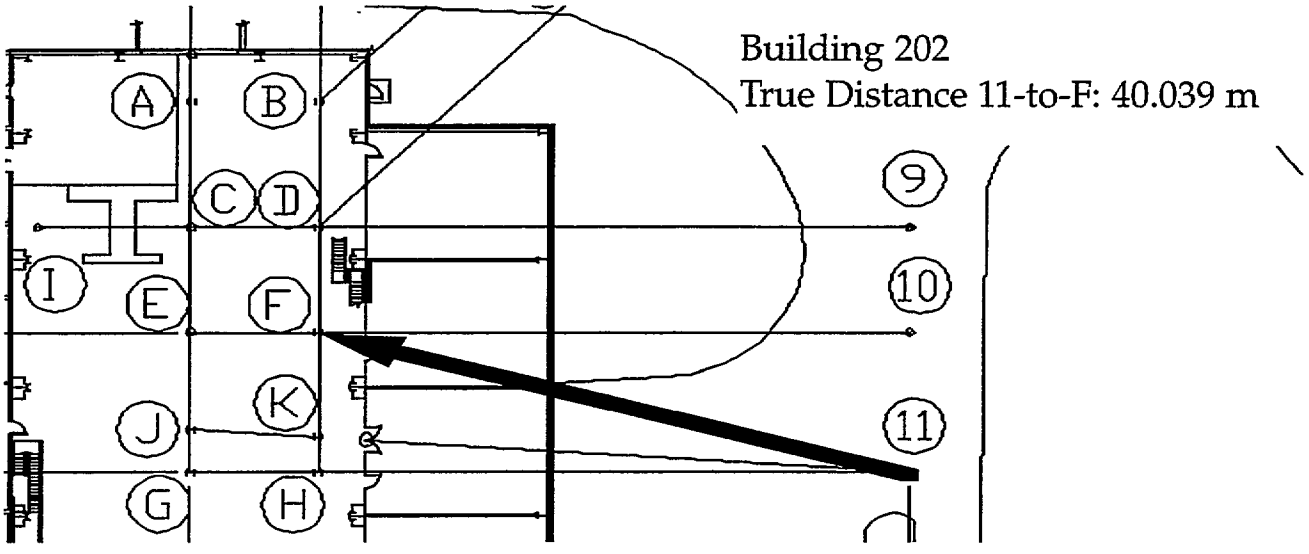

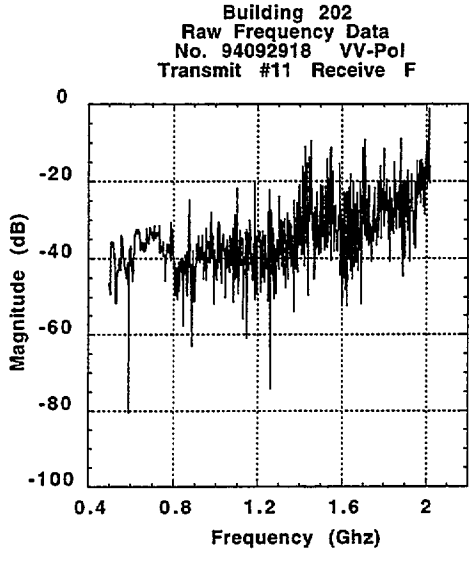

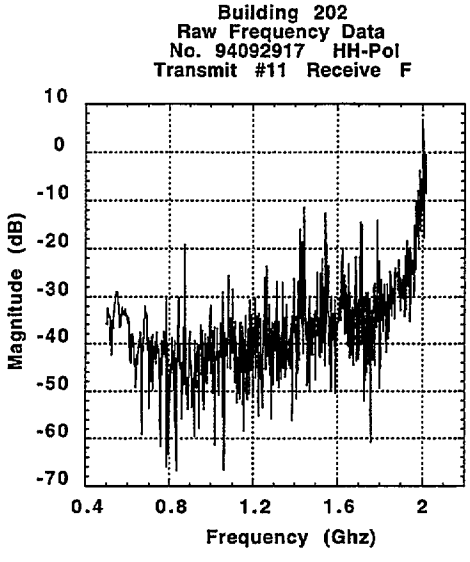

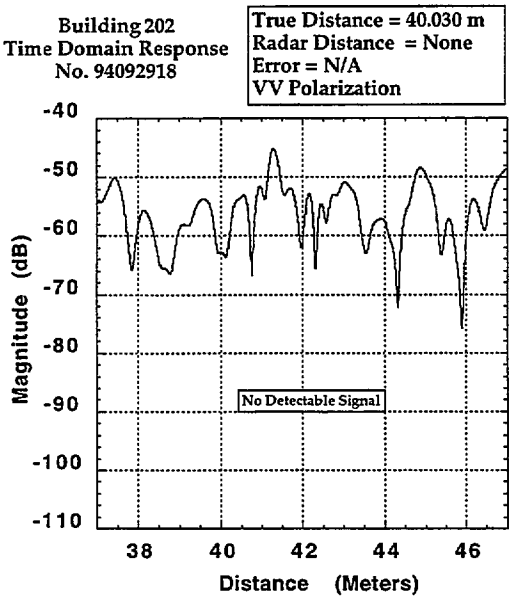

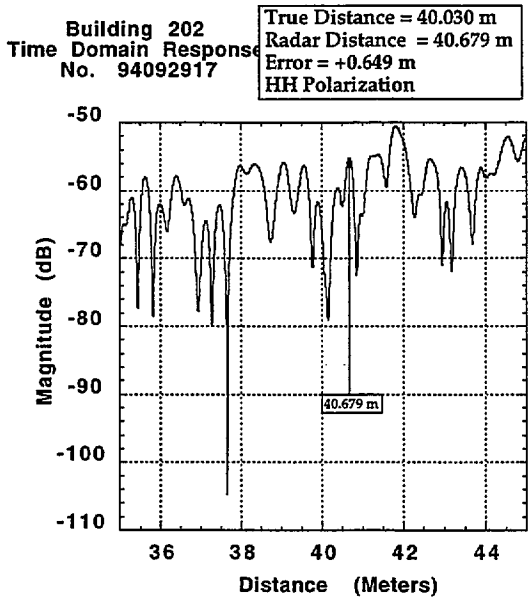

Fig 32a: Transmission at Station #11 to Receive Station F. Vertical Polarization.

Fig 32b: Transmission at Station #11 to receive Station F. Horizontal Polarization.

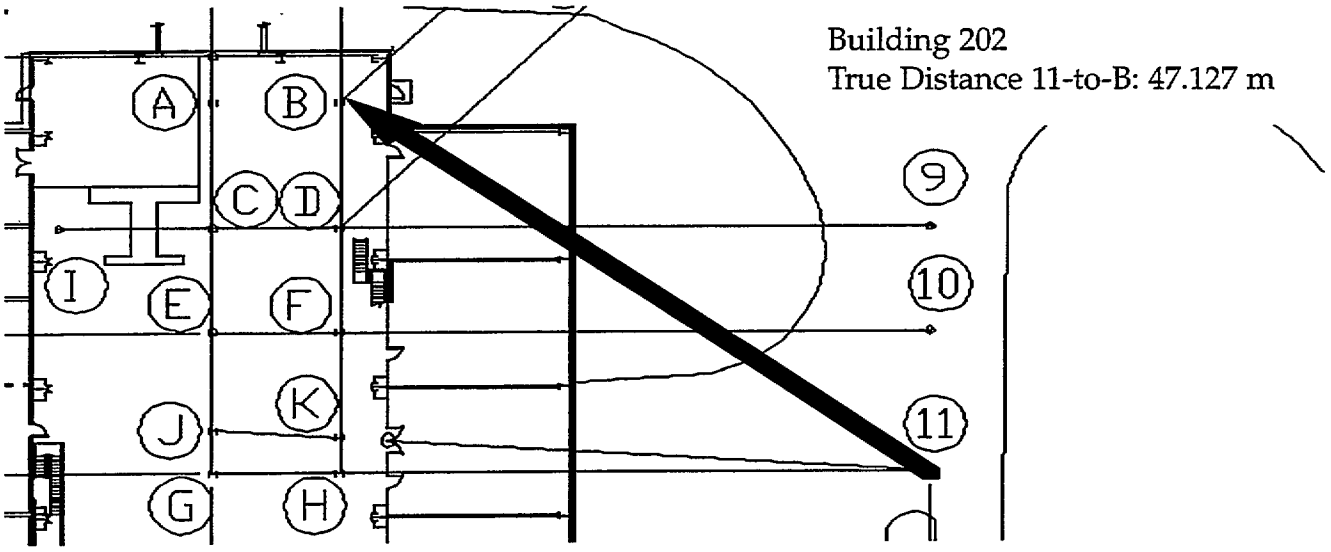

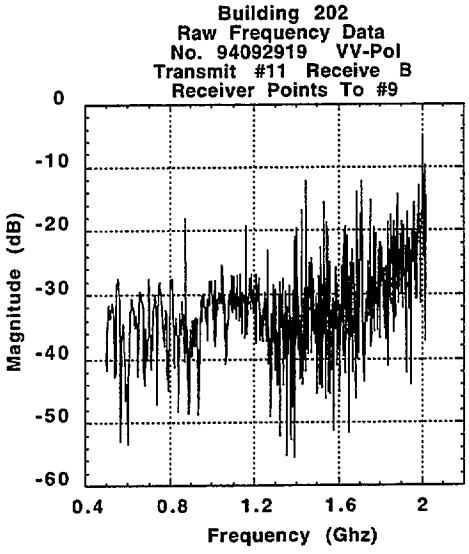

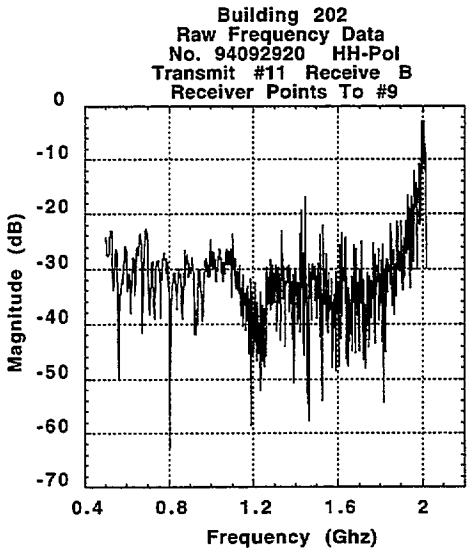

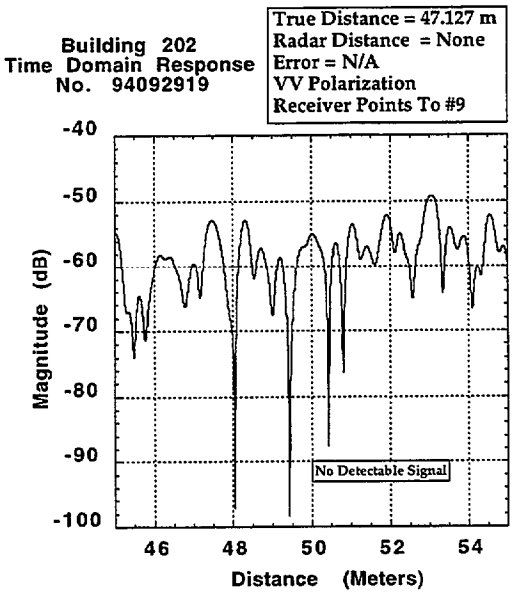

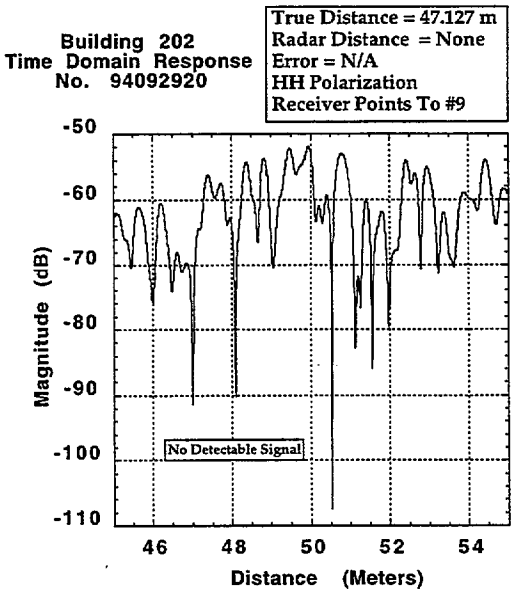

Fig 33a: Transmission at Station #11 to Receive Station B. Vertical Polarization.

Fig 32b: Transmission at Station #11 to Receive Station B. Horizontal Polarization.

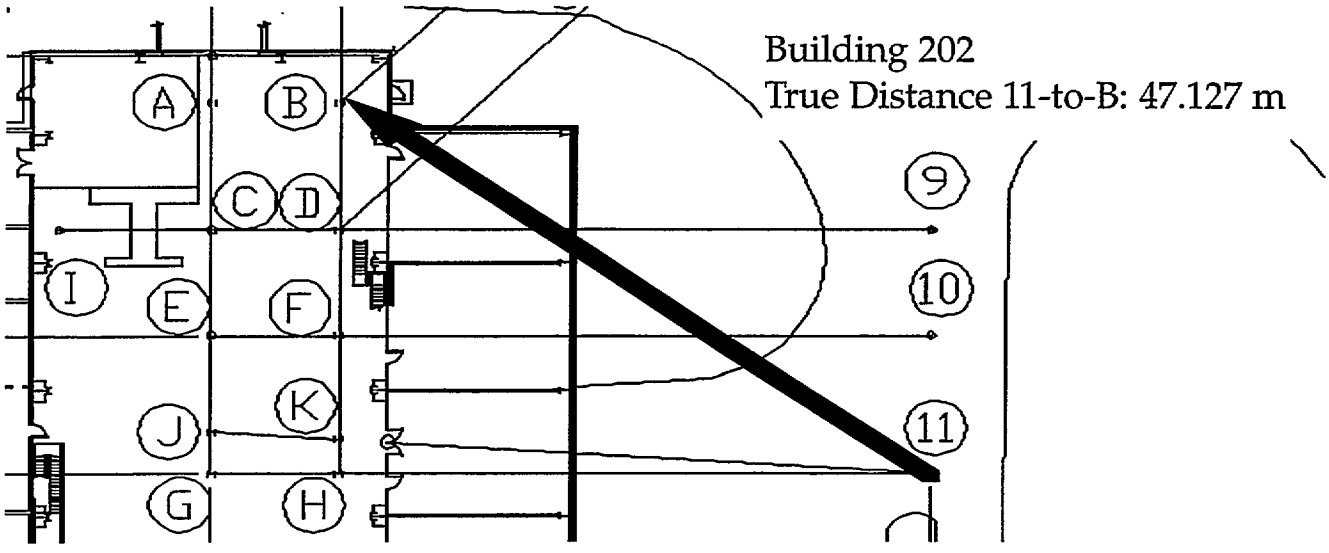

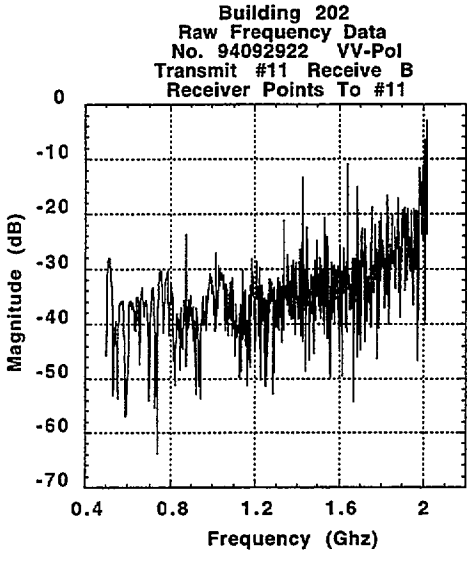

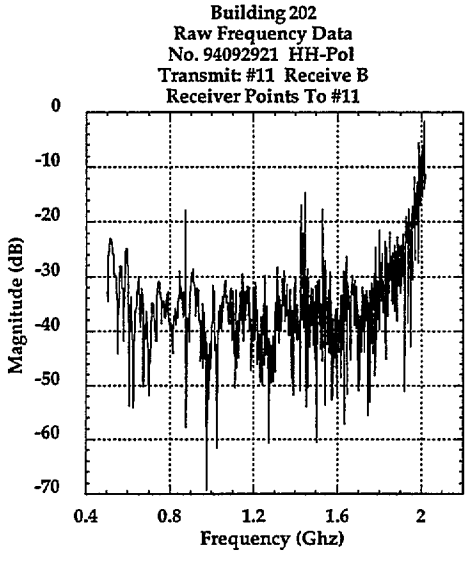

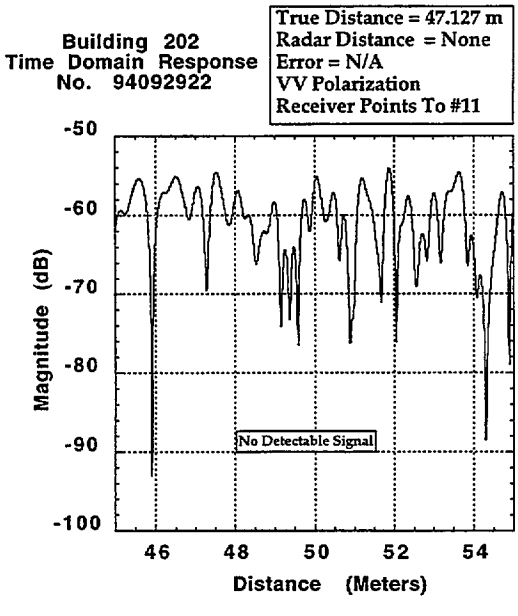

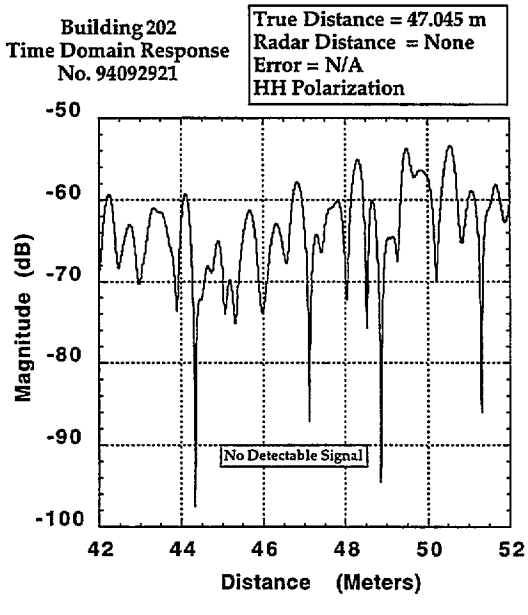

Fig 34a: Transmission at Station #11 to Receive Station B. Vertical Polarization.

Fig 34b: Transmission at Station #11 to Receive Station B. Horizontal Polarization.

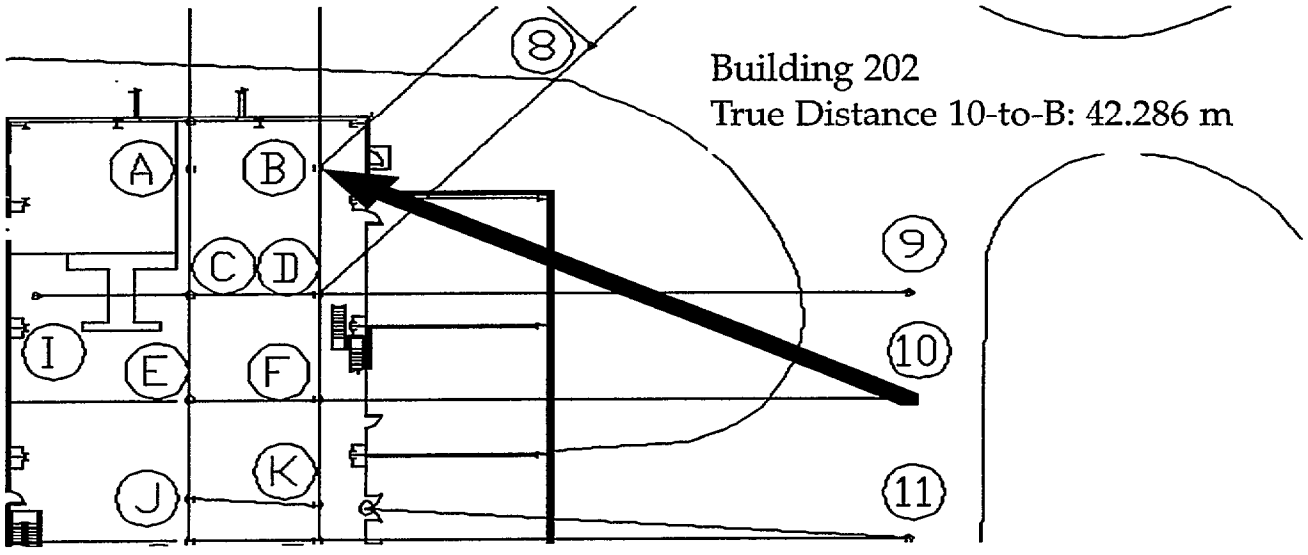

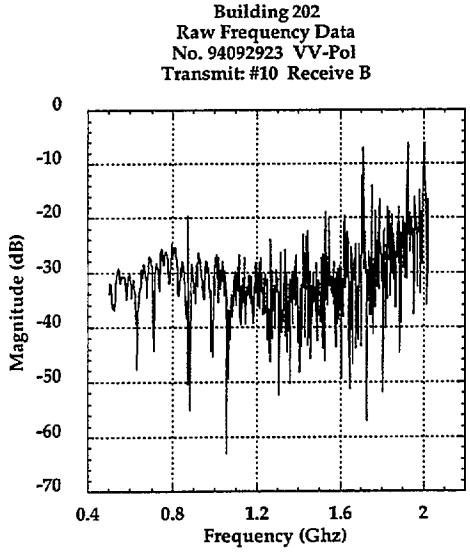

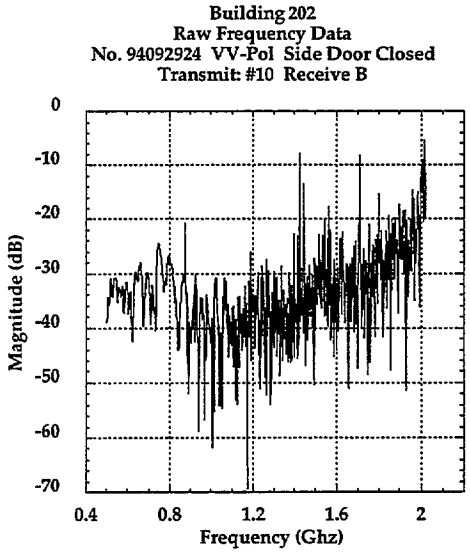

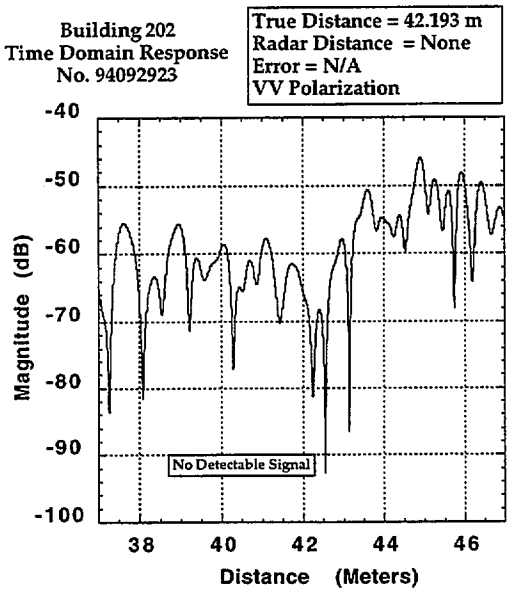

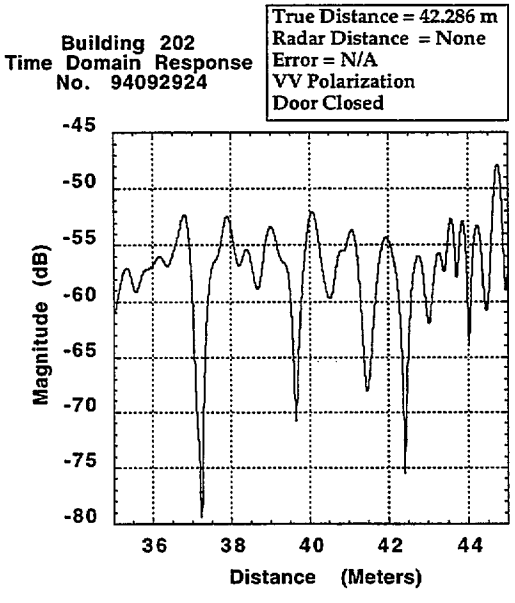

Fig 35a: Transmission at Station #10 to Receive Station B. Vertical Polarization.

Fig 35b: Transmission at Staion #10 to Receive Station B. Horizontal Polarization.

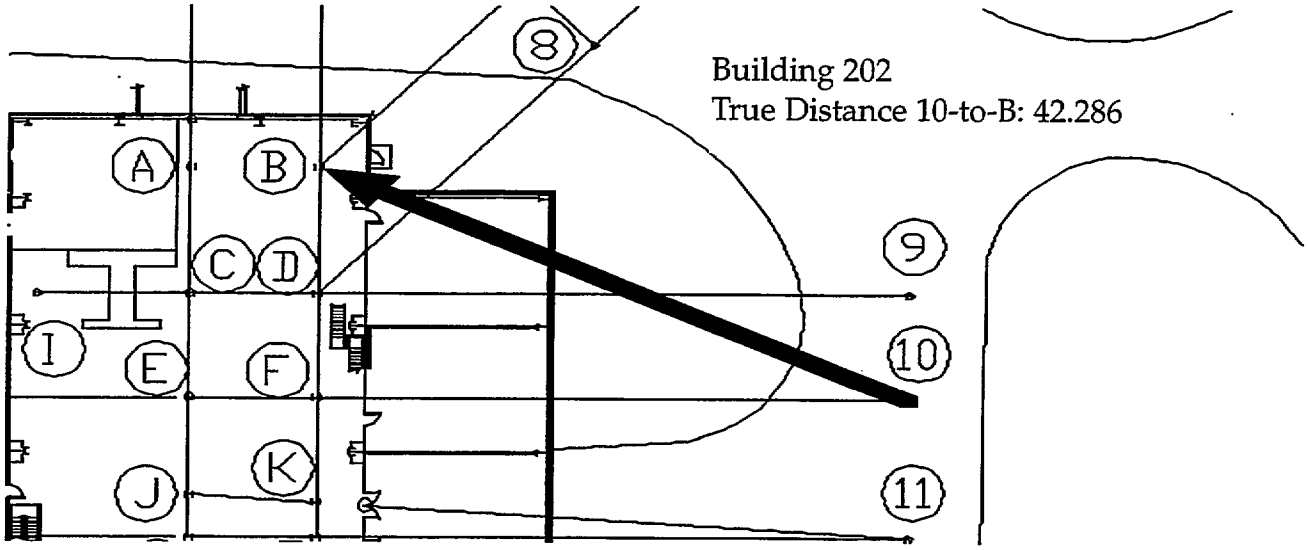

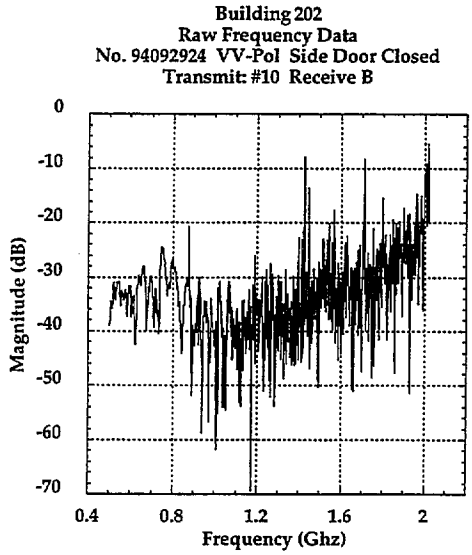

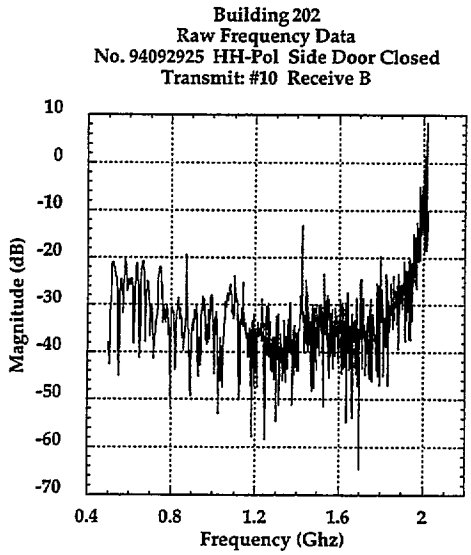

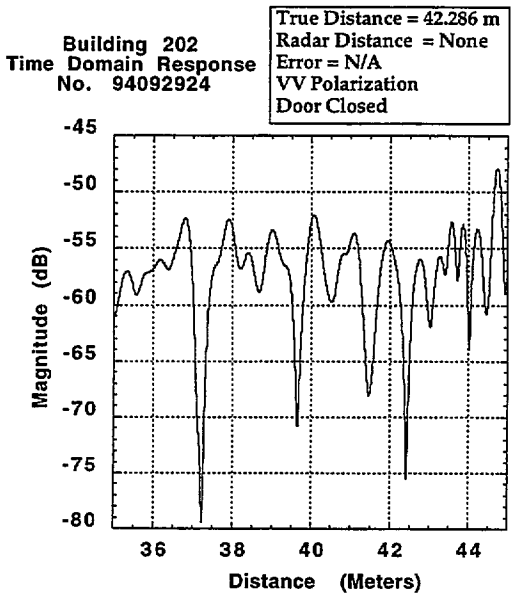

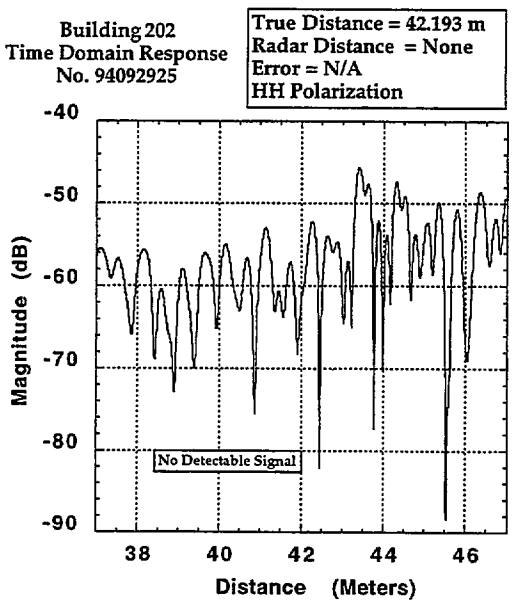

Fig 36a: Transmission at Station #10 to Receive Station B. Vertical Polarization.

Fig 36b: Transmission at Station #10 to Receive Station B. Horizontal Polarization.

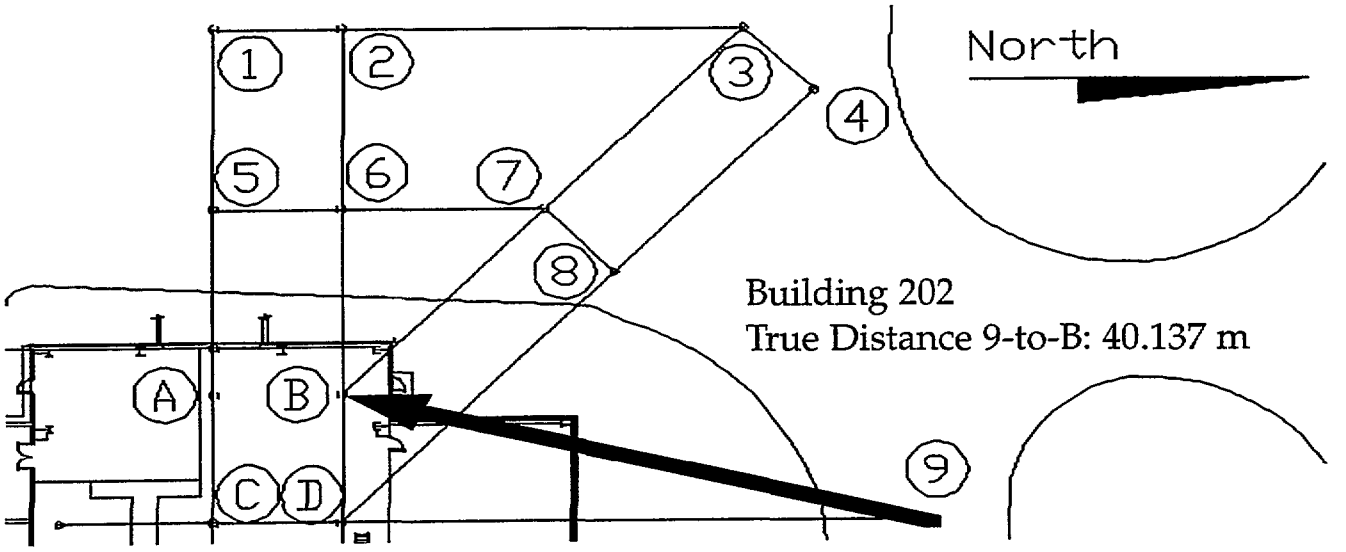

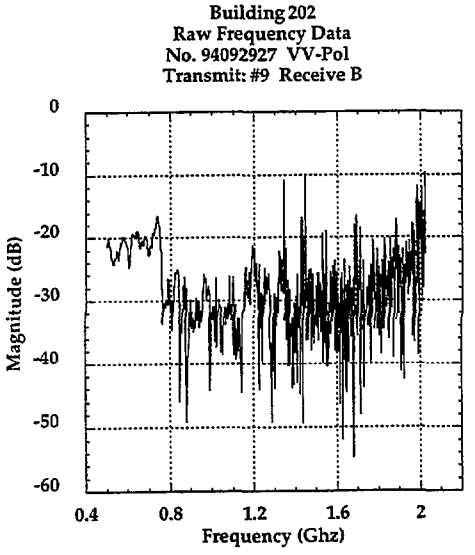

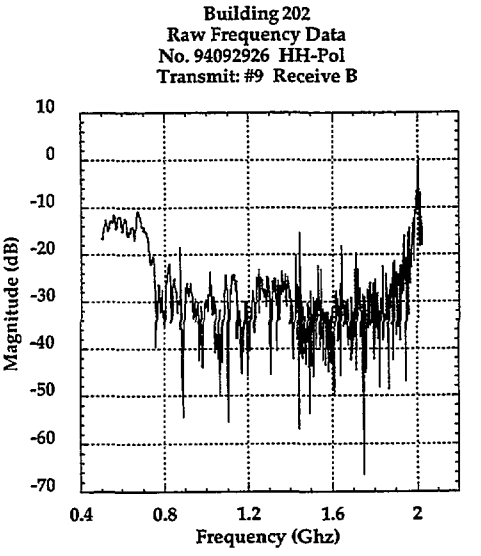

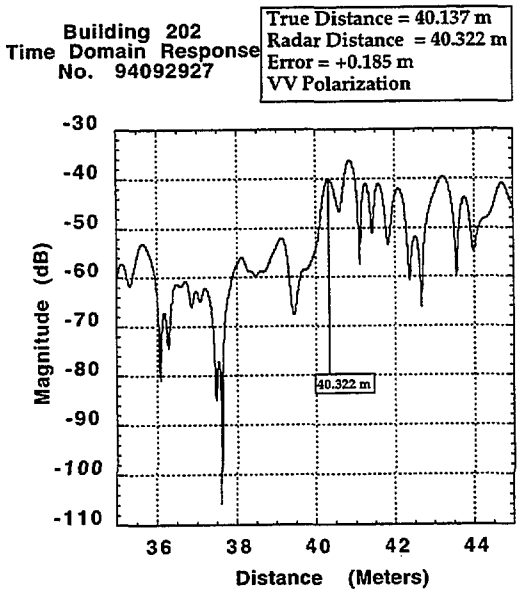

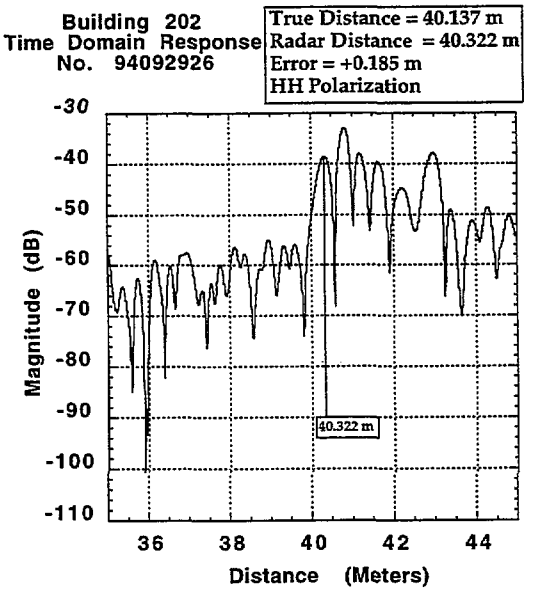

Fig 37a: Transmission at Station #9 to Receive Station B. Vertical Polarization.

Fig 37b: Transmission at Station #9 to Rceive Station B. Horizontal Polarization.

Building 202
True Distance 5-to-6: 8.229 m

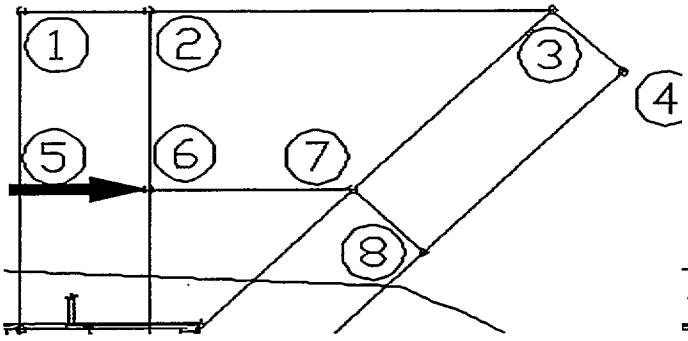

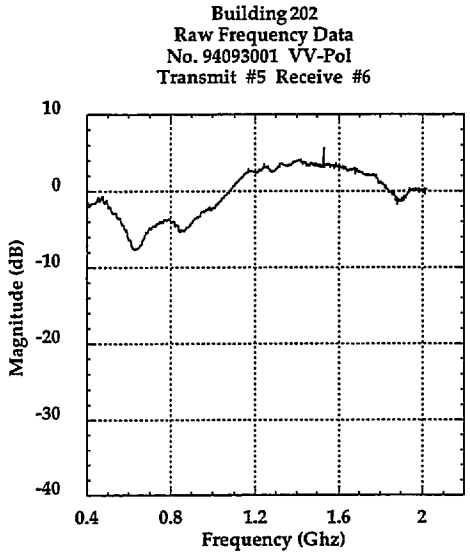

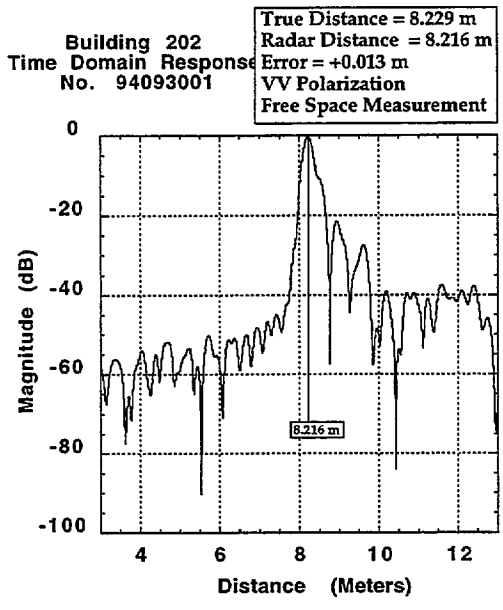

Fig 38a: Transmission at Station #5 to Receive Station #6. Vertical Polarization.

Building 202
True Distance 5-to-7: 21.582 m

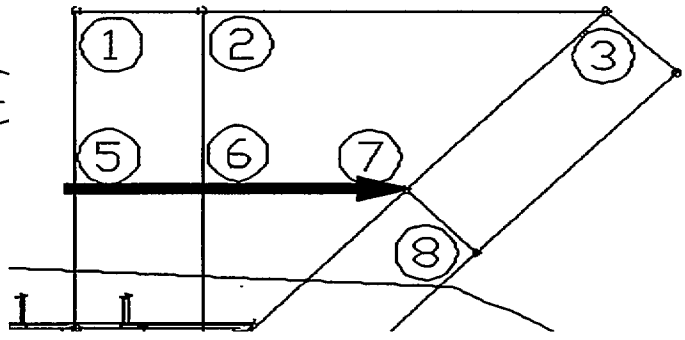

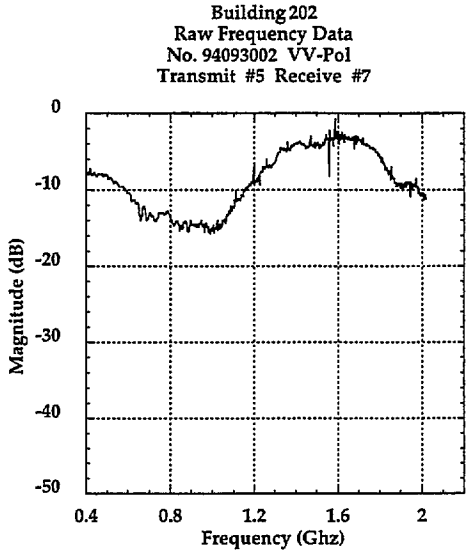

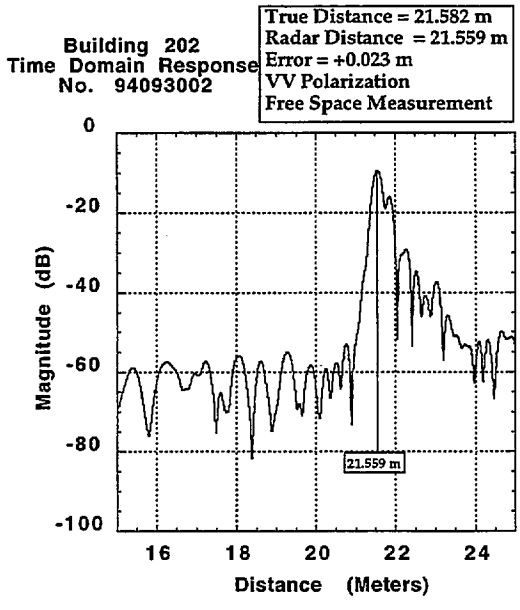

Fig 38b: Transmission at Station #5 to Receive Station #7. Vertical Polarization.

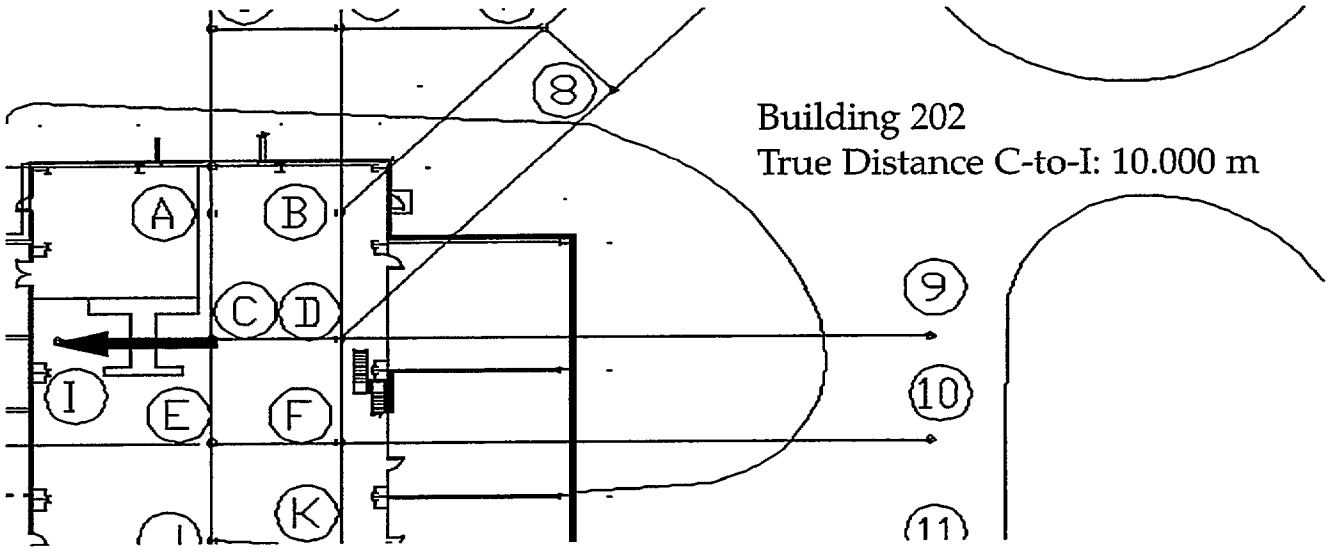

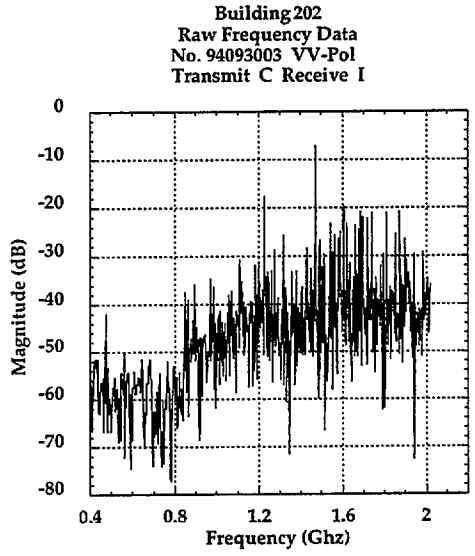

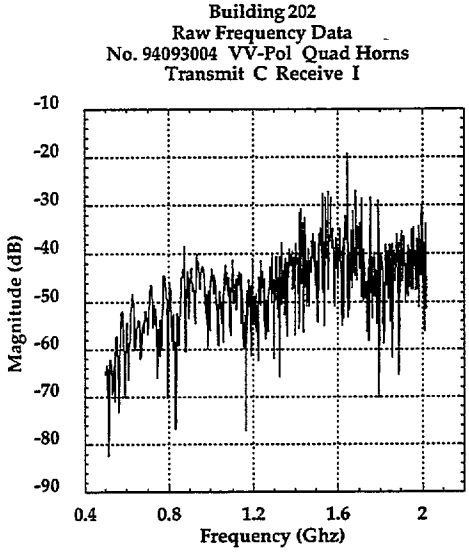

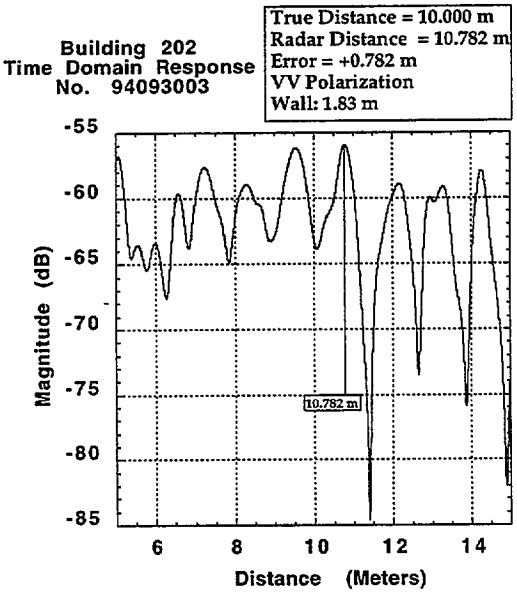

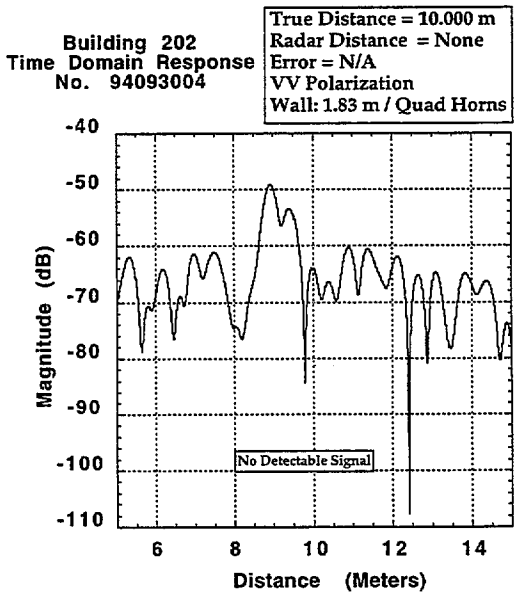

Fig 39a: Transmission at Station C to Receive Station I. Vertical Polarization.

Fig 39b: Transmission at Station C to Receive Station T. Vertical Polarization.